



**PLACE IN RETURN BOX**  
to remove this checkout from your record.  
**TO AVOID FINES** return on or before date due.

DATE DUE	DATE DUE	DATE DUE
<del>1005</del> MAR 28 2004		

THE ROLE OF SUBUNIT II IN CYTOCHROME *c* OXIDASE IN  
CYTOCHROME *c* BINDING AND ELECTRON TRANSFER

By

Yuejun Zhen

A DISSERTATION

Submitted to  
Michigan State University  
in partial fulfillment of the requirements  
for the degree of

DOCTOR OF PHILOSOPHY

Department of Biochemistry

1998



## ABSTRACT

### THE ROLE OF SUBUNIT II IN CYTOCHROME *c* OXIDASE IN CYTOCHROME *c* BINDING AND ELECTRON TRANSFER

By

Yuejun Zhen

Subunit II of cytochrome *c* oxidase (CcO), contains a unique binuclear Cu<sub>A</sub> center that is the entry site for electrons from cytochrome *c* (Cc). In order to use site-directed mutagenesis techniques to define the protein structure of Cc binding, to clarify the function of Cu<sub>A</sub>, and to test various models of electron transfer (ET), a strain of *Rhodobacter sphaeroides* was engineered with a chromosomal deletion of the entire *coxII* gene, part of the *coxIII* gene, and two intervening open reading frames (*orf1* and *orf3*) contained in the same operon. This resulted in the loss of the *aa<sub>3</sub>*-type oxidase from the membrane of the deletion strain (YZ200). Upon complementation of YZ200 with the entire *coxII/III* operon in a multicopy plasmid (pRK415-1), the *aa<sub>3</sub>*-type oxidase was restored. Two mutagenesis systems have been established, which, together with the YZ200 strain, enable all the residues in subunit II to be mutated.

CcO from *R. sphaeroides* is a good model system for the homologous mammalian oxidase. To take full advantage of this bacterial system, the wild-type CcO gene was overexpressed at levels up to seven-fold higher than in native strains by ligating the two operons for the CcO genes together and reintroducing them into *R. sphaeroides*, and by growing cells at a high pH (pH 8.0). The enzyme from the overexpression strain has properties identical to the native wild-type enzyme. A high-yield protocol for purifying homogeneous CcO by coupling metal-affinity chromatography and anion-exchange chromatography is also described.



A number of mutants were designed to create different forms of the Cu<sub>A</sub> site by altering its ligands. H260N and M263L, while retaining two copper atoms at the Cu<sub>A</sub> center, lost the electronic coupling between the two coppers, resulting in an increase of its redox potential and severe inhibition of ET from Cu<sub>A</sub> to heme *a*. In spite of their low activity, these two mutants still retain the ability to pump protons. The results suggest that the unique binuclear character is important for rapid ET from Cu<sub>A</sub> to heme *a*, but it is not required for proton pumping.

To define the interaction domain for Cc, a number of carboxylated residues on subunit II were changed to neutral residues, creating E148Q, D151N/E152Q, E157Q, D188N/E189Q, D195N, D214N, D229N and E254A. The mutants were characterized by UV-Vis and EPR spectroscopies, ultracentrifugation binding assays, steady-state and time-resolved kinetics. In all these mutants, except D229N and E254A, all of the metal centers are undisturbed, indicating localized effects. The mutants of internal residues, D229N and E254A, have altered heme centers and fail to bind Mg/Mn atoms. Analysis of intrinsic ET rates by a photo-induced ET assay revealed inhibition of intracomplex and second-order rates in the order of greatest to least: D214N > E157Q > E148Q > D195N > D151N/E152Q > D188N/E189Q = wild-type. The effects of the mutations on the binding of Cc to CcO complex were measured using analytical ultracentrifugation and steady-state kinetics. The degree of inhibition followed the same order. These results indicate that Asp-214, Glu-157, Glu-148 and Asp-195 are at the interface where Cc binds, while Asp-151, Glu-152, Asp-188, and Glu-189 are not.

In W143A and W143F mutants, the ET rate from Cc to Cu<sub>A</sub> is severely inhibited (1:1000 of wild-type), indicating that Trp-143 is the specific conduit for delivering electrons into Cu<sub>A</sub>, and that Cu<sub>A</sub> is the sole electron acceptor from Cc. The results favor a through-bond mechanism of ET.

**Dedicated to**

**my mom**

**and**

**my wife**

## ACKNOWLEDGMENTS

I would like to take this opportunity to express my deepest gratitude to my advisor, Dr. Shelagh Ferguson-Miller, for her support, encouragement, and for sharing her unique scientific thinking and insight during the course of this work. I would also like to thank my committee members: Dr. Robert Hausinger, Dr. Rawle Hollingsworth, Dr. John McCracken, and Dr. William Smith, for their guidance. A special thanks to Dr. Hausinger for reading through my thesis and providing valuable suggestions.

It is impossible for me to finish this project without the help from so many scientists with whom I had chance to interact in the past several years. First, I would like to thank Jon Hosler and John Fetter for helping me start my project, and continually giving me advice even after they left the lab. Next, to all the current members in Shelagh's lab: Dr. Denise Mills, Dr. Carrie Hiser, Dr. Laurence Florens, Dr. Uan Gen Kang, Jie Qian, Yasmin Hilmi, for their help at different aspects. I cherish the experiences I had with many undergraduates, past and current: Ann Tobin, Heidi Hoard, Michael Dahn, Marykey Lehman and Shawnon Langdon.

I would like to thank several collaborators for their help, including Dr. Frank Millett at the University of Arkansas for letting me stay in his lab to do some rapid kinetics experiments, and Kefei Wang for his generous help and allowing me to have

dinner at his home all week-long; and Dr. Gerald Babcock for inspiring the knowledge of chemistry into a biochemist's mind, and Dr. Wenjun Shi, Dr. Curtis Hoganson, Dr. Michelle Pressler for running EPR and Raman analyses for me.

A special thanks to Dr. William Hughes for spending so much time with me polishing my English and introducing me to American culture.

I thank my parents back in China and my brother here for their love and support. It is much to be regretted that I was not around with my parents when they needed me the most.

Last, to my wife, Yanbo, for her love, unconditional support and understanding, for accompanying me in the lab so many late nights and weekends.

## TABLE OF CONTENTS

LIST OF TABLES .....	xii
LIST OF FIGURES .....	xiii
LIST OF ABBREVIATIONS .....	xvii
<b>CHAPTER I</b>	
LITERATURE REVIEW .....	1
<b>I Respiratory chain and cytochrome <i>c</i> oxidase</b> .....	<b>4</b>
<b>1 The Respiratory chain</b> .....	<b>4</b>
1.1 Complex I (NADH:ubiquinone oxidoreductase) .....	5
1.2 Complex II (Succinate:quinone oxidoreductase) .....	5
1.3 Complex III (Cytochrome <i>bc</i> <sub>1</sub> ) .....	6
1.4 Complex IV (Cytochrome <i>c</i> oxidase) .....	7
<b>2 Heme-copper oxidases</b> .....	<b>7</b>
<b>3 The structure of cytochrome <i>aa</i><sub>3</sub> oxidase and the prosthetic groups</b> .....	<b>10</b>
3.1 Structural information .....	10
3.1.1 Subunit I .....	11
3.1.2 Subunit II .....	17
3.1.3 Subunit III .....	21
3.1.4 Other subunits .....	22
3.2 The oxygen reactions .....	23
3.3 Proton pumping .....	27
3.3.1 Characteristics of proton pumping .....	27
3.3.2 Proton pumping models .....	28
3.3.3 Proton channels .....	31
<b>4 Cu<sub>A</sub> center</b> .....	<b>33</b>
4.1 General characteristics of copper proteins .....	33
4.2 Cu <sub>A</sub> site in cytochrome <i>c</i> oxidase .....	35
4.2.1 Spectroscopic studies and chemical analyses .....	36
4.2.2 Molecular biology studies .....	40
4.2.3 Crystallographic studies .....	42
4.2.4 The advantages of being a binuclear center .....	43
4.2.5 Mutagenesis studies on Cu <sub>A</sub> .....	43
<b>5 Kinetics studies</b> .....	<b>44</b>
5.1 Steady-state kinetics .....	44
5.2 Rapid kinetics studies .....	48

II Electron transfer (ET) theories .....	52
1 Marcus theory .....	52
2 Dutton's distance dependent theory .....	55
3 Tunneling-pathway model .....	56
III The interactions of cytochrome <i>c</i> with its redox partners .....	58
1 Chemical modification studies .....	59
2 The interaction of cytochrome <i>c</i> with CcP— A case study .....	61
2.1 Crystallography studies .....	61
2.2 Mutagenesis studies .....	63
IV <i>c</i> -type cytochromes in <i>R. sphaeroides</i> .....	66
1 Properties of <i>c</i> -type cytochromes .....	68
1.1 Cytochrome <i>c</i> <sub>1</sub> .....	68
1.2 Cytochrome <i>c</i> <sub>2</sub> .....	69
1.3 Isocytochrome <i>c</i> <sub>2</sub> .....	73
1.4 Cytochrome <i>c</i> ' .....	74
1.5 Cytochrome <i>c</i> <sub>554</sub> .....	75
1.6 A diheme cytochrome .....	76
1.7 Cytochrome <i>c</i> <sub>551.5</sub> .....	76
1.8 <i>Sphaeroides</i> heme protein (SHP) .....	77
1.9 Cytochrome <i>cbb</i> <sub>3</sub> oxidase .....	77
2 Which cytochrome <i>c</i> is the physiological substrate for the <i>aa</i> <sub>3</sub> -type oxidase in <i>R. sphaeroides</i> .....	78
2.1 Soluble cytochrome <i>c</i> .....	78
2.2 Membrane bound cytochrome <i>c</i> .....	82
2.2.1 Cytochrome <i>c</i> <sub>552</sub> .....	82
2.2.2 Cytochrome <i>c</i> <sub>γ</sub> .....	83
2.2.3 Is there a membrane-bound cytochrome <i>c</i> in <i>R. sphaeroides</i> ? .....	84
3 Summary .....	85
V Research significance .....	86

**CHAPTER II**  
**DEVELOPMENT OF SYSTEMS FOR**  
**SITE-DIRECTED MUTAGENESIS IN SUBUNIT II OF**  
**CYTOCHROME *c* OXIDASE FROM *RHODOBACTER SPHAEROIDES*** ..... 88

Introduction .....	89
Materials and Methods .....	90
Results .....	95
Creation of a mutant strain lacking <i>coxII</i> .....	95
Characterization of the subunit II deletion strain (YZ200) .....	96
Complementation of the deletion strain .....	96
Characterization of the complemented cytochrome <i>c</i> oxidase .....	99
Construction of mutation systems .....	99
Discussion .....	103

**CHAPTER III**  
**OVEREXPRESSION AND**  
**PURIFICATION OF CYTOCHROME *c***  
**OXIDASE FROM *RHODOBACTER SPHAEROIDES*** ..... 108

Introduction .....	109
Materials and Methods .....	110
Results .....	118
Construction of the overexpression plasmid pRK-pYJ123H .....	118
Comparison of expression levels in different strains .....	119
Effect of pH on cytochrome <i>c</i> oxidase expression .....	121
Effect of salt concentration on cytochrome <i>c</i> oxidase expression .....	123
Expression of cytochrome <i>c</i> oxidase using a small vector pBBR1MCS and <i>fruP</i> gene .....	123
Fine-tuning the metal-affinity chromatography .....	126
A combined purification method .....	127
Comparison of overexpressed and wild-type oxidases .....	130
Discussion .....	131
Requirements for overexpression of cytochrome <i>c</i> oxidase .....	131
Purification strategies .....	135
Summary .....	136

<b>CHAPTER IV</b>	
<b>DEFINITION OF INTERACTION DOMAIN</b>	
<b>FOR THE REACTION OF CYTOCHROME <i>c</i> WITH</b>	
<b><i>RHODOBACTER SPHAEROIDES</i> CYTOCHROME <i>c</i> OXIDASE</b>	137
Introduction	138
Materials and methods	143
Results	149
Design of mutants	149
Metal analyses	150
Spectral characteristics of mutants	150
Optical spectra	150
Cu <sub>A</sub> /heme EPR spectra	158
Mn EPR spectra	161
The activities of mutants	163
Effect of ionic strength on the interaction of cytochrome <i>c</i> with cytochrome <i>c</i> oxidase	166
Steady-state kinetics assay	168
Laser flash photoreduction study of electron transfer rates into, and within <i>R. sphaeroides</i> cytochrome <i>c</i> oxidase	174
Kinetics of wild-type oxidase	174
Kinetics of cytochrome <i>c</i> oxidase mutants	182
Analytical ultracentrifuge measurement of the equilibrium dissociation constant K <sub>D</sub>	187
Discussion	190
The surface region of cytochrome <i>c</i> that interacts with various redox partners	190
Nature of the interaction between cytochrome <i>c</i> and cytochrome <i>c</i> oxidase: ionic strength effects	191
The effects of mutations in charged residues on cytochrome <i>c</i> binding and electron transfer	195
Comparison of horse and <i>R. sphaeroides</i> cytochrome <i>c</i> interaction with <i>R. sphaeroides</i> cytochrome <i>c</i> oxidase	197
Distinction between effects on cytochrome <i>c</i> binding and electron transfer	199
Trp-143 as the electron conduit to Cu <sub>A</sub> , and Cu <sub>A</sub> as the solo entry site for electrons from cytochrome <i>c</i>	201
A model of cytochrome <i>c</i> /cytochrome <i>c</i> oxidase interaction	204
Summary	206

<b>CHAPTER V</b>	
<b>IMPORTANCE OF ELECTRONIC COUPLING</b>	
<b>OF THE TWO COPPERS IN THE <math>Cu_A</math> CENTER</b>	
<b>FOR ELECTRON TRANSFER, NOT PROTON PUMPING</b>	207
Introduction	208
Materials and methods	211
Results	216
Expression levels of the mutants in cell membranes	217
Spectral characterizations of H260N and M263L	220
Time-resolved kinetics of electron transfer in H260N and M263L	229
Proton translocation	236
Discussion	239
The cytochrome <i>c</i> oxidase expression levels in subunit II mutants	239
The effects of mutations in H260N and M263L	240
The disruption of the proposed electron transfer pathway in H260N	244
Summary	245
<b>CHAPTER VI</b>	
<b>SUMMARY AND PERSPECTIVES</b>	246
Deletion of subunit II gene	247
Overexpression and purification of cytochrome <i>c</i> oxidase	248
Structural significance of the binuclear $Cu_A$ center and its control on electron transfer	249
Residues involved in cytochrome <i>c</i> binding	250
Trp-143, the electron entry site, and $Cu_A$ , the solo initial electron acceptor in cytochrome <i>c</i> oxidase	252
<b>APPENDIX</b>	254
<b>BIBLIOGRAPHY</b>	255

## LIST OF TABLES

Table 3.1	Bacterial strains and plasmids.....	111
Table 3.2	Purification of cytochrome <i>c</i> oxidase from overexpression strain YZ200.....	112
Table 4.1	Characteristic of subunit II mutants of cytochrome <i>c</i> oxidase from <i>R. sphaeroides</i> .....	151
Table 4.2	Protein and heme assays of subunit II cytochrome <i>c</i> oxidase mutants from <i>R. sphaeroides</i> .....	154
Table 4.3	The $K_M$ values for the interactions of <i>R. sphaeroides</i> cytochrome <i>c</i> oxidases with <i>R. sphaeroides</i> cytochrome $c_2$ and horse cytochrome <i>c</i> .....	173
Table 4.4	Electron transfer from Ru-55-Cc to <i>R. sphaeroides</i> cytochrome <i>c</i> oxidase.....	176
Table 4.5	Equilibrium dissociation constant $K_D$ ( $\mu\text{M}$ ) from analytical ultracentrifuge assays for the binding of horse cytochrome <i>c</i> to <i>R. sphaeroides</i> cytochrome <i>c</i> oxidase .....	189
Table 5.1	Characteristics of <i>R. sphaeroides</i> cytochrome <i>c</i> oxidase subunit II H260N and M263L enzymes.....	222
Table 5.2	Electron transfer from Ru-55-Cc to cytochrome <i>c</i> oxidase H260N and M263L enzymes.....	231

## LIST OF FIGURES

### CHAPTER I

Figure 1.1	Mitochondrial respiratory chain.....	3
Figure 1.2	The metal centers and their ligands in cytochrome <i>c</i> oxidase.....	13
Figure 1.3	Stereoview of the Mg site in cytochrome <i>c</i> oxidase.....	14
Figure 1.4	Stereoview of the calcium site in cytochrome <i>c</i> oxidase.....	16
Figure 1.5	Sequence alignments of subunits II of cytochrome <i>c</i> oxidases and quinol oxidase.....	18
Figure 1.6	Stereoview of the Cu <sub>A</sub> site in cytochrome <i>c</i> oxidase.....	20
Figure 1.7	Mechanism of oxygen reduction by cytochrome <i>c</i> oxidase.....	26
Figure 1.8	Potential energy diagram for electron transfer between to nearly equivalent complexes.....	53
Figure 1.9	An overview of the respiratory pathways in <i>Rhodobacter sphaeroides</i> .....	67
Figure 1.10	Sequence alignments of <i>c</i> -type cytochromes.....	72

### CHAPTER II

Figure 2.1	Restriction map of pYJ100 with <i>coxII/III</i> operon.....	91
Figure 2.2	The procedure for deletion of the <i>coxII/III</i> operon.....	93
Figure 2.3	Physical maps of the <i>coxII/III</i> operons in Ga and YZ200, and the southern blots analysis results.....	97

Figure 2.4	The difference spectra of membranes derived from wild-type Ga, <i>coxII</i> deletion strain YZ200 and the complemented strain YZ300.....	98
Figure 2.5	System I for site-directed mutagenesis of residues at the N-terminal half of subunit II of cytochrome <i>c</i> oxidase.....	102
Figure 2.6	System II for site-directed mutagenesis of residues at the C-terminal half of subunit II of cytochrome <i>c</i> oxidase.....	104

### CHAPTER III

Figure 3.1	The procedures for construction of the overexpression plasmid pRK-pYJ123H.....	114
Figure 3.2	Cytochrome <i>c</i> oxidase content in cytoplasmic membrane prepared from different <i>R. sphaeroides</i> strains.....	120
Figure 3.3	Effect of pH on cytochrome <i>c</i> oxidase expression in YZ100 strain.....	122
Figure 3.4	Constructs made for expressing cytochrome <i>c</i> oxidase using fructose promoter gene ( <i>fruP</i> ).....	125
Figure 3.5	SDS-polyacrylamide gel electrophoresis of cytochrome <i>c</i> oxidase e purified from Ni <sup>2+</sup> -NTA and FPLC column.....	128
Figure 3.6	Purification of Ni <sup>2+</sup> -NTA purified cytochrome <i>c</i> oxidase on DEAE-5PW.....	129

### CHAPTER IV

Figure 4.1	The structure of subunit II C-terminal domain of cytochrome <i>c</i> oxidase.....	141
Figure 4.2	Optical spectra of <i>R. sphaeroides</i> wild-type oxidase and subunit II mutants.....	153

Figure 4.3	Near-infrared spectra of the wild-type and mutants cytochrome <i>c</i> oxidase from <i>R. sphaeroides</i> .....	157
Figure 4.4	Cu <sub>A</sub> and heme EPR spectra of cytochrome <i>c</i> oxidase.....	160
Figure 4.5	Mn EPR spectra of wild-type cytochrome <i>c</i> oxidase and subunit II mutant enzymes.....	162
Figure 4.6	The maximum turnover numbers of subunit II mutants with <i>R. sphaeroides</i> <i>c</i> <sub>2</sub> (A) and horse heart cytochrome <i>c</i> (B) as substrates.....	165
Figure 4.7	Ionic strength dependent turnover numbers of subunit II mutants.....	167
Figure 4.8	Steady-state kinetics assay of <i>R. sphaeroides</i> cytochrome <i>c</i> oxidase with <i>R. sphaeroides</i> cytochrome <i>c</i> <sub>2</sub> .....	169
Figure 4.9	Steady-state kinetics assay of <i>R. Sphaeroides</i> cytochrome <i>c</i> oxidase with horse cytochrome <i>c</i> .....	170
Figure 4.10	Steady-state kinetics assay of <i>R. sphaeroides</i> CcO with <i>R. sphaeroides</i> cytochrome <i>c</i> <sub>2</sub> .....	171
Figure 4.11	Photoinduced electron transfer from Ru-55-Cc to cytochrome <i>c</i> oxidase.....	178
Figure 4.12	Ionic strength dependent of electron transfer from Ru-55-Cc to cytochrome <i>c</i> oxidase .....	181
Figure 4.13	Ionic strength dependent of the slow phase electron transfer from Ru-55-Cc to cytochrome <i>c</i> oxidase.....	183
Figure 4.14	Analytical ultracentrifugation assay of the equilibrium dissociation constant between cytochrome <i>c</i> and <i>R. sphaeroides</i> cytochrome <i>c</i> oxidase.....	188
Figure 4.15	Space-filling models of subunit II C-terminal domain of cytochrome <i>c</i> oxidase (A) and horse cytochrome <i>c</i> (B).....	192

## CHAPTER V

Figure 5.1	Schematic representation of site-specific mutagenesis using overlap extension method.....	213
Figure 5.2	Optical spectra of Cu <sub>A</sub> ligand mutants.....	219
Figure 5.3	Near-infrared spectra of the wild-type and M263L enzymes.....	223
Figure 5.4	EPR spectra of wild-type, M263L and H260N enzymes.....	226
Figure 5.5	Ionic strength dependent electron transfer from Ru-55-Cc to wild-type, M263L and H260N enzymes.....	232
Figure 5.6	Electron transfer between Ru-55-Cc and M263L at 150 mM NaCl.....	234
Figure 5.7	Ionic strength dependent electron transfer from cytochrome <i>c</i> to Cu <sub>A</sub> and from Cu <sub>A</sub> to heme <i>a</i> in M263L enzyme.....	235
Figure 5.8	Proton pumping activities of the purified M263L and H260N.....	238

## LIST OF ABBREVIATIONS

3-CP	3-carboxyl-2,2,5,5-tetramethyl-1-pyrrolidinyloxy free radical
AP	ampicillin
Cc(Y)	yeast cytochrome <i>c</i>
Cc(H)	horse cytochrome <i>c</i>
CcO(s)	cytochrome <i>c</i> oxidase(s)
CcP	cytochrome <i>c</i> peroxidase
EPR	electron paramagnetic resonance spectroscopy
Eq.	equation
ET	electron transfer
<i>fruP</i>	fructose promotor gene
ICP	inductively coupled plasma emission spectroscopy
Kn	kanamycin
LM	lauryl maltoside
LpM	subunit II loop mutant with the Cu <sub>A</sub> binding loop replaced with the short one from blue copper protein.
N <sub>2</sub> OR	nitrous-oxide reductase
Ni-NTA	nickel nitrilotriacetic acid resin
PIXE	proton induced x-ray emission spectroscopy
Ru	ruthenium
Ru-55-Cc	cytochrome <i>c</i> with ruthenium labeled at lys-55 position
Sm	streptomycin
Sp	spectinomycin
Tc	tetracycline
TMPD	N,N,N',N'-tetramethyl-p-phenylenediamine
TXRF	total-reflection x-ray fluorescence spectrometry

**CHAPTER I**  
**Literature Review**

One of the striking features of living organisms is their active engagement in energy transformation to maintain homeostasis and movement. However, most of them cannot use solar energy directly through photosynthesis, like plants do; instead, they acquire energy through metabolizing foodstuffs and storing it in the form of fat and carbohydrate. The major energy form that living organisms use directly is the chemical energy stored as ATP. There are generally three steps for converting energy from foodstuffs into ATP: 1) Glycolysis, where the foodstuffs are degraded to smaller building blocks; 2) Tricarboxylic acid (TCA) cycle, in which the small building blocks from glycolysis are further degraded to CO<sub>2</sub> and H<sub>2</sub>O with the production of a reducing agent, NADH; 3) Oxidative phosphorylation, in which the electrons from NADH are fed into a chain of membrane-bound complexes, the respiratory chain (Figure 1.1), and are eventually accepted by oxygen and some other inorganic molecules. In the process of electron transfer through the respiratory chain, the energy is stored in the form of a transmembrane potential, which drives ATP synthesis (Mitchell & Moyle, 1965; Mitchell, 1976).

The enzyme that I have worked on is cytochrome *c* oxidase (CcO), a complex that belongs to the respiratory chain. The function of CcO is to reduce oxygen to water by accepting electrons from its substrate, cytochrome *c* (Cc), meantime, contributing to the establishment of the transmembrane potential. So in this chapter, I am going to review some related issues with CcO as listed below:

- 1) Respiratory chain and CcO.
- 2) Electron transfer theories.
- 3) The interaction of Cc with its redox partners.
- 4) C-type cytochromes in *R. sphaeroides*.

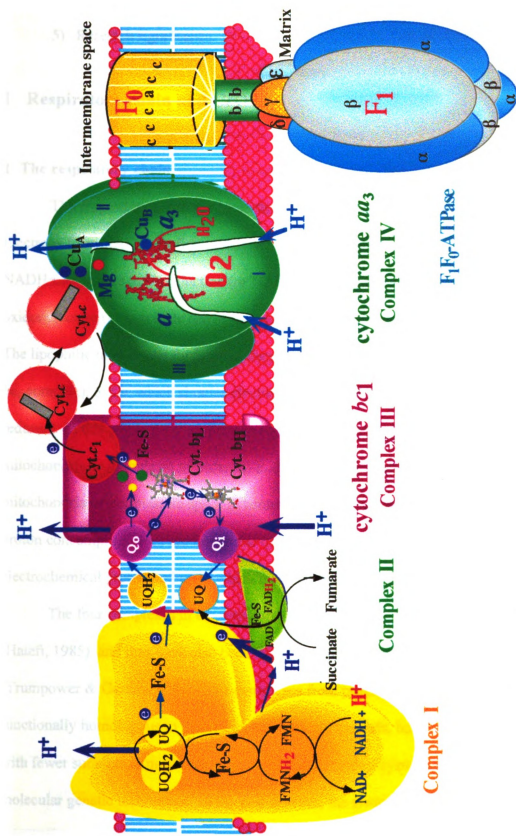


Figure 1.1 Mitochondrial Respiratory Chain

5) Research significance.

## **I Respiratory chain and CcO**

### **1 The respiratory chain**

The respiratory chain produces the most energy of all the three steps listed above. Electrons from NADH are first transferred to complex I and complex II, also known as NADH:ubiquinone oxidoreductase (*or* NADH dehydrogenase) and succinate:quinone oxidoreductase (*or* succinate dehydrogenase), and then are used to reduce ubiquinone. The lipophilic ubiquinone further transfers electrons, through complex III (cytochrome  $bc_1$  complex), to Cc, which shuttles electrons to complex IV (CcO), where oxygen is reduced. In this whole process, protons were translocated from the inside (matrix of mitochondria *or* cytoplasm of bacteria) to the outside (intermembrane space of mitochondria *or* periplasmic space in bacteria). The proton translocation, together with proton consumption from the inside due to water formation, creates a transmembrane electrochemical proton potential, which is the driving force for ATP synthesis.

The four complexes in the respiratory chain have been isolated from mitochondria (Hatefi, 1985), and they have also been found in many aerobically growing prokaryotes (Trumpower & Gennis, 1994). The complexes from prokaryotes are structurally and functionally homologous to their mitochondrial counterparts, but structurally simpler with fewer subunits in most complexes, making them ideal systems to study using molecular genetic techniques. In the past decades, the studies on the prokaryotic systems

10  
11  
12  
13  
14  
15  
16  
17  
18  
19  
20  
21  
22  
23  
24  
25  
26  
27  
28  
29  
30  
31  
32  
33  
34  
35  
36  
37  
38  
39  
40  
41  
42  
43  
44  
45  
46  
47  
48  
49  
50  
51  
52  
53  
54  
55  
56  
57  
58  
59  
60  
61  
62  
63  
64  
65  
66  
67  
68  
69  
70  
71  
72  
73  
74  
75  
76  
77  
78  
79  
80  
81  
82  
83  
84  
85  
86  
87  
88  
89  
90  
91  
92  
93  
94  
95  
96  
97  
98  
99  
100

have greatly advanced our understanding of energy conservation in the respiratory chain, but our understanding of each complex varies greatly due to their different complexities and the amount of structural information available.

### **1.1 Complex I (NADH:ubiquinone Oxidoreductase)**

Complex I is the initial electron acceptor from NADH and catalyzes electron transfer from NADH to ubiquinone in a reaction that is coupled with proton translocation across the membrane with a stoichiometry of  $4H^+/2e^-$ .

Complex I is the largest complex in the respiratory chain, with about 43 subunits in bovine mitochondria; as a result, it is also the least well understood. In this complex, there is one flavin mononucleotide (FMN) and unknown numbers of iron-sulfur groups. Two dimensional structure studies using electron microscopy suggest that the protein has an overall L-shaped structure, with one arm located in the membrane and the other one in the matrix side (for review see Friedrich et al., (1998)).

### **1.2 Complex II (Succinate:quinone oxidoreductase)**

Complex II is the only protein that is involved in both the TCA cycle and the respiratory chain. It catalyzes the oxidation of succinate and produces fumarate. Because of the low redox potential change in the overall reaction, there is not enough energy to drive proton translocation, as the other three complexes in the respiratory chain do. It is interesting to notice that quinone:fumarate reductase, while catalyzing the opposite reaction as complex II, is structurally similar to complex II.

Complex II from different species have three to four subunits, including a flavoprotein subunit with a flavin adenine dinucleotide (FAD) prosthetic group, and an

iron-sulfur subunit with three Fe-S groups. These two subunits form the cytoplasm (*or* matrix) domain of the protein, while the rest of the subunit(s) is(are) located in the membrane with one or two cytochrome *b* groups (for review see Hagerhall, (1997)).

### 1.3 Complex III (Cytochrome *bc*<sub>1</sub>)

The cytochrome *bc*<sub>1</sub> complex is one of the most well studied complexes in the respiratory chain. It catalyzes the oxidation of ubiquinone and transfers electrons to *c*-type cytochromes, coupled with proton translocation across the membrane at a stoichiometry of  $4\text{H}^+/2\text{e}^-$  (Trumpower, 1990(a); 1990(b)). This complex is involved in both anaerobic photosynthesis and aerobic respiration processes, by transferring electrons to either reaction centers or CcO, respectively.

It has been found that the *bc*<sub>1</sub> complex is composed of at least four subunits in *Rhodobacter sphaeroides* (Yu et al., 1984), and as many as eleven in mammalian mitochondria (Schägger et al., 1986; Iwata et al., 1998). All of the *bc*<sub>1</sub> complexes from different species have four redox centers: a low (*b*<sub>L</sub>) and a high potential (*b*<sub>H</sub>) cytochrome *b*, a "Rieske" iron-sulfur [2Fe-2S] cluster and a membrane-bound cytochrome *c*<sub>1</sub>. The *b*<sub>L</sub> is located at the middle of the membrane, and *b*<sub>H</sub> close to the cytoplasmic surface. The *c*-type heme group of cytochrome *c*<sub>1</sub> and the iron-sulfur cluster are located at the periplasm (*or* intermembrane space), anchored to the membrane through transmembrane helices.

Recently, several cytochrome *bc*<sub>1</sub> crystal structures have been resolved, including a 1.5 Å resolution structure of the soluble domain of the Fe-S protein from the beef heart (Iwata et al., 1996), a 2.9 Å structure of the *bc*<sub>1</sub> complex from bovine heart (Xia et al., 1997), several structures from chicken heart (3.0 Å), beef heart (3.8 Å, in a different space

group from Xia's crystal) and rabbit (3.5 Å) (Berry et al., 1998; Zhang et al., 1998) and a 3.0 Å bovine structure (Iwata et al., 1998), which resolved all the eleven subunits. These crystallographic studies confirm most of the early biochemical and biophysical study results, regarding the locations and arrangements of the prosthetic groups in the protein. But the big surprise is the distance between the Fe-S cluster and cytochrome *c<sub>1</sub>*, which, when measured from the crystal structure, is too long to explain the kinetic study data. More interestingly, the distances calculated from different crystals vary significantly. It has been suggested that the Fe-S protein can be rotated, and this movement is a necessary part of the turnover cycle of this complex (Zhang et al., 1998).

#### 1.4 Complex IV (CcO)

CcO sequentially accepts four electrons from four Cc and uses them to reduce oxygen molecules to water (Saraste, 1990). In addition to the electron transfer and the consumption of protons from the cytoplasm (*or* matrix) side, CcO also pumps protons at a stoichiometry of  $4\text{H}^+/4\text{e}^-$  (Wikström, 1977; 1984).

CcO, with thirteen subunits in bovine heart and three to four subunits in some bacteria (Kadenbach et al., 1983; Hosler et al., 1992; Iwata et al., 1995; Tsukihara et al., 1996), belongs to the heme-copper oxidases family.

## 2 Heme-copper oxidases

Heme-copper terminal oxidases catalyze the four electron reduction of oxygen to water, coupled with the generation of an electrochemical gradient across the membrane in which they are embedded (García-Horsman et al., 1994a). The distinct characteristics of

all the members of this superfamily are that the subunits I are homologous to each other, and in this subunit there is always a heme-copper binuclear site, where the oxygen reaction takes place. Besides the heme groups at the binuclear centers, which are high spin five coordinate hemes, there is usually another low spin heme located in subunit I close to the high spin heme at the binuclear center. Most of the terminal oxidases found so far belong to this family, the only exception being the cytochrome *bd* oxidase, where the oxygen reduction site is a *d*-type heme with no associated copper (Junemann, 1997).

In mammalian mitochondria, the only type of oxidase present is the *aa*<sub>3</sub>-type oxidase, characterized by the presence of two heme A groups in subunit I. This *aa*<sub>3</sub>-type oxidase, together with several alternative oxidases from this superfamily, is also found in some bacteria, and they are inducible by oxygen in the environment. In *R. sphaeroides*, three respiratory oxidases have been identified: *aa*<sub>3</sub>- and *cbb*<sub>3</sub>-type CcOs and a *bb*<sub>3</sub>-quinol oxidase (Hosler et al., 1992; García-Horsman et al., 1994b; Yun et al., 1994). At high oxygen tension (under aerobic growth conditions), the *aa*<sub>3</sub>-type oxidase is the dominant form, while at low oxygen tension (semi-aerobic conditions), the *cbb*<sub>3</sub>-type oxidase is induced and the *aa*<sub>3</sub>-type oxidase is repressed. The presence of more than one kind of terminal oxidase enables organisms to survive under different environmental conditions.

Although all the members from the heme-copper oxidase family have a similar structure in subunit I, they are diversified in several aspects:

- 1) **Substrate:** Substrate utilization for the members of the heme-copper oxidase family differ, and can be categorized into two groups: CcOs use soluble or membrane-bound Cc as their substrate, while quinol oxidases use membrane-bound quinol, rather than Cc, as the electron donor.

2) **Prosthetic groups:** So far four types of heme groups have been found among the members of the heme-copper oxidases family: A-, B-, C-, and O-type hemes. These four types of heme groups all share the same basic tetrapyrrole porphyrin rings structure, but their differences lie in the types of the side chains, which also impart to them different visible absorption spectra. Among these four types of heme groups found in the heme-copper oxidase family, only hemes A, B and O are found to be present at the binuclear center. The c-type hemes are only found covalently linked to subunit II of some members of the family, like *caa<sub>3</sub>*- and *cbb<sub>3</sub>*-type oxidases (Mather et al., 1993; García-Horsman et al., 1994b). In these types of oxidases, the covalently bound c-type hemes, acting as the substrates for the oxidases, can transfer electrons directly to the oxidases (Nicholls & Sone, 1984).

Besides the variation of the heme components, another difference among the prosthetic groups is the presence or absence of a Cu<sub>A</sub> site among the heme-copper oxidases. In most CcOs, Cu<sub>A</sub>, as the initial electron acceptor from Cc (see below), is located at the C-terminus of subunit II. This copper site is found to be present in *aa<sub>3</sub>*-, *caa<sub>3</sub>*- and *ba<sub>3</sub>*-type CcO, but not in any known quinol oxidases or other CcOs, including the *cbb<sub>3</sub>*-type oxidases (García-Horsman et al., 1994a). The membrane-bound feature of quinol may enable it to transfer electrons directly to the low spin hemes in subunit I of the quinol oxidases, in the absence of a Cu<sub>A</sub> site. In this regard, the covalently bound C-type hemes in the *cbb<sub>3</sub>*-type CcO may also transfer electrons directly to the low spin hemes at subunit I.

3) **Proton pumping capability:** Although heme-copper oxidases have been found in many species, few have been purified and very well characterized, especially for

100

101

102

103

104

105

106

107

108

109

110

111

112

113

114

115

116

117

118

119

120

their proton pumping activities. Among them, the *aa*<sub>3</sub>-type CcO and the *bo*<sub>3</sub>-type quinol oxidases are the most well understood. The proton pumping activities of the oxidases do not correlate with the substrates used, either Cc or quinol. Both *aa*<sub>3</sub>-type CcO and *bo*<sub>3</sub>-type quinol oxidases show proton pumping activities; so do the *cbb*<sub>3</sub>-type CcO found in *R. sphaeroides* and *Paraccous. denitrificans* (de Gier et al., 1996). The *bb*<sub>3</sub>-type CcO from *Thermophilic bacterium* PS3 (Sone et al., 1990) and the *ba*<sub>3</sub>-type CcO from *Thermus thermophilis* (M. Denise and S. Ferguson-Miller, unpublished) have not been demonstrated to pump protons.

### **3 The structure of cytochrome *aa*<sub>3</sub> oxidase and the prosthetic groups**

#### **3.1 Structural information**

The *aa*<sub>3</sub>-type CcO is the best characterized among the heme-copper oxidases. Most of the early work on this enzyme was done on the enzyme isolated from bovine heart using a variety of spectroscopic and biochemical techniques (Wikström et al., 1981). In bovine heart, CcO has thirteen subunits (Kadenbach et al., 1983), with the three largest encoded by mitochondria, and the other ten by nucleus. In contrast, the *aa*<sub>3</sub>-type oxidases from bacteria have a much simpler structure, with three to four subunits, and the three largest ones from bacterial oxidases are highly homologous to the three largest subunits in mammalian oxidases (Cao et al., 1991; Shapleigh & Gennis, 1992).

Extensive mutagenesis has been done on the gene encoding subunit I of CcO from *R. sphaeroides* and the homologous subunit in the *E. coli bo*<sub>3</sub> quinol oxidase (Hosler et al., 1993). The combination of biochemical, biophysical and spectroscopic analyses correctly

predicted the structures of the metal centers (except the newly discovered Ca site) in subunit I and their arrangements in the membrane. In 1995, a landmark time for CcO research, two crystal structures were resolved simultaneously from different species: a thirteen subunit bovine heart oxidase (Tsukihara et al., 1995; 1996) and a four subunit oxidase from *P. denitrificans* (Iwata et al., 1995), with the three largest subunits in both oxidases sharing almost identical secondary structures and local metal structures. It is noteworthy that, although mammalian and prokaryotes are evolutionarily distantly related, the features of the core structures in the  $aa_3$ -type CcO are essentially identical in both systems. The crystal structures, besides confirming results of early studies, provide more detailed structural information for further functional analysis. The following review is based on the information from these two crystal structures and their newly refined versions (Ostermeier et al., 1997; Yoshikawa et al., 1998), with emphasis on the three core subunits. All the residue numbers, unless otherwise specified, are based on the *R. sphaeroides* oxidase system (for a more general review, see Ferguson-Miller & Babcock, (1996)).

### 3.1.1 Subunit I

Subunit I, being the most conserved subunit in CcO, has twelve transmembrane helices, as suggested by amino acid hydropathy plot analysis (Hosler et al., 1993), with the exceptions that the helices from the structures are generally longer than predicted and are more tilted in the membrane.

With the discovery of the new Ca site, there are five metal centers in this subunit: the redox active heme  $a$ , heme  $a_3$  and  $Cu_B$  sites, and the non-redox active Mg and Ca

sites. The overall arrangements of these sites, together with Cu<sub>A</sub> located in subunit II, are shown in Figure 1.2. The low spin heme *a* is ligated by two histidine residues, His-102 and His-421, from helix II and helix X, respectively, while the high spin heme *a*<sub>3</sub> uses another histidine residue (His-419) in helix X as its ligand. This arrangement puts the two heme centers in close proximity, with an edge to edge distance between the two hemes of 4.7 Å in the bacterial oxidase, and an iron to iron distance of 13.2 Å in the *P. denitrificans* oxidase (14 Å in the bovine oxidase). The heme planes are almost perpendicular to each other with the interplanar angles of 108° and 104°, respectively, for the *P. denitrificans* and bovine oxidases. As suggested from spectroscopic analyses, the heme *a*<sub>3</sub> and Cu<sub>B</sub> are located in close proximity at about 5.0 Å apart (4.5 Å in bovine and 5.2 Å in *P. denitrificans*), with Cu<sub>B</sub> ligated by three histidine residues, His-284, -333 and -334. The high spin heme *a*<sub>3</sub> and the Cu<sub>B</sub> are strongly electronically coupled, rendering both of them EPR invisible.

The non-redox active Mg site is located at the interface between subunit I and II. As the mutagenesis and spectroscopy studies suggested (Espe et al., 1995; Hosler et al., 1995; Witt et al., 1997), this metal center has an octahedral structure with side chains of His-411 and Asp-412 from subunit I and the carbonyl oxygen of Glu-254 from subunit II as ligands (Figure 1.3). The other three ligands are water molecules, with one of them hydrogen-bonded to Asp-229 in subunit II. This Mg site has been found to be important for stabilizing the overall structure and modulating the redox potentials of the neighboring metal centers (Florens et al., 1998). Its possible involvement in proton/water exit has also been proposed (Ferguson-Miller & Babcock, 1996).

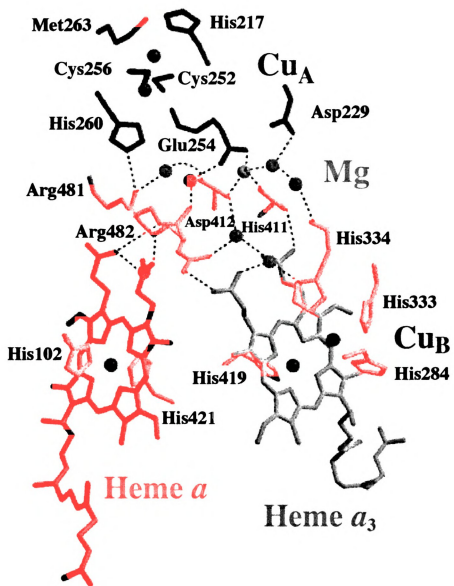


**Figure 1.2** The metal centers and their ligands in cytochrome *c* oxidase. The structure is from Ostermeier (1997) with modification.

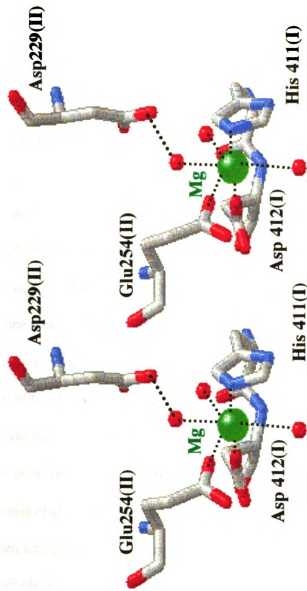
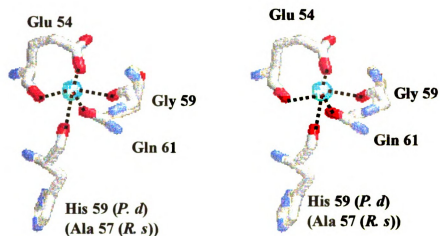


**Figure 1.3** Stereoview of the Mg site in cytochrome *c* oxidase. The roman numerals (I) and (II) refer to subunit I and II, respectively. The structure created is from 2.3 Å bovine oxidase coordinates (Yoshikawa, 1998).

With the availability of the two-subunit structure of the bacterial oxidase (Ostermeier et al., 1997) and the refinement of the bovine oxidase to 2.3 Å resolution (Yoshikawa et al., 1998), a new Ca site has been discovered in both systems. This metal site is located at the periplasmic end of the first transmembrane helix of subunit I, with five oxygen molecules as direct ligands. It is noteworthy that, although the new Ca sites were identified at roughly the same positions in subunit I of the two oxidases, the resolved ligands in the two structures are not all the same. In the two-subunit oxidase from *P. denitrificans*, the five oxygen molecules are from the carbonyl oxygen of Ala-57 (His-59 in *P. denitrificans*), Glu-54 and Gly-59, as well as the side chain oxygens of Glu-54 and Gln-61 (Figure 1.4), while in the bovine oxidase, they are from the carbonyl oxygens of Glu-54, Gly-59 and Ile-484 (Ser-441 in bovine oxidase), the side chain of Glu-54 and one water molecule (Figure 1.4). The center to center distances from Ca to Cu<sub>A</sub> and heme *a* in *P. denitrificans* oxidase from is about 18 Å and 17 Å, respectively. The function of this Ca site is unknown so far.

Another unexpected result from the high resolution structures is the presence of a covalent bond between the highly conserved Tyr-288 and His-284, one of the Cu<sub>B</sub> ligands (Ostermeier et al., 1997; Yoshikawa et al., 1998). The electron densities between them have been interpreted as a hydrogen bond in early structures, while the high resolution structures clearly show the presence of a covalent bond. It previously had been noted that substitutions of this tyrosine residue in the oxidases from *R. sphaeroides* and *E. coli* result in disruption of the heme *a*<sub>3</sub>-Cu<sub>B</sub> center, suggesting its importance in stabilizing this copper site (Hosler et al., 1993; Thomas et al., 1994). The function of this linkage is still

A



B

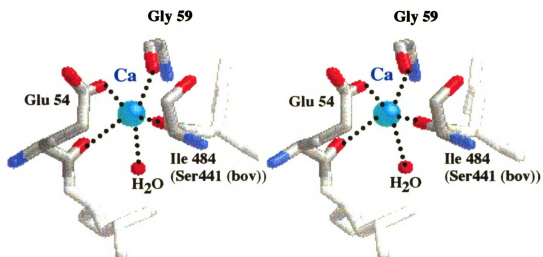


**Figure 1.4 Stereoview of the calcium site in cytochrome *c* oxidase.**

All the numbers are from *R. sphaeroides* oxidase numbering, unless otherwise specified. Panel A and B are the Ca structures from *P. denitrificans* and bovine oxidases, respectively. In *R. sphaeroides* the equivalent residues to His-59 in *P. denitrificans* and Ser-441 in bovine are Ala-57 and Ile-484, respectively.

elusive, but clearly, it will change the charge distribution around the Cu<sub>B</sub> site, which will influence the oxygen reduction. It has been proposed that this Tyr-His dimer may become a tyrosine radical at the "peroxy stage" during the oxygen reaction (see below), and involved in electron transfer and protonations of the oxygen intermediates (Ostermeier et al., 1997; Yoshikawa et al., 1998). Obviously, more experimental work is needed to address this issue.

The involvement of tyrosine (or tryptophan) radicals in oxygen reactions are not without precedents. In CcP (Millett et al., 1995), prostaglandin synthase (Dietz et al., 1988), and photosystem II (Babcock et al., 1997), a tyrosine (or tryptophan) residue has been found to be essential for the oxygen reaction. The identification of the Tyr-His dimer near the binuclear center in CcO undoubtedly will provide new insights for studying the oxygen chemistry in this system (Proshlyakov et al., 1998).

### 3.1.2 Subunit II

Subunit II has only two transmembrane helices, located at the N-terminus of this subunit. The hydrophilic C-terminal part of the protein forms a globular domain, which consists of a ten-stranded  $\beta$ -barrel, similar to the blue copper protein structures. This C-terminal domain is the substrate binding site and also the place where Cu<sub>A</sub> resides. Among all the *aa*<sub>3</sub>-type CcO, several features are conserved in all known subunit II sequences (Figure 1.5):

- 1) **Cu<sub>A</sub>**: Cu<sub>A</sub> is a binuclear center with a mixed-valence state [Cu(1.5)-Cu(1.5)]. The ligands of the two copper atoms are two histidine residues (His-217 and -260), two cysteines (Cys-252 and -256), a methionine (Met-263) and the backbone carbonyl oxygen

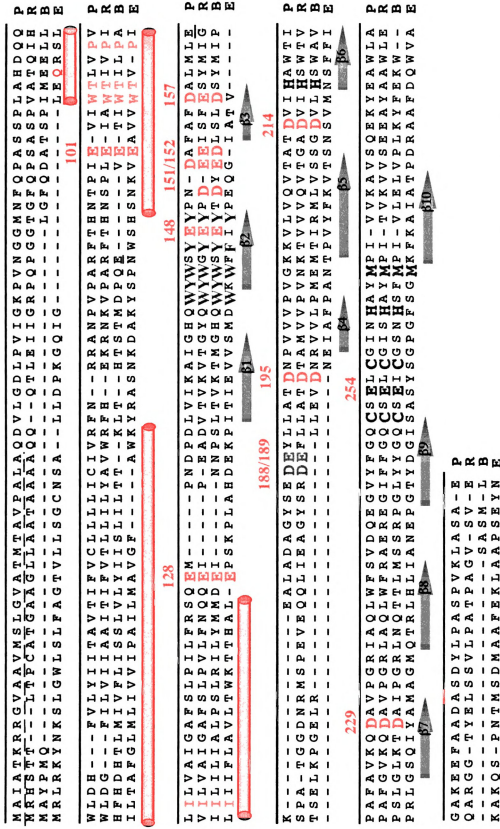


Figure 1.5 Sequence alignments of subunit II of cytochrome c oxidases and quinol oxidase. P. *P. denitrificans*, R. *R. sphaeroides*; B: Bovine heart; E. *E. coli bo3* oxidase. The cylinders and arrows indicate the locations of the transmembrane helix and the  $\beta$ -sheet structures, respectively. The numbers are from the *R. sphaeroides* sequence.

of Glu-254 (Figure 1.6), which is also ligated to the Mg atom using its carboxyl side chain. All the Cu<sub>A</sub> ligands are highly conserved in all the oxidases with a Cu<sub>A</sub> site. The two cysteines bridge the two copper atoms, while the two histidine residues provide terminal ligands. Glu-254 and Met-263 ligate one Cu ion each in a symmetric configuration. The distances between the two copper atoms are in the range of 2.5 to 2.7 Å in different species and among different crystal forms (Iwata et al., 1995; Tsukihara et al., 1995; Wilmanns et al., 1995; Ostermeier et al., 1997), consistent with strong electronic coupling.

2) **Conserved residues in the transmembrane region:** Subunit II of the *aa*<sub>3</sub>-type CcO has two transmembrane helices at the N-terminus, which anchor the C-terminal soluble domain to the membrane. In the second helix, there are several invariant residues (Glu-101, Trp-104, Thr-105, Pro-108 and Ile-121) in close contact with helix VIII in subunit I, and among them, Pro-108 is within van der Waals distance from the farnesyl group of heme *a*<sub>3</sub>. These same residues are also present in the homologous cytochrome *bo*<sub>3</sub> oxidase. In the space-filling model of the oxidases, the farnesyl tail can be seen from the cleft of the two transmembrane helices in subunit II. An oxygen channel has been proposed to reach Cu<sub>B</sub> by way of the farnesyl group (Tsukihara et al., 1996), which puts these conserved residues in subunit II in the vicinity of this proposed oxygen channel. No mutagenesis has been reported for this group of residues.

3) **Aromatic stretch:** Another striking feature in subunit II of CcO is the stretch of well-conserved aromatic residues (Trp-43, Tyr-144, Trp-145, Tyr-147, and Tyr-149) (Figure 1.5). In an early study, these residues had been suggested to be involved in electron transfer (Steffens & Buse, 1979b). The more recent crystal structure from *P. denitrificans* indicates that Trp-143 is in van der Waals contact with one of the Cu<sub>A</sub> ligands, Met-263,

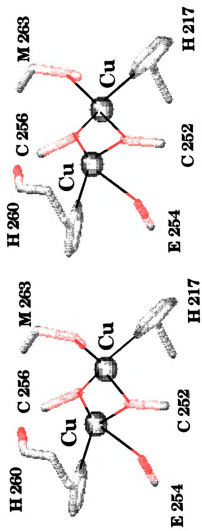


Figure 1.6 Stereoview of the  $\text{Cu}_A$  site in cytochrome *c* oxidase

113  
114  
115  
116  
117  
118  
119  
120  
121  
122  
123  
124  
125  
126  
127  
128  
129  
130  
131  
132  
133  
134  
135  
136  
137  
138  
139  
140  
141  
142  
143  
144  
145  
146  
147  
148  
149  
150  
151  
152  
153  
154  
155  
156  
157  
158  
159  
160  
161  
162  
163  
164  
165  
166  
167  
168  
169  
170  
171  
172  
173  
174  
175  
176  
177  
178  
179  
180  
181  
182  
183  
184  
185  
186  
187  
188  
189  
190  
191  
192  
193  
194  
195  
196  
197  
198  
199  
200

and is also hydrogen-bonded to His-217 (Iwata et al., 1995), which places it in a favorable position for transferring electrons from Cc to Cu<sub>A</sub>. It is interesting to notice that, although cytochrome *bo*<sub>3</sub> oxidase does not have a Cu<sub>A</sub> site and uses quinol, rather than Cc, as substrate, this stretch of aromatic residues is also present in this quinol oxidase.

4) **Carboxyl residues:** The subunit II C-terminal domain has been suggested to be the substrate binding site (Steinrucke et al., 1987). Moreover, chemical modification studies indicated that some of carboxyl residues are involved in Cc binding (Millett et al., 1983; Witt et al., 1995). As a matter of fact, in this domain, beside the Cu<sub>A</sub> ligands and the aromatic residues, several carboxyl residues (Glu-148, Glu-152, Glu-157, Asp-195, Asp-214 and Asp-229) are also highly conserved in most *aa*<sub>3</sub>-type CcO, but not in cytochrome *bo*<sub>3</sub> oxidase (Figure 1.5), implying a functional importance for them.

### 3.1.3 Subunit III

Subunit III has seven transmembrane helices, which form two bundles; one containing helix I and II, and the other one helices III to VII. These two bundles form a V-shaped structure with each bundle as an arm. The function of subunit III is still not clear, and the evidence against its involvement in proton pumping is strong (Thompson et al., 1985; Haltia et al., 1991). The gene of subunit III from *R. sphaeroides* has been deleted, which results in a two-subunit oxidase in which the binuclear center is undergoes rapid inactivation (J. Hosler, personal communication), suggesting that subunit III may be involved in protein assembly or stability. Structural analysis also suggests that subunit III may provide a reservoir for efficient oxygen diffusion from the membrane to the binuclear center in subunit I (Tsukihara et al., 1996). In the space-filling model of the oxidases, Glu-286, a conserved residue close to Cu<sub>B</sub>, can be seen from the cleft in subunit

1  
2  
3  
4  
5  
6  
7  
8  
9  
10  
11  
12  
13  
14  
15  
16  
17  
18  
19  
20  
21  
22  
23  
24  
25  
26  
27  
28  
29  
30  
31  
32  
33  
34  
35  
36  
37  
38  
39  
40  
41  
42  
43  
44  
45  
46  
47  
48  
49  
50  
51  
52  
53  
54  
55  
56  
57  
58  
59  
60  
61  
62  
63  
64  
65  
66  
67  
68  
69  
70  
71  
72  
73  
74  
75  
76  
77  
78  
79  
80  
81  
82  
83  
84  
85  
86  
87  
88  
89  
90  
91  
92  
93  
94  
95  
96  
97  
98  
99  
100

III. The blockage of this channel by introducing a bulky side chain has been found to sterically hinder the oxygen diffusion (Riistama et al., 1996).

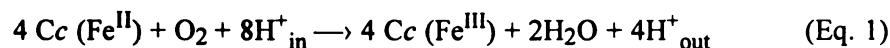
### 3.1.4 Other subunits

A fourth subunit, has been resolved in the crystal structure of *P. Denitrificans* oxidase, with one transmembrane helix and in contact with all the other three subunits (Iwata et al., 1995). This subunit shows no homology to the ten small subunits in the bovine oxidase. The function of this small subunit is unknown, and the deletion of this subunit from *P. denitrificans* has no obvious effect on the catalytic functions of the enzyme (Witt & Ludwig, 1997).

CcO in bovine heart has been crystallized as a dimer, with the ten nuclear-encoded subunits surrounding the three core subunits. Seven of the ten nuclear subunits have transmembrane regions which vary in length. Subunit VI<sub>a</sub> is found to be involved in stabilizing the dimer structure. A zinc site, with four cysteine ligands, is located at the matrix side of subunit V<sub>b</sub>, forming a tetrahedral structure. Subunits VI<sub>a</sub> and VI<sub>b</sub>, together with subunit II and the top of subunit I, form a concave surface, which has been suggested to be the Cc binding site in the bovine oxidase (Tsukihara et al., 1996). ADP and ATP have been shown to regulate allosterically the oxidase activity (Anthony et al., 1993; Frank & Kadenbach, 1996), and two possible ADP binding sites have been located by their resemblance to cholate binding sites in the bovine oxidase structure, with one of them interacting with subunits I and III at the cytosolic side, while the other interacts with subunit VI<sub>a</sub> toward the matrix (Tsukihara et al., 1996).

### 3.2 The oxygen reactions

The overall reaction catalyzed by CcO involves transferring electrons from Cc to oxygen, according the following scheme:



The evolutionary choice of using oxygen as the electron acceptor is due to its high redox potential, which will maximize the free energy production. The energy produced from this reaction is not solely dispersed as heat, but is efficiently stored as the transmembrane electrochemical proton gradient. For the reduction of one oxygen molecule, four electrons are required, which results in four protons being consumed from the matrix to form water; concomitantly, four ( $\text{H}^+_{\text{out}}$ ) are pumped across the membrane.

In the process of reduction of oxygen, several events occur: electron transfer, protonation, and oxygen bond cleavage. Any of these events can be the overall rate-limiting step, which will result in different reaction kinetics. Unlike cytochrome P450 enzymes, in which electron transfer is the rate-limiting step and the oxygen intermediates are transient, CcO shifts the rate-limiting step to proton transfer (Ferguson-Miller & Babcock, 1996). This proton-transfer control ensures that the protons are loaded at the proton-pumping site before the electron transfer event takes place, enabling the proton pumping to be tightly coupled with electron transfer. Moreover, this proton control feature allows the oxygen intermediates to build up to substantial levels to be characterized spectroscopically.

The reaction of CcO with oxygen is so fast that conventional stopped-flow techniques are impractical; To overcome this problem, Gibson & Greenwood, (1963) invented the flow-flash technique by using CO-bound oxidase. After mixing CO-inhibited

oxidase with oxygen, the reaction can be initiated using a laser to photodissociate CO from the reduced oxidase. This technique can essentially completely convert the CO complex to the oxygen complex, and it has been used widely in combination with other spectroscopic techniques to detect the oxygen reaction intermediates. These techniques include the low temperature optical and EPR trapping measurement (Chance et al., 1975(a);1975(b); Hansson et al., 1982), time resolved resonance Raman (Han et al., 1990; Varotsis & Babcock, 1990; Ogura et al., 1991; Varotsis et al., 1993; Proshlyakov et al., 1994; 1996), and time-resolved optical absorption techniques (Georgiadis et al., 1994; Bose et al., 1997). By slowing down the reaction progress at low temperatures, Chance *et al.* (1975) first identified several reaction intermediates. On the other hand, Georgiadis et al. (1994) used time-resolved optical absorption techniques combined with singular value decomposition and global exponential fitting analysis to pull out the spectra of several oxygen species in the overall reaction. Optical spectroscopy provides information about the kinetics of the internal electron transfer processes, but the uncertainty of the theoretical spectra of some of the oxygen intermediates that are used in the analyses may undermine their assignments. Time-resolved resonance Raman, coupled with isotope and model compound studies, provides more definitive information, and a number of oxygen-isotope sensitive Raman bands have been observed in the reaction. But the shortcomings of this technique are that it is less quantitative and the assignments of the isotope-sensitive bands sometimes are not straightforward.

Besides the technical aspects, there is also a variety of ways to study the oxygen reaction using enzymes in different redox states. The fully reduced and mixed-valence oxidases can react with oxygen directly, while the fully oxidized enzyme can react with

11  
12  
13  
14  
15  
16  
17  
18  
19  
20  
21  
22  
23  
24  
25  
26  
27  
28  
29  
30  
31  
32  
33  
34  
35  
36  
37  
38  
39  
40  
41  
42  
43  
44  
45  
46  
47  
48  
49  
50  
51  
52  
53  
54  
55  
56  
57  
58  
59  
60  
61  
62  
63  
64  
65  
66  
67  
68  
69  
70  
71  
72  
73  
74  
75  
76  
77  
78  
79  
80  
81  
82  
83  
84  
85  
86  
87  
88  
89  
90  
91  
92  
93  
94  
95  
96  
97  
98  
99  
100

hydrogen peroxide to produce some compounds with similar spectroscopic properties to the intermediates formed in the oxygen reaction with the fully reduced oxidase. Wikström (Wikström, 1989; Wikström & Morgan, 1992) has studied the same reaction in “reverse” in the whole mitochondria. He noticed that under highly oxidizing conditions with a high electrochemical proton gradient created by hydrolysis of ATP, one or two electrons can flow back from water through enzyme to form the “peroxy” intermediate, similar to the oxygen intermediate observed in the forward reaction.

By using the different biochemical and spectroscopic methods listed above in different laboratories, the oxygen reaction with CcO has been studied thoroughly, and a consensus of the reaction scheme has begun to emerge, although there is still controversy (Babcock & Wikström, 1992; Ferguson-Miller & Babcock, 1996). A simplified reaction scheme for the oxygen reaction with CcO is shown in Figure 1.7. In the fully reduced state, oxygen was found to bind to Cu<sub>B</sub> first, before forming the oxy form in which oxygen binds to heme a<sub>3</sub> in an end-on configuration. The initial oxy form and the last hydroxyl form are the best resolved intermediates in the whole reaction cycle. In the subsequent steps following oxygen binding, the oxy form is reduced to the peroxy (“P”) form first, and then to the ferryl (“F”) form, where the oxygen bond is broken, and finally to the hydroxy form after the third and the fourth electrons are transferred into the binuclear center, respectively. It is only the last two steps in the oxygen reaction that are coupled with proton pumping activity with a stoichiometry of 2H<sup>+</sup>/e<sup>-</sup> for each electron (Wikström, 1989). Peroxy and ferryl forms have been identified using different techniques and different redox stages of the oxidases; the controversies associated with

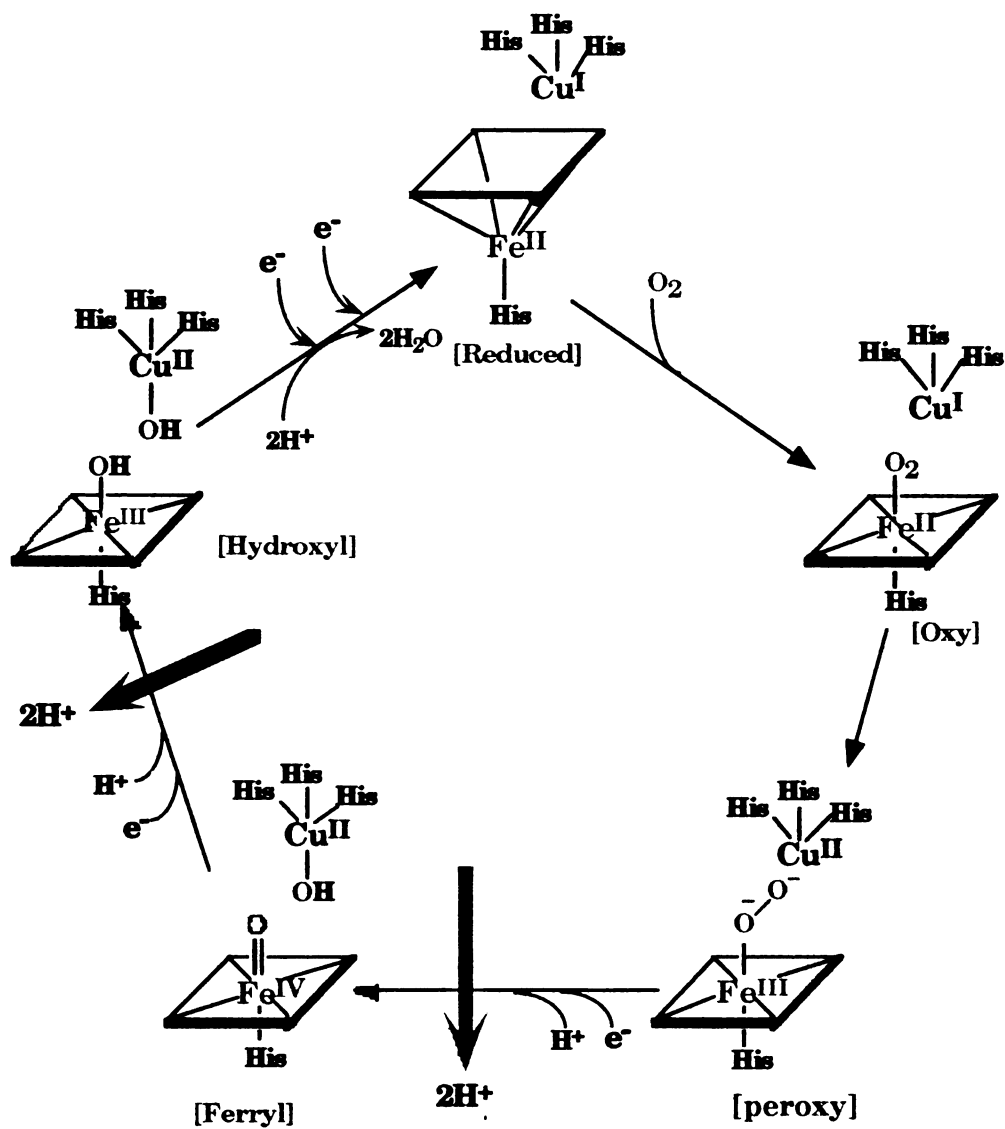


**Figure 1.7** Mechanism of oxygen reduction by cytochrome c oxidase. The simplified mechanism is adopted from (Ferguson-Miller and Babcock, 1996), and only the changes occurring at the heme  $a_3$ -Cu $_B$  are shown.

these two forms are the detailed structure and the time-sequence of the intermediates that occur.

### **3.3 Proton pumping**

#### **3.3.1 Characteristics of proton pumping**

One intrinsic property of CcO is its proton-pumping function. When one molecule of oxygen is reduced, besides four protons consumed for water formation, four more protons are pumped across the membrane. The proton pumping activity of the oxidase is tightly coupled with the electron transfer activity, with the proton pumping controlling the overall activity under most conditions. The principle underlying this tight coupling is electroneutrality, as advanced by Rich (1995). The essence of the principle is that the movement of negative electrons into a region of low dielectric is always compensated by protonation, which will decrease the electrostatic energy created by electron movement. To keep the overall charge balance, the theory suggests that protonation of the oxygen intermediates to form water will repulse an equal number of the protons (brought in to neutralize the electron events) from the binuclear center areas to the outside of the membrane, and result in proton pumping. This electroneutrality theory is supported by the experimental facts that many of the electron transfer steps are pH dependent and show a D/H isotope effect (Oliveberg et al., 1991; Hällén & Nilsson, 1992). The pumping of four protons is not coupled uniformly with the input of four electrons; only the last two electron transfer events that convert the peroxy to the ferryl and the ferryl to the hydroxy forms are coupled to the translocation of two protons at each step (Wikström, 1989). This result was further confirmed from the study of oxidase

with hydrogen peroxide, which, bypassing the first two electron transfer steps, and shows that a total of four protons are pumped in the last two electron transfer steps (Konstantinov et al., 1997). A successful model about CcO proton pumping mechanism has to implement all these requirements.

### 3.3.2 Proton pumping models

Since the discovery of the proton pumping activity associated with the oxidase, several models have been proposed to explain the pumping mechanism. They generally can be categorized into two kinds, direct and indirect coupling mechanisms.

The indirect coupling mechanisms propose that electron transfer causes an overall conformational change, causing protons to be pumped at some sites at a distance from the site where the oxygen chemistry occurs. A representative of these models is the two-conformation model proposed by Brzezinski & Malmström (1986), based on the biphasic steady-state kinetics of CcO. This model suggested that CcO has two conformations, the non-proton-pumping and the proton-pumping conformations. With the electron transfer, one conformation switches to the other. From analyzing the bovine oxidase structure, Yoshikawa *et al.* also observed a hydrogen-bonded network involving some residues from helices III and V in subunit I, remote from the binuclear heme  $a_3$ -Cu<sub>B</sub> centers (Tsukihara et al., 1996; Yoshikawa et al., 1998). They suggested that conformational change will induce a unidirectional proton transfer along this hydrogen bond network.

In the latest 2.3 Å resolution structures of the bovine oxidase (Yoshikawa et al., 1998), an aspartate residue (Asp-51 in bovine) located at the periplasmic side of subunit I is found to change conformations associated with the changes of the redox states of the oxidase, and a hydrogen-bond network has been identified, which connects this residue,

through hydrogen-bonds to heme *a* and eventually to the bulk solution at the matrix side. An indirect proton-pumping mechanism associated with this residue has been proposed, but inconsistent with such a model, this residue and some other residues involved in the proposed proton-pumping model are not conserved in a number of oxidases.

Most of the models proposed are based on a direct coupling mechanism, using one or more of the redox active metal centers as the coupling site. The first well developed model was proposed by Chan *et al.* (Chan & Li, 1990), who based it on the unusual spectral characteristics of the Cu<sub>A</sub> (At that time, the binuclear nature of the Cu<sub>A</sub> was not known). In this “ligand-exchange” model, the reduction of Cu<sub>A</sub> causes a structural conformational change in the Cu<sub>A</sub> site from planar to tetrahedral, and drawing in a nearby tyrosine residue to ligate Cu<sub>A</sub>, replacing one of its cysteine ligands. This ligand exchange enables the tyrosine proton, which is from the inside of the membrane, to be transferred to the displaced cysteine residue. In turn, when the cysteine ligates back to the Cu<sub>A</sub> site, it releases the proton to the outside of the membrane. In this model, each electron transfer step is coupled with one pumped proton. Babcock & Callahan (1983) also proposed that a change in the hydrogen binding of the formyl group of heme *a*, in response to its redox state, controls the proton pumping. Arguments against these models are based on the facts that quinol oxidases, which are homologous to CcOs but do not have the Cu<sub>A</sub> site or the formyl substituent of heme *a*, can pump protons.

The latest direct coupling models are focused on the binuclear site, where the oxygen reaction takes place, and a ligand-shuttling mechanism resembling the model of Chan *et al.* was adopted to Cu<sub>B</sub>. Woodruff (1993) proposed that when oxygen binds to Cu<sub>B</sub>, one of its ligands with a labile proton can dissociate and bind to the distal position

12  
13  
14  
15  
16  
17  
18  
19  
20  
21  
22  
23  
24  
25  
26  
27  
28  
29  
30  
31  
32  
33  
34  
35  
36  
37  
38  
39  
40  
41  
42  
43  
44  
45  
46  
47  
48  
49  
50  
51  
52  
53  
54  
55  
56  
57  
58  
59  
60  
61  
62  
63  
64  
65  
66  
67  
68  
69  
70  
71  
72  
73  
74  
75  
76  
77  
78  
79  
80  
81  
82  
83  
84  
85  
86  
87  
88  
89  
90  
91  
92  
93  
94  
95  
96  
97  
98  
99  
100

of heme  $a_3$ , replacing the proximal histidine; and in the meantime, the labile proton is released. Subsequent protein conformational change enables the proximal histidine, now with a proton from the inside of the membrane, to reprotonate the shuttling  $\text{Cu}_B$  ligand and dissociate it from heme  $a_3$ . In this model, the proton pumping does not couple with the electron transfer reaction, but rather with the initial oxygen binding. A similar model was proposed by Rousseau *et al.* (1993); rather than using the  $\text{Cu}_B$  ligand, they proposed that the conserved Tyr-422 was involved in ligand exchange with the proximal ligand of heme  $a_3$ . Mutagenesis study of this tyrosine residue in *R. sphaeroides* has ruled out this possibility (Mitchell *et al.*, 1996).

A current working model is the “Histidine-cycle” model, involving  $\text{Cu}_B$  ligands, first proposed by Wikström (Morgan *et al.*, 1994; Wikström *et al.*, 1994), and further modified by Iwata *et al.* (1995), based on the crystal structure of the *P. denitrificans* oxidase. This model fits with the electroneutrality principle, the  $2\text{H}^+/\text{e}^-$  stoichiometry for the third and fourth electrons, and the known oxygen reaction scheme. The essence of the model is that histidine, functioning as a  $2\text{H}^+$  carrier, can cycle between imidazolate ( $\text{Im}^-$ ), imidazole ( $\text{ImH}$ ) and imidazolium ( $\text{ImH}_2^+$ ) states. At the  $\text{ImH}_2^+$  state, the histidine ligand dissociates from  $\text{Cu}_B$  and assumes another configuration. The protonation of the peroxy and ferryl intermediates will repulse the two protons from the  $\text{ImH}_2^+$  to the proton exit channel. From the peroxy form to the ferryl and from ferryl to the hydroxyl states (Figure 1.7), the  $\text{Cu}_B$  will be reduced twice; as a result, two water molecules are formed, and four protons are translocated. In this model, the proton translocation is directly associated with the oxygen reaction. In the original crystal structure of the oxidized form

of *P. denitrificans* oxidase, the electron density of His-333 was not resolved, suggesting the presence of multiple conformations for this residue. Thus, Iwata et al. (1995) used this residue, rather than His-284, the one Wikström originally proposed in his early model (Wikström et al., 1994), as the shuttling ligand in their modified version. Recently, this “Histidine-cycle” proton-pumping models has lost some attraction due to the fact that in all the latest structures, whether reduced or oxidized, the electron densities for the Cu<sub>B</sub> ligands are all clearly resolved.

### 3.3.3 Proton channels

In the oxygen reaction, two kinds of protons are required: substrate protons for water formation and pumped protons. To make sure no proton short-circuiting takes place at the binuclear center, protonic insulation is required; otherwise, the pumped protons may be used for water formation. As a result, the presence of two proton channels have been suggested, one for the pumped protons and one for the substrate protons. In order to acquire protons from the cytoplasmic side, the two channels have to originate from the cytoplasmic side and lead the substrate protons to the binuclear center, and the pumped proton eventually to the proton exit channel. Studies on bacteriorhodopsin suggest that a hydrogen-bond network involving water molecules and protonable residues is a good relay system for proton movement (Krebs & Khorana, 1993). Much effort has been spent on trying to identify polar residues important for proton pumping (Fetter et al., 1995).

Mutation of Asp-132 in *R. sphaeroides*, or the equivalent residue in cytochrome *bo<sub>3</sub>* oxidase in *E. coli*, completely abolishes the proton pumping activities, but the

enzyme can still turn over, albeit at a slower rate (Thomas et al., 1993; Fetter et al., 1995; García-Horsman et al., 1995). The proton pumping activity of this mutant can be restored by placing a carboxyl group near Asp-132 (García-Horsman et al., 1995). The straightforward explanation for these results is that Asp-132 is involved in proton pumping. A hydrogen-bonded network for pumped protons has been identified in the bacterial oxidase structure, which starts from Asp-132, involving several water molecules, and leads to Glu-286 in the interior of the protein on helix VI (Iwata et al., 1995). A similar pathway for the substrate protons in the structure was also suggested, beginning at Lys-362 and leading to the hydroxyl group of heme  $a_3$ . This identification of a substrate proton pathway was also originally suggested by mutagenesis results, which showed that the mutation of Lys-362 caused complete inactivation of the oxidase (Hosler et al., 1993; Junemann et al., 1997).

Glu-286 is one of the highly conserved residues in heme-copper oxidases; replacement of this residue in CcO from *R. sphaeroides* and cytochrome  $bo_3$  oxidase from *E. coli* almost completely inactivates the enzymes (Puustinen et al., 1992; Hosler et al., 1993; Puustinen et al., 1997). Modeling of the position of water in the structure indicates that Glu-286 could be hydrogen bonded to a water molecule, and further connect to His-334, the  $Cu_B$  ligand (Puustinen et al., 1997). The movement of the side chain of Glu-286 during proton transfer, coupled with the switching of one of the histidine ligands, has been suggested to be the proton translocation mechanism. In Wikström's latest model, the ligand involved in the histidine shuttle is proposed to be residue His-334, due to its closeness to Glu-286 (Puustinen et al., 1997).

Based on computational simulation analysis of the bacterial oxidase structure with the placement of water molecules, Schulten and co-workers (Hofacker & Schulten, 1997) suggest a pumping-proton channel which also involves the movement of the side chain of Glu-286. In this model, the protonated glutamic acid side chain can flip upwards and deliver the pumped protons to the propionate group of heme  $a_3$ , which is located at the bottom of the suggested proton exit channel. A change in the environment of the Glu-286 carboxyl, consistent with both these models, is supported by FTIR analysis (Puustinen et al., 1997; Behr et al., 1998; Hellwig et al., 1998)

The proton exit channel has been suggested to be located at the interface of subunits I and II, where the Mg is located (Iwata et al., 1995). A negative charge cluster has been found in this area, which consists of some carboxyl residues from subunits I and II. The recent high resolution structures from both *P. denitrificans* and bovine identify several water molecules in this area, which, together with the carboxyl residues, the propionate groups of heme  $a_3$  and His-334 ( $\text{Cu}_B$  ligand), form an extended hydrogen bonded network, making it a likely candidate for the proton exit pathway.

## **4 $\text{Cu}_A$ center**

### **4.1 General characteristics of copper proteins**

Copper is one of the essential trace elements for living organisms. As a cofactor, it is present in many enzymes that carry out biological oxidation-reduction reactions, either simple electron transfer, as in blue copper proteins, or oxygen binding and activation, as in hemocyanin and Cu/Zn superoxide dismutase which binds superoxide

(Adman, 1991). The  $aa_3$ -type CcOs have two copper sites, with  $Cu_A$  involved in electron transfer, and  $Cu_B$  in oxygen reduction. Historically, the copper proteins have been categorized into three kinds based on their spectroscopic properties and structures: the type I (*or* blue) copper proteins, type II (*or* normal) copper proteins and the type III coupled binuclear copper proteins. With the discoveries of new kinds of copper centers, including the  $Cu_A$  sites in CcO and nitrous-oxide reductase ( $N_2OR$ ) (Kroneck et al., 1989), and the multicopper sites in ascorbate oxidases (Avigliano et al., 1983), this list was further expanded.

The type I copper proteins, including plastocyanins and azurins, exhibit strong absorption in the 600 nm region, giving these proteins an intense blue color (Solomon & Lowery, 1993). The electron paramagnetic resonance (EPR) spectra of the blue copper proteins have smaller parallel hyperfine splitting ( $A_{II} < 70$  G) compared to the type II copper proteins. The typical structure of the blue copper site has two histidine ligands and one cysteine ligand coplanar with the copper atom and a methionine as a weak axial ligand. The strong absorption at 600 nm is due to the metal to ligand charge transfer between the copper atom and the cysteine ligand. In the blue copper proteins, the copper atoms are in a distorted tetrahedral geometry, which is intermediate between that preferred by  $Cu^{II}$  (square planar) and  $Cu^I$  (tetrahedral). As a result, the structure of blue copper sites show little change on reduction, which lowers the reorganization energy and favors rapid electron transfer.

The type II copper proteins, such as Cu/Zn superoxide dismutase, exhibit distinct EPR spectra with larger parallel hyperfine splitting ( $A_{II} > 120$  G). The absorption spectra in the visible region is much weaker than that of blue copper proteins due to the

weak ligand field transition. In Cu/Zn superoxide dismutase, the copper atom is ligated with four histidines and one water molecule.

The type III coupled binuclear copper proteins, including hemocyanin, can bind oxygen reversibly, as reviewed by Solomon et al. (1996). In the oxygenated form of hemocyanin, where the two Cu atoms are 3.6 Å apart from each other and each Cu atom is ligated with three histidine residues, the oxygen binds to the two Cu<sup>II</sup> in the peroxide form in a side-on geometry (Magnus et al., 1994). Because of the strong antiferromagnetic coupling between the electrons on each copper atom, the oxygenated form, with a weak absorption band at 600 nm and an intense band at 350 nm, does not have an EPR signal. In the deoxygenated form, the two copper atoms are in the reduced form, which is also EPR silent.

Multicopper proteins, like ascorbate oxidase (Avigliano et al., 1983), have more than two copper atoms. These copper atoms usually are a combination of the three types of copper centers discussed above. In the case of ascorbate oxidase, the four copper atoms in each monomer of the enzyme form a mononuclear and a trinuclear species. The mononuclear copper, which is involved in transferring electrons from the substrate to the trinuclear center, has two histidines, one cysteine, and one methionine as ligands, as a typical type I copper. The trinuclear site, with 8 histidines as ligands, is the oxygen binding site.

#### 4.2 Cu<sub>A</sub> site in CcO

Now it is general understood that there are two copper centers, Cu<sub>A</sub> and Cu<sub>B</sub>, in the *aa*<sub>3</sub>-type CcOs, with Cu<sub>A</sub> being a dinuclear copper site with each metal in a mixed-valence state. In the past half century, since Keilin and Hartree first discovered copper in

CcO in the 1930s (Keilin & Hartree, 1939), until the emergence of the crystal structures several years ago (Iwata et al., 1995; Tsukihara et al., 1995), the studies of Cu<sub>A</sub> have always been associated with controversies. Is copper a functional part of the oxidase and how many are there? Is there one or two copper atoms in the Cu<sub>A</sub> site? What is the structure of the Cu<sub>A</sub> site? All these questions have puzzled people through these years. The study of Cu<sub>A</sub> has also demonstrated the importance of developing new methodologies for solving problems. The unfolding of the Cu<sub>A</sub> history has been recently related by H. Beinert, a pioneer in this field (Beinert, 1997).

#### 4.2.1 Spectroscopic studies and chemical analyses

When copper atoms were first found to be present in CcO samples, their true identities were not clear. Are they an intrinsic and functional part of the oxidase or just fortuitously bound? Early studies showed that the Cu to Fe ratio in CcO was approximately 1:1, with two Cu and two Fe ions per monomer (Griffiths & Wharton, 1961; Li et al., 1987b; Naqui et al., 1988). Although most of these studies observed slightly higher Cu/Fe ratios than 1:1, it was generally attributed to contaminating copper atoms in the samples. Several groups later also observed slightly higher Cu/Fe ratios with 5 Cu/4 Fe per dimer of bovine oxidase (Einarsdottir & Caughey, 1984; 1985; Moubarak et al., 1987; Yoshikawa et al., 1988; Pan et al., 1991b), and suggested that the “extra” copper was important for the dimerization of the enzyme. A few groups using different techniques, including inductively coupled plasma atomic emission spectroscopy (ICP-AES) (Steffens et al., 1987), proton induced X-ray emission (PIXE) spectroscopy (Bombelka et al., 1986), and energy dispersive X-ray fluorescence (EDXRF)

spectrometry (Oblad et al., 1989), found a 3:2 ratio for the Cu and Fe. The inconsistency of metal analysis results laid the ground for the controversies about the structure of Cu<sub>A</sub>.

The copper atoms in CcO were found early not to be removed during the enzyme purification and by EDTA dialysis (Griffiths & Wharton, 1961). The final proof that copper atoms are a functional part of the oxidase came from EPR studies, which showed that the copper signals disappeared upon substrate addition, and this disappearance was reversible. Moreover, the oxidation states of the copper paralleled that of the EPR-visible heme, suggesting that EPR-visible copper is involved in electron transfer (Beinert et al., 1962).

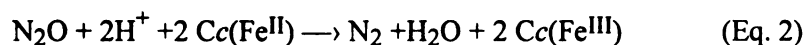
EPR spectroscopy was used intensively in early CcO studies (Malmstrom & Vangard, 1960; Beinert et al., 1962; Aasa et al., 1976; Froncisz et al., 1979), but the Cu<sub>A</sub> EPR spectra showed no similarity with those of known copper proteins. At X-band frequency, unlike other copper proteins which showed hyperfine splitting in the  $g_{II}$  region, the hyperfine splitting in CcO is not resolved due to the overlap with low spin heme signal; furthermore, it has an unusually low  $g$  value ( $g = 1.99$ ) at the  $g_I$  region. EPR analysis also revealed that the low spin heme represents only about 50% of the total heme content (Beinert et al., 1962). The quenching of one of the two hemes was suggested to be the result of the antiferromagnetic coupling between this heme and a copper ion (Cu<sub>B</sub>). Indeed, the  $g = 2$  signal of CcO accounts for only about 40% of the intrinsic copper (Beinert et al., 1962). This antiferromagnetic coupling idea was subsequently confirmed by magnetic circular dichroism (MCD) studies (Babcock et al., 1976). MCD studies also revealed that the absorption at around 830 nm is an attribute of

the Cu<sub>A</sub> site (Greenwood et al., 1983; 1988) and thereby provided a Cu<sub>A</sub> optical marker for further kinetics studies.

Redox titration of CcO suggests that Cu<sub>A</sub> functions as a one electron carrier (Blair et al., 1986). This result, together with the early metal analyses which indicated the presence of a 1:1 ratio of Cu/Fe, led to general acceptance that there were two copper atoms in CcO, one at Cu<sub>A</sub> and one at Cu<sub>B</sub> (Wikström et al., 1981).

To identify the ligands of Cu<sub>A</sub>, yeast CcO was labeled with [1,3-<sup>15</sup>N<sub>2</sub>]histidine or [β,β-<sup>2</sup>H<sub>2</sub>]cysteine, and was studied using EPR and electron nuclear double resonance spectra (ENDOR) techniques (Stevens et al., 1982). It was concluded that there are at least one cysteine and one histidine as Cu<sub>A</sub> ligands. This result was further supported by copper extended X-ray absorption fine structure (EXAFS) study (Li et al., 1987a), which, by using Cu<sub>A</sub>-depleted, Cu<sub>A</sub> modified, and intact oxidase, showed that there are two histidine and two cysteine ligands. Based on these studies, a model of Cu<sub>A</sub> was proposed with two histidines and two cysteines as the ligands, with delocalization of the unpaired electron in the Cu ion to the two cysteine ligands, to account for the unusual EPR signal (Stevens et al., 1982; Martin et al., 1988). With the availability of more protein sequences for CcO from different species, two cysteine residues in the C-terminus of subunit II were found to be highly conserved (Saraste, 1990). The similarity of the Cu<sub>A</sub> binding and the blue copper sequences gave further support to the idea that Cu<sub>A</sub> was a mononuclear center with two cysteine ligands, and together with the protein sequence information, the Cu<sub>A</sub> site was assigned to be located at the C-terminus of subunit II (Holm et al., 1987).

An unexpected breakthrough in the Cu<sub>A</sub> study came from unrelated studies of N<sub>2</sub>OR. N<sub>2</sub>OR is a terminal enzyme in the energy-conserving denitrification process of many denitrifying bacteria; it converts N<sub>2</sub>O to N<sub>2</sub> in the last denitrification step by accepting electrons from Cc (reviewed by Zumft (1997)):



N<sub>2</sub>OR from most species is a homodimer with 4 Cu ions per monomer. The Cu<sub>A</sub> center in N<sub>2</sub>OR is found to be the electron transfer site, while another copper center, Cu<sub>Z</sub>, is the substrate binding site. In the resting state of the reductase, Cu<sub>Z</sub> is EPR silent due to the presence of two antiferromagnetically coupled copper ions at this site. Because of the lack of interference from other metal centers, a seven line hyperfine pattern was observed for N<sub>2</sub>OR at X-band frequency, which was interpreted as arising from a mixed-valence [Cu(1.5)-Cu(1.5)] binuclear center.

N<sub>2</sub>OR, like CcO, has a broad absorption band around 830 nm, that is distinct from other type I and type II copper proteins (Malmstrom & Aasa, 1993). Based on the similarity of X-, S- and C-band EPR spectra between N<sub>2</sub>OR and beef CcO (Antholine et al., 1992), Kroneck et al. (1988; 1989) proposed that the Cu<sub>A</sub> site in CcO was also a binuclear center with mixed-valence states. Although this suggestion was immediately received with skepticism (Li et al., 1989), the relationship between N<sub>2</sub>OR and CcO was cemented by the availability of the amino acid sequences of N<sub>2</sub>OR (Scott et al., 1989; Zumft et al., 1992; Hoeren et al., 1993). These sequences clearly showed that the Cu<sub>A</sub> binding domain in the C-terminus of N<sub>2</sub>OR is highly similar to that in CcO, with all the potential ligands, two histidines, two cysteines and one methionine, present in both

enzymes (The peptide carboxyl of glutamate as a ligand in CcO was replaced by a tryptophan carboxyl group in N<sub>2</sub>OR in most species).

It is noteworthy that, early on, the small hyperfine splitting of CcO had been resolved at 2 to 4 GHz in EPR spectra (Froncisz et al., 1979), but unfortunately it was interpreted as arising from the interaction of Cu<sub>A</sub> and heme *a*. Beinert et al. (1962) in their early paper suggested that the unusual EPR copper spectrum of CcO could be interpreted as arising from two copper ions in close proximity, but this idea was largely ignored because of inadequate support from early metal analyses.

#### 4.2.2 Molecular biology studies

With the advances in molecular biology techniques, substantial progress was made on the Cu<sub>A</sub> studies. To eliminate the interference of the low spin heme on the Cu<sub>A</sub> optical and EPR spectra, the soluble Cu<sub>A</sub> domains from *P. denitrificans* (Lappalainen et al., 1993), *Bacillus subtilis* (von Wachenfeldt et al., 1994) and *Thermus thermophilus* (Slutter et al., 1996) were engineered to be overexpressed in bacteria. The Cu<sub>A</sub> sites were reconstituted by incubating these protein domains in the presence of Cu<sup>I</sup> and Cu<sup>II</sup>. Metal analyses and EPR studies on these proteins have unambiguously shown that the Cu<sub>A</sub> site consists of two copper ions. The optical spectrum of Cu<sub>A</sub> has also been resolved with absorption at 530 and 480 nm, in addition to the weak one at around 830 nm, as suggested from MCD studies (Greenwood et al., 1983), which is very similar to the absorption reported for N<sub>2</sub>OR (Zumft, 1997). Without the interference of heme *a*, the hyperfine splitting at the g<sub>II</sub> region has also been partially resolved. An EXAFS study of the recombinant Cu<sub>A</sub>-domain from *B. subtilis*, in comparison with a directly-bonded Cu(1.5)-

Cu(1.5) inorganic model complex, revealed a Cu-Cu distance of 2.5 Å, suggesting a direct metal-metal bond (Blackburn et al., 1994).

Another important development in Cu<sub>A</sub> study has been the restoration of the Cu<sub>A</sub> site in the CyoA subunit of *E. coli* cytochrome *bo*<sub>3</sub> quinol oxidase (van der Oost et al., 1992). Quinol oxidases do not have the Cu<sub>A</sub> site in subunit II, nor its ligands. However, circular dichroism (CD) study has indicated that the cupredoxin fold, a Greek key β-barrel, is present in both the soluble Cu<sub>A</sub> domain of CcO and the CyoA domain of quinol oxidase (Wittung et al., 1994). By introducing back these ligands at the corresponding positions in the CyoA sequence, van der Oost *et al.* (1992) have successfully restored the Cu<sub>A</sub> site, with an EPR spectrum similar to the native Cu<sub>A</sub> site in CcO. This study also further confirmed the binuclear characteristic of the Cu<sub>A</sub> site. Mutagenesis studies using this system identified two cysteines, two histidines, and one methionine as the ligands for this engineered Cu<sub>A</sub> center (Kelly et al., 1993). Meanwhile, this work has provided the source for a high-resolution Cu<sub>A</sub> crystal structure (Wilmanns et al., 1995). The ability to reintroduce the Cu<sub>A</sub> center to quinol oxidase further supports the notion that CcO and quinol oxidase are evolutionarily related and the quinol oxidase resulted from the loss of the Cu<sub>A</sub> site (Saraste et al., 1989).

The type I copper proteins have only one copper atom, with one histidine ligand remote in the primary sequence from all the others, which are located in a short loop. This structure is similar to the Cu<sub>A</sub> binding domains in CcO, except that one cysteine is missing in the blue copper proteins and the loop is longer in CcO. By replacing the short loop in blue copper proteins with a corresponding longer one from CcO, the blue copper sites in amicyanin (Dennison et al., 1995) and azurin (Hay et al., 1996) have been

converted to a Cu<sub>A</sub>-like centers. Spectroscopic analyses of the engineered Cu<sub>A</sub> centers in amicyanin and azurin show that they are similar to the native Cu<sub>A</sub> sites in CcO, with two copper ions at the engineered Cu<sub>A</sub> sites.

### 4.2.3 Crystallographic studies

Although the binuclear characteristics of Cu<sub>A</sub> was firmly established and the potential ligands have been identified, the actual structure of the Cu<sub>A</sub> site was still an open question before the crystal structures were obtained. Several models were proposed with no bridging ligand between the two Cu ions (Blackburn et al., 1994; Farrar et al., 1995; Larsson et al., 1995), or one cysteine (Kelly et al., 1993; Steffens et al., 1993), or two cysteines (Lappalainen & Saraste, 1994; Farrar et al., 1995) as bridging ligands. But none was correct as revealed by the crystallographic studies.

The purple CyoA domain with the engineered Cu<sub>A</sub> center was crystallized at 2.3 Å (Wilmanns et al., 1995), and CcOs from *P. denitrificans* and bovine heart at 2.8 Å (Iwata et al., 1995; Tsukihara et al., 1995). The Cu<sub>A</sub> structures revealed by the three different crystals were almost identical, with two thiolate groups from the two cysteines (Cys-252, -256) bridging the two Cu ions, and two histidines (His-217, -260) as the terminal ligands for each Cu (Figure 1.6). The sulfur group from the methionine (Met-263) and the carbonyl oxygen from glutamate-264 symmetrically bind one Cu atom each. The Cu-Cu distance and the bond lengths are slightly different in each structure.

#### 4.2.4 The advantages of being a binuclear center

As the detailed Cu<sub>A</sub> structure has emerged, new questions have arisen with it. What are the advantages of being a binuclear center for electron transfer versus the mononuclear center in blue copper proteins? What are the electronic properties of Cu<sub>A</sub>?

In small electron-transfer proteins, like Cc and azurin, electrons generally enter and leave the redox centers through the same path. The binuclear character may enable Cu<sub>A</sub> to receive and donate electrons using separate pathways, enhancing electron transfer rates, as suggested by Larsson et al. (1995). Malmström and colleagues also suggested that the delocalization of one electron over two nuclei centers will result in the reduction of the reorganization energy to 25% of that of the mononuclear copper center (Larsson et al., 1995; Ramirez et al., 1995). The decrease of the reorganization energy will enable rapid electron transfer from Cu<sub>A</sub> to heme *a*.

#### 4.2.5 Mutagenesis studies on Cu<sub>A</sub>

To study the structure and function of the Cu<sub>A</sub> site, several mutants have been made on the engineered Cu<sub>A</sub> site at CyoA domain (Kelly et al., 1993), the soluble Cu<sub>A</sub> domain (Farrar et al., 1995), and the holoenzyme from *P. denitrificans* (Zickermann et al., 1995; 1997). In CyoA domain studies, the mutation of Glu-254 to alanine does not cause a dramatic change of the copper content, consistent with the fact that the backbone carbonyl oxygen, rather than the side-chain, of the residue at this position is the ligand.

Studies in both the engineered CyoA domain from the *E. coli* quinol oxidase and the soluble Cu<sub>A</sub> domain from *P. denitrificans* have shown that mutation of the ligands in H217N and M263T completely abolish Cu binding, while mutation of the same residues

in the holoenzyme from *P. denitrificans* had no obvious effect on the copper content of the Cu<sub>A</sub> site, which may indicate stability differences between these two Cu<sub>A</sub> centers. The M263I mutation in the holoenzyme of *P. denitrificans* did not change the Cu stoichiometry, but EPR studies indicated that the two Cu ions are decoupled, with the unpaired electron localized at one of the copper ions (Zickermann et al., 1995).

Mutation of the cysteine ligand, C252, produced a mononuclear site in both soluble domains and in the holoenzyme (Zickermann et al., 1997).

## **5 Kinetics studies**

CcO catalyzes the oxidation of reduced Cc to oxidized Cc and subsequently reduces oxygen to water. This reaction has been investigated extensively using different techniques to study the rates of Cc oxidation, electron transfer (rates and pathways) in the oxidase and the oxygen reaction process as discussed above.

### **5.1 Steady-state kinetics**

The electron transfer rate from Cc to the oxidase is very fast, and traditional techniques are impractical to follow a single turnover of the reaction. At steady-state, where the Cc concentration is at least 100 times that of the oxidase, the enzyme is continuously turned over on a relatively longer time scale, and the reaction can be followed (reviewed by Cooper, (1989); Millett, (1996)).

Traditionally, two methods have been used to study the steady-state kinetics: either by following the Cc oxidation spectrophotometrically (Errede et al., 1976; Smith et al., 1981; Sinjorgo et al., 1984; 1986), or by following the oxygen consumption

polarographically (Ferguson-Miller et al., 1976; 1978; Millett, 1996). In the spectrophotometric assay, pre-reduced *Cc* is mixed with the oxidase and electrons subsequently are transferred from *Cc* to the oxidase, and the ET rate was measured by following *Cc* oxidation; while in the polarographic assay *Cc* is kept reduced in the presence of ascorbate and N,N,N',N'-tetramethylphenylenediamine dihydrochloride (TMPD) is used as an artificial donor to *Cc*, and the oxygen consumption rate was measured. Although the two systems differ in getting the ET rate, similar events take place in a turnover cycle in both systems. First, reduced *Cc* approaches the oxidase through electrostatic interactions forming a complex; then, electron transfer takes place within this complex; finally, the oxidized *Cc* dissociates from the complex before another reduced cytochrome binds to it.

Although the approaches differ in their methods to study the steady-state kinetics, both methods show saturation kinetics. At low ionic strength, the kinetics measured using both methods exhibit two phases in the Eadie-Hofstee plots: a high affinity phase with smaller  $K_M$  and  $V_{max}$  values, and a low affinity phase with larger  $K_M$  and  $V_{max}$  values. The  $K_M$  value of the high affinity phase, measured using both methods, is about  $5 \times 10^{-8}$  M. But the  $V_{max}$  value for the high affinity phase measured from the polarographic assay is much larger than the one measured from the spectrophotometric assay. This difference has been suggested to be due to the presence of a different rate-limiting step in each method. In the spectrophotometric assay, the association/dissociation of ferri-*Cc* is often rate-limiting, while in the polarographic assay these steps are bypassed because TMPD can reduce *Cc* directly while it is bound to the oxidase in the high affinity site. Thus the rate-limiting step in the high affinity phase of

polarographic assay can be the reduction of bound Cc by TMPD, as evidenced by the fact that the  $V_{\max}$  of the high affinity phase increases with the increase of TMPD concentrations, and the TMPD reduction rate has been found to be significantly faster than the dissociation rate, accounting for the larger  $V_{\max}$  observed in the polarographic assay.

In the polarographic assay, the high-affinity  $K_M$  value has been found to be similar to the  $K_D$  value for the binding of the first Cc to the high-affinity site, as measured by gel-filtration and ultracentrifugation methods (Ferguson-Miller et al., 1976; Osheroff et al., 1980). This phenomena can be explained by the fact that in the polarographic assay, the  $V_{\max}$  of the high-affinity phase is proportional to the amount of complex present, so the Eadie-Hofstee plot is analogous to the Scatchard binding plot. The direct binding assay also shows that the  $K_D$  of binding the second molecule is similar to the  $K_M$  values ( $10^{-5}$  -  $10^{-6}$  M) of the low affinity phases measured polarographically and spectrophotometrically (Brautigan et al., 1978; Ferguson-Miller et al., 1978). In a practical way, the polarographic assay becomes an easy method (though not rigorous) for measuring the binding strength of Cc to CcO.

The interaction between Cc and the oxidase has a large electrostatic component, and thus is ionic strength and pH dependent. At above 100 mM ionic strength, the reaction becomes monophasic, with a straight line in the Eadie-Hofstee plot, and this phase has been suggested to reflect the high-affinity reaction (Sinjorgo et al., 1986). Upon raising of pH, the  $V_{\max}$  for both the high- and the low-affinity phase reactions increase in both the spectrophotometric and the polarographic assays. However, the contradictory effects on the  $K_M$  values persist. Polarographic assays have shown that the  $K_M$  of the

high-affinity phase did not change in the pH range examined (Ferguson-Miller et al., 1976), while the spectrophotometric assay has shown a decrease of the high-affinity  $K_M$  in the similar pH range (Sinjorgo et al., 1986). The  $K_M$  of the low affinity phase is even more complicated; it is affected not only by the ionic strengths and pH, and also by the kinds of ions present in the solution, either cations or anions (Ferguson-Miller et al., 1976).

The steady-state reaction between *Cc* and the oxidase is easy to follow, but the interpretation of the biphasic kinetics is not so straightforward. Several models have been proposed to explain the biphasic kinetics behavior. Early models have proposed that there are two *Cc* binding sites with different binding affinities and turnover rates (Ferguson-Miller et al., 1976). This two binding site model is consistent with the direct binding assays which show that the binding stoichiometry between *Cc* and the oxidase is 2:1. This model has been further supported by the kinetic studies of cytochrome *caa*<sub>3</sub> oxidases (Nicholls & Sone, 1984). The *caa*<sub>3</sub> oxidase is homologous to the *aa*<sub>3</sub> type oxidase, except that a *c*-type cytochrome has been covalently linked to the C-terminus of subunit II. This covalently-linked *Cc*, in the absence of external *Cc*, can efficiently transfer electrons from TMPD to Cu<sub>A</sub> and heme *a*. Additional *Cc*, in the presence of TMPD, can only slightly increase the turnover rate. Furthermore, the reaction with external *Cc* displays monophasic kinetics, which suggests that the high affinity site has been occupied by the intrinsic *Cc* in the *caa*<sub>3</sub> oxidase, and the external *Cc* can only bind to the low affinity site and transfer electrons.

The second class of models proposes that there is only one electron transfer site, but two *Cc* binding sites (Garber & Margoliash, 1990). The presence of the second

molecule, although not involved in electron transfer directly, will decrease the binding affinity of the first molecule through electrostatic repulsion and increase the dissociation rate, which will result in high turnover rate. This model is supported by the fact that Cc can bind to lipids, and different lipid compositions of the oxidase will affect the low affinity phase reaction (Bisson et al., 1980).

The third class of models correlates the biphasic kinetics with the proton pumping function of the oxidase (Brzezinski & Malmström, 1986). It suggests that the oxidase has two conformations, a proton-pumping conformation and a non-pumping conformation, and that each conformation has different binding affinities for Cc, resulting in biphasic kinetic plots. So far there is no direct experimental data to support this.

## 5.2 Rapid kinetics studies

The internal electron transfer rates in CcO are very fast, and these rates cannot be measured using the conventional steady-state kinetics assay or stopped-flow methods. Understanding the internal electron transfer rates and pathways is critical for understanding the overall enzymatic function. Over the past two decades various techniques have been used to address these issues.

*Stopped-flow techniques:* Early studies on the electron transfer have been carried out using stopped-flow apparatus under anaerobic conditions (Wilson et al., 1975; Antalis & Palmer, 1982). At low ionic strength, a second-order rate constant of  $3 \times 10^7 \text{ M}^{-1}\text{s}^{-1}$  has been observed for the reaction of Cc and the oxidase. Only two electrons were found to be transferred to each oxidase molecule, distributed equally between heme *a* and Cu<sub>A</sub>. The observed similar rates for the oxidation of Cc, monitored at 550 nm, and the

reduction of heme *a*, followed at 605 nm and 443 nm, promoted the early suggestions that heme *a* was the initial electron acceptor from Cc.

*Flow flash with fully reduced oxidase:* Hill (1991; 1994) has studied the electron transfer events using fully reduced CO-bound oxidase under single turnover conditions . After mixing reduced Cc, CO bound oxidase and O<sub>2</sub>-containing buffer, and then photodissociating the CO from the binuclear center, two electrons are transferred to the binuclear center at a rate of  $6 \times 10^4 \text{ s}^{-1}$ . In addition, these investigators observed the concomitant oxidation and then re-reduction of heme *a*, which suggests that heme *a* is the electron mediator between Cu<sub>A</sub> and the binuclear center.

*Flash photolysis of the mixed-valence oxidase:* Similar to Hill's experiment, the Malmström group uses "mixed-valence" CO-bound oxidase in which Cu<sub>A</sub> and heme *a* are oxidized and heme *a*<sub>3</sub> and Cu<sub>B</sub> are reduced with CO bound to *a*<sub>3</sub> (Brzezinski & Malmstrom, 1987; Oliveberg & Malmström, 1991), rather than the fully reduced oxidase. After dissociation of the CO from heme *a*<sub>3</sub> by a short laser flash, the redox potential of heme *a*<sub>3</sub> drops, resulting in electrons at the binuclear center flowing back to heme *a* and Cu<sub>A</sub>. The rate constants for electron transfer from heme *a*<sub>3</sub> to heme *a* and from heme *a* to Cu<sub>A</sub> were found to be  $2 \times 10^5$  and  $1.3 \times 10^4 \text{ s}^{-1}$ , respectively. The slower rate from heme *a* to Cu<sub>A</sub>, compared to the reverse reaction, indicates an equilibrium in favor of heme *a* and suggest that Cu<sub>A</sub> is the initial electron acceptor in the normal electron transfer sequence.

*Carboxymethylated cytochrome c (CmCyt. c) and Zn-cytochrome c:* Brzezinski *et al.* (1995; 1997) use both CmCyt. *c* and Zn-Cc to inject electrons into the oxidase . In the CmCyt. *c* system, the methionine-80 ligand of the heme is carboxymethylated, so it can not bind to the heme iron anymore, which allows CO to bind to this five-coordinated

heme. The reduced CO-bound form of CmCyt. *c* has a higher redox potential, and upon rapid photodissociation of CO, the redox potential of the five-coordinated heme dramatically decreases, which makes it a good electron donor. A rate constant of  $10^4 \text{ s}^{-1}$  has been observed for delivering electrons to the oxidase using this system (Brzezinski & Wilson, 1997).

It is well known that iron in the heme of *Cc* can be replaced by Zn ions, and the triplet state Zn-*Cc* can be an efficient electron donor. At low ionic strength and with the oxidized oxidase, biphasic triplet decay kinetics are observed with rate constants of  $2 \times 10^5$  and  $2 \times 10^3 \text{ s}^{-1}$  to the oxidase (Brzezinski et al., 1995).

*Ruthenium-cytochrome c*: Electron injection was also studied using an artificial electron donor, tris(2,2'-bipyridyl)ruthenium(II) (Nilsson, 1992). After a laser flash, electron transfer from the photoexcited ruthenium to the oxidase occurs within 1 ms, and the rapid heme *a* reduction is observed with a rate constant of  $2 \times 10^4 \text{ s}^{-1}$ . By following the 830 nm band, a rapid reduction followed by an oxidation is observed for the  $\text{Cu}_A$  center, suggesting that  $\text{Cu}_A$  is the initial electron acceptor.

Millett *et al.* used a technique which allows the (bipyridine)ruthenium group to be singly linked to the lysine or cysteine groups in *Cc* (Pan et al., 1988; 1991a; 1993; Durham et al., 1989; Geren et al., 1995). This system allows electrons to be injected into the oxidase rapidly from its own substrate, avoiding the traditional rapid mixing methods. Early studies suggested that *Cc* uses several lysine residues located at the upper left on the front face to interact with *CcO* (see below); so linking the ruthenium group at the back of the molecule would not interfere with its interaction with the oxidase. The rate constants for the photoinduced electron transfer from the excited  $\text{Ru}^{\text{II}}$  on different lysine

positions to the *Cc* are in the range of  $10^5$  to  $10^7$  s<sup>-1</sup>. A rate constant of greater than  $10^5$  s<sup>-1</sup> has been observed for electron transfer from horse *Cc*, labeled at the 7, 39, 55, or 60 positions, to Cu<sub>A</sub>, and the rate constant from Cu<sub>A</sub> to heme *a* is about  $2 \times 10^4$  s<sup>-1</sup>. These studies again suggest that Cu<sub>A</sub> is the initial electron acceptor from *Cc*.

Now it is generally accepted that Cu<sub>A</sub> is the initial electron acceptor from *Cc* (Hill, 1993), which is in agreement with its location at the periplasmic surface, close to the likely *Cc* binding site (Millett et al., 1983). The electron transfer sequence in *CcO* is believed to be from *Cc*, to Cu<sub>A</sub>, to heme *a*, and then to the binuclear center, where Cu<sub>B</sub> has been suggested to be the initial acceptor followed by transfer of electrons to heme *a*<sub>3</sub>. The rate constants from *Cc* to Cu<sub>A</sub> are in the range of  $10^4$  to  $10^5$  s<sup>-1</sup>, and the rate from Cu<sub>A</sub> to heme *a* has been measured in the range of  $10^3$  to  $10^4$  s<sup>-1</sup>, or even  $10^5$  s<sup>-1</sup>, as our recent data in *R. sphaeroides* oxidase indicated (See Chapter IV). This explains why the measured rates for *Cc* oxidation and heme *a* reduction are similar, due to the fact that the rate-limiting step in the sequential transfers is from *Cc* to Cu<sub>A</sub>. The electron transfer rates from heme *a* to the binuclear center have the widest variation, ranging from 3 s<sup>-1</sup> to  $10^5$  s<sup>-1</sup> (Greenwood & Gibson, 1967; Antalis & Palmer, 1982; Hill, 1991; Oliveberg & Malmström, 1991), and this rate has been shown to be sensitive to the overall redox states of the metal centers and is likely to be controlled by protonation and deprotonation events. No direct electron transfer between Cu<sub>A</sub> and heme *a*<sub>3</sub> has been reported, although there are similar distances between Cu<sub>A</sub>-heme *a* (19.5 Å) and Cu<sub>A</sub>-heme *a*<sub>3</sub> (22 Å). The lack of direct electron transfer from Cu<sub>A</sub> to heme *a*<sub>3</sub> has been suggested to be due to the larger reorganization energy associated with heme *a*<sub>3</sub> than with heme *a* (Brzezinski, 1996).

## II Electron transfer (ET) theories

Electron transfer processes are essential for biological systems. In the respiratory system, the energy released from the ET is indirectly used to drive biological functions. The ET theory has been thoroughly reviewed by Marcus (Marcus & Sutin, 1985), and two experimental groups (Gray, H & Dutton, P) have further studied the influences of protein structures on ET rates. This review briefly summarizes the main points of their theories.

### 1 Marcus Theory

In biological systems, the electron donor and acceptor are usually far away from each other ( $> 10 \text{ \AA}$ ), and ET is an “out-sphere” reaction, in which the two reactants do not share a common atom, and the interaction of the relevant electronic orbitals of the two reactants is usually weak. In the ET process, the environments of the two reactants will reorganize to facilitate the electron transfer.

In Marcus’ quantum-mechanical theory (Marcus & Sutin, 1985), the nuclei of reactants and products, together with their environment, are treated as two harmonic oscillators. The potential energy surface of the reactants and the products are shown in Figure 1.8, with the lowest energies as the equilibrium positions ( $DA_{eq}$  and  $D^+A^-_{eq}$ ).

The rate of the ET is given by

$$k \propto (\text{electronic coupling})^2 (\text{nuclear factor}) \quad (\text{Eq. 3})$$

$$k = \frac{2}{\hbar} H_{DA}^2 \frac{1}{(4 \lambda RT)^{1/2}} e^{-(\Delta G^0 + \lambda)^2 / 4\lambda RT} \quad (\text{Eq. 4})$$

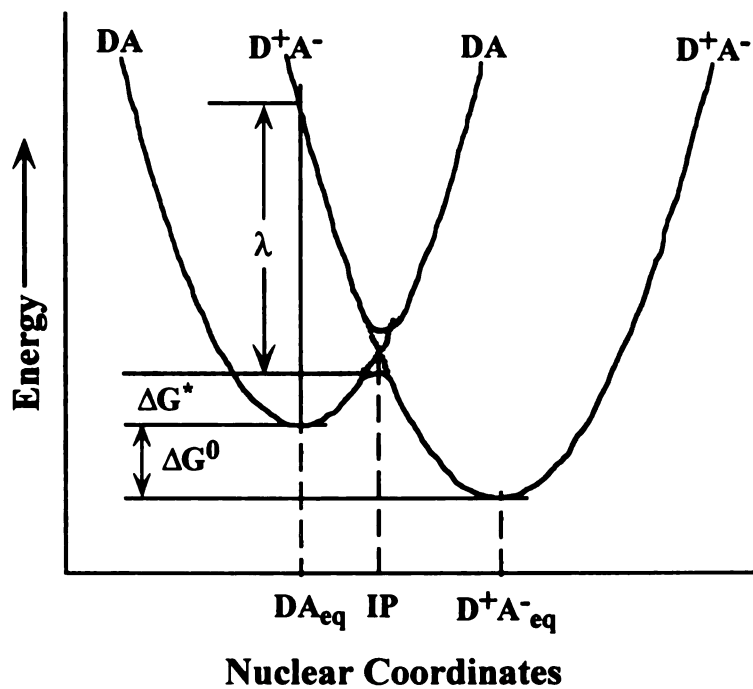


**Figure 1.8** Potential energy diagram for electron transfer between two nearly equivalent complexes.  $DA_{eq}$  and  $D^+A^-_{eq}$  correspond to the equilibrium configurations of the reactant and product complexes, respectively.  $\Delta G^*$  reflects the activation energy,  $\Delta G^0$  the driving force,  $\lambda$  the reorganization energy.

$$H_{DA}^2 = H_0^2 * e^{-\beta(r_{DA} - r_{\text{van der Waals}})} \quad (\text{Eq. 5})$$

where  $H_{DA}$  is the electronic coupling element, describing the electronic coupling of the reactants' electronic states with the products, and reflecting how readily the protein allows an electron to leak across the protein from donor to acceptor. The rate of electron tunneling through the protein matrix is expected to decay exponentially with increasing distance ( $r_{DA}$ ) between donors and acceptors according to the Eq. 5, where  $H_0^2$  is the maximum electronic coupling when the donor and the acceptor are within van der Waals distance. The parameter  $\beta$  reflects the effectiveness of the protein in mediating ET.

The nuclear factor is associated with the activation barrier. This barrier arises because the nuclei around the redox groups adjust their position to accommodate the change of the redox states. The energy required for reorganizing the ligands to overcome the activation barrier and to reach the crossing point (IP in Figure 1.8) is denoted  $\lambda_i$ . When the redox state of the redox centers changes, the solvent molecules around the redox centers will also need adjustments, and the energy required for rearranging the solvent molecules is denoted  $\lambda_o$ . The value of  $\lambda_i$ , together with that of  $\lambda_o$ , forms the term of reorganization energy ( $\lambda = \lambda_i + \lambda_o$ ), which is the amount of the energy that must be added to the reactant at its potential minimum to bring the nuclei into the geometry resembling the product at its potential minimum without transferring the electron.

The factor of  $\Delta G^0$  in Eq. 4 is the total free energy change for the ET reaction (Figure 1.8), equivalent to the energy difference between reactant and product states. It is also the driving force for the reaction to take place. When  $-\Delta G^0 = \lambda$  (in Figure 1.8,  $\Delta G^*$

= 0), the ET reaction has the maximum rate. The Gaussian dependency of ET rate versus  $-\Delta G^0$  allows the estimation of the value of  $\lambda$ , which is equivalent to the  $-G^0$  at the maximum rate.

## 2 Dutton's Distance Dependent Theory

In Marcus' ET theory, the ET rates are affected by the nuclear factor, including the total free energy ( $-\Delta G^0$ ), the reorganization energy ( $\lambda$ ), and the electronic factor  $H_{DA}^2$ , in which the dominant factor is the donor-acceptor distance ( $r_{DA}$ ) (see Eq. 5 above). The electronic effects on ET can be separated from the nuclear effects, when comparing electronic effects on electron transfer rates, by keeping the nuclei effect constant at the conditions where  $-\Delta G^0 = \lambda$ .

Under this principle, Dutton and coworkers have systematically studied the donor-acceptor distance effects on the maximum ET rates (when the free energy ( $-\Delta G^0$ ) matches the reorganization energy ( $\lambda$ )) in biological systems, and in some synthetic and semi-synthetic compounds in a wide range of separation (from 5 to 25 Å ) between centers (Moser et al., 1992; 1995). Comparing the maximum rates in a variety of reactions at different distances allows evaluation of the distance effects on the ET rate.

The biological systems that Dutton and coworkers have used in their studies are the reaction centers from *R. sphaeroides* and *R. viridis*, which have been crystallized (Deisenhofer et al., 1984; Allen et al., 1986; Chang et al., 1986). In these systems, the photo-reduced bacteriopheophytin, BPh<sup>-</sup>, can transfer an electron to the quinone at the Q<sub>A</sub> site. This rate can be altered by replacing the native quinone at the Q<sub>A</sub> site with

artificial quinones with different redox potentials, which results in a change of the free energy ( $-G^0$ ). In their survey, some ruthenated Cc data have also been included (see below).

By plotting the free energy dependence of electron transfer rates, the maximum ET rates at specific distances (measured from the crystal structures) can be determined. Dutton and coworkers found that the logarithms of the maximum ET rates compiled from different proteins are linearly dependent on the edge-to-edge distances (R) between donors and acceptors, with a  $\beta$  value of  $1.4 \text{ \AA}^{-1}$ , which is intermediate between the values for a vacuum ( $2.8 \text{ \AA}^{-1}$ ) and for covalent systems ( $0.7 \text{ \AA}^{-1}$ ). An empirical equation which includes all three parameters for ET has been proposed (Moser et al., 1995):

$$\log k = 15 - 0.6R - 3.1(\Delta G^0 + \lambda)^2/\lambda \quad (\text{Eq. 6})$$

Dutton's theory implies that the proteins present a uniform barrier to electron tunneling, and the specific amino acid bonding structure of the intervening protein does not affect the coupling between the redox centers. In this ET model, there is no specific pathway involved in ET between donors and acceptors, and electrons tunnel into the protein medium in all directions and in large regions between cofactors. The directional specificity for an electron from donor to acceptor rests on the nuclear factors.

### 3 Tunneling-pathway model

A dramatically different model of the protein matrix effect on ET, compared to Dutton's model which describe that the protein matrix as homogenous for ET, has been proposed by Onuchic and Beratan: a tunneling-pathway model (Onuchic et al., 1992; Curry et al., 1995). The essence of this model is that there are three basic elements in ET

pathways: covalent, hydrogen-bonded, and through-space interactions. Each of these elements is associated with different decay factors. The through-covalent-bonds tunneling is the most effective way, with lower tunneling barriers and smaller decay factors (electrons propagate faster and longer). In contrast, the through-space jumps have the highest tunneling barriers with larger decay factors which are explicitly distance dependent. Because of the difference between these two types of ET mediators, generally electronic coupling interactions mediated through-bonds are longer range than those mediated through space. The hydrogen-bond interactions are also excellent tunneling mediators because they introduce relatively small through-space gaps (Regan et al., 1995).

Because of the above differences in the way the protein matrix is treated in the two different models, the logarithms of maximum ET rates in Onuchic and Beratan's model are not linearly dependent on the edge-to-edge distance, as in Dutton's model; instead, they are linearly dependent on the so-called effective tunneling lengths ( $s^{-1}$ ), which is determined by calculating the number of covalent bonds that are energetically equivalent to the shortest pathway through the protein via covalent and hydrogen bonds and through space jumps, and then multiplying the effective number (nonintegral number) of bonds in a pathway by an average bond length of 1.4 Å.

This model has been experimentally tested by Gray and coworkers by attaching ruthenium groups to proteins via surface histidines (Bjerrum et al., 1995; Langen et al., 1995; Regan et al., 1995; Gray & Winkler, 1996). The systems that they used are ruthenated-Cc and ruthenated azurins. In these systems, photoexcitation of the Ru groups can result in rapid ET from Ru<sup>II</sup> to the Fe<sup>III</sup> in Cc or Cu<sup>II</sup> in azurins. The

combination of photoexcitation and bimolecular quenching reaction (flash-quench procedure) allows them to measure the reverse electron transfer rates from  $\text{Fe}^{\text{II}}$  to  $\text{Ru}^{\text{III}}$  and from  $\text{Cu}^{\text{I}}$  to  $\text{Ru}^{\text{III}}$ . The distances between donors and acceptors can be varied by placing the ruthenium group at different positions on the protein surface, and the driving force can be changed by using ruthenium groups with different ligands.

The Ru-modified-proteins studies give strong support to the tunneling pathway model, and further indicate that there is no universal  $\beta$  value in proteins. The balance of through-bond and through-space contacts between donors and acceptors have been proposed to set the coupling strength. It is noteworthy that in Dutton's survey, some of the data from ruthenium-Cc has also been included, and among these ruthenium-Cc systems, the edge-to-edge distances are found to be linearly related to the effective tunneling lengths ( $\sigma$ -1), but the difference between the two different theories is the  $\beta$  values they found, and whether edge-to edge or center to center distance are used.

### **III The interactions of cytochrome *c* with its partners**

Cytochrome *c* is one of the most versatile proteins in its redox activities. In the respiratory system, it shuttles electrons from the cytochrome *bc<sub>1</sub>* complex to a variety of oxidases belonging to the heme-copper oxidase family. It also transfers electrons to reaction centers and nitric oxide-reducing systems, in some species, involved in photosynthesis and denitrification processes. In the yeast system, ferro-Cc can also be oxidized by CcP and sulfite reductase. Besides these physiological reactions, this protein

shows reactivities with a large number of nonphysiological redox partners, including cytochrome *b*<sub>5</sub>, and plastocyanin (for review see Margoliash & Schejter (1996)).

A variety of techniques have been used to study the interaction of *Cc* with its partners, and to try to answer the following questions: What surface area of *Cc* is involved in docking with other proteins? Does *Cc* use the same, or a different, binding surface to interact with its different redox partners? Answering these questions is important for understanding the electron transfer process. This section briefly summarizes several well studied cases, including chemical modification studies and interactions with plastocyanin and *CcP*.

## **1 Chemical modification studies**

The interactions between *Cc* and its partners have a significant electrostatic component, which is affected by the ionic strength of the reaction medium. In bovine *Cc*, the importance of the lysine residues in the interactions of *Cc* with its partners was recognized early. To understand which specific residue was important for the binding, chemical modification studies were done with several reagents, including 4-carboxyl-2,5-dinitrophenyl (CDNP) (Brautigan et al., 1978; Osheroff et al., 1980), trifluoroacetyl (TFA) (Staudenmayer et al., 1976) and trifluoromethylphenylcarbonyl (TFC) (Smith et al., 1977), to modify the lysine residues.

The singly labeled cytochrome species were separated through several rounds of chromatography, and the specific location of the chemical reagents on the proteins were identified through protease digestion, two-dimensional thin-layer peptide mapping and coupled with amino acid sequence analysis or other techniques. Spectroscopic analyses

of these *Cc* derivatives indicated that the chemical modifications had little effect on the overall conformation and redox properties of *Cc*, making the interpretation of the kinetic analyses of these derivatives much easier.

The reactions of these *Cc* derivatives have been tested under steady-state conditions either spectrophotometrically or polarographically (Smith et al., 1977; Ferguson-Miller et al., 1978; Osheroff et al., 1980). Early studies suggested that the  $K_M$  of the high affinity phase in the oxidase reaction is equivalent to the  $K_D$  of the binding strength between *Cc* and oxidases (Ferguson-Miller et al., 1976; Smith et al., 1981), so measuring the  $K_M$  values of these derivatives allowed a semi-quantitative measurement of the modification effects on their interactions with the oxidase. The results from different laboratories using different reagents all showed that the modifications of Lys-8, -13, -27, -72, -86, and -87 in horse *Cc* have the most dramatic effects on its binding to the oxidase, suggesting that these lysine residues (of a total of 19) are important in binding *Cc* to the oxidase. These six derivatives also show the biggest effects in their reactions with cytochrome *bc<sub>1</sub>* (Smith et al., 1981) and *CcP* (Smith & Millett, 1980), suggesting that *Cc* uses the same patch on its surface to interact with its various redox partners.

A different approach, called differential protection technique, has also been used to address the same issue (Rieder & Bosshard, 1980). In this experiment, the reactivities of the chemical modification reagents with the lysine residues, in both free and complexed cytochromes *c*, have been compared. In the complexed *Cc*, the lysine residues important for the interaction will be protected from the modification, because they are located at the bimolecular interface. It is reassuring that this study also points to the same residues suggested from chemical modification studies as important for *Cc* binding. Now it is

generally accepted that the upper-left of the “front” face of *Cc*, close to where the heme is exposed, is involved in its interactions with its redox partners.

## **2 The interaction of cytochrome *c* with *CcP* — A case study**

The reaction between *Cc* and cytochrome *c* peroxidase (*CcP*) from yeast has been a good model system for studying long-range electron transfer in a biological system. Unlike other physiological partners of *Cc* in mammalian systems, which are usually membrane-bound, *CcP* is a small soluble protein with a molecular weight of 34.2 kDa and a single heme group. In addition, the high-resolution crystal structure of *CcP* is available (Poulos et al., 1980). Pelletier and Kraut (1992) have also resolved the crystal structures of horse *Cc/CcP* complex (*CcP:Cc(H)*) and yeast iso-1-*Cc/CcP* complex (*CcP:Cc(Y)*), which makes it an even more favorable system for testing the electron transfer theories and available computational docking methods.

### **2.1 Crystallography studies**

The crystal structures of *CcP:Cc(Y)* and *CcP:Cc(H)* were resolved under different conditions with *CcP:Cc(H)* at low ionic strength (5 mM) and *CcP:Cc(Y)* at high ionic strength (150 mM). Although they were crystallized under different conditions, the two complexes are similar, with *CcP* using a similar domain to interact with *Cc(Y)* and *Cc(H)*. In *CcP:Cc(H)*, the interaction domain can be considered in terms of three regions of *CcP* making contact with *Cc(H)*. The first region includes Glu-290, which is hydrogen-bonded with Lys-72 from *Cc*. The second region has several carboxyl residues, including Glu-32, Asp-33, Asp-34 and Glu-35, with Glu-35 forming a hydrogen-bond with Lys-87 of *Cc(H)*. The crystal structure also shows that the carboxyl side-chain of Asp-34 may

form potential hydrogen-bond with the side-chain of Lys-13 of Cc(H). In the second region, Asn-38 from CcP is also hydrogen-bonded with Lys-8 of Cc(H). It is noteworthy that the lysine residues (Lys-8, -13, -72 and -87) in horse Cc that have been identified to be involved in hydrogen-bond interactions with CcP in the CcP:Cc(H) crystal structure are the same residues that have been suggested from early chemical modification studies (Kang et al., 1978), and these residues were also determined to be important for the interaction between Cc and CcO (Smith et al., 1977; Ferguson-Miller et al., 1978; Osheroff et al., 1980). The third region of interaction between horse Cc and CcP is between the heme methyl group of Cc(H) and Ala-193 and Ala-194 of CcP. Overall the predominant forces holding the CcP:Cc(H) complex together appear to be hydrogen-bonds and van der Waals interactions.

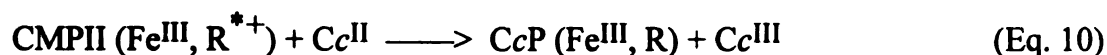
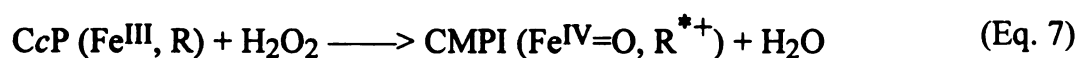
The overall structure of the CcP:Cc(Y) complex is similar to that of CcP:Cc(H), and CcP uses similar regions to interact with Cc(Y). The most noticeable difference between them is the slight relative rotation-translation of Cc molecule, which results in different hydrogen-bond interactions in two complexes (Pelletier & Kraut, 1992). In CcP:Cc(Y), the three interaction regions in CcP are similar to those in the CcP:Cc(H) complex, with potential hydrogen bonds between Glu-290 (CcP) and Lys-73 and Asn-70 of Cc(Y). Ala-193 and Ala-194 from CcP are again in van der Waals contact with the methyl group in the heme group of Cc(Y). An electron transfer pathway, which is also the shortest straight line between the two hemes groups, has been identified in the CcP:Cc(Y) complex: it involves the backbone chains of Ala-194, Ala-193, Gly-192 and Trp-191 (Pelletier & Kraut, 1992). The indole ring of Trp-191, in van der Waals contact with the peroxidase heme, is located at one end of the chain, while Ala-193 and Ala-194,

in van der Waals distance with the methyl group of the Cc heme, are located at the other end. Because of the slight differences between the two cytochromes *c* in the two complexes, there is a gap of 7 Å between Ala-193 and Ala-194 and the methyl group of the *c*-type heme in the CcP:Cc(H) complex, suggesting a less efficient ET complex.

## 2.2 Mutagenesis studies

One of the biggest concerns regarding the crystallography studies is whether the crystallized complexes represent the solution interaction which is required for rapid electron transfer. The crystallography studies of cytochromes *c* and CcP raise another question: is the geometry difference between the two cytochromes in CcP:Cc(H) and CcP:Cc(Y) due to the different crystal growth conditions or because of the intrinsic difference between the two cytochromes? These questions have been addressed through mutagenesis and kinetics studies (Wang et al., 1996).

Before talking about the experimental approach, it is worthwhile to discuss the reactions that CcP catalyzes. The overall reaction that CcP catalyzes is the reduction of hydrogen peroxide by ferro-Cc, according to the following schemes (Millett et al., 1995):



The resting ferric state of CcP is oxidized to CMPI (Fe<sup>IV</sup>=O, R<sup>\*+</sup>), which contains an oxyferryl heme, Fe<sup>IV</sup>=O, and Trp-191 cation radical, R<sup>\*+</sup>. The CMPI is reduced to CMPII after the cation radical is reduced by an electron from ferro-Cc. In CMPII, the

intramolecular electron transfer converts CMPII ( $\text{Fe}^{\text{IV}}=\text{O}$ , R) to CMPII ( $\text{Fe}^{\text{III}}$ ,  $\text{R}^{*+}$ ), which is further converted to the resting ferric state after accepting the second electron. In these schemes, Trp-191 is the initial electron acceptor, which is consistent with the crystallography studies, which indicate that Trp-191 is closer to the *c*-type heme than the peroxidase heme.

To probe the *Cc* binding site on *CcP*, mutants have been made at the three contact regions in *CcP*. These include E32Q, D34N, E35Q, E290N and E291N, which convert the carboxyl groups to amide groups, and A193F and A193C-MPB (the cysteine was labeled with a bulky group of 3-(*N*-maleimidylpropionyl)biocytin) (MPB), which introduced a bulky group at the interface (Fishel et al., 1987; Miller et al., 1994;1996). The mutational effects on electron transfer from *Cc*(Y) have been measured using the ruthenium-*Cc* photolysis technique. The rate constants of  $k_{\text{eta}}$  for D34N, E290N and A193F were found to decrease 2 to 4-fold, and the binding constants ( $K_{\text{D}}$ ) of these mutants decreased from 6 to 15-fold, while the mutations E32Q and E291Q had no obvious effect on both  $k_{\text{eta}}$  and  $K_{\text{D}}$  (Wang et al., 1996). These results are consistent with the use of the binding domain identified by crystal structures. The modification of *Cc*-A193C with a bulky reagent, MPB, resulted in a decrease of  $k_{\text{eta}}$  about 150-fold, in agreement with the crystal structure analysis, which shows that Ala-193 is located at the electron transfer interface. The mutational effects on  $k_{\text{etb}}$  were about the same as the effects on  $k_{\text{eta}}$ , suggesting that the two *Cc* involved in each turnover cycle use the same binding site in *CcP*.

To answer the question of whether the different conformations of *Cc* in *CcP*:*Cc*(Y) and *CcP*:*Cc*(H) are due to the different crystal growth conditions, as suggested

of

to

the

the

in

and

the

the

and

the

the

the

of

the

the

of

of

ES

199

and

AIS

com

bona

by the authors, or because of the intrinsic difference between the two cytochromes, a technique was developed to introduce a bulky MPB group at position 193, the point of closest contact between *Cc* and *CcP* (Miller et al., 1996). The introduction of MPB presumably weakens the binding of *Cc* due to steric effects. But because of the orientational differences between *CcP:Cc(Y)*, where Ala-193 is in van der Waals contact with *c*-type heme, and *CcP:Cc(H)*, where Ala-193 is 7 Å away from the *c*-type heme, the introduction of MPB will affect the electron transfer rates in the two complexes to different degrees. Indeed, the modification causes a 20 to 100-fold decrease in transient and steady-state electron transfer rates with yeast *Cc* in buffers of 20-160 mM ionic strength, while only 2-3-fold decrease in the reaction with horse *Cc*. This suggests that the geometry difference observed in the crystal structures is also present in solutions and this difference is due to the intrinsic difference between the two cytochromes, not a result of the crystallographic or ionic strength effects.

Bound water molecules are ubiquitous in protein-protein interfaces, and are important in mediating the interaction by forming hydrogen bonds. In the 2.3 Å structure of *CcP:Cc(Y)*, 21 interface water molecules have been resolved. Thermodynamic analyses of the mutational effects on complex formation show that the mutations E291Q and E35Q have no effects on either the enthalpy and entropy of the reactions (Erman et al., 1997), which is consistent with the rapid kinetics assays and the crystal structure analysis, indicating that they are not involved in the binding. The entropies of E35Q, A193F, D34N and E290N decrease, with no dramatic changes in their enthalpies. The complex formation between *Cc* and *CcP* is endothermic, and the formation of hydrogen bonds contribute to the enthalpy changes. In E35Q, D34N and E290N, the small

enthalpy changes observed in the reactions suggest that the substituted amide groups can still form the hydrogen bonds, like the carboxyl groups do in wild-type CcP. In the process of complex formation, some water molecules are released, which contribute to the increase in entropy for the reactions. Due to the charge differences between the carboxyl and amide groups, the hydration states for each of them are different. As a result, the degree of water exclusion from amide groups is less than the corresponding carboxyl groups, which accounts for the decrease of the entropy for E35Q, D34N and E290N. It is suggested that the lower affinity for these mutants is also mainly due to a decrease of the entropy changes upon complex formation.

The mutagenesis analyses support the crystal structure results, and *vice versa*, the mutagenesis results were also validated from the crystallography studies. This gives us confidence in using similar approaches to study the interaction of Cc with CcO.

#### **IV C-type cytochromes in *R. sphaeroides***

*R. sphaeroides*, a purple nonsulfur bacterium, has been a popular subject for biochemical, biophysical and genetic studies of photosynthesis and respiration processes. This microorganism can grow chemoheterotrophically in the dark under aerobic respiration conditions or photoheterotrophically in the light under anaerobic photosynthesis conditions; some species can grow anaerobically in the dark using N<sub>2</sub>O as electron acceptor. Because of its versatile growth conditions, the cells have adapted branched electron transfer systems to support their growth under different environments (Figure 1.9). Among these branched electron transfer systems, several c-type

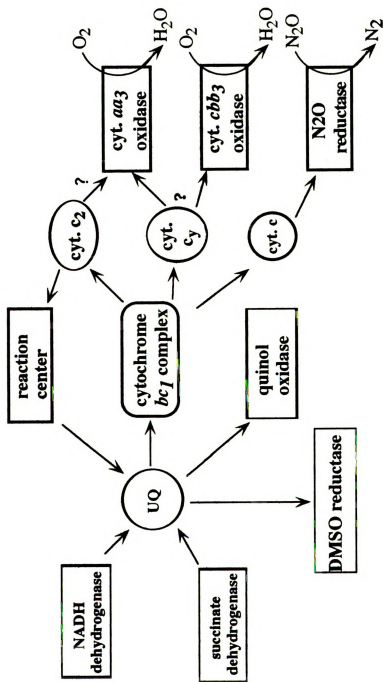


Figure 1.9 An overview of the respiratory pathways in *Rhodobacter sphaeroides*

cytochromes have been found to be important in shuttling electrons between membrane-bound complexes (Meyer & Cusanovich, 1985).

Cytochromes *c* are very small, stable proteins and can be purified relatively easily in large amounts; moreover, they are present ubiquitously in most organisms. Because of these features, cytochromes *c* have been a favorite protein for multidisciplinary research, which has led to a wealth of information about them (Bartsch, 1978; Meyer & Kamen, 1982; Pettigrew & Moore, 1987; Moore & Pettigrew, 1990; Scott & Mauk, 1996). This discussion will focus on the different *c*-type cytochromes found in *R. sphaeroides*, with emphasis on their biochemical properties. The question regarding which protein is the physiological electron donor to the  $aa_3$  oxidase is also addressed. Although a number of cytochromes have been identified over several decades, the functional roles of most of them are still elusive.

## 1 Properties of cytochromes *c*

Cytochromes *c* are electron transfer proteins that have protoheme covalently attached via two thioether bonds between two cysteine residues of the apoprotein and the vinyl side chains of the heme. No other types of heme are known to be covalently bound, and cysteine is the only amino acid residue which is known to covalently bind heme. Because of this unique characteristic of *C<sub>c</sub>*, almost all the *c*-type cytochromes have a CxxCH heme binding motif in their sequences (Meyer & Kamen, 1982), but not all sequences with this motif bind heme; some Fe-S proteins also share this binding motif.

### 1.1 Cytochrome *c*<sub>1</sub>

Cytochrome *c*<sub>1</sub> is a subunit of the *bc*<sub>1</sub> complex, not a soluble protein, and it has been isolated from the complex using Triton X-100 and shown to have a molecular weight of 30 kDa (Yu et al., 1986). Sequence analysis indicates that it consists two parts (Gabellini & Sebald, 1986; Xia et al., 1997): an N-terminal hydrophilic domain located at

the peripheral side of the membrane and a hydrophobic membrane-spanning segment near the C-terminus. Heme  $c_1$  is located in the N-terminal domain. The  $bc_1$  complex from bovine heart mitochondria has been crystallized at 2.9 Å (Xia et al., 1997), but because of the poor quality of the crystals at this region, the detailed structure of the N-terminal domain was not clearly resolved. Based on sequence analysis and a more recent high resolution  $bc_1$  structure (Iwata et al., 1998), the two cysteines that covalently bind the heme to the protein are established as Cys-37 and Cys-40 in bovine (Cys-58 and Cys-61 in *R. sphaeroides*). The two axial ligands are His-41 and Met-160 in bovine (His-62 and Met-207 in *R. sphaeroides*).

The functional role of cytochrome  $c_1$  is to transfer electrons from  $bc_1$  complex to soluble Cc (Trumpower, 1990(b)), which is analogous to the role of cytochrome  $f$ , a component of the chloroplast cytochrome  $b_6f$  complex. The primary difference between cytochrome  $c_1$  and cytochrome  $f$  is that the axial ligands to the  $c$ -type heme are histidine and methionine and those to the  $f$ -type heme are histidine and the amino group of the N-terminal tyrosine (Cramer et al., 1994; Martinze et al., 1996).

Cytochrome  $c_1$  from *R. sphaeroides* has a redox potential of 228 mV (Yu et al., 1986), identical with that of isolated mammalian cytochrome  $c_1$ , and also similar to the redox potential of soluble mitochondrial Cc. Its reduced optical spectrum has an  $a$ -peak at 552.5 nm, and the Soret absorption maximum at 417 nm.

## 1.2 Cytochrome $c_2$

Cytochrome  $c_2$  is also known as cytochrome  $c_{550}$ , because its reduced  $a$ -peak is at 550 nm. This low spin cytochrome is one of the bacterial counterparts of mitochondrial Cc with a similar molecular weight of 14 kDa. Cytochrome  $c_2$  from *R. sphaeroides* has been crystallized (1cxa.pdb), and the crystal structure reveals that its overall structure is similar to that of bovine Cc, with the heme surrounded by 5 helices and the N-terminal and C-terminal helices interacting with each other, a typical "cytochrome  $c$  fold"

se  
ov  
ber  
ig  
of  
po  
for  
em  
be  
w  
&  
Th  
con  
ed  
che  
res  
be  
L  
are  
ten  
of  
se  
B  
cyc

structure. All the residues conserved in mammalian Cc and important for keeping the overall structure are also present at *R. sphaeroides* cytochrome  $c_2$  (Figure 1.10). The heme binding motif CXXCH is located at the N-terminus of the protein, and the sixth ligand, Met-100, is located at the C-terminus. Because of the presence of insertions, *R. sphaeroides* cytochrome  $c_2$  is slightly larger than the mammalian proteins.

Unlike mitochondrial Cc, cytochrome  $c_2$  from *R. sphaeroides* has a high redox potential of 356 mV (*versus* 260 mV for bovine Cc) and a low pI value of 5.5 (*versus* 10 for bovine Cc) (Meyer & Cusanovich, 1985), reflecting the differences in the heme environment and the surface charge of these two proteins. The nine lysine residues in bovine Cc (Lys-8, 13, 25, 27, 72, 73, 79, 86, 87), which are important for interacting with its electron transfer partners (Smith et al., 1977; Ferguson-Miller et al., 1978; Rieder & Bosshard, 1980), are not all present in *R. sphaeroides* cytochrome  $c_2$  (Figure 1.10). The counterparts of Lys-13 and Lys-72 in bovine Cc are missing, while the rest of the conserved lysine residues and some additional amino acids surrounding the exposed heme edge, remain. Although *R. sphaeroides* cytochrome  $c_2$  is acidic, and has more negatively charged residues overall, the protein itself is a dipole, with most of the positively charged residues located at the front surface, where the heme edge is exposed. Cytochrome  $c_2$  has been found to use this positively charged face to interact with its physiological partners (Long et al., 1989). The insertions in *R. sphaeroides* are located outside the front face, and these extra residues will not likely interfere with its interaction with other proteins.

Cytochrome  $c_2$  is one of the major *c*-type components in *R. sphaeroides*, and it tends to stay reduced when isolated (Meyer & Cusanovich, 1985). The expression levels of the gene encoding *R. sphaeroides*  $c_2$  have been found to be approximately four- to seven-fold higher under phototrophic growth condition than growing aerobically (Brandner et al., 1989).

The primary function of cytochrome  $c_2$  is in cyclic electron transfer from the cytochrome  $bc_1$  complex to the photooxidized reaction center (Overfield et al., 1979;

**Figure 1.10** **Sequence alignment of c-type cytochromes.** Horse: horse Cc, pdcM: *P. denitrificans* membrane-bound Cc ( $c_{552}$  or  $c_{mem}$ ), Rscy: *R. sphaeroides* membrane cyt. c, Rccy: *R. capsulatus* membrane Cc, pdc<sub>2</sub>: *P. denitrificans* soluble cyt.  $c_2$ , Rsc<sub>2</sub>: *R. sphaeroides* soluble cyt.  $c_2$ , Rsic<sub>2</sub>: *R. sphaeroides* soluble iso-cyt.  $c_2$ . The alignment were done using the program DNASTar, and some regions were adjusted manually based on 3-D structure comparison of horse Cc and *R. sphaeroides* cyt.  $c_2$ . Some lysine residues are highlighted with the horse numberings.



Chory et al., 1984). In this process, light causes electrons to transfer from the reaction center to the ubiquinone pool; in the meantime, protons are taken from the cytoplasmic side. The electrons lost in the reaction center are replaced later by electrons coming from the cytochrome  $bc_1$  complex carried by soluble cytochrome  $c_2$ . Evidence supporting the involvement of cytochrome  $c_2$  in cyclic electron transfer comes from a genetic study (Donohue et al., 1988). When the cytochrome  $c_2$  gene was deleted from *R. sphaeroides*, the deletion strains could not grow photosynthetically, but a photosynthetic phenotype of the deletion strain could be restored when a plasmid-born copy of the cytochrome  $c_2$  gene was introduced. However, recent experiments also indicate that cytochrome  $c_2$  is dispensable for photosynthesis because an alternative  $c$ -type cytochrome, isocytochrome  $c_2$ , can substitute it (Rott & Donohue, 1990; Rott et al., 1992).

### 1.3 Isocytochrome $c_2$

A cytochrome  $c_2$  deletion strain of *R. sphaeroides* cannot sustain phototrophic growth; however, spontaneous mutations (*spd* mutants) suppress this photosynthesis deficiency and have led to the discovery of a new cytochrome, isocytochrome  $c_2$  (Rott & Donohue, 1990). When *spd* mutants are grown under photosynthetic conditions, isocytochrome  $c_2$  is present at 20 to 40% of the level of cytochrome  $c_2$  in wild-type, and the highest level of isocytochrome  $c_2$  is found when the *spd* mutants are grown under aerobic conditions (Rott et al., 1992). Detailed analysis also reveals that isocytochrome  $c_2$  is also present at lower levels in wild-type strains.

Isocytochrome  $c_2$  has been purified and its gene has been cloned (Fitch et al., 1989; Rott et al., 1993). The size of the mature isocytochrome  $c_2$ , deduced from the nucleotide sequence, is about 14 kDa, about the same as cytochrome  $c_2$ . It is also highly homologous to cytochrome  $c_2$ , sharing 44% identical residues (Figure 1.10).

With fewer internal insertions, isocytochrome  $c_2$  is more structurally related to horse Cc than cytochrome  $c_2$  is, however, the counterpart of Lys-72 in horse Cc is

missing. But unlike horse Cc and cytochrome  $c_2$ , isocytochrome  $c_2$  from *R. sphaeroides* has absorption maxima of 552 nm and 415 nm for the  $\alpha$  and Soret peaks, respectively, and it has more negatively charged residues (pI 4.5) than cytochrome  $c_2$ . The redox potential for isocytochrome  $c_2$  is 294 mV, lower than that of cytochrome  $c_2$  (Fitch et al., 1989).

#### 1.4 Cytochrome $c'$

Cytochrome  $c'$  is widely distributed in purple phototrophic bacteria and some nonphotosynthetic bacteria (Amber et al., 1981), and its synthesis is regulated by the oxygen levels (Cusanovich, 1971). Under aerobic growth conditions, the expression level of cytochrome  $c'$  in wild-type *R. sphaeroides* strains is almost undetectable. Instead, it is present in appreciable amounts in photosynthetically grown cells (Meyer & Cusanovich, 1985; Rott & Donohue, 1990).

In *R. sphaeroides*, cytochrome  $c'$  is present as a homodimer with a molecular weight of 28 kDa (Cusanovich, 1971; Meyer & Cusanovich, 1985). The two subunits can be dissociated in the presence of 6 M guanidine and each monomer has 130 residues in *R. sphaeroides*. A number of cytochromes  $c'$  have been crystallized from several strains (Weber et al., 1980; Yasui et al., 1992), including from *Rhodobacter capsulatus* (Tahirov et al., 1996), a strain closely related to *R. sphaeroides*. Although cytochromes  $c'$  from different bacteria show very little sequence similarity (Amber et al., 1981), X-ray crystallography indicates that the tertiary structure is conserved in all the known structures. Despite its widespread occurrence and the fact that the structure is conserved, the functional roles of cytochrome  $c'$  remain unknown.

The structure of cytochrome  $c'$  is different from mitochondrial Cc or bacterial cytochrome  $c_2$  in the following aspects:

(1) It has a four parallel helical bundle with a covalently bound heme group in the center, and with the binding motif CXXCH located at the C-terminus of the protein rather than at the N-terminus, as in mammalian Cc.

(2) The heme iron is penta-coordinated, with the histidine residue ligated to the fifth position, and the sixth position open. The sixth empty coordination site faces the protein interior and the access to this site is hindered primarily by the side chains of aromatic residues. Because of the special heme environment, most of the small molecules which can bind to hemoglobin, such as O<sub>2</sub>, CN<sup>-</sup>, N<sub>3</sub><sup>-</sup>, cannot bind to cytochrome *c'*; the exceptions are carbon monoxide for the reduced form and nitric oxide for the oxidized form.

(3) The absorption spectra of reduced cytochrome *c'* has a pronounced splitting of the Soret peak around 425 nm and a single broad peak for the *a*- band around 552 nm. As is typical of the cytochrome *c'*, the Soret absorption maxima changes with pH. The redox potential of cytochrome *c'* is about 30 mV at pH 7.0, much lower that of mitochondrial Cc (Meyer & Cusanovich, 1985),

### 1.5 Cytochrome *c*<sub>554</sub>

When photosynthetically grown, *R. sphaeroides* cells are switched to aerobic growth conditions, the type of cytochrome that is induced most is cytochrome *c*<sub>554</sub>, which is five- to eight-fold more abundant in aerobically cultured cells than those grown anaerobically in the light (Meyer & Cusanovich, 1985; Bartsch et al., 1989). The level of cytochrome *c*<sub>554</sub> is about three times that of cytochrome *c*<sub>2</sub> under aerobic condition. As its name indicated, the absorption spectrum of the reduced cytochrome *c*<sub>554</sub> has a wavelength maxima of 554 nm for the *a*-peak and 419 nm for the Soret peak. The redox potential of cytochrome *c*<sub>554</sub> is 203 mV at pH 7.0. Cytochrome *c*<sub>554</sub> is found to be located in the periplasm (Flory & Donohue, 1995).

The gene of *R. sphaeroides* *c*<sub>554</sub> has been cloned and the deduced protein sequence is homologous to that of cytochrome *c'* from *R. sphaeroides* with 36% identity (Flory & Donohue, 1995). Like cytochrome *c'*, the single heme in cytochrome *c*<sub>554</sub> is attached at the C-terminus of the protein. Instead of being a high spin heme, as in the case of cytochrome *c'*, the *c*-type heme in cytochrome *c*<sub>554</sub> is low spin, with the sixth ligand being Met-16 near the N-terminus.

Cytochrome *c*<sub>554</sub>, with a pI of 4.1, binds much tighter to a DEAE-cellulose column than any other soluble cytochrome components due to its acidic nature. The mature cytochrome *c*<sub>554</sub> has 133 residues with a molecular weight of about 14 kDa, but the native size of purified *c*<sub>554</sub> is 44 kDa, suggesting that the protein is present as a trimer (Meyer & Cusanovich, 1985).

### 1.6 A diheme cytochrome

In the process of cloning cytochrome *c*<sub>554</sub> from *R. sphaeroides*, a new *Cc* was discovered (Flory & Donohue, 1995), which is encoded by *cycG*, and is located in the same operon as cytochrome *c*<sub>554</sub> and is transcriptionally linked to it. The predicted gene product for *cycG* is a diheme *Cc* with a subunit molecular weight of 32 kDa. The two *Cc* binding motifs, CXXCH, are located in the middle of the protein, 145 residues from each other. The sixth ligand, if there is one, has not been identified yet. This cytochrome has been shown to be located in the cytoplasmic membrane with its N-terminal 20 residues as the anchor. This protein has not been purified, and its spectroscopic and structural properties are unknown.

### 1.7 Cytochrome *c*<sub>551.5</sub>

Under photosynthetic conditions, *R. sphaeroides* also synthesizes a small amount of cytochrome *c*<sub>551.5</sub> with an absorption maxima at 551.5 nm for the *α* peak and 419 nm for the Soret peak (Meyer & Cusanovich, 1985). In this 16 kDa protein, two *c*-type

hemes are found to bind at each end of the molecule. The redox potential of cytochrome *c*<sub>551.5</sub> (about -254 mV) is the lowest among all the *c*-type cytochromes known so far. Cytochrome *c*<sub>551.5</sub> has not been found in any other species, and it is not related to any other protein.

### 1.8 *Sphaeroides* heme protein (SHP)

This green-colored heme protein is present in small amounts in *R. sphaeroides* grown anaerobically in the light, and was the first to come out from a DEAE-cellulose purification column (Meyer & Cusanovich, 1985). SHP, with a high-spin heme, is more like myoglobin in spectral properties, and binds oxygen and carbon monoxide. But unlike myoglobin, the absorption intensity of the Soret band decreases when the protein is reduced from the oxidized form. The absorption maxima for the reduced form are at 548 nm for the *a* peak and 429 for the Soret peak. The absorption peak changes in different buffers, reflecting the binding of small ligands to the high spin heme.

### 1.9 Cytochrome *cbb*<sub>3</sub> oxidase

Cytochrome *cbb*<sub>3</sub> oxidase belongs to the heme-copper oxidase family (García-Horsman et al., 1994a) and has been found in several species (Thony-Meyer et al., 1994; de Gier et al., 1996; Kaminski et al., 1996), including *R. sphaeroides* (García-Horsman et al., 1994b). This enzyme is induced at low O<sub>2</sub> condition and is important for N<sub>2</sub> fixation for some species (Kaminski et al., 1996).

The subunit II of *cbb*<sub>3</sub> oxidase has an N-terminal transmembrane region and a hydrophilic C-terminal domain. Unlike *aa*<sub>3</sub>-type oxidase, *cbb*<sub>3</sub> oxidase does not have a Cu<sub>A</sub> site at the C-terminus of subunit II; instead, it has two covalently bound *c*-type cytochromes with methionines as the sixth ligands (García-Horsman et al., 1994b; de Gier

et al., 1996). The subunit III of *cbb*<sub>3</sub> oxidase has another covalently bound *c*-type cytochrome in the middle of the protein. All three *c*-type cytochromes in *cbb*<sub>3</sub> oxidase have predominantly negatively charged residues, and all the conserved lysine residues in mammalian Cc are not present, suggesting that difference forces, other than electrostatic interaction, are involved in stabilizing these cytochromes and the oxidase. How electrons are transferred within these three cytochromes is still unknown.

The purified *cbb*<sub>3</sub> oxidase from *R. sphaeroides* has characteristics of a *c*-type cytochrome with an absorption maxima of 551 nm for the *a* band and a Soret peak of 415 nm (García-Horsman et al., 1994b). The redox potential of the Cc in subunit III from *R. capsulatus* has been reported to be 320 mV and this heme has been suggested to be the direct electron donor to the *b*-type hemes in subunit I (Gray et al., 1994).

## **2 Which cytochrome *c* is the physiological substrate for *aa*<sub>3</sub>-type oxidase in *R. sphaeroides*?**

### **2.1 Soluble cytochrome *c***

Although *aa*<sub>3</sub>-type CcO in *R. sphaeroides* has been very well characterized, little is known about its physiological substrate. Among several *c*-type cytochromes known so far (see above), the real substrate for the *aa*<sub>3</sub>-type CcO is still an open question. The motivation to address this question has been reduced by the fact that bovine Cc is an excellent substrate for bacterial CcOs, but solving this basic problem is important in understanding electron flow in the respiratory chain and its physiological regulation.

The *aa*<sub>3</sub>-type oxidase is present at higher levels when the cells are grown aerobically in the dark. Under these conditions, the synthesis of photosynthetic pigments is suppressed. To qualify for the physiological substrate of *aa*<sub>3</sub>-type oxidase,

the *c*-type cytochromes have to be present at relatively higher levels under aerobic conditions too. In all the *c*-type cytochromes discussed above, only two of them meet this criteria: cytochrome  $c_2$  and cytochrome  $c_{554}$ .

**2.1.1 cytochrome  $c'$  and cytochrome  $c_{551.5}$**  In aerobically grown wild-type cells, the expression levels of cytochrome  $c'$  and cytochrome  $c_{551.5}$  are very low, and also they have the lowest redox potentials among all the known *Cc* in *R. sphaeroides*. All these facts suggest that they may not be the substrates for the  $aa_3$ -type oxidase.

**2.1.2 isocytochrome  $c_2$**  Isocytochrome  $c_2$  is also presented at a very low level in wild-type cells, although under aerobic growth conditions the expression level increases. The low abundance of isocytochrome  $c_2$  may not be enough to support cell growth by aerobic respiration. So far there is no evidence that isocytochrome  $c_2$  is involved in electron transfer to the  $aa_3$ -type oxidase, but this does not exclude the possibility that it can transfer electrons to the oxidase. Isocytochrome  $c_2$ , having less internal deletions and insertions, is more structurally related to bovine *Cc* than cytochrome  $c_2$ . Besides the fact that the redox potential of isocytochrome  $c_2$  is closer to that of bovine *Cc*, the important lysine residues (Lys-13, 27, 73, 79, 86, 87 in bovine *Cc*) are also present in isocytochrome  $c_2$  (Figure 1.10), so it will not be surprising to see that it can transfer electrons effectively to the  $aa_3$  oxidase.

**2.1.3 cytochrome  $c_{554}$**  Cytochrome  $c_{554}$  is the most abundant *c*-type cytochrome under aerobic respiration (Bartsch et al., 1989; Flory & Donohue, 1995). Based solely on its high expression level under aerobic growth conditions, it is suitable as a candidate for the oxidase substrate; but little is known about it besides its sequence, and its deletion has no effects on cell growth photosynthetically or aerobically, making deciphering its function more difficult.

The oxidases from both *R. sphaeroides* and bovine are very similar. Based on the similarity of the oxidases, it is reasonable to speculate that the substrate for *R. sphaeroides* *Cc*O should also share similarity with mammalian *Cc*, which is a good

substrate for both oxidases. In this regard, cytochrome  $c_{554}$  may be not the substrate for  $aa_3$  oxidase. Protein sequence analysis indicated that there is no similarity between cytochrome  $c_{554}$  and mammalian Cc, except for the presence of the heme binding motif. In cytochrome  $c_{554}$  (a type II cytochrome), the heme binding motif is located at the C-terminus, whereas in bovine Cc (a type I cytochrome) it is located at the N-terminus. Although there are several lysine residues in cytochrome  $c_{554}$ , it is difficult to correlate them to the lysine residues in bovine Cc without structural information.

**2.1.4 Cytochrome  $c_2$**  When  $aa_3$ -type oxidase was identified early in *R. sphaeroides*, cytochrome  $c_2$  was found to transfer electrons to the oxidase *in vitro*, although with a much lower rate than with bovine Cc does (Kituchi et al., 1965). In steady-state assays with *R. sphaeroides* wild-type oxidase, the maximum turn-over rate with *R. sphaeroides* cytochrome  $c_2$  is about one-fourth of that of bovine Cc.

Although cytochrome  $c_2$  can transfer electrons to the oxidase in *R. sphaeroides*, the deletion of the cytochrome  $c_2$  gene (except to abolish the strain's photosynthetic growth capability) has no obvious effects on the cells' aerobic growth rate (Donohue et al., 1988; Rott & Donohue, 1990), and the deletion strain has a similar generation time as wild-type strains. In the deletion strains, isocytochrome  $c_2$  might substitute for cytochrome  $c_2$  in electron transfer to  $aa_3$  oxidase as in the case of the photosynthesis process, but the deletion of both cytochrome  $c_2$  and isocytochrome  $c_2$  genes still has no major effect on cells aerobic growth (Rott et al., 1993). The expression levels of the  $aa_3$ -type oxidase and the potential effects of the deletion on the oxidase expression has not been addressed in the papers.

An alternative approach to study the electron transfer activity of cytochrome  $c_2$  from *R. sphaeroides* has been to measure the steady-state kinetics of its interaction with bovine CcO and cytochrome  $bc_1$  complex. It has been found that *R. sphaeroides* cytochrome  $c_2$  reacts at 1% of the rate of bovine Cc with bovine CcO (Errede & Kamen, 1978). The different reactivity of *R. sphaeroides* cytochrome  $c_2$  and bovine Cc with

bovine CcO suggests that the protein structures and heme electronic structures are different. Although the overall secondary structure is conserved in both *R. sphaeroides* and bovine Cc, other changes are present. Lys-13 in bovine Cc has been identified to be important in its interaction with its physiological partners (Ferguson-Miller et al., 1978). It is located next to the heme binding motif in the protein sequence, and located in the heme exposed front face on the 3-D structure, which was used to interact with other proteins. The equivalent residue of Lys-13 in *R. sphaeroides* is replaced by an glutamine residue (Figure 1.10), which can partially explain its low reactivity due to its expected wrong binding orientation. Similarly, Lys-72 was identified as critical in horse Cc binding, but is missing in *R. sphaeroides*  $c_2$  too. Moreover, the difference in redox potentials between *R. sphaeroides* and bovine Cc may also contribute to the low reactivity.

Meanwhile, it is interesting to notice that *R. sphaeroides* cytochrome  $c_2$  reacts equally well as bovine Cc with  $bc_1$  complex (Errede & Kamen, 1978). The high reactivity of with *R. sphaeroides* cytochrome  $c_2$  with bovine  $bc_1$  complex, in contrast to its low reactivity with bovine oxidase, suggests that cytochrome  $c_2$  has evolved the characteristics required for rapid electron transfer from the  $bc_1$  complex, but not for the electron transfer to the oxidase, which is also supported by the established fact that cytochrome  $c_2$  is important for photosynthesis but not for the aerobic respiration. These studies also suggest that *R. sphaeroides* cytochrome  $c_2$  may use some different residues to interact with the  $bc_1$  complex and the oxidase.

All this evidence speaks against the involvement of cytochrome  $c_2$  in mediating electron transfer from the  $bc_1$  complex to  $aa_3$  oxidase under physiological conditions. It is more likely important in mediating electron transfer from the  $bc_1$  complex to the reaction center than to the  $aa_3$  oxidase.

## 2.2 Membrane bound cytochrome *c*

Cytochrome *c*<sub>1</sub>, a membrane-bound cytochrome, is the direct electron donor to cytochrome(s) *c*, which then transfer(s) the electron to the reaction center or the CcO. Besides cytochrome *c*<sub>1</sub>, another membrane-bound Cc, cytochrome *c*<sub>552</sub>, was discovered in *P. denitrificans* (Turba et al., 1995) and *R. capsulatus* (Jenney Jr. & Daldal, 1993), two strains closely related to *R. sphaeroides*.

**2.2.1 cytochrome *c*<sub>552</sub>** In *P. denitrificans*, a complex with cytochrome *bc*<sub>1</sub>, cytochrome *aa*<sub>3</sub> oxidase and cytochrome *c*<sub>552</sub> has been isolated (Berry & Trumpower, 1985). This complex can oxidize ubiquinone rapidly in the absence of soluble cytochrome *c*<sub>2</sub>, and the activity is not significantly enhanced by added horse Cc. Anti-*c*<sub>552</sub> antibody was found to inhibit the electron transfer in the wild-type *P. denitrificans* membrane (Smith & Davies, 1991; Steinrücke et al., 1991; Turba et al., 1995). All these experiments suggest the importance of membrane-bound Cc in shuttling electrons from the *bc*<sub>1</sub> complex to the *aa*<sub>3</sub> oxidase.

The genes for cytochrome *c*<sub>552</sub> have been cloned from *P. denitrificans* (Turba et al., 1995), *R. capsulatus* (Jenney Jr. & Daldal, 1993), and *Bradyrhizobium japonicum* (Bott et al., 1991), and the protein has been purified from *P. denitrificans* (Turba et al., 1995). The molecular weights are about 20 to 22 kDa, larger than that of bovine Cc. Amino acid sequences, translated from nucleotide sequences, indicate the presence of a hydrophobic N-terminal domain and a C-terminal globular domain. The N-terminal 30 to 40 residues will form a transmembrane helix and anchor the proteins to the membrane. The C-terminal domain is highly homologous to bovine Cc, with less internal insertions and deletions than cytochrome *c*<sub>2</sub> from both *P. denitrificans* and *R. sphaeroides*. With most of the important residues conserved, this C-terminal domain will likely to form the typical "cytochrome *c* fold" structure. The lysine residues conserved in mammalian Cc are retained in the *Paracoccus c*<sub>552</sub> and to different degrees among species. The neck region between the N-terminal transmembrane region and the C-terminal domain is rich in alanine

and negatively charged residues, which may give the C-terminal domain flexibility to interact with the  $bc_1$  complex and the  $aa_3$  oxidase.

**2.2.2 cytochrome  $c_y$**  *R. capsulatus* and *R. sphaeroides* are closely related phylogenetically, but each of them still has its own distinct genetic characteristics. It has been found that the *R. capsulatus* strains lacking cytochrome  $c_2$  can still grow phototrophically (Daldal et al., 1986), while *R. sphaeroides* lacking cytochrome  $c_2$  is unable to do so (Donohue et al., 1988). The difference is also indicated by the fact that *R. capsulatus* does not have the  $aa_3$  oxidase, as *R. sphaeroides* does; instead, the terminal oxidase identified in *R. capsulatus* is a  $cbb_3$  oxidase.

The reason for the ability of the cytochrome  $c_2$  deletion strain of *R. capsulatus* to grow photosynthetically is because of the presence of a membrane-bound Cc, cytochrome  $c_y$  (Jenney Jr. & Daldal, 1993). Double deletion of both cytochrome  $c_2$  and cytochrome  $c_y$  from *R. capsulatus* completely abolishes its ability to grow phototrophically. This double deletion strain can be complemented to grow phototrophically with either cytochrome  $c_2$  or cytochrome  $c_y$  genes, indicating that either cytochrome  $c_2$  or cytochrome  $c_y$  is essential for photosynthesis only in the absence of the other. More interestingly, it has been found that the cytochrome  $c_y$  gene from *R. capsulatus* can also enable the cytochrome  $c_2$ -lacking strain of *R. sphaeroides* to grow phototrophically, further suggesting that cytochrome  $c_y$  can shuttle electrons from  $bc_1$  complex to the reaction center.

The capability of growing aerobically for the cytochrome  $c_2$  and cytochrome  $c_y$  double deletion strain of *R. capsulatus*, suggests that there must be present another electron mediator between the  $bc_1$  complex and the  $cbb_3$  oxidase in this strain. The  $cbb_3$  oxidase has two covalently bound cytochromes  $c$  at the C-terminus of subunit II, and another one at subunit III. One of them may shuttle electrons from the  $bc_1$  complex to the oxidase itself, although more experimental data is needed to prove it. However, one

fact needs to be pointed out; that subunit III of the *cbb*<sub>3</sub> oxidase and cytochrome *c*<sub>γ</sub> from *R. capsulatus* show little similarity.

In *Bradyrhizobium japonicum*, the insertional inactivation of membrane-bound cytochrome also renders the strain an *aa*<sub>3</sub> oxidase-negative phenotype (Bott et al., 1991). The authors explain that the assembly of the *aa*<sub>3</sub> oxidase is dependent on the incorporation of the membrane bound cytochrome to the cytoplasmic membrane. The effect on the *aa*<sub>3</sub> oxidase of the deletion of cytochrome *c*<sub>γ</sub> from *R. capsulatus* is not discussed in that paper.

**2.2.3 Is there a membrane-bound cytochrome *c* in *R. sphaeroides*?** Although membrane-bound cytochrome *c*<sub>γ</sub> from *R. capsulatus* can enable the cytochrome *c*<sub>2</sub> deletion strains of *R. sphaeroides* to grow phototrophically, the membrane-bound cytochrome *c*<sub>γ</sub> from *R. sphaeroides*, if there is one, has not been purified and its gene has not been cloned. Its presence in *R. sphaeroides* has been suggested from kinetics study by measuring the TMPD oxidase activity with the cytoplasmic membranes (Hosler et al., 1992). A substantial oxygen consumption rate has been observed when TMPD was added to the membranes. However, this result is complicated to interpret because of the presence of the *cbb*<sub>3</sub> oxidase in *R. sphaeroides*. The *cbb*<sub>3</sub> oxidase in *R. sphaeroides*, having three covalently attached *c*-type cytochromes, can efficiently accept electrons from TMPD and reduce oxygen.

**Footnote:** The membrane-bound cytochrome *c*<sub>γ</sub> in *R. sphaeroides* was cloned after this chapter was finished (F. Daldal, personal communication), and found to be highly similar to the *c*<sub>552</sub> from *P. denitrificans*, with a transmembrane domain at the C-terminus of the protein. The lysine counterparts for Lys-8, -13, -72, -79, -87 in horse *Cc* are present in *c*<sub>γ</sub> from *R. sphaeroides* too, while the lysine residues equivalent to Lys-27, -86, -88 are missing (Figure 1.10).

### 3 Summary

To accommodate its versatile growth conditions, *R. sphaeroides* cells have evolved several electron transfer systems. These systems are branched at the quinone pool and after the  $bc_1$  complex. Both the photosynthesis and respiration processes share the  $bc_1$  complex, which enables the cells to adapt from one environment to another very rapidly by using already established complexes. Among these systems, cytochromes *c* are involved in transferring electrons. Several *c*-type cytochromes have been identified in *R. sphaeroides*, and it may be expected that more will be discovered. In wild-type cells, the primary function for cytochrome  $c_2$  is transferring electrons from the  $bc_1$  complex to the reaction center. *In vitro* experiments also indicate that it can transfer electrons to the  $aa_3$  oxidase at a much slower rate than bovine Cc.

A membrane-bound Cc has been identified in several systems, including *R. sphaeroides*. Except for having an N-terminal transmembrane region and a neck region, these membrane-bound cytochromes are highly homologous to the mammalian Cc. Genetic studies found that these membrane-bound cytochromes *c* can transfer electron rapidly to the  $aa_3$  oxidase in the cytoplasmic membrane, and it is probably the physiological substrate for the  $aa_3$  oxidase.

Chemical modification studies have indicated that mammalian Cc using similar residues to interact with the  $bc_1$  complex and CcO, and electrons enter and exit by that same way. As the physiological substrate for the  $aa_3$  oxidase, the membrane-bound Cc will interact with the  $bc_1$  complex and the  $aa_3$  oxidase through lateral diffusion, rather than free diffusion. The transmembrane region of the membrane-bound Cc will anchor itself to the membrane, and the neck region, acting as a hinge, would moves the C-terminal globular domain back and forth from the  $bc_1$  complex to the  $aa_3$  oxidase. The localization of membrane-bound Cc close to both the  $bc_1$  complex and the  $aa_3$  oxidase will enable more efficient electron transfer to take place.

## V. Research significance

Previous studies have shown that subunit II of CcO is the primary Cc binding site, and the Cu<sub>A</sub> center in CcO has resolved to be a binuclear center, but the exact binding site for Cc and the functional significance of the binuclear character of the Cu<sub>A</sub> center are still not clear. In this study, site-directed mutagenesis, in combination with biochemical and biophysical techniques, was used to address these questions.

In order to use site-directed mutagenesis technique to study related issues associated with subunit II, the gene encoding subunit II of CcO in *R. sphaeroides* has to be deleted from the chromosome. The procedure for the deletion of the *coxII/III* operon was described in chapter II. The deletion of *coxII/III* operon in strain YZ200 was confirmed through genetic and spectral analyses. More important, this deletion strain, YZ200, can be complemented with the *coxII/III* operon through plasmid pRK415-1, which making it a good system for mutational analysis of subunit II of CcO.

The expression level of CcO in wild-type *R. sphaeroides* strains are very low, and the levels in some of the low activity mutant strains are even lower, making the purification of CcO even difficult. In chapter III, several strategies for attempting to overexpress CcO in *R. sphaeroides* were described, including the method by ligating the two operons of CcO gene together and introducing them back into *R. sphaeroides* through a multicopy plasmid pRK415-1, which yielded up to seven-fold production of CcO. A high-yield protocol for purifying homogeneous oxidase was also reported.

With the establishments of the *coxII/III* deletion strain and the CcO overexpression systems, a number of residues in subunit II of CcO in *R. sphaeroides* has been mutated and the oxidases have been purified in a large amount for biochemical and biophysical studies, which is reported in chapter IV and V.

Chapter IV describes the mutational studies on Cc binding. Several mutants were created, and characterized using optical spectra, EPR spectroscopy, metal analysis, steady-state and rapid kinetics. These studies suggest that Glu-148, Glu-157, Asp-195 and Asp-214 in subunit II of CcO are involved in Cc binding, and Trp-143 is the electron entry site to CcO.

The Cu<sub>A</sub> ligands were mutated and the analysis of these mutants were described in chapter V. In this study, the binuclear character of Cu<sub>A</sub> center was found to be important for maintaining the right redox potential for rapid electron transfer from Cu<sub>A</sub> to heme *a*, while it is not required for proton pumping.

The overexpression system described here not only enables this study to be finished, but will also provide materials for other studies on CcO, including x-ray crystallography. The definition of the Cc binding site in subunit II and the study on the functional significance of the binuclear character of Cu<sub>A</sub> will enable us to further understanding the energy conservation mechanism of this important enzyme.

## CHAPTER II

### **Development of systems for site-directed mutagenesis in subunit II of cytochrome *c* oxidase from *Rhodobacter sphaeroides***

These experiments were based on previous unpublished results done by John Fetter and Scott Boley, who designed the plasmid pJB101A.

## Introduction

The sequences of the three largest subunits of CcO in bacteria are highly homologous to the three largest subunits of the mitochondrial enzyme, and, in fact, the resolved crystal structures from both the *Paracoccus denitrificans* and bovine heart enzymes have shown that these subunits in both systems are structurally almost identical (Iwata et al., 1995; Tsukihara et al., 1996). The genes for the three subunits of the  $aa_3$ -type CcO from *Rhodobacter sphaeroides* have been cloned and show similar high homology to the corresponding genes from bovine heart (Cao et al., 1991; 1992; Shapleigh & Gennis, 1992).

*R. sphaeroides*, with a branched electron transfer system, can thrive not only as an anaerobic phototroph, but also as a facultatively microaerophilic to aerobic chemotroph. Within this branched electron transfer system, the  $aa_3$ -type CcO functions when cells are grown under aerobic conditions, induced by high oxygen tension. Because of the presence of multiple electron transfer pathways in *R. sphaeroides*, the cells can survive when one pathway malfunctions by relying on alternatives. This characteristic of *R. sphaeroides*, together with the well-characterized genetic properties of this strain (Donohue & Kaplan, 1991), enable us to use genetic techniques, including deletions and mutations, to study the structural and functional aspects of  $aa_3$ -type CcO.

Due to the fact that  $aa_3$ -type oxidase from *R. sphaeroides* has a simpler but highly homologous structure to the eukaryotic enzymes, it has become a good model system for studying CcO, as evidenced by the fact that mutational analysis using the *R. sphaeroides* system (Hosler et al., 1993) was successful in determining the structures and the arrangements of the metal centers in the oxidase that were later confirmed from

crystallography (Iwata et al., 1995; Tsukihara et al., 1995).

Among the three largest subunits of CcO, subunit II is the likely primary site for substrate binding (Millett et al., 1983). A unique binuclear Cu<sub>A</sub> center in subunit II accepts electrons from Cc and transfers them to heme *a* and the heme *a*<sub>3</sub>-Cu<sub>B</sub> centers, which reside in subunit I. To accurately define the Cc binding site and to study the structure and function of the Cu<sub>A</sub> center, It is necessary to delete the operon encoding subunit II and subunit III (*coxII/III*) in *R. sphaeroides*. An insertional/deletion strain has been created Cao et al., (1992), which, abolishes the ability of expressing *aa*<sub>3</sub> oxidase, but this is not a good system for mutagenesis due to the possibility of recombination between the inactivated copy in the genome and the copy in the plasmid. In this study, the *coxII/III* operon, including the two intervening open reading frames (*orf1* and *orf3*), has been deleted from the bacterial chromosome, resulting in the loss of the *aa*<sub>3</sub>-type CcO from the membrane in the deletion strain. Upon complementation of this deletion strain with the entire *coxII/III* operon, the *aa*<sub>3</sub>-type oxidase can be restored, which makes it possible to use site-directed mutagenesis techniques to study the structure and functions associated with subunit II.

## Materials and Methods

**Material** All restriction endonucleases, other DNA-modifying enzymes and the DIG/Genius<sup>TM</sup> system were from Boehringer Mannheim (Indianapolis, IN); Plasmids pHP45Ω, pRK415-1 and *E. coli* strain S-17-1 were obtained from the sources indicated in Shapleigh and Gennis (Shapleigh & Gennis, 1992). Plasmid pYJ100 containing the sequence of *coxII* and *coxIII* was originally prepared by Cao et al. (1992) (Figure 2.1).

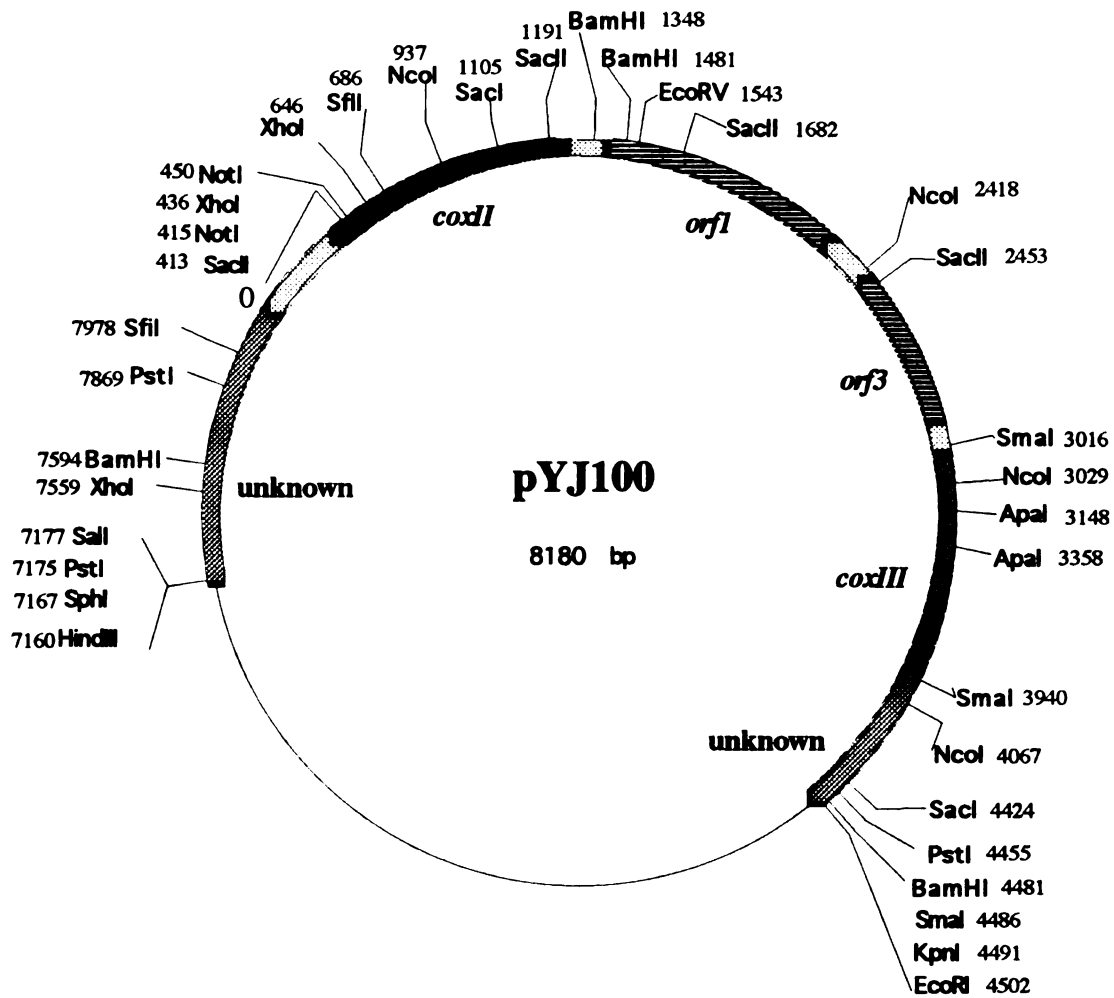


**Figure 2.1** Restriction map of pYJ100 with *coxII/III* operon. The positions of the restriction sites located within the *coxII/III* operon are from Cao (1991; 1992), and the others are based on the best estimations from the available sequence information.

pJP5603 was obtained from the University of Illinois.

**Cell growth** *E. coli* strains S-17-1 and TG1 were grown in LB medium at 37°C.

Plasmids pUC19, pRK415-1, pJP5603 and their derivatives were maintained in the presence of the following antibiotics: ampicillin (Ap) (50 µg/ml), streptomycin (Sm) (50 µg/ml), spectinomycin (Sp) (50 µg/ml), kanamycin (Kn) (25 µg/ml) and tetracycline (Tc) (15 µg/ml).

*R. sphaeroides* strain Ga was grown aerobically in Siström's media at 30°C in flasks with rapid swirling. Strains of *R. sphaeroides* harboring a Sm/Sp resistance cartridge were maintained in the presence of Sm (50 µg/ml) and Sp (50 µg/ml). For cells containing pRK415-1 derivatives, Tc was added to the medium at 1 µg/ml.

**Isolation of genomic DNA** *R. sphaeroides* genomic DNA was isolated from cells by the method of Davis et al. (Davis et al., 1980). Briefly, after growing to late exponential phase, cells were lysed by a freeze/thaw protocol in the presence of lysozyme and sodium dodecyl sulfate. Protein was extracted repeatedly using phenol and chloroform to remove DNA, and the residual RNA was degraded by treatment with RNase prior to storage.

**Construction of plasmid pJP-pJB** Creation of a mutant strain of *R. sphaeroides* with a deleted *coxII* gene was accomplished by a plasmid, pJP-pJB (Figure 2.2). pYJ100 was digested with *SfiI* and *ApaI*, followed by blunt-ending with T4 DNA polymerase. The 4.6-Kb fragment from the pYJ100 digestion, without *coxII* and *orf* genes, was ligated with the Ω fragment, to create plasmid pJB101A (Figure 2.2). The Ω fragment, containing the Sm/Sp drug resistance cartridge, was isolated from a *SmaI* digestion of plasmid pHP45Ω. Plasmid pJP-pJB was created by inserting the *EcoRI/HindIII* fragment

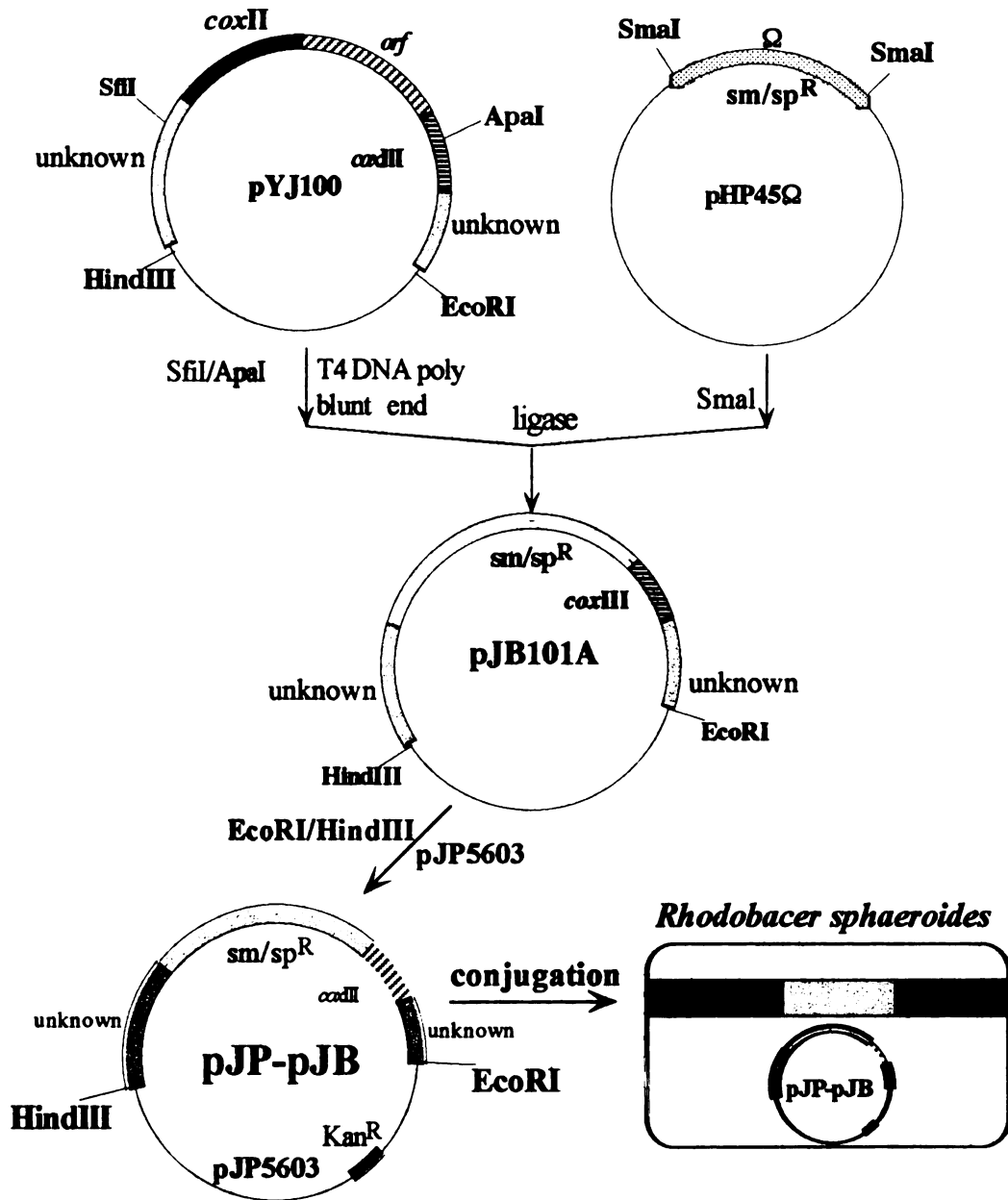


**Figure 2.2** Procedure for deletion of the *coxII/III* operon. Plasmid pYJ100 was digested with *SfiI* and *ApaI*, and the fragment without the *coxII* gene was treated with T4 DNA polymerase to blunt-end, which was ligated with the *SmaI/SmaI* Ω fragment and created pJB101A. The *EcoRI/HindIII* fragment of pJB101A was ligated to a suicide vector, pJP5603, creating pJP-pJB, which was transferred to *R. sphaeroides* through conjugation.

from pJB101A, containing the Sm/Sp resistant cartridge, into the suicide vector pJP5603.

**Conjugation** Plasmid pJP-pJB was mobilized into *R. sphaeroides* Ga by biparental conjugation using *E. coli* strain S-17-1 as the donor. Briefly, 1 ml of late exponential phase of *R. sphaeroides* Ga cells was mixed with 1 ml early exponential phase of *E. coli* S-17-1 which contains plasmid pJP-pJB. The mixture of cells was pelleted for 1 min, resuspended in 0.1 ml of LB medium, and spotted onto a nitrocellulose filter on an LB plate. After 6 h incubation at 30°C, the filter was washed with 1 ml of Sistrom's medium, and the recovered cells were further washed twice with cold Sistrom's medium before plating them on Sistrom's agar plates containing Sm/Sp antibiotics.

**Southern blots** Approximately 10 µg of genomic DNA was digested by *Sma*I overnight at 25°C and the digestion was separated on a 0.8% agarose gel. DNA was transferred to a nitrocellulose membrane through standard capillary transfer method. DNA probes were labeled with Digoxigenin using DIG/Genius™ DNA labeling and detection kit. The hybridization was detected colorimetrically according to the Genius™ detection protocol.

**Spectrophotometric analysis** Membranes were isolated from Ga and YZ200 as described in Hosler et al. (1992), and were solubilized in 100 mM KH<sub>2</sub>PO<sub>4</sub>, pH 7.0, 0.2% lauryl maltoside (LM), and the spectra were taken on a UV/visible spectrometer (Perkin Elmer, Lambda 40P). Dithionite and ferricyanide were used to fully reduce or oxidize the samples, respectively.

## Results

**Creation of a mutant strain lacking *coxII*** In plasmid pJB101A (Figure 2.2), a 3.6-Kb *SfiI/ApaI* fragment containing the *coxII* gene, 37% of the *coxIII* gene (corresponding to the first 114 residues in subunit III), the intervening open reading frames and some of the unknown region upstream of the *coxII* sequence, was replaced by a 2.0-Kb  $\Omega$  fragment which contained the Sm/Sp antibiotic resistance gene. The remaining of *coxIII* gene and the unknown sequence flanking each end of the W fragment in pJB101A were critical for providing templates for homologous recombinations. Since pJP5603 and its derivatives cannot replicate in *R. sphaeroides*, the only way to maintain the drug-resistant phenotype in cells under the selective pressure of antibiotics in Sm/Sp plates was through homologous recombination. The Sm/Sp-resistant colonies could have been created through two different mechanisms: a single-crossover, which resulted in the insertion of the whole plasmid of pJP-pJB into the genome of the bacteria, or a double-crossover, in which case the 3.6-Kb *SfiI/ApaI* fragment in the genome was replaced by the Sm/Sp-resistant  $\Omega$  fragment from plasmid pJP-pJB. The colonies derived from double-crossover could be distinguished from those from single-crossover due to the fact that the latter were also Kn-resistant, while the former were not. Among the Sm/Sp-resistant colonies acquired after conjugation, only about 1% of the colonies were Kn-nonresistant, derived from double-crossover. This low percentage was unexpected compared with the 20% observed in the subunit I deletion experiment (Shapleigh & Gennis, 1992). This may have been due to the intrinsic differences between the two suicide plasmids, pSUP202 versus pJP5306, used in these two experiments, but it was more likely due to the fact that the deleted piece in this experiment (3.6 Kb) is much longer than the one in

subunit I (1.5 Kb). One colony was picked from the Sm/Sp-resistant, Kn-nonresistant group. This mutant strain derived from *R. sphaeroides* Ga is designated YZ200.

**Characterization of the subunit II deletion strain (YZ200)** The deletion of the *coxII/III* operon was analyzed using the southern hybridization technique, as shown in Figure 2.3. The probes used in this experiment were a 1.8-Kb *SacI/SmaI* fragment (Probe C), and a 1.9-Kb *BamHI/BamHI* fragment (Probe D). The DIG-dUTP labeled probe C did not hybridize to YZ200, but hybridized to a 4.3-Kb *SmaI/SmaI* fragment in wild-type Ga, which corresponded to fragment E, as shown in Figure 2.3. This result was expected, since the *SacI/SmaI* sequence corresponding to probe C was absent from the genome of YZ200 due to the deletion. The same nitrocellulose membrane was further hybridized with probe D, which overlapped with the known sequence located upstream of the *coxII/III* operon. As expected, a 3.7-Kb band was detected in YZ200, which corresponded to fragment F (Figure 2.3). These analyses fully confirmed the deletion of the *coxII*, *orfs* and part of the *coxIII* gene, and the replacement by a 2.0-Kb Sm/Sp-resistance gene at the corresponding position.

The deletion was further confirmed by comparing the reduced minus oxidized spectra of the solubilized membranes from both wild-type Ga and YZ200 strains (Figure 2.4). The typical 606-nm peak, resulting primarily from heme *a* in the *aa<sub>3</sub>*-type oxidase, was completely absent in mutant YZ200, indicating the absence of the *aa<sub>3</sub>*-type oxidase due to the deletion.

**Complementation of the deletion strain** To test whether the *coxII* deletion strain, YZ200, could be complemented, the *HindIII/EcoRI* fragment from pYJ100, containing the whole *coxII/III* operon and some flanking sequences, was cloned into the

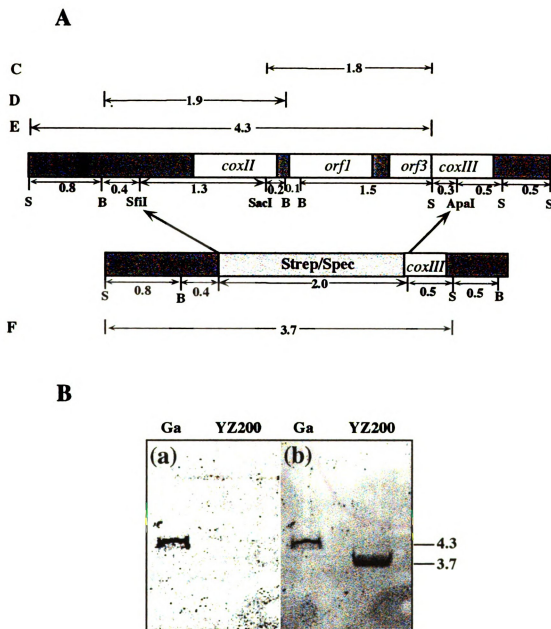


**Figure 2.3 Physical maps of the *coxII/III* operons in Ga and YZ200, and the southern blots analysis results.** Panel A: the restriction maps of the *coxII/III* operons of Ga and YZ200. S and B indicate restriction sites for *SmaI* and *BamHI*, respectively. All numbers are in kilobases. Four restriction fragments are shown in their positions relative to the operons, and their designated names are on the left. Panel B: Southern blot analyses of Ga and YZ200. Genomic DNA from Ga and YZ200 were digested with *SmaI* and separated on a 0.8% agarose gel. The digestion fragments were transferred to a nitrocellulose membrane, and first hybridized with probe C in (a), then with probe D in (b).

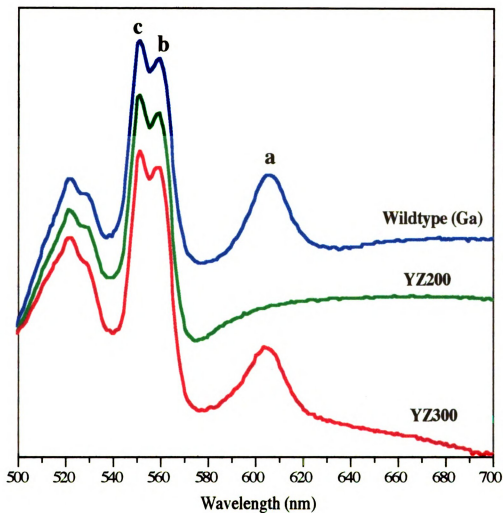


**Figure 2.4** The difference spectra of membranes derived from wild-type Ga, *coxII* deletion strain YZ200 and the recomplemented strain YZ300. The spectra were recorded as dithionite-reduced *minus* ferricyanide-oxidized difference spectra for the solubilized membranes. The peaks labeled with a, b and c correspond to the absorption peaks for heme a, b and c, respectively.

broad host range plasmid vector pRK415-1 and mobilized into YZ200 through conjugation. The difference spectrum of the solubilized membranes from this complemented strain (YZ300) clearly showed the restoration of the 606-nm peak (Figure 2.4), indicating the presence of  $aa_3$ -type oxidase. The ability to complement YZ200 from a plasmid-borne copy of *coxII/III* gene made YZ200 a potentially good system for mutational analysis of subunit II of CcO.

**Characterization of the complemented CcO** The complemented strain, YZ300, was grown in Siström's medium and the  $aa_3$ -type oxidase was isolated as described in Hosler *et al.* (1992). The purified oxidase was checked by running an SDS-PAGE gel (data not shown). All three subunits of CcO are present in YZ300, and the molecular weights and the stoichiometries of the three subunits from YZ300 were the same as those from native wild-type oxidase, indicating that genes for all three subunits were equally well expressed in YZ300, albeit from different sources; that is, genes encoding subunit I from the chromosome and subunit II and III from the plasmid. The optical spectra, CO-binding ability, the maximum turnover rate and the proton pumping activity of the purified  $aa_3$ -type oxidase from YZ300 were the same as those of the native wild-type oxidase (data not shown).

**Construction of mutation systems** Two systems were created for making mutants using a PCR technique by splitting the subunit II gene into two shorter pieces. A shorter template in a PCR reaction will reduce the error rate associated with this technique, and moreover, it is easier to get all the sequence of a short PCR product, to confirm the presence of the desired mutation and the absence of random errors. System I contains the 522-bp *NotI*<sup>415</sup>/*NcoI*<sup>937</sup> fragment from *coxII* (Figure 2.1), which covers residues from Ala-

24 to Ala-197 in subunit II. In this fragment, the *NotI*<sup>450</sup> site in the original sequence was removed, making *NotI*<sup>415</sup> a unique site. System II contains the remaining *coxII* gene and some of the *orf1* sequence in a 606-bp *NcoI*<sup>937</sup>/*EcoRV*<sup>1543</sup> fragment, including residues from Met-198 to the C-terminal of subunit II. These two systems allowed most of the residues in subunit II to be mutated.

Because of the shortage of unique restriction sites in pYJ100, the PCR fragments could not be ligated back into the *coxII*/III operon directly. To avoid this problem, several constructs were created for each system. In system I (Figure 2.5), these constructs were: pYJ006, a pUC19 derivative with the *NotI*<sup>415</sup>/*NcoI*<sup>937</sup> fragment from *coxII*; pYJ005, a pUC19 derivative with *NcoI*<sup>937</sup>/*EcoRV*<sup>1543</sup> fragment from *coxII*, with the *XhoI*<sup>436</sup>/*XhoI*<sup>646</sup> fragment located in this region being deleted; pYJ003, a construct similar to pYJ100, except that the 133-bp *BamHI*<sup>1348</sup>/*BamHI*<sup>1481</sup> fragment was deleted. Among these three constructs, pYJ006 was the template for the PCR reaction for mutating residues located at this region. After the PCR reaction and DNA sequencing confirmation, the mutagenized *NotI*/*NcoI* fragment from pYJ006 was used to replace the *NotI*/*NcoI* fragment in pYJ005, in order to recover the whole *coxII* gene. The deletion of the *XhoI*/*XhoI* fragment in pYJ005 facilitated the identification of the mutagenized fragment from the wild-type one in pYJ005, which was 210-bp shorter than the mutagenized one from pYJ006. The ligation of the mutagenized *NotI*/*EcoRV* fragment from pYJ005 with the longer *NotI*/*EcoRV* piece from pYJ003 resulted in the recovery of the whole *coxII*/III operon. The deletion of the *BamHI*/*BamHI* fragment in pYJ003 also helped to identify the mutagenized gene.

**Figure 2.5 System I for site-directed mutagenesis of residues at the N-terminal half of subunit II.** The 522 bp *NotI/NcoI* fragment in pYJ006 is the template for PCR reactions, and the \* denoted the location of the desired mutation. After sequencing confirmation, the *NotI/NcoI* piece from pYJ006 was used to replace the *NotI/NcoI* piece from pYJ005, creating pYJ004. In pYJ005, the 210 bp *XhoI/XhoI* fragment has been deleted, which would help to distinguish the two *NotI/NcoI* pieces from pYJ006 and pYJ005 in the ligation reactions based on their size differences. In pYJ003, the 133 bp *BamHI/BamHI* piece has been deleted, which will facilitate the subcloning of the *NotI/EcoRV* piece from pYJ004 with the desired mutation to pYJ003, recovering the whole *coxII/III* operon.

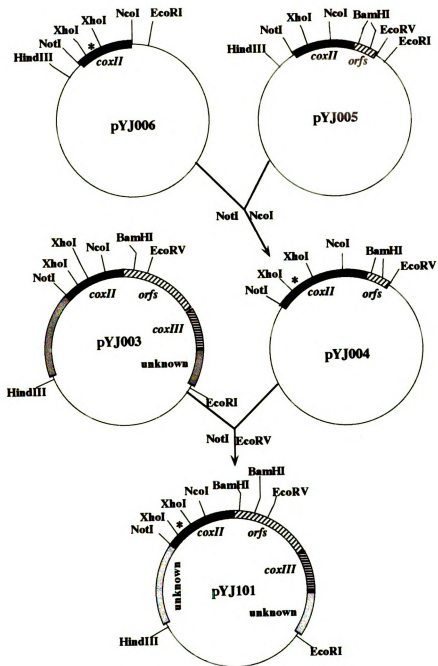


**Figure 2.5** System I for site-directed mutagenesis of residues at the N-terminal half of subunit II

A similar system was also created in system II (Figure 2.6) for mutating residues located at the C-terminus half of *coxII* gene. The three constructs were: pYJ302, a pUC19 derivative with the *NcoI*<sup>937</sup>/*EcoRV*<sup>1543</sup> fragment from pYJ100; pYJ401, a pUC18 derivative with the *HindIII*<sup>7160</sup>/*EcoRV*<sup>1543</sup> fragment, containing the upstream unknown sequence of *coxII*, the whole *coxII* gene and some *orf* sequence with the *BamHI*<sup>1348</sup>/*BamHI*<sup>1481</sup> fragment being deleted; pYJ501, a pUC18 derivative with the *EcoRV*<sup>1543</sup>/*EcoRI*<sup>4502</sup> fragment from pYJ100. Like pYJ006 in system I, pYJ302 was the template for the PCR reaction in this system. Following the similar strategy used in system I, the whole *coxII/III* operon can be recovered with the desired mutations with the help of pYJ501 and pYJ402; in the latter, the 133-bp *BamHI/BamHI* piece has been deleted.

## Discussion

Early on, the genes encoding subunit II and subunit III of *aa*<sub>3</sub>-type CcO and the intervening open reading frames were cloned and sequenced from *R. sphaeroides* (Cao et al., 1991; Cao et al., 1992). An insertional mutation of the *coxII/III* operon in the chromosome of *R. sphaeroides* Ga was created by placing a Sm/Sp-resistance gene cartridge into the *coxII* gene (Cao et al., 1992), which results in the elimination of the *aa*<sub>3</sub>-type oxidase from the membrane. The oxidase in this insertional mutation strain can be fully restored by a plasmid-borne copy of the whole operon, as shown with YZ200. However the insertional mutant strain is not sufficient for performing site-directed mutagenesis, and a complete deletion of the *coxII* gene from the chromosome is required

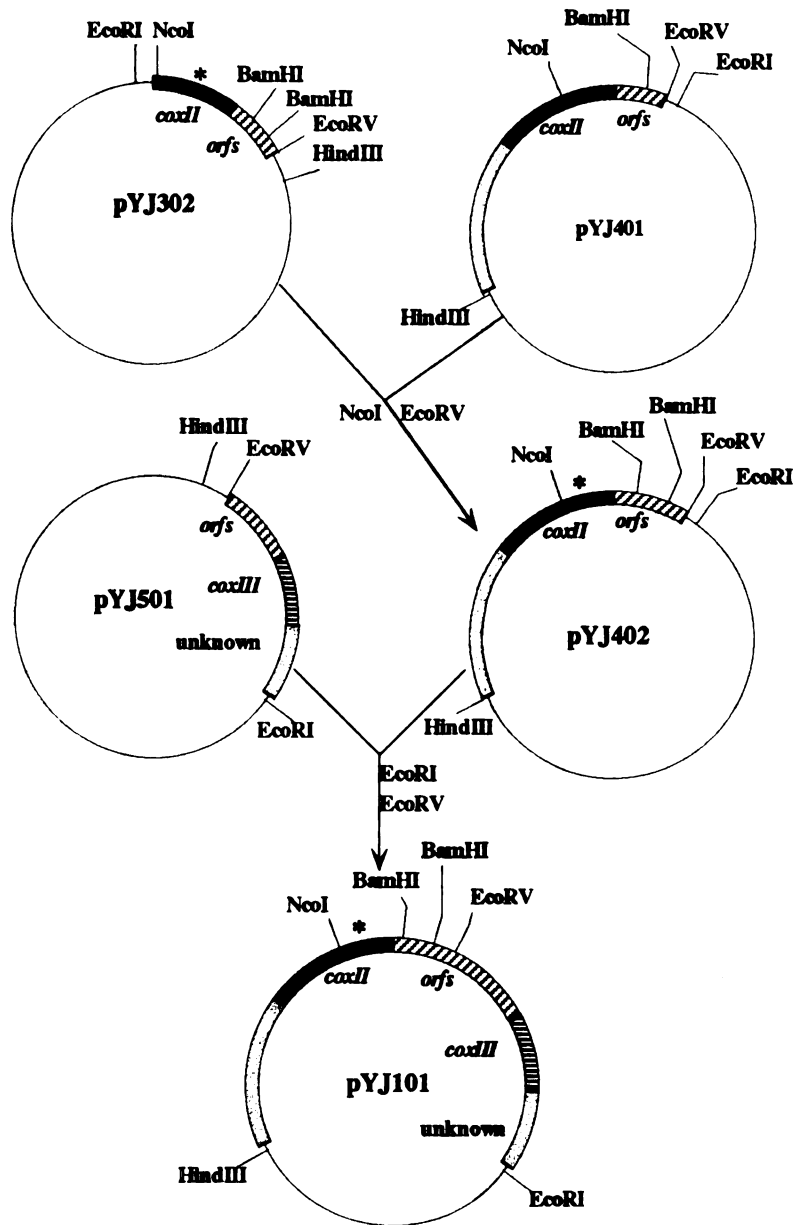


**Figure 2.6** System II for site-directed mutagenesis of residues at the C-terminal half of subunit II. The 606 bp *NcoI/EcoRV* fragment in pYJ302 is the template for PCR reactions, and the \* denoted the location of the desired mutation. The *coxII* gene can be recovered after replacing the *NcoI/EcoRV* fragment in pYJ401 with the mutagenized *NcoI/EcoRV* fragment from pYJ302. The deletion of the 133-bp *BamHI/BamHI* fragment from pYJ401 would help the identification of the fragment with the desired mutation. After ligating the *HindIII/EcoRV* fragment from pYJ402 and the *EcoRV/EcoRI* fragment from pYJ501 with *coxIII* gene, the whole *coxII/III* operon could be recovered in pYJ101

to prevent possible recombination of the plasmid-borne mutant copy with the native chromosomal gene.

In this report, *coxII*, the two *orfs* and part of the *coxIII* gene were deleted from the chromosomal DNA, as confirmed by genetic and spectroscopic analyses. The absence of the 606 nm heme *a* absorption peak in the *coxII* deletion strain indicates the absence of the *aa*<sub>3</sub>-type oxidase. In *aa*<sub>3</sub>-type oxidase, the *coxI* gene is not clustered with the genes coding for subunit II and subunit III. Therefore a *coxII/III* operon deletion is not likely to have a direct genetic effect on subunit I expression; as a result, a plasmid copy of subunit I gene is not required to complement YZ200.

The *orfI* gene encodes a protein which shows homology to the COX10 peptide in yeast and the *cyoE* peptide in *E. coli*. Genetic analysis of the COX10 mutation strain in the yeast system has suggested the important roles of COX10 in enzyme assembly and heme A synthesis (Nobrega et al., 1990). In fact, an *in vitro* assay using the *cyoE* gene product from *E. coli* indicates that the *cyoE* product is a farnesyl transferase, necessary for converting protoheme IX to heme O, an intermediate for heme A synthesis (Saiki et al., 1993). The *orf3* gene product, on the other hand, is homologous to the COX11 peptide in yeast, and the disruption of COX11 gene in yeast produced defects similar to those produced from COX10 mutation (Tzagoloff et al., 1990). COX11 protein has been suggested to be involved in heme A synthesis in the formation of the formyl group at the position 8 of the porphyrin ring (Tzagoloff et al., 1993). In this regard, the *orfI* and *orf3* gene products presumably have the same functions as COX10 and COX11, respectively. This is in line with the fact that the *coxII* gene alone can not reconstitute cytochrome *aa*<sub>3</sub> synthesis (Cao et al., 1992). YZ200, in which the *orf* genes have also been deleted,

should not have any heme A, explaining the lack of heme  $aa_3$  spectral signal.

The *coxIII* gene was not found to be essential for the complementation of the *coxII/III* operon insertionally inactivated strain (Cao et al., 1992), which can be partially complemented with only *coxII* and the *orf* genes. The oxidase produced by this complemented strain has an altered absorption spectrum (Haltia et al., 1989; Cao et al., 1992), which is similar to the one observed for the *P. denitrificans* strain in which the subunit III gene has been deleted (Haltia et al., 1989). In order to get oxidase from YZ200 with properties similar to those of the wild-type, the whole *coxII/III* operon is required for the complementation.

Two systems have been established for making site-directed mutants in the subunit II region of CcO in *R. sphaeroides*. In these two systems, several small deletion plasmids were created: in pYJ005, a 210-bp *XhoI/XhoI* fragment was deleted, while in pYJ003 and pYJ401, a 133-bp *BamHI/BamHI* fragment was deleted. These deletions will help to identify the mutagenized fragments from the wild-type ones in the ligation reactions, simply based on their size differences, thus avoiding the tedious work involved in using DNA sequencing to distinguish them. System I covers all the residues at the transmembrane region, the N-terminal fragment and part of the C-terminal soluble domain of subunit II; while system II covers the C-terminal residues around the Cu<sub>A</sub> binding site. These two systems have been tested, and the *coxII/III* operon created from these two systems can efficiently complement YZ200 strain creating desired mutants.

In summary, the *coxII/III* operon has been deleted from *R. sphaeroides*, and the deletion confirmed by genetic and spectroscopic analyses. This deletion strain can be complemented with a plasmid-borne copy of the *coxII/III* operon gene. Two systems

have also been set up for using site-directed mutagenesis techniques to study the structure and function of subunit II of CcO in *R. sphaeroides*.

## CHAPTER III

### **Overexpression and purification of cytochrome *c* oxidase from *Rhodobacter sphaeroides***

This chapter has been published as:

Overexpression and purification of cytochrome *c* oxidase from *Rhodobacter sphaeroides*  
Zhen, Y., Qian, J., Follmann, K., Hayward, T., Nilsson, T., Dahn, M.,  
Hilmi, Y., Hamer, A. G., Hosler, J. P., and Ferguson-Miller, S.

*Protein Expression and Purification*, vol. 13, n 3, 1998, p326-336

## Introduction

CcO, the last component of the energy-transducing electron-transfer chain of mitochondria and many aerobic bacteria, catalyzes electron transfer from Cc to oxygen coupled with vectorial translocation of protons to generate a transmembrane pH gradient. The mechanism of the redox-coupled proton pump is still not understood. But recently, this key enzyme was crystallized at atomic resolution from both mitochondria and bacteria (Iwata et al., 1995; Tsukihara et al., 1995; 1996; Ostermeier et al., 1997), providing the structural information necessary for more incisive mechanistic analysis.

Mammalian CcO has 13 different subunits, as well as seven metal centers (Cu<sub>A</sub>, Cu<sub>B</sub>, heme *a*, heme *a*<sub>3</sub>, Mg, Zn and Ca), resulting in a complexity of physical and genetic structure that makes structure/function analysis at a molecular level difficult. In contrast, CcO from *Rhodobacter sphaeroides*, has a simpler structure that can be manipulated with molecular genetic techniques (Cao et al., 1992; Hosler et al., 1992; 1993). The *aa3*-type oxidase from *R. sphaeroides* has only three subunits (molecular masses, 62.6, 32.9 and 30.1 kDa), but these show strong homology to the three largest subunits of its mitochondrial counterpart. Spectroscopic characterizations, and now the crystal structures, show that the six metal centers (Cu<sub>A</sub>, Cu<sub>B</sub>, heme *a*, heme *a*<sub>3</sub>, Mg, and Ca) in this bacterial oxidase are essentially identical to those in mitochondrial oxidase. The genes for CcO from *R. sphaeroides* have been cloned, sequenced, deleted and reintroduced into the bacterium (Cao et al., 1991; Shapleigh & Gennis, 1992), allowing extensive mutational analysis that successfully predicted the arrangements of the metal centers in subunit I of the oxidase (Hosler et al., 1993). Yet, relatively low expression of CcO in aerobically grown *R. sphaeroides* has somewhat limited the use of this model system. Here we

report the results of several strategies to overexpress CcO in *R. sphaeroides*, including the consolidation of all the required genes on one plasmid, the use of a fructose promoter, the use of a smaller expression plasmid and varying growth conditions of the cells. We also show that combining Ni<sup>2+</sup> affinity chromatography and anion exchange chromatography results in an enzyme preparation of purity suitable for crystallographic studies.

## **Materials and methods**

### *Materials*

All restriction endonucleases and T4 DNA ligase were obtained from Life Technologies, Inc. (Gaithersburg, MD). The gel purification kit and Ni<sup>2+</sup>-NTA resin were from QIAGEN (Santa Clarita, CA). Ultrafree-15 centrifugal filters were from Millipore (Bedford, MA), lauryl maltoside from Anatrace Inc. (Maumee, OH) and protein assay reagent from Bio-Rad (Hercules, CA). All other chemicals were reagent grade or better.

### **Growth of bacteria**

The bacterial strains and plasmids involved in this work are listed in Table 3.1. Both wild-type and overexpression strains of *R. sphaeroides* were grown at 30 °C in 2.8 liter Fernbach flasks containing 800 ml of Siström's minimal medium A (Cohen-Bazire et al., 1957). The cultures were shaken at 300 rpm and harvested at an OD<sub>660</sub> of 1.5 (late exponential phase). Approximately 60 g of wet weight cells were obtained from 10 liters of culture, containing about 90 mg of membrane-bound oxidase in the YZ100 strain (Table 3.2). The following concentrations of antibiotics were added to the corresponding

**Table 3.1 Bacterial strains and plasmids**

Strain or Plasmid	Parent	Relevant characteristics	Source or Reference
<i>E. coli</i>			
TG1		<i>supE hsd 5 thi Δ(lac-proAB) F</i> [ <i>traD36 proAB<sup>+</sup> lacI<sup>A</sup> lacZΔM15</i> ]	(Sambrook <i>et al.</i> , 1989)
S-17-1		<i>pro, res-, mod+, recA, Tp<sup>R</sup>, Sm<sup>R</sup>, integrated Rp4-2 (TC::Mu) (Kn::Tn7)</i>	(Simon <i>et al.</i> , 1983)
<i>R. sphaeroides</i>			
2.4.1		wild-type	(Van. Niel, 1944)
Ga	2.4.1	mutation in carotenoid biosynthesis	(Cohen <i>et al.</i> , 1957)
CY91	Ga	cyt. b562; Kn <sup>R</sup>	(Yun <i>et al.</i> , 1994)
JS100	Ga	<i>ΔctaD (coxI)::sm/sp</i>	(Shapleigh <i>et al.</i> , 1992)
YZ200	Ga	<i>ΔctaC (coxII), ΔctaB (orf1), ΔctaG (orf3) ΔctaE (coxIII)::sm/sp</i>	(Zhen <i>et al.</i> 1998)
YZ100	JS100	with pYJ123H	This work
YZ300	YZ200	with pYJ123H	This work
YZ400	CY91	with pYJ123H	This work
<b>Plasmids</b>			
pUC19		Ap <sup>R</sup> , ori, <i>lacZ</i>	(Yanisch <i>et al.</i> , 1985)
pRK415-1		Tc <sup>R</sup> , oriT, <i>lacZ</i>	(Keen <i>et al.</i> , 1988)
pJS3-X6H	pT7T318	His-tagged <i>ctaD (coxI)</i>	(Mitchell <i>et al.</i> , 1995)
pJS100	pT7T318	<i>ctaD (coxI)</i>	(Shapleigh <i>et al.</i> , 1992)
pYJ100	pUC19	<i>ctaC (coxII), ctaB (orf1), ctaG (orf3), ctaE (coxIII)</i>	(Zhen <i>et al.</i> 1998)
pYJ123H	pUC19	<i>ctaC (coxII), ctaB (orf1), ctaG (orf3), ctaE (coxIII) and His-tagged ctaD (coxI)</i>	This work
pJQ100	pUC19	<i>ctaC (coxII), ctaB (orf1), ctaG (orf3), ctaE (coxIII) and non-His-tagged ctaD (coxI)</i>	This work
pTN100	pUC18	FruP, <i>ctaC (coxII), ctaB (orf1), ctaG (orf3), ctaE (coxIII), ctaD (coxI) and two promoters .</i>	This work
pTN200	pUC18	FruP, <i>ctaD (coxI) and its promoter region.</i>	This work
pTN300	pUC18	FruP, <i>ctaC (coxII), ctaB (orf1), ctaG (orf3), ctaE (coxIII), ctaD (coxI) and coxI promoter</i>	This work
pTN400	pUC18	FruP, <i>ctaC (coxI).</i>	This work
pBBR1MCS-2		Kn <sup>R</sup> , <i>lacZ</i> , mob, pT7P3	(Kovach <i>et al.</i> , 1994)
pBBR1MCS-4		Ap <sup>R</sup> , <i>lacZ</i> , mob, pT7P3	(Kovach <i>et al.</i> , 1994)
pFRKI		Ap <sup>R</sup> , Gm <sup>R</sup> , Kn <sup>R</sup> , Ble <sup>R</sup> , FruP	(Duport <i>et al.</i> , 1994).

**Table 3.2 Purification of cytochrome *c* oxidase from overexpression strain YZ100**

Steps	Specific heme A content nmol/mg protein	Purification (fold)	Total <i>aa3</i> (mg) (from 10 L culture)	Yield (%)
Broken cells	0.3	1	90	100
solubilized inner membrane	0.8	3	86	96
Ni <sup>2+</sup> -NTA	12.2	41	77	85
DEAE-5PW	17.2	57	61	68

cultures: streptomycin (Sm), 50  $\mu\text{g/ml}$ ; spectinomycin (Sp), 50  $\mu\text{g/ml}$ ; tetracycline (Tc), 1  $\mu\text{g/ml}$ ; kanamycin (Kn), 25  $\mu\text{g/ml}$ . The *Escherichia coli* strains, TG1 and S-17-1, were grown aerobically at 37 °C in LB broth. Plasmids were maintained in *E. coli* in the presence of ampicillin (Ap), 50  $\mu\text{g/ml}$ , or Tc, 15  $\mu\text{g/ml}$ .

In the experiments testing the effect of pH on oxidase expression, the cells were grown at 30 °C in 500 ml flasks with 100 ml of Siström's medium; the flasks were inoculated with identical aliquots of a YZ100 culture to achieve an initial OD<sub>660</sub> of 0.1. The pH of the pH 6.5 culture was kept constant during the whole experiment, by adding hydrochloric acid. The other cultures, started at pH 7.0, were allowed to reach the desired pH at which they were maintained. All cells were harvested at an OD<sub>660</sub> of about 1.5.

### **Construction of the overexpression plasmid pRK-pYJ123H**

The procedure for creating pRK-pYJ123H is shown in Figure 3.1. Briefly, plasmid pJS3-X6H2, which contains the His-tagged subunit I gene, was digested with restriction endonuclease *Sma*I. The 2.0-kb *Sma*I/*Sma*I fragment, containing the subunit I gene (*cox*I), was then subcloned into pUC19 at the unique *Sma*I site at the polylinker region, creating pJS3-SH. A 4.8-kb *Pst*I/*Pst*I fragment from pYJ100, which contains *cox*II, *orf*1, *orf*3 and *cox*III genes, was subcloned into pJS3-SH through the unique *Pst*I site, located between *Hind*III and *Sma*I site in the polylinker region. The new plasmid, containing all the three subunit genes of CcO, is named pYJ123H. All the CcO genes were cloned into the broad-host-mobile expression vector pRK415-1, using *Eco*RI and *Hind*III to prepare pRK-pYJ123H, which was mobilized into *R. sphaeroides* by

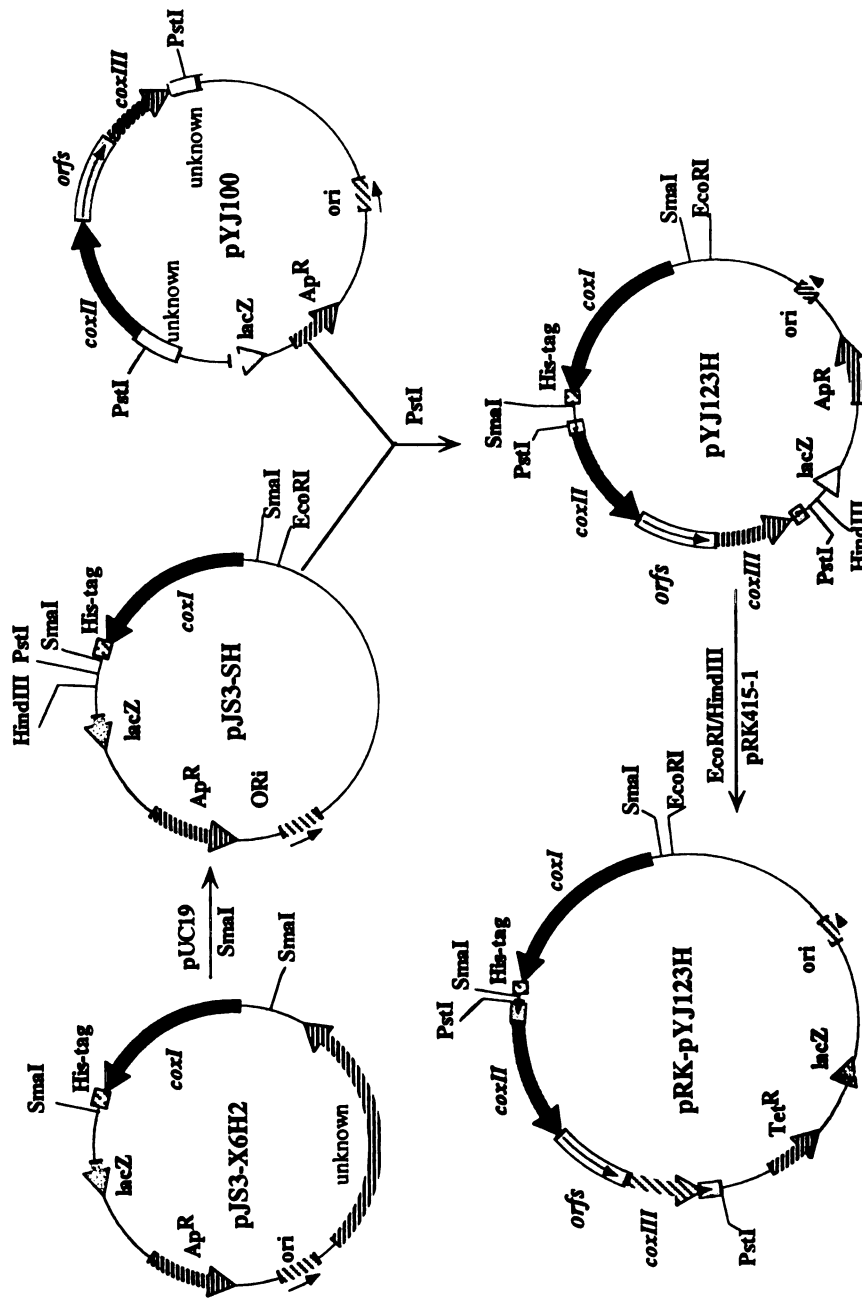


**Figure 3.1** The procedures for construction of the overexpression plasmid pRK-pYJ123H. The detail is described as in Materials and methods.

biparental conjugation using *E. coli* strain S-17-1 as the donor (Cao et al., 1992).

Incubation with bacteriophage T4 was omitted for the conjugation procedure.

### **Construction of pBBR1MCS expression and fructose promoter (*fruP*)-containing plasmids**

A series of broad-host-range cloning vectors, pBBR1MCS1-5, have been constructed for gram-negative bacteria (Kovach et al., 1994). These vectors are smaller than pRK415-1 (5 kb *versus* 9 kb) and have five different antibiotic resistant forms. Small vectors presumably will shorten the replication cycle and enhance the expression level, and they are also more stable than large plasmids which are frequently observed to be partially deleted during conjugation processes. Vector pBBR1MCS-2 (Km<sup>R</sup>) and pBBR1MCS-4 (Ap<sup>R</sup>) were tested because of the presence of an *EcoRI* site at the polylinker site. The *EcoRI/HindIII* fragment from pYJ123H, containing the *coxI* and *coxII/III* operons was ligated into the polylinker regions of pBBR1MCS-2 and -4. These constructs were transferred into strains JS100 and YZ200 through conjugation with S-17-1 strains, which contain these constructs.

Plasmid pFRKII contains the fructose promoter (*fruP*) isolated from *Rhodobacter capsulatus*. To facilitate subcloning foreign genes downstream of *fruP*, a *NdeI* restriction site (CATATG) was constructed immediately after *fruP* (Duport et al., 1994). This arrangement allows insertion of any foreign gene into *fruP* when a CAT sequence is added in front of the start codon (ATG), creating the *NdeI* site. The 660-bp *BamHI/HindIII* fragment from pFRKII, which contains *fruP*, was subcloned into pUC18 first, and the *EcoRI/HindIII* fragment from pYJ123H, containing the *coxI* and *coxII/III* operons, was then subcloned downstream of *fruP* through standard molecular biology techniques,

creating pTN100. Three more plasmids were derived from pTN100. In pTN200, the *coxII/III* operon was removed and *fruP* was placed in front of the *coxI* operon. In plasmids pTN300 and pTN400, the upstream sequences of *coxII* and *coxI* were removed, which placed *fruP* immediately in front of the coding regions of *coxII* and *coxI*, respectively. All four plasmids were ligated to pRK415-1 and transferred to strains JS100 and YZ200 through conjugations. The cells containing these plasmids were grown in Siström's medium with and without the presence of 5 mM fructose.

### **Preparation of cytoplasmic membranes**

Membranes were prepared as described previously (Mitchell & Gennis, 1995; Qian et al., 1997) with some modifications. Approximately 40 g of wet weight cells were resuspended in 200 ml of 50 mM  $\text{KH}_2\text{PO}_4$ , pH 6.5, 1 mM EDTA, 50 mg/ml DNaseI, and broken by two passages through a French pressure cell at 20,000 psi. Whole cells and debris were removed by centrifugation at 30,000 g for 30 min. The membranes were pelleted by centrifugation of the supernatant at 200,000 g for 1.5 h and the pellets were resuspended in 10 mM Tris-HCl, 40 mM KCl, pH 8.0, at 6 mg protein/ml (Bradford, 1976). Lauryl maltoside (LM) was added to a final concentration of 1% for solubilization. The membranes were stirred in LM at 4 °C for 20 min, and then centrifuged at 200,000 g for 30 min to remove unsolubilized material.

### **$\text{Ni}^{2+}$ -NTA purification of CcO**

The solubilized membranes were mixed with  $\text{Ni}^{2+}$ -NTA resin at a ratio of 1 ml of packed resin for every 2.5 mg of oxidase. To prevent nonspecific binding, 10 mM imidazole was included. The mixture was stirred at 4 °C for 1 h and then poured into a

gravity column and washed with 10 mM Tris-HCl, pH 8.0, 40 mM KCl, 10 mM imidazole, 0.1% LM until the brown colored membrane proteins were completely washed away and the flow-through was clear of color and turbidity. The column was further washed with 5 bed volumes of 10 mM Tris-HCl, pH 8.0, 40 mM KCl, 20 mM imidazole, 0.1 % LM, followed by 5 vol of 10 mM Tris-HCl, pH 8.0, 40 mM KCl, 0.1% LM to remove the imidazole. The enzyme was eluted slowly with 100 mM histidine, 10 mM Tris-HCl, pH 8.0, 40 mM KCl, 0.1 % LM. The oxidase containing fractions (green colored) were pooled and washed several times using 10 mM  $\text{KH}_2\text{PO}_4$ , pH 7.6, 1 mM EDTA, 0.2% LM by centrifugal filtration in Ultrafree-15 centrifugal filters to reduce the histidine level to less than 1 mM.

#### **FPLC-DEAE chromatography**

Approximately 15 mg of  $\text{Ni}^{2+}$ -NTA purified CcO in 10 ml of final wash buffer (above) made up to 3% in LM at 0 °C for 30 min, was applied to tandem DEAE-5PW columns (8 mm x 7.5 cm, TosoHaas) attached to an FPLC system (Pharmacia LKB Biotechnology Inc.). The columns were preequilibrated with 10 mM  $\text{KH}_2\text{PO}_4$ , pH 7.6, 1 mM EDTA, 0.2 % LM, and the oxidase was eluted with a 45-ml gradient of 0.01-0.35 M KCl in the same buffer at a flow rate of 0.5 ml/min. Oxidase-containing fractions were collected and stored at -80 °C.

#### **Visible spectra**

Visible spectra of dissolved membranes were recorded with a Perkin-Elmer Lambda 40P UV-Visible spectrophotometer at 25 °C after the membranes were resuspended in 10 mM Tris-HCl, pH 8.0, 40 mM KCl and 0.1 % LM. The extinction

coefficients used were  $\Delta\epsilon_{606-640} = 40 \text{ cm}^{-1} \text{ mM}^{-1}$  for dithionite-reduced spectra, and  $\Delta\epsilon_{606-630} = 24 \text{ cm}^{-1} \text{ mM}^{-1}$  for dithionite-reduced minus ferricyanide-oxidized difference spectra (Vanneste, 1966).

### **Protein and heme A determinations**

Protein concentrations were determined using the Bradford method (Bradford, 1976) and bovine serum albumin was used as the standard. The concentration of heme A was determined by the pyridine hemochrome method (Berry & Trumpower, 1987). Briefly, NaOH and pyridine were added to the dissolved samples to a final concentrations of 0.2 N and 10 %, respectively, the solutions were clarified by brief centrifugation in a microcentrifuge, and reduced *minus* oxidized spectra were recorded. A  $\Delta\epsilon_{588-620} = 25 \text{ cm}^{-1} \text{ mM}^{-1}$  was used to calculate the heme A content.

## **Results**

### **Construction of the overexpression plasmid pRK- pYJ123H**

The genes for the three subunits of CcO from *R. sphaeroides* are located in two separate operons along with two genes that code for proteins (ORF1 and ORF3) involved in heme A synthesis (Tzagoloff et al., 1990; 1993). In the construct described here (Figure 3.1), the two CcO operons were linked together, with each operon retaining its own promoter region. A 207-bp 5'-region in front of the *coxI* was found to be sufficient for the expression of subunit I; this region appears to contain an oxygen-regulated promoter for *coxI* (Shapleigh & Gennis, 1992). Similarly, an oxygen-regulated promoter

for *coxII/III* has been located 150-bp upstream of the *coxII* coding region (Flory & Donohue, 1997). Constructs made with either orientation of the *coxII/III* operon, with respect to that of *coxI*, showed equal overexpression, consistent with the presence of separate promoters for the two operons.

### **Comparison of expression levels in different strains**

To study the yield of *aa<sub>3</sub>*-type oxidase, pRK-pYJ123H was transferred into JS100, YZ200, and CY91 through pRK415-1, creating strains YZ100, YZ300 and YZ400, respectively (Table 3.1). These strains, along with three wild-type strains containing only the genomic copies of the oxidase genes, were grown in Siström's media starting with an initial pH of 7.0, and with no pH adjustment during cell growth. When the cells were harvested at OD<sub>660</sub> of 1.5, (about 30 h for the wild-type strains and 48 h for the overexpression strains), the pH had risen to 8.6 - 8.9. The reduced minus oxidized spectra for membranes isolated from these strains are shown in Figure 3.2.

Cytochrome *aa<sub>3</sub>* expression was compared by the ratio of absorbance at 606 nm to that of 560 nm (cytochrome *a*/cytochrome *b* or *a/b* ratio). Two wild-type strains, 2.4.1 and Ga, shared similar *aa<sub>3</sub>* expression with *a/b* ratios of 0.20. CY91, another wild-type strain with a kanamycin insertion in the gene for cytochrome *b<sub>562</sub>*, showed somewhat higher *aa<sub>3</sub>* expression, as observed previously (Hosler et al., 1992; Yun et al., 1994). In contrast, all the strains containing the plasmid pRK-pYJ123H gave much higher expression. The *a/b* ratios for YZ100 and YZ300 are 1.29 and 1.40, respectively, while YZ400, with the additional background oxidase level, has an *a/b* ratio of 1.5. Based

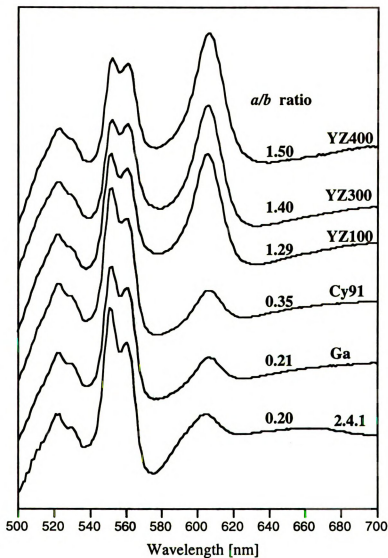


**Figure 3.2** Cytochrome *c* oxidase content in cytoplasmic membrane prepared from different *R. sphaeroides* strains. All the strains were grown at 100 ml of Siström's medium and harvested at  $OD_{660}$  of 1.5. Dithionite-reduced minus ferricyanide-oxidized spectra were recorded for the solubilized membrane from different strains. The cytochrome *a* to cytochrome *b* (*a/b*) ratios were calculated as  $A_{606-630}/A_{560-580}$ ; the ratios for different strains are shown on their spectra.

on the  $a/b$  ratios, all of the pRK-pYJ123H-containing strains increase the  $aa_3$  expression levels about four fold over CY91 and seven-fold over Ga and 2.4.1 (Figure 3.2).

Heme A content per milligram of membrane protein was also determined, giving values of 0.20 and 0.82 nmol of heme A/mg protein for the cytoplasmic membranes of CY91 and YZ100, respectively, consistent with over four fold increase of CcO content estimated by the  $a/b$  ratio. The oxidase content in the cytoplasmic membrane increases from 1.2% in CY91 to 5 % in YZ100, based on the results of protein assays. The high content of oxidase in the overexpression strains renders their cytoplasmic membrane a greenish color, in contrast to the reddish color of CY91 membrane.

#### **Effect of pH on CcO expression**

*R. sphaeroides* is routinely grown in Siström's medium prepared with an initial pH of 7.0. Due to the consumption of succinic acid (the carbon source) during growth, the pH of the medium slowly increases to a maximum of 8.9 after 48 h cell growth. To test the effect of pH on the expression of the oxidase, four batches of YZ100 cells were grown in Siström's media at pH values of 6.5, 7.0, 7.5 and 8.0, respectively. After 20 h, cells grown in pH 6.5 and 7.0 media reached an  $OD_{660}$  of 1.5, while cells grown in pH 7.5 and 8.0 media required about 40 and 48 h, respectively, to reach that OD. Spectra of membranes from these cells are shown in Figure 3.3. The  $a/b$  ratios increase from 0.37 to 1.32 with the increase in initial pH. Thus, higher pH results in higher  $aa_3$  expression, although the growth rate is slowed. The difference in the  $a/b$  ratio between pH 8.0 and pH 6.5 is over three fold. The final  $a/b$  ratio at pH 8.0, however, is not significantly different from the experiment of Figure 3.2, where the culture was allowed to continuously increase in pH with time. For CY91 the effect of pH is also significant,

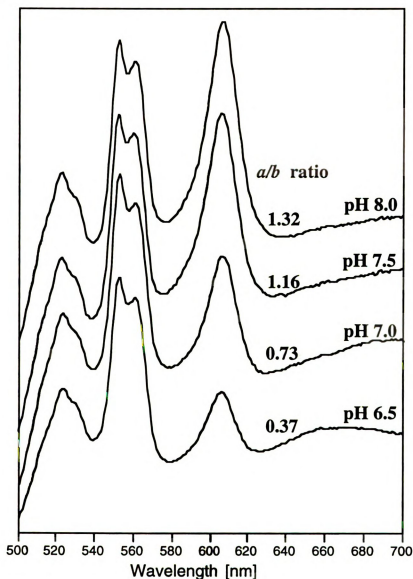


**Figure 3.3** Effect of pH on cytochrome *c* oxidase expression in YZ100 strain. The growth of the cells is as described in Materials and Methods. Reduced minus oxidized spectra were recorded for the solubilized membranes. The cytochrome *a* to cytochrome *b* (*a/b*) ratios are shown on the spectra.

giving an increase in the  $a/b$  ratio from 0.12 to 0.35 with an increase in pH from 6.5 to 8.9. Initiating the growth at pH 7.0 is advantageous, since it allows the cells to get started under conditions favorable to rapid growth.

#### **Effect of salt concentration on CcO expression**

Under stress conditions, such as high pH, cells tend to express more oxidase than under optimal growth conditions. The stress effect of high salt on *aa3* expression was also tested for all the *R. sphaeroides* strains. The presence of extra NaCl (200 mM) in addition to the 9 mM NaCl in Sistrom's media had no major effect on cell growth rate. However, the oxidase expression levels in the wild-type strains are slightly decreased, and no dramatic changes are seen in the overexpression strains. Under high salt growth conditions, the cultures of all strains, except CY91, began to turn green after the cell density reached an OD<sub>660</sub> of over 1.0. The optical spectra of the whole membranes from these strains showed the presence of an extra absorption peak at 475 nm, indicating the presence of large amounts of carotenoid and bacteriochlorophyll, the important components in the light harvesting photosynthetic system. High salt begins to induce the synthesis of the photosynthetic pigments at the late growth phase for most of the strains, except in CY91. In CY91, the gene for cytochrome *b<sub>562</sub>* is deleted, which appears to inhibit the induction of the photosynthetic pigments.

#### **Expression of genes encoding CcO using a small vector pBBR1MCS and *fruP* gene**

After the pBBR1MCS-2 and -4 plasmids, together with the oxidase genes, were transferred into JS100 and YZ200 through conjugation, the cells were plated in Sm/Sp/Kn (SSK)- and Sm/Sp/Ap (SSA)-resistant plates for pBBR1MCS-2 and pBBR1MCS-4

containing cells, respectively. Cells containing plasmid pBBR1MCS-4 failed to grow on SSA plates, while a small number of colonies from pBBR1MCS-2 containing cells were observed on SSK plates, and these cells were further grown in Siström's medium. The optical spectra of the isolated membranes from pBBR1MCS-2 containing cells showed that CcO genes were expressed in these cells, but the expression level was relatively low. The *a/b* ratio of 0.3 is comparable to that of wild-type strains, but significantly lower than those using pRK415-1 as expression vector.

Transcription of the CcO genes in pYJ123H is controlled by the native promoters. In an attempt to induce even better expression, a more efficient promoter was sought. The fructose promoter (*fruP*) from *Rb. capsulatus*, has been shown to be capable of inducing  $\beta$ -Gal expression over 100-fold in the presence of fructose when the *lacZ* genes were placed under the control of *fruP* (Duport et al., 1994). In addition, the expression of ferredoxin was found to be inducible by fructose when a promoterless copy of *fdxN* gene was placed behind *fruP*. To test whether *fruP* can induce *aa3* expression in *R. sphaeroides*, four constructs were made with *fruP* at different positions relative to *coxI* and *coxII/III* operons (Figure 3.4). In the absence of fructose, the expression levels of oxidase in the cells containing pTN100 and pTN200 were comparable to those of the cells containing the equivalent plasmids without *fruP*. In these two constructs, the native promoters for *coxI* and *coxII* are still present, and the similar expression levels of oxidase observed in constructs with and without *fruP* suggests that the upstream *fruP* did not control the expression of the oxidase, but rather it was regulated by its native promoters. Surprisingly, in the presence of 5 mM fructose, the expression of the oxidase decreased by about 20%. Both pTN300 and pTN400 failed to express CcO when placed in JS100

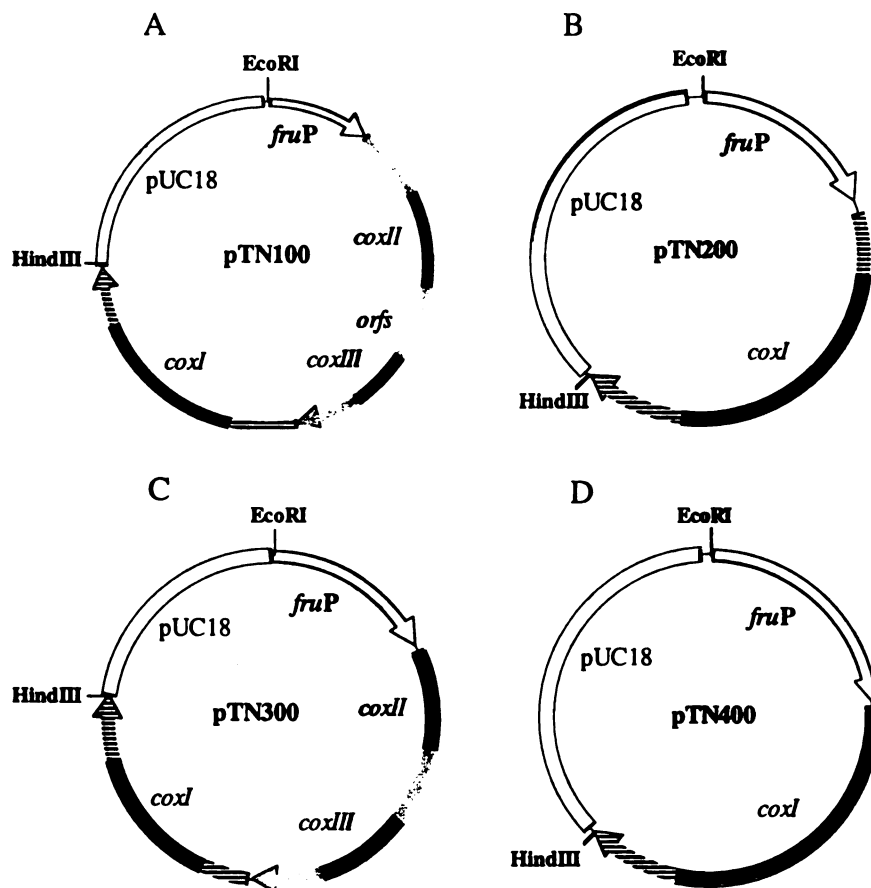


**Figure 3.4** Constructs made for expressing cytochrome *c* oxidase using fructose promoter gene (*fruP*). Cytochrome *c* oxidase genes and some upstream sequences were placed downstream of *fruP*. (A) (pTN100) three subunit genes together with 1-kb upstream sequence of *coxII* coding region and 400 bp upstream sequence of *coxI* coding region; (B) (pTN200) *coxI* gene and 400 bp upstream sequence of *coxI* coding region; (C) (pTN300) similar to pTN100, except the 1-kb upstream sequence of *coxII* coding region was removed and the *fruP* gene was put immediately in front of the *coxII* gene; (D) (pTN400) *coxI* gene alone. The *EcoRI* and *HindIII* sites were used to subclone these constructs into pRK415-1 for expression.

or YZ200 in the presence or absence of fructose. Further studies to determine the cause of the lack of expression and promoter insensitivity have not been conducted.

### **Fine-tuning the metal-affinity chromatography**

Two protocols have been published for purifying the *aa*<sub>3</sub>-type CcO of *R. sphaeroides* (Hosler et al., 1992; Mitchell & Gennis, 1995). One protocol combines hydroxylapatite and anion exchange chromatography, while the other method, taking advantage of six histidines added at the C-terminus of subunit I, uses Ni<sup>2+</sup>-NTA affinity chromatography. The His-tagged method is rapid, and gives a high yield (Mitchell & Gennis, 1995). However, the elution of oxidase from the Ni<sup>2+</sup>-NTA column using 100 mM imidazole leads to a blue-shift in the *α*-band and some loss of heme A, likely due to the insertion of imidazole into the heme *a* binding site as an alternative ligand to the iron. Histidine, due to its larger size and more hydrophilic character, was used to replace imidazole in the final elution step, allowing elution without distortion of the optical spectrum or loss of heme A. A purple Ni<sup>2+</sup>-histidine complex that coelutes with the enzyme can be washed away using a membrane filtration device. Histamine was also tested, but it did not elute oxidase from the resin. Many His-tagged proteins can be eluted from Ni<sup>2+</sup>-NTA column by lowering the pH of the buffer, but at pH 5.0 CcO did not elute from the resin, and further reduction in pH was likely to damage the protein.

The previously published metal-affinity method did not indicate the optimal protein concentration and protein/detergent ratio required for efficient binding and elution (Mitchell & Gennis, 1995). We tested loading conditions ranging from 6 to 28 mg protein/ml using 1% LM. The final yields of purified enzyme were higher when more dilute solutions were loaded; 70% yield at 28 mg/ml protein; 87% yield at 6 mg/ml

protein. Five purified oxidase samples that were chromatographed at different protein concentrations were run on SDS-PAGE, and all showed a similar level of purity (data not shown).

Rapid Ni<sup>2+</sup>-NTA purification does not prevent the formation of, or separate, the two different forms of oxidase with differently processed subunit II. The smaller subunit II band is presumably formed by the proteolytic cleavage of a 2 kDa fragment from the C-terminus (Lane 1 in Figure 3.5). An attempt to convert all the subunit II to the smaller form by adding trypsin and chymotrypsin to the solubilized membranes was not successful, indicating the presence of a distinct proteolytic processing step during post-translational modification inside the cells, which also takes place for another homologous enzyme, cytochrome *bo* oxidase, in *E coli* (Rumbley et al., 1997).

#### **A combined purification method**

In order to prepare highly homogeneous oxidase suitable for crystallization, a combination of the metal-affinity and DEAE-chromatography methods was devised. The Ni<sup>2+</sup>-NTA purified oxidase has an  $A_{280}/A_{420}$  value of 2.2, identical to that of the enzyme purified by DEAE chromatography (Hosler et al., 1992). After the Ni<sup>2+</sup>-histidine complex was removed and the oxidase was exchanged into 10 mM KH<sub>2</sub>PO<sub>4</sub>, pH 7.6, 1 mM EDTA, 3% LM was added and the sample was chromatographed on a DEAE-5PW column. Several peaks were resolved (Figure 3.6). A fraction containing mainly subunit I, subunit III and some contaminants elutes at 160 mM KCl. In the 190 mM KCl fraction, the dominant component is a 68-kDa peptide that is tightly associated with CcO, and not removed by NaBr washing of the membranes, hydroxylapatite chromatography, or

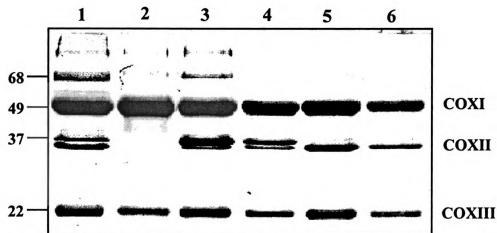


**Figure 3.5** SDS-polyacrylamide gel electrophoresis of cytochrome *c* oxidase purified from  $\text{Ni}^{2+}$ -NTA and FPLC columns.

Lane 1,  $\text{Ni}^{2+}$ -NTA alone purified oxidase; Lane 3 to 6, different oxidase fractions from FPLC. Lane 2, the fraction eluted at 160 mM KCl with only subunit I and subunit III; Lane 3 and 4, two fractions from the first oxidase peak; Lane 5 and 6, two fractions from the second oxidase peak; The apparent molecular mass (kD) of each band is indicated. A 15% polyacrylamide gel was used in this experiment.

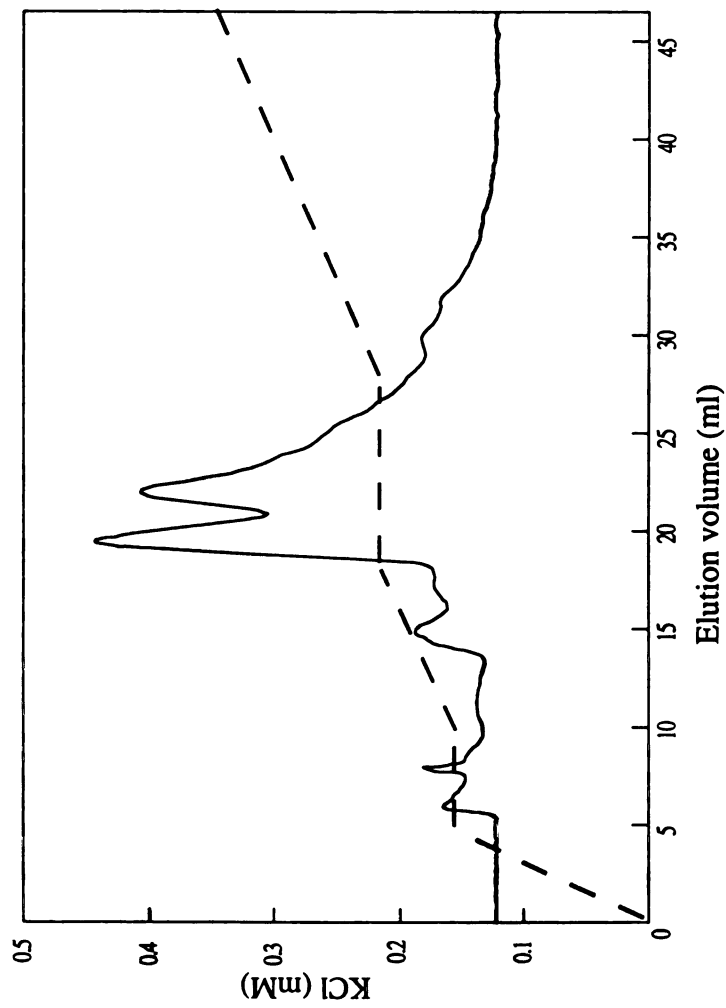


**Figure 3.6 Purification of Ni<sup>2+</sup>-NTA purified cytochrome *c* oxidase on DEAE-5PW.** The FPLC chromatographs of Ni<sup>2+</sup>-NTA purified oxidase are plotted against the KCl concentration (dashed line). Protein concentration is monitored at the bottom of the columns with a wavelength of 280 nm.

the Ni<sup>2+</sup>-NTA column. DEAE-5PW chromatography can partially separate this peptide from the oxidase, but variable amounts of it are still seen in SDS gels (Figure 3.5). The oxidase fractions eluting at 220 mM KCl resolved into two fractions, the first containing mostly cleaved, and the second mostly full-length subunit II.

The ratio of A<sub>280</sub>/A<sub>420</sub> for the enzyme purified by using the combination of metal-affinity and DEAE chromatography is 1.8, compared to 2.2 for preparations purified by either procedure alone. A value of 17.2 nmol of heme A/mg of protein is obtained for the Ni<sup>2+</sup>-affinity/DEAE purified enzyme by pyridine hemochromagen determination. This is about 107% of the calculated maximum value of 15.9 nmol of heme A/mg of protein, using the molecular weights predicted from the amino acid sequence and assuming two heme A per oxidase. This “more than 100%” purity is due to the fact that the Bradford protein assay method used in this study and the bicinchoninic acid method and modified Lowry assay in another study (Hosler et al., 1992) all underestimate the actual amount of protein when applied to membrane proteins (C. Hiser, D. Mills, S. Ferguson-Miller, in preparation).

### **Comparison of overexpressed and wild-type enzyme**

CcO from *R. sphaeroides* was previously purified as a two-subunit enzyme in Triton X-100 (Gennis et al., 1982) and a three-subunit enzyme in LM (Hosler et al., 1992). SDS-PAGE shows the Ni<sup>2+</sup>-NTA purified oxidase also has three subunits (Mitchell & Gennis, 1995) The ratios of each subunit in the overexpression strain are the same as those in the wild-type strain, indicating that the overexpression strains retain the correct stoichiometry of the individual subunits. A subunit IV, equivalent that in *Paracoccus denitrificans* oxidase (Haltia et al., 1994; Iwata et al., 1995), is not observed

in the purified *R. sphaeroides* oxidase using a 16% SDS gel. The Soret to  $\alpha$ -band ratio ( $A_{445-490}/A_{606-630}$ ) of the reduced enzyme from the overexpression strains is 5.6, similar to the value of wild-type reported previously (Hosler et al., 1992), showing that both hemes are present. The steady-state turnover of the overexpressed enzyme determined polarographically is equivalent to that measured for the enzyme from CY91 ( $V_{\max} \approx 2000 \text{ sec}^{-1}$ ). The overall characterization indicates that the overexpressed oxidase is identical to that synthesized at lower levels by CY91.

## Discussion

### Requirements for overexpression of CcO

*Gene copy number:* The three structural subunits of the mitochondrial-like CcO in *R. sphaeroides* are encoded in two separate regions of the bacterial chromosome. The subunit I gene (*coxI*) is separate from the subunit II (*coxII*) and subunit III (*coxIII*) genes; the latter are grouped in one operon and separated by two open reading frames, *orf1* and *orf3*. The predicted amino acid sequences for ORF1 and ORF3 are homologous to COX10 and COX11 from yeast (Cao et al., 1991). Tzagoloff and coworkers (Tzagoloff et al., 1990; Tzagoloff et al., 1993) and Saiki and coworkers (Saiki et al., 1992) have reported that COX10 is a heme A biosynthetic enzyme involved in adding the 15 carbon farnesyl group to the vinyl group at position 2 of the porphyrin ring. COX11 has been suggested to be involved in the conversion of the methyl at position 8 to a formyl group (Tzagoloff et al., 1993). ORF1 and ORF3 in *R. sphaeroides* presumably have the same functions and thus are indispensable for expression of the *aa3*-type oxidase.

In strain JS100, in which *coxI* has been deleted in the genomic DNA, high copy numbers of *coxI* alone on the exogenous plasmid pRK415-1 complement the chromosomal deletion but do not lead to overexpression (Shapleigh & Gennis, 1992). Similarly in YZ200, in which the genomic *coxII/III* operon has been deleted (chapter II), multiple copies of the *coxII/III* operon on pRK415-1, complement but do not lead to overexpression. To overproduce the enzyme, high copy numbers of both operons, including the ORF1 and ORF3, were required. In fact, *coxIII* is not essential for overexpression: the presence of a high copy number of *coxI*, *coxII*, *orf1* and *orf3* alone can allow overproduction of a two-subunit enzyme (data not shown).

Strain YZ300 was created by placing pRK-pYJ123H into YZ200, the deletion strain lacking the *coxII/III*, but containing the genomic *coxI*. When the solubilized membrane from this strain was loaded onto Ni<sup>2+</sup>-NTA column, approximately 20% of the oxidase in the solubilized YZ300 membranes fails to bind to Ni<sup>2+</sup>-NTA resin. Presumably this fraction of oxidase originates from the genomic copy of subunit I which does not contain the His-tag. The remaining 80% of the solubilized oxidase binds to the Ni<sup>2+</sup>-NTA resin. The 4 to 1 ratio between the His-tagged and native oxidase is consistent with the overexpression level achieved using pRK-pYJ123H and agrees with the copy number (4 to 6) of pRK415 in *R. sphaeroides* reported by Donohue et al. (Donohue & Kaplan, 1991).

Since the overexpression plasmid does not contain a gene for any subunit IV, as observed in *P. denitrificans* (Haltia et al., 1994; Iwata et al., 1995), such an additional subunit is not critical for assembly or activity of *R. sphaeroides* oxidase.

*Growth conditions.* When bacteria are subject to unfavorable growth conditions, they synthesize more electron-transfer/energy-transducing components to maintain homeostasis. Growth at high pH requires more energy to maintain a membrane potential and therefore promotes CcO synthesis. This is true for wild-type strains as well as those containing pRK-pYJ123H, but only the latter can produce high levels of oxidase. Similarly, high salt conditions should demand more oxidase production, but instead of using the energy generated from the oxidative phosphorylation pathway, the cells appear to induce photosynthesis, as indicated by the presence of large amounts of carotenoid and bacteriochlorophyll in the membranes.

The expression level of CcO in *R. sphaeroides* was affected not only by the pH of the Sistrom's medium, but also by the apparatus used for growing cells. When the cells are grown in a 14-liter fermentor at 30 °C, vigorously stirred and sparged with air supplemented to 30% oxygen, the oxidase expression level (mg/liter) is about 50-70% of that in rapidly-swirled Fernbach flasks. The expression of CcO genes in *R. sphaeroides* has been found to be oxygen-regulated (Flory & Donohue, 1997). As a result, the higher expression observed by using Fernbach flasks is likely due to the better aeration condition in Fernbach flasks.

*Vector size and drug-resistance.* pRK415-1 is the tetracycline resistant broad host-range vector used for expressing CcO in *R. sphaeroides*. Presumably due to the large size of pRK-pYJ123H (15.9 kb), a high percentage of exconjugates (2-4%) that contain a deletion of part of the plasmid arise. The partially deleted smaller plasmids allow a faster growth rate and their exconjugates produce larger colonies. The large colonies retain tetracycline resistance, but they do not express the oxidase gene.

Transcription and translation in *R. sphaeroides*, as in other prokaryote systems, occur concomitantly. Moreover, the tetracycline resistance protein, like CcO, is a membrane protein (Tait & Boyer, 1978) whose transcription, translation and insertion into the membrane occurs in a concerted manner, tethering the genes to the membrane and hindering the unwinding process. The combined effect of synthesizing a number of membrane proteins off the same plasmid presumably slows down the protein synthesis. To address the problem of a large plasmid with several membrane proteins encoded, a new expression vector system, pBBR1MCS, was tested. The pBBR1MCS plasmids have several different antibiotic resistance genes, including kanamycin resistance (pBBR1MCS-2) and ampicillin resistance (pBBR1MCS-4), both soluble protein-based drug-resistance systems (Davies & Smith, 1978; Waxman & Strominger, 1983). However, we observed no growth of pBBR1MCS-4 containing colonies, likely due to *R. sphaeroides* not being able to express resistance to ampicillin, as noted previously (Donohue & Kaplan, 1991). The pBBR1MCS-2 was capable of expressing CcO in *R. sphaeroides*, but at a lower level than pRK415-1. The failure to increase the expression level of CcO when combined with soluble antibiotic resistance proteins suggests that the transcription and translation of too many membrane proteins may not be the rate limiting step in the oxidase expression.

*Fructose promoter.* The purple, non-sulfur photosynthetic bacteria, including *R. sphaeroides*, typically possess DNA with G + C content between 68 and 70% (Pfenning & Truper, 1974), while the *E. coli* genome has an average G + C content of about 51% (Fujita et al., 1994). Because of this genetic difference, *E. coli* genes are not highly expressed in *R. sphaeroides* from their own promoters (Nano & Kaplan, 1982), nor are

genes from *R. sphaeroides* generally transcribed from their own promoters when placed in *E. coli* (Kiley & Kaplan, 1988). The ability to express  $\beta$ -Gal from *fruP* in *Rb. capsulatus* suggested that *fruP* is strong enough to overcome this problem for at least one *E. coli* gene. However, the expression of the native gene for ferredoxin in *Rb. capsulatus* was low when it was placed under the control of *fruP*, suggesting that *fruP* is not as strong as the native promoter (Duport et al., 1994). The failure to overexpress CcO in *R. sphaeroides* with *fruP* also suggests that it is not as strong as the native promoter. The lack of synthesis of CcO in *R. sphaeroides* using the *fruP* promoter gene from *R. capsulatus* is unlikely to be due to incompatibility of transcription and translation mechanisms in these two strains. Previous studies have shown that a gene from *Rb. capsulatus*, which includes its promoter region and ribosome binding site, is expressed in *R. sphaeroides* (Jenney Jr. & Daldal, 1993).

### **Purification strategies**

Table 3.2 clearly indicates that Ni<sup>2+</sup>-NTA is a most efficient method of separating other proteins from CcO, and the resulting purified enzyme is suitable for general spectroscopy studies (Mitchell & Gennis, 1995), especially when histidine is substituted for imidazole to avoid spectral shifts and heme displacement. But Ni<sup>2+</sup>-NTA chromatography cannot resolve the two oxidase fractions with different lengths of subunit II, nor the contaminating fraction with subunit I and subunit III alone, due to the location of the histidine tag on subunit I. Purified cytochrome *bo*<sub>3</sub> oxidase from *E. coli*, homologous to the *aa*<sub>3</sub> oxidase in *R. sphaeroides*, also shows the presence of two subunit II bands on SDS-PAGE, and a recent study suggests that the proteolytic cleavage site is

located at the C-terminal of subunit II (Rumbley et al., 1997). The crystal structure of the cytochrome *aa<sub>3</sub>* oxidase from *P. denitrificans* does not resolve a complete C-terminus of subunit II, and protein sequencing of subunit II from this enzyme also shows the C-terminus to be processed at the predicted site (Steinrucke et al., 1987). A sequence of subunit II from *E. coli bo<sub>3</sub>*, *R. sphaeroides aa<sub>3</sub>*, and *P. denitrificans aa<sub>3</sub>* reveals very little conservation in the terminal cleaved region, and its total absence in bovine *aa<sub>3</sub>* suggesting this region is not functionally important.

The purity of the oxidase can be further improved after Ni<sup>2+</sup>-NTA purification by chromatography on a DEAE-5PW column, and the different subunit II cleavage forms can be separated. This more homogeneous cytochrome oxidase is likely to be more suitable for crystallization efforts. Molecular genetic approaches are also being taken to remove the cleavable C-terminus of subunit II.

### Summary

This paper describes successful overexpression of CcO genes in *R. sphaeroides*, dependent on a new plasmid construct and optimized growth conditions. Ligating the two operons of CcO genes together and introducing them back into *R. sphaeroides* yielded up to 7-fold overproduction of the whole enzyme with identical properties to the wild-type. Growth at high pH achieves even higher expression. A high-yield protocol for purifying homogeneous oxidase by coupling metal-affinity chromatography and anion-exchange chromatography is also described. These procedures now allow purification of large amounts of enzyme relatively easily, which will facilitate rigorous characterization of mutants and eventual understanding of the mechanism of CcO.

## CHAPTER IV

### **Definition of the interaction domain for the reaction of cytochrome *c* with *R. sphaeroides* cytochrome *c* oxidase**

This work was done in collaboration with Dr. Frank Millett at the University of Arkansas and Dr. Gerald Babcock, and will be published in two papers (in preparation):

Definition of the interaction domain for cytochrome *c* on *Rhodobacter sphaeroides* cytochrome *c* oxidase: I. Biochemical spectral and kinetic characterization of surface mutants in subunit II.

Zhen, Y., Hoganson, C. W., Mills, D., Babcock, G., and Ferguson-Miller, S

Definition of the interaction domain for cytochrome *c* on *Rhodobacter sphaeroides* cytochrome *c* oxidase: II. Rapid kinetics analysis of electron transfer from cytochrome *c* to *Rhodobacter sphaeroides* cytochrome oxidase mutants

Wang, K., Zhen, Y., Sadosky, R., Grinnell, S., Geren, L., Durham, B., Ferguson-Miller, S., and Millett, F.

A special thanks to Dr. Honggong Yan for helping us develop the equation to fit the steady-state kinetic data.

## Introduction

Electron transfer plays an important role in biological systems. In the respiratory chain, electrons from reducing agents (NADH or succinate) are transferred through three multisubunit membrane-bound complexes before reducing oxygen to water. In this process, a small water-soluble molecule, *Cc*, shuttles electrons between complex III (cytochrome *bc*<sub>1</sub>) and complex IV (*CcO*).

The electron transfer reaction between *Cc* and *CcO* has been extensively studied under steady-state conditions spectrophotometrically and polarographically (Ferguson-Miller et al., 1976; Antonini et al., 1991). In these studies, biphasic kinetics were observed which could be analyzed in terms of two different  $K_M$  and  $k_{cat}$  values (Errede et al., 1976; Ferguson-Miller et al., 1976; 1978). Different models have been proposed to explain the biphasic kinetics (for review see, Cooper, (1989)), but still there is no consensus, making the interpretation of steady-state kinetics difficult.

The electron transfer process between *Cc* and *CcO* is generally thought to involve the formation of *Cc/CcO* complexes guided by electrostatic interactions. Extensive chemical modification studies identified several lysine residues, Lys-8, -13, -27, -72 and -87 in horse *Cc* numbering, located on the upper half of the front surface surrounding the heme edge, as forming the binding interface between *Cc* and *CcO* (Smith et al., 1977; Ferguson-Miller et al., 1978). This result was further supported by the fact that formation of *Cc* and *CcO* complexes prevent chemical modification of the same lysine side chains on *Cc* (Rieder & Bosshard, 1980). These lysine residues surround the edge of heme *c* that is mostly solvent-exposed. The arrangement of these lysine residues

presumably enables the heme group of *Cc* to come into proximity with *CcO*, facilitating the rapid electron transfer between them. A similar surface domain of *Cc* was also identified to interact with other redox partners (Kang et al., 1978; Speck & Margoliash, 1984; Margoliash & Schejter, 1996).

The location of the *Cc* binding site on *CcO* has been investigated using chemical reagents and monoclonal antibodies (Millett et al., 1982; 1983; Taha & Ferguson-Miller, 1992). In these studies, the reagent 1-ethyl-3-[3-(dimethylamino)propyl]carbodiimide (EDC) reacts specifically with carboxyl groups in subunit II of *CcO* and inhibits the high-affinity phase of the reaction between oxidase and *Cc*. Similarly, the presence of *Cc* protected several carboxyls in *CcO* from labeling and inhibition by EDC (Millett et al., 1983). Epitope mapping studies have indicated that the C-terminal domain of subunit II of *CcO* is the primary binding site for antibodies that inhibit *Cc* binding (Taha & Ferguson-Miller, 1992). Furthermore, Lys-13-modified arylazido horse *Cc* has been found to cross-link specifically with His-161 (His-217 in *R. sphaeroides*; all the numbers below, unless otherwise specified, are refer to the *R. sphaeroides* oxidase numbering), within this domain in horse *CcO* (Bisson et al., 1982).

These modification studies are consistent with time-resolved electron transfer kinetic studies, which have shown that  $\text{Cu}_A$ , located in the C-terminal region of subunit II, is the initial electron acceptor from *Cc* (Hill, 1991; Pan et al., 1993). Crystallography studies of *CcO* from both bovine and *Paracoccus denitrificans* are consistent with this general location of the *Cc* binding site (Iwata et al., 1995; Tsukihara et al., 1995; 1996), with both structures revealing a concentration of negatively charged residues above the

Cu<sub>A</sub> site in subunit II. In mammalian oxidase, the structure suggests the possibility that other subunits may also contribute to the binding.

Analyses of the available sequences of cytochrome oxidases that use Cc as a substrate reveal that there are seven highly conserved carboxylated residues (Glu-148, Glu-152, Glu-157, Asp-195, Asp-214, Asp-229 and Glu-254) in the solvent-exposed C-terminal region of subunit II (Figure 4.1). Chemical modification protection studies identified Asp-151 (Asp-112 in bovine), Glu-152 (Glu-114 in bovine), and Glu-254 (Glu-198 in bovine) (Millett et al., 1983) as candidates in Cc binding.

Site-directed mutagenesis studies in the genetically-engineered soluble Cu<sub>A</sub> domain in *P. denitrificans* CcO suggested several residues (Gln-142, Glu-148, Asp-214, Asp-229 and Glu-254) as being important in Cc binding (Lappalainen et al., 1995). A similar study on subunit II of the holoenzyme from *P. denitrificans* also revealed that Asp-214 and Glu-254 are involved in binding Cc (Witt et al., 1995). With the isolated holoenzyme, steady-state kinetics assays have shown that the catalytic efficiencies ( $k_{cat}/K_M$ ) of these two mutants are severely decreased. Further studies in this system have also indicated that Glu-148, Glu-157 (Asp-135 in *P. denitrificans*), and Asp-195 in subunit II and Asp-257 in subunit I are involved in Cc binding (Witt et al., 1998a). In many of the studies mentioned above (Millett et al., 1983; Lappalainen et al., 1995; Witt et al., 1995), Glu-254 has been identified as an important residue in Cc binding. However the crystal structures clearly show that this residue ligates both Cu<sub>A</sub> and Mg, and is buried inside the protein (Iwata et al., 1995; Tsukihara et al., 1996), excluding its possible involvement in Cc binding. The Mg center has been shown to be important in stabilizing the subunit I and subunit II interface (Florens et al., 1998), and any modifications at this position will

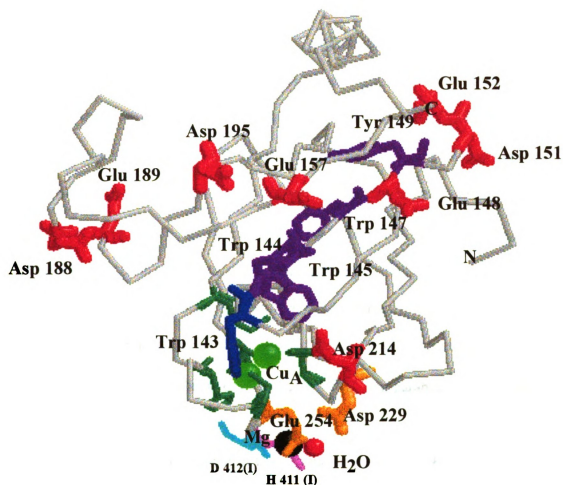


**Figure 4.1** Structure of subunit II C-terminus domain of cytochrome c oxidase.

The  $\text{Cu}_A$  ligands are in green; the aromatic residues Trp 143 in blue and all others in purple; the carboxyl residues in red, except that Asp 229 and Glu 254 in orange. The structure is created using the coordinates of *P. denitrificans* oxidase.

likely to alter the Mg center, destabilizing the interface and changing the electron transfer kinetics, as observed in this study.

Electron transfer from  $Cc$  to  $CcO$  is very rapid, and conventional stopped-flow spectroscopy does not have sufficient time resolution to resolve the initial electron transfer rate from  $Cc$  to  $Cu_A$ . Flow-flash experiments, in which CO-inhibited  $CcO$  is mixed with oxygen and then CO flashed off to allow the oxygen reaction to proceed, have shown that the electron transfer rate between  $Cc$  and  $Cu_A$  in beef heart oxidase is about  $70,000\text{ s}^{-1}$  (Hill, 1991). An additional valuable technique in studying electron transfer events is laser flash photoinduced electron transfer events (Pan et al., 1993; Geren et al., 1995). This method is initiated by photoactivating a ruthenium group attached to  $Cc$ , resulting in a rapid reduction of the heme  $c$  followed by electron transfer from  $Cc$  to  $Cu_A$ , with a rate constant for the latter of  $(6 \pm 2) \times 10^4\text{ s}^{-1}$ , comparable to that measured by flow-flash.

Here, I report my studies of the  $Cc$  binding site on *R. sphaeroides*  $CcO$ . A number of conserved carboxylate residues in the subunit II C-terminal domain of  $CcO$  from *R. sphaeroides* have been mutated to neutral charges. These residues include the highly conserved Glu-148, Glu-152, Glu-157, Asp-195, Asp-214, Asp-229 and Glu-254. A pair of residues, Asp-188/Glu-189, which are only present in an extra loop in *R. sphaeroides* and *P. denitrificans*, have also been mutated. Besides these carboxyl residues, several aromatic residues are also conserved in the subunit II C-terminal domain of  $CcO$  and even in quinol oxidases (Saraste, 1990). Among these residues, Trp-143 has been mutated to phenylalanine and alanine. The analysis of these two mutants is also reported. The ability to measure intra-complex and intra-oxidase electron transfer

kinetics, along with steady state and binding parameters, has revealed important new information about the nature of the Cc/CcO complex and the nature of electron transfer within it.

## Materials and Methods

**Materials:** Horse heart Cc (Sigma type VI) was purchased from Sigma and was purified on a carboxymethyl cellulose column before use (Brautigan et al., 1978). All the mutated oxidases were constructed using the overlapping extension PCR method (Ho et al., 1989) and the mutagenesis systems described in chapter II of this thesis. In the PCR reactions, the high fidelity *Pfu* polymerase (Stratagene, La Jolla, CA) was used, and all PCR products were sequenced to make sure that no secondary mutations were introduced. The mutated oxidases were overexpressed and purified using Ni-NTA affinity column chromatography as described the chapter III.

**Purification of *R. sphaeroides* cytochrome  $c_2$ :** *R. sphaeroides* cytochrome  $c_2$  was isolated from a cytochrome  $c_2$  overexpression strain, pC2P404.1 (Brandner et al., 1989). The cells were grown photosynthetically to maximize cytochrome  $c_2$  expression, and harvested at late exponential phase. The harvested cells were resuspended in a solution of 20 mM  $\text{KH}_2\text{PO}_4$ , pH 7.0, in the presence of small amounts of DNase and RNase, and were broken by two passages through a French pressure cell at 20,000 psi. Whole cells and debris were removed by centrifugation at 20,000 g for 20 min. The supernatant was adjusted to pH 5.0 with HCl and centrifuged again at 15,000 g for 15 min. The red photosynthetic pigments were precipitated in this step. The pellet was washed by

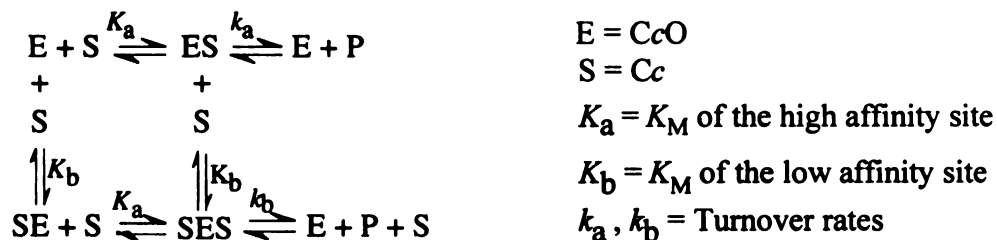
resuspending in the same buffer and homogenized using a glass homogenizer. The pH of the mixture was adjusted to pH 5.0 and centrifuged at 15,000 g for another 15 min. The supernatants from the two spins were pooled and adjusted to pH 7.0 before being subjected to another centrifugation at 200,000 g for 1 hour to removed any remaining membrane proteins. The supernatant from the ultracentrifugation was loaded onto a hydroxylapatite column pre-equilibrated with buffer of 20 mM  $\text{KH}_2\text{PO}_4$ , pH 7.0; cytochrome  $c_2$  binds to the column under these conditions. The column was washed with 30 mM  $\text{KH}_2\text{PO}_4$ , pH 7.0, and cytochrome  $c_2$  was eluted with 150 mM  $\text{KH}_2\text{PO}_4$ , pH 7.0. The cytochrome solution was dialyzed against 5 mM Tris, pH 7.0, and was loaded onto a DEAE-cellulose column pre-equilibrated with 5 mM Tris, pH 7.0. The column was washed with 20 mM Tris, pH 7.0, 25 mM NaCl, and cytochrome  $c_2$  was eluted with 50 mM NaCl in the same buffer. The purity of cytochrome  $c_2$  can be improved by running the sample through a second DEAE-cellulose column. The purified *R. sphaeroides* cytochrome  $c_2$  after two runs on DEAE-cellulose column has a ratio of  $A_{280}/A_{416}$  of 0.2, similar to the reported value (Meyer & Cusanovich, 1985).

**Activity assay:** The maximum turnover number (molecular activity) of CcO from *R. sphaeroides* was measured polarographically using a Gilson model 5/6H oxygraph at 25°C in a reaction medium containing 50 mM  $\text{KH}_2\text{PO}_4$ , pH 6.5, in the presence of 0.05% LM, 2.8 mM ascorbate, 0.55 mM TMPD, 1.1 mg/ml phospholipid (asolectin), and 30  $\mu\text{M}$  of horse Cc. The presence of asolectin in the medium stabilizes the oxidase and gives up to two-fold higher turnover rate. The oxidase concentrations were in the range of 5 to 50 nM.

For comparing the activities of CcO with horse Cc and *R. sphaeroides* cytochrome  $c_2$ , turnover numbers were also measured in 10 mM Tris/acetate, pH 8.0, 0.05% lauryl maltoside, 2.8 mM ascorbate, 0.55 mM TMPD, with no asolectin. The Cc concentrations were 30  $\mu\text{M}$ .

The ionic strength effect on the oxidation of reduced Cc was measured at 25 °C by following the 550 nm transients using an Olis-RSM stopped-flow spectrophotometer (On-Line Instrument systems, Inc., GA) in 5 mM Tris/acetate, pH 7.0, 0.1% LM, with 20  $\mu\text{M}$  reduced horse heart Cc or *R. sphaeroides* cytochrome  $c_2$ . The oxidases in the assays were in the range of 50 to 80 nM. The ionic strengths of the reactions were varied from 0 to 150 mM by using a 4 M NaCl solution.

***Steady-state kinetics assay:*** The steady-state kinetics of CcO were measured polarographically in a solution of 10 mM Tris/acetate, pH 8.0, 0.05% lauryl maltoside, 2.8 mM ascorbate, 0.55 mM TMPD, with *R. sphaeroides* cytochrome  $c_2$  ranging from 0.1 to 40  $\mu\text{M}$ , or pre-reduced horse Cc from 0.02 to 30  $\mu\text{M}$ . All the data were measured from single Cc additions, and Cc was added to the reaction solutions after the addition of oxidase, without waiting for the establishment of the baseline rate. Asolectin was not included in these assays, since it tends to bind Cc and deplete free Cc concentrations in the assays with lower Cc concentration. The kinetic data were analyzed using scheme 1 and assuming that only the high affinity site is involved in electron transfer, and the binding of the second Cc increases the dissociation rate of the tightly bound Cc due to



Scheme 1

charge repulsion. The following equation was used to fit the steady-state kinetics data by means of the nonlinear least square method using program ORIGIN™ (Microcal Software, Inc.):

$$v = \frac{V_a \frac{[S]}{K_a} + V_b \frac{[S]^2}{K_a K_b}}{1 + \frac{[S]}{K_a} + \frac{[S]}{K_b} + \frac{[S]^2}{K_a K_b}}$$

$V_a = V_{\max}$  for the high affinity phase  
 $V_b = V_{\max}$  for the low affinity phase

(Eq. 11)

**Electron paramagnetic resonance(EPR) spectroscopy :** Measurements were performed as described in Hosler et al. (1992), with the exception that the samples were in 10 mM Tris-HCl, 40 mM KCl, pH 8.0, 0.1 % lauryl maltoside. The sample preparations for high Mg/low Mn content, or low Mg/high Mn content oxidases were as described (Hosler et al., 1995). The EPR spectra were recorded using a Bruker EP-300E spectrometer.

**Metal analyses:** Metal analyses were done using inductively coupled plasma emission spectroscopy (ICP) at the chemical analysis laboratory in the University of Georgia and total-reflection X-ray fluorescence spectrometry (TXRF) at the physics department of the University of Göteborg, Sweden. The sample concentrations were in the range of 30-70  $\mu$ M.

**Flash photolysis:** Transient absorbance measurements were carried out in a 1 cm glass microcuvette by flash photolysis of 300 ml solutions containing about 10 mM of CcO and equal or less amounts of ruthenium labeled Cc (Millett & Durham, 1991), in order to measure a 1:1 reaction between Cc and CcO. Also included were 10 mM aniline and 1 mM 3-carboxyl-2,2,5,5-tetramethyl-1-pyrrolidinyloxy free radical (3-CP). Ru-55-Cc, a horse Cc derivative with the inorganic complex ruthenium trisbipyridine (Ru(bpy)<sub>3</sub>) covalently attached at the Lys-55 position, was used in the experiments. Upon a laser flash, electron transfer from Cc to the Cu<sub>A</sub> center of CcO was measured by monitoring the decrease of absorbance at 550 nm for Ru-55-Cc, as well as at 830 nm for Cu<sub>A</sub> reduction, and the increase of absorbance at 605 nm for the heme *a* reduction. The ionic strength dependencies for electron transfer from Ru-55-Cc to wild-type and mutated CcO were determined by varying the ionic strength of the solution from 5 mM to 300 mM using a 5.0 M NaCl stock solution.

**Equilibrium dissociation constant measurement:** The equilibrium dissociation constant ( $K_D$ ) was measured using an analytical ultracentrifuge (Beckmann, XLA model) as described in Cann (1970). A solution of 300 ml of 5 mM Tris-HCl, pH 8.0, 0.1% lauryl maltoside with 5 μM of horse Cc and 6 μM of *R. sphaeroides* CcO was spun at 48,000 rpm for 1 hour. The concentrations of NaCl in the solutions were from 0 to 250 mM. Each sample was scanned every 15 min at 410 nm (Soret peak of Cc) to follow the sedimentation of Cc in free and bound states. The concentrations of free Cc in the samples were obtained from the absorbance in the free Cc plateau region, using an extinction coefficient of 106 cm<sup>-1</sup>mM<sup>-1</sup>. The concentration of Cc in complex with oxidase

was the difference between total Cc and free Cc. The  $K_D$  was calculated using the following equation:

$$K_D = [Cc]_{\text{free}}[CcO]_{\text{free}}/[Cc/CcO]_{\text{complex}} \quad (\text{Eq. 12})$$

**Protein and heme assay:** The protein concentrations were measured using the BCA method (Pierce), and bovine serum albumin (BSA) was used as the standard. A modification to the original protocol is that the BSA standard and the oxidase were diluted with a solution of 10 mM Tris, 40 mM KCl, 0.25% deoxycholate, pH 8. The concentration of heme A was determined by the pyridine hemochrome method (Berry & Trumpower, 1987). Briefly, 100 ml of 2 N NaOH and 100 ml of neat pyridine were added to 800 ml of oxidase solution in 10 mM Tris, 40 mM KCl, pH 8.0, 0.1% LM. The solution was clarified by brief centrifugation in a microfuge, and reduced *minus* oxidized spectra were recorded. An extinction coefficient of  $\Delta\epsilon_{588-620} = 25 \text{ cm}^{-1} \text{ mM}^{-1}$  was used to calculate the heme A content.

**CO-binding assay:** The CO-binding ability of oxidase was measured from the CO difference spectrum of CO bound form *minus* the reduced form of the oxidase. To prepare CO bound oxidase, the enzyme at a concentration of about 1  $\mu\text{M}$  in a solution of 100 mM Tris, pH 8.0, 0.1 % LM was reduced with dithionite, and a reduced spectrum was taken. Then 1 ml of CO was bubbled slowly (5 min total time) into 1 ml of the dithionite-reduced oxidase at 25 °C, and a second spectrum was taken. The trough at 447 nm in the difference spectrum indicates the CO bound form. For wild-type oxidase, the extinction coefficient ( $\epsilon_{475-447}$ ) of the trough at 447 nm in the difference spectrum is 80  $\text{mM}^{-1}\text{cm}^{-1}$ .

## Results

### Design of mutants

Early studies have implied that the hydrophilic subunit II C-terminal domain of CcO is the major binding site for Cc, and negatively charged residues in this region play a pivotal role in the binding. In fact, a number of carboxyl residues are conserved in this region among all the known CcOs (Figure 1.5), but not in quinol oxidases which, although having considerable homologies to CcOs, use membrane-bound quinol instead of Cc as their electron donor.

To test the involvement of these carboxyl residues in Cc binding, the acidic side chains were mutated to their corresponding neutral amide forms, creating E148Q, D151N/E152Q, E157Q, D195N, D214N and D229N. In E254A, the glutamic side chain of Glu-254 has been changed to a methyl group. Two carboxyl residues, Asp-188 and Glu-189, which are not conserved but have been suggested to be involved in Cc binding (Cao et al., 1991), have also been mutated in a double mutant, D188N/E189Q. Besides the presence of these carboxyl residues and the conserved Cu<sub>A</sub> ligands, another feature of subunit II C-terminal domain is the presence of a set of highly conserved aromatic residues (Trp<sup>143</sup>-Tyr<sup>144</sup>-Trp<sup>145</sup>-x-Tyr<sup>147</sup>-x-Tyr<sup>149</sup>), located at the second β-sheet on the surface of the molecule (Figure 4.1). These aromatic residues have been postulated to play a role in electron transfer from Cu<sub>A</sub> to heme *a* (Steffens & Buse, 1979a). Trp-143, shown in the crystal structures (Iwata et al., 1995; Tsukihara et al., 1996) to be in proximity to the Cu<sub>A</sub> center, has been implicated in transferring electrons from Cc to Cu<sub>A</sub> (Witt et al., 1998a). To test the function of this residue, Trp-143 has been mutated to

phenylalanine and alanine, creating W143F and W143A, respectively. Another mutant, Y144A/W145A, has been created as well.

### **Metal assay**

The metal contents of wild-type and mutant forms of CcO were measured using either ICP or TXRF techniques, or both (Table 4.1). For wild-type oxidase, the Cu/Fe ratio measured by ICP is 1.51, which is in agreement with the fact that there are three Cu and two Fe atoms per oxidase molecule resolved by crystal structures, while the ratio for wild-type oxidase measured by TXRF is slight lower than the theoretical value of 1.5, indicating the different sensitivities of the two methods. For all the mutants, except D229N and E254A, the Cu/Fe ratios measured using either technique are comparable to that of the wild-type oxidase, indicating that the copper atoms in Cu<sub>A</sub> center were not preferably lost in these subunit II mutants, while the ratios for D229N and E254A are about 1.

### **Spectral characteristics of mutants**

**Optical spectral assay:** All the mutants have been successfully purified and some of their properties are summarized in Table 4.1. Among these mutants, Y144A/W145A has a very low expression level in the cell membrane and a severely shifted  $\alpha$  - peak in the visible spectrum, indicating structural alteration at the heme centers in this mutant. The widespread structural change would make it difficult to interpret any localized effects of removing aromatic side chains, so this double mutant was not further pursued. All the other mutants were first characterized using visible, near-infrared and EPR spectra.

**Table 4.1** Characteristic of subunit II mutants of cytochrome *c* oxidase from *R. sphaeroides*

Enzymes	$\alpha$ -band (nm)	Soret/ $\alpha$ (ratio)	Turn-over* (s <sup>-1</sup> )	CO-binding	Cu/Fe ratio		Cu <sub>A</sub> EPR	Mn EPR
					ICP	TXRF		
wild-type	606	5.58	1700	100%	1.51	1.26	normal	normal
E148Q	606	5.54	1100	100%	ND	1.34	normal	normal
D151N E152Q	606	5.53	1300	100%	ND	1.35	normal	normal
E157Q	606	5.60	600	100%	1.48	1.38	normal	normal
D188N E189Q	606	5.60	1600	100%	ND	1.38	normal	normal
D195Q	606	5.58	1200	100%	ND	1.34	normal	normal
D214N	606	5.53	400	100%	1.51	1.38	normal	normal
D229N	602	4.35	400	50%	0.99	0.85	normal	None
E254A	604	4.80	600	70%	0.84	ND	normal	None
W143A	606	5.50	20	100%	1.50	ND	normal	normal
W143F	606	5.50	40	100%	1.49	1.35	normal	normal
Y144A W145A	601	ND	ND	ND	ND	ND	ND	ND

\* The turn-over numbers are measured with 30  $\mu$ M horse Cc in 50 mM KH<sub>2</sub>PO<sub>4</sub>, pH6.5.

In the reduced form, wild-type CcO from *R. sphaeroides* has characteristic absorbance at 445 nm and 606 nm for the Soret and  $a$ -peaks, respectively, with a Soret to  $a$ -peak ratios ( $A_{445-490}/A_{606-630}$ ) of 5.6. The majority of the carboxyl mutant proteins and W143A/F have wild-type spectral characteristics (Table 4.1), indicating alteration of activity is not due to any global change in enzyme structure, but rather due to localized effects of the altered side-chains. In contrast, the two mutant proteins, D229N and E254A, in which the mutated residues are revealed by the X-ray structures to be internally located (Iwata et al., 1995; Tsukihara et al., 1996), have the severely disrupted heme centers, indicated by the shift of the visible spectra (Figure 4.2). Furthermore, in the resting forms, the hemes  $a$  in D229N and E254A tend to stay partially reduced, suggesting changes of the redox potentials of heme  $a$  or  $a_3$  in these two mutants. Besides the shift of the visible spectra, the Soret to  $a$ -peak ratios for D229N and E254A are much lower than that of wild-type (Table 4.1), suggesting the loss of heme in these mutants, which is supported by the results of pyridine hemochromogen assays showing that the heme contents in D229N and E254A are lower than that in wild-type oxidase (Table 4.2). It is well known that in CcO, heme  $a$  and  $a_3$  contribute differently to the Soret and  $a$ -peak absorption, with heme  $a$  accounting for about 80% of the  $a$ -peak, and 50% of the Soret peak (Liao & Palmer, 1996). The lower Soret to  $a$ -peak ratios for D229N and E254A indicate a preferential loss of heme  $a_3$  in these two mutants. Based on the Soret to  $a$ -peak ratios, it is estimated that the heme  $a_3$  contents in D229N and E254A are about 40% and 60%, respectively. In this regard, D229N and E254A may not be homogenous samples, but contain some "apo-cytochrome  $a_3$ " form.

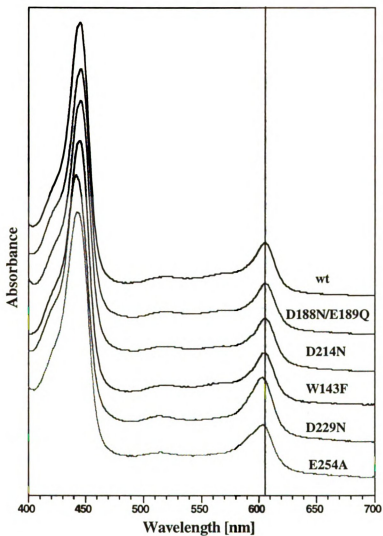


**Figure 4.2** Optical spectra of *R. sphaeroides* wild-type oxidase and subunit II mutants. All the enzymes were purified using Ni-NTA resin, and were reduced by dithionite in 100 mM Tris, pH 7.0.

**Table 4.2 Protein and heme assays of subunit II cytochrome *c* oxidase mutants from *R. sphaeroides***

	col. #1	col. #2	col. #3	col. #4	col. #5	col. #6	col. #7	col. #8	col. #9	col. #10
Enzymes	Protein <sup>a</sup> assay (mg/ml)	Heme <sup>b</sup> assay ( $\mu$ M)	Heme/Prot. <sup>c</sup> (nmole/mg)	Soret/ $a$ <sup>d</sup> (ratio)	$A_{280}/A_{424}$ <sup>e</sup> (ratio)	$[aa_3]$ <sup>f</sup> ( $\mu$ M)	$aa_3$ <sup>g</sup> protein (mg/ml)	$[aa_3]$ <sup>h</sup> content (%)	Heme/ $aa_3$ <sup>i</sup> (ratio)	$a_3$ <sup>j</sup> content (%)
wild-type	0.7	11.8	16.9	5.6	2.1	5.9	0.7	100	2.0	100
W143A	0.7	8.1	11.6	5.6	2.4	4.8	0.6	86	1.7	100
W143F	0.6	7.6	12.7	5.6	2.2	4.8	0.6	100	1.6	100
D229N	6.3	71.1	11.3	4.4	2.2	48.3	6.0	95	1.5	40
E254A	6.1	69.3	11.4	4.8	2.3	44.1	5.5	90	1.6	60

c. Heme/Prot. ratio is calculated by dividing col. #2 with the values in col. #1. The theoretical value for wild-type is 15.9..

e. The  $A_{280}/A_{424}$  ratio is calculated as  $A_{280-310}/A_{424-490}$  from the spectrum of the resting form of enzyme.

f. The  $aa_3$  amount is based on spectral assay with  $\epsilon_{606-640} = 40 \text{ mM}^{-1} \text{ cm}^{-1}$  in the reduced form.

g. The amount of oxidase calculated as mg/ml based on a sequence molecular weight of 125 kDa. col. #7 = col. #6 x 0.125.

h. The percentage of  $aa_3$  in the total amount of protein; ratio of mg oxidase calculated from spectrum to mg total protein measured from the protein assay. col. #8 = col. #7/ col. #1.

i. Heme A content per mole of oxidase. col. #9 = col. #2 / col. #6.

j. Heme  $a_3$  content in the oxidase. Assuming heme  $a_3$  contributes 50% and 20% to the Soret and  $\alpha$ -peak absorbances, respectively. For wild-type oxidase,  $\epsilon_{444-490} = 200 \text{ mM}^{-1} \text{ cm}^{-1}$  and  $\epsilon_{606-630} = 36 \text{ mM}^{-1} \text{ cm}^{-1}$ .

CO can bind to the heme  $a_3$ -Cu<sub>B</sub> binuclear center quantitatively, and structural changes at this center will affect its CO-binding capability. For most of the mutants, except D229N and E254A, their CO-binding abilities are identical to that of wild-type. The lower CO-binding abilities for D229N and E254A suggest structural alterations at the binuclear centers, which is in agreement with the heme assay results showing that some portion of heme  $a_3$  has been lost.

Beside loss of some heme  $a_3$ , a significant portion of D229N and E254A purified using Ni-NTA method also lost subunit II, as revealed from further purification using FPLC and SDS-gel analysis. This portion of sample without subunit II (20% for E254A and 40% for D229N) failed to bind to the DEAE-cellulose column. The lower Cu/Fe ratios measured for these two mutants can be explained by the loss of some subunit II. Since EPR suggests no major alteration in the Cu<sub>A</sub> signal (see below) in D229N and E254A, the portion of sample with subunit II likely retains an intact Cu<sub>A</sub> center.

In the oxidized form, bovine CcO has a broad absorption peak at the near-infrared region centered at 830 nm, which has been assigned to be from Cu<sub>A</sub>. A similar absorption band is also observed in CcO from *R. sphaeroides* with an extinction coefficient of 2.0 mM<sup>-1</sup>cm<sup>-1</sup> for the oxidized minus reduced spectra (Figure 4.3), the same as reported for bovine CcO (Blair et al., 1983), suggesting that the Cu<sub>A</sub> centers in CcOs from bovine and *R. sphaeroides* are similar. However, the peak position of *R. sphaeroides* CcO is at 850 nm, instead of at 830 nm as observed in bovine oxidase, suggesting the electronic structures of these Cu<sub>A</sub> centers are in fact slightly different. However, the term of “830 nm band” is retained for simplicity. The near-IR spectra for other mutant enzymes are

**Figure 4.3 Near-infrared spectra of the wild-type, D229N and E254A CcO.**

**A.** Reduced and oxidized spectra of wild-type cytochrome *c* oxidase *R. sphaeroides*. The wild-type enzyme concentration was 31.5  $\mu\text{M}$ . The *inset* provides the oxidized, reduced, and the oxidized minus reduced difference spectra of wild-type oxidase in the region of 700 to 1000 nm.

**B.** The oxidized minus reduced difference spectra for wild-type, D229N and E254A enzymes. The enzyme concentrations for all three samples are averaged to 31  $\mu\text{M}$  in this figure. To prepare the fully oxidized oxidases, ferricyanide was added to 300  $\mu\text{l}$  of oxidases in 100 mM Tris, pH 8.0, 40 mM KCl, 0.1% LM, and was subsequently removed by running the samples through Sephadex G-10 spin columns. The run-through oxidase solution was diluted to 800  $\mu\text{l}$  with 100 mM Tris, pH 8.0, 40 mM KCl, 0.1% LM, and the oxidized spectra were recorded. Dithionite was added to the cuvettes to completely reduce the samples.

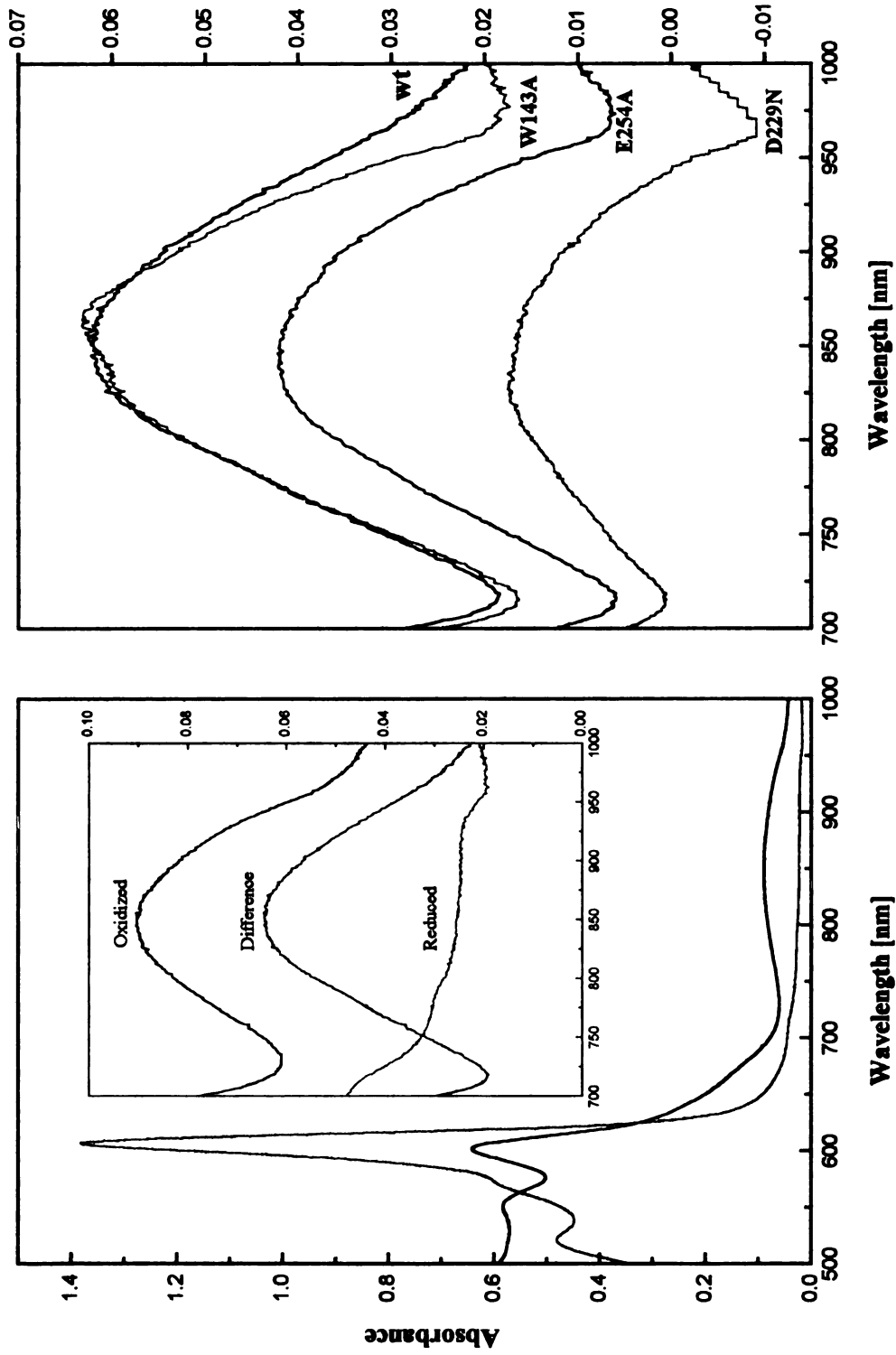


Figure 4.3. Near-infrared spectra of wild-type and mutant cytochrome *c* oxidases from *Rb. sphaeroides*

similar to that of the wild-type, indicating that the Cu<sub>A</sub> centers in these mutant proteins are not altered. The corresponding spectra are shown in Figure 4.3. For D229N and E254A, their peak positions are same as that of the wild-type, but the calculated extinction coefficients are lower, with a value of 0.6 and 1.4 mM<sup>-1</sup>cm<sup>-1</sup> for D229N and E254A, respectively. The lower extinction coefficients calculated for these two mutants also reflect the loss of both copper atoms at the Cu<sub>A</sub> center in a portion of the mutant.

**Cu<sub>A</sub>/heme EPR spectral assays:** For the X-band EPR spectrum of *R. sphaeroides* CcO, the signals at  $g = 2.83$ , 2.31 and 1.62 arise from the low spin heme *a*, and the signals at  $g = 2.0$  and 2.19 from Cu<sub>A</sub> (Figure 4.4) (Hosler *et al.*, 1992). Most of the surface carboxylate-deficient mutant proteins showed wild-type character (Figure 4.4). In contrast, as expected from the visible spectra and CO binding, the heterogeneity of the heme centers in D229N and E254A is reflected in the changes of the heme *a* EPR signals (Figure 4.4), indicated by the splitting and shift of the  $g = 2.83$  signal to lower field values, and the decreased amplitudes of the three heme *a* signals. The extra signal at  $g = 2.95$  in D229N and E254A appears in a position closer to that found in the native bovine CcO. In *R. sphaeroides*, the low spin heme *a* at  $g = 2.83$  has been interpreted to be the result of ligation by one neutral and one deprotonated histidine. When heme *a* is ligated by two neutral histidine ligands, the corresponding signal is shifted to  $g = 2.96$  position (Hosler *et al.*, 1992). The presence of both  $g = 2.83$  and 2.96 signals in these two mutants suggests more than one conformation around heme *a* in D229N and E254A. Besides the changes observed for the heme *a* signals, the amplitude of  $g = 6.0$  signal, arising from the decoupled high spin heme *a*<sub>3</sub>, is also somewhat larger than that in wild-type, indicating that some Cu<sub>B</sub> is lost, but the signal represents a very small amount of high spin form.



**Figure 4.4 Cu<sub>A</sub> EPR spectra of cytochrome c oxidase.** (A) wild-type, W143A/F, (B) carboxylate-deficient mutants. EPR spectra of 20 to 50  $\mu$ M oxidases in 10 mM Tris, pH 8.0, 40 mM KCl, 0.1% LM were recorded at X-band using a Bruker EP-300E spectrometer. The related g values are indicated in the plots. The EPR spectra were recorded at 10 K with the following settings: microwave frequency 9.482 GHz; microwave power 2 mW; modulation amplitude 12.7 G; sweep time 335.5 s; The cells were grown in high Mg/low Mn media. The hyperfine structures present in E148Q are from Mn.

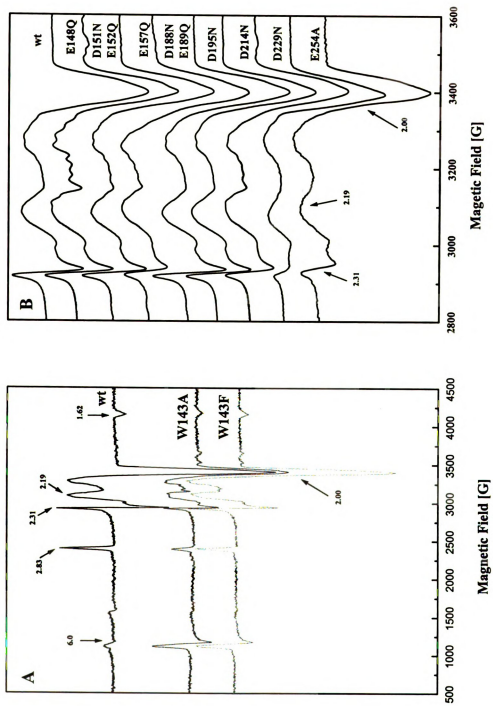
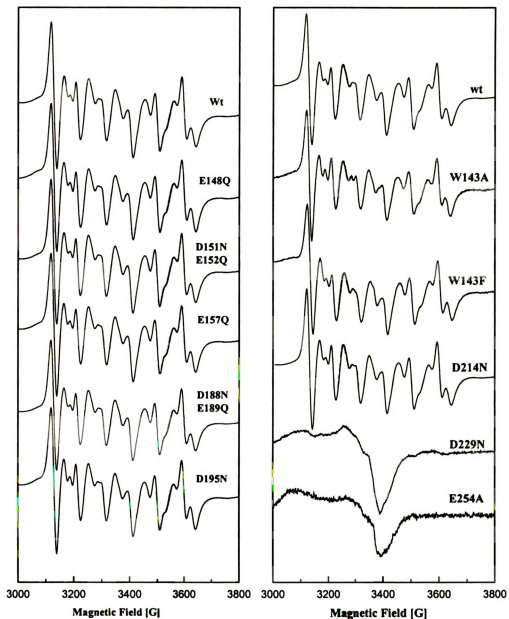


Figure 4.4  $\text{Cu}_A$  EPR spectra of cytochrome *c* oxidases.

The EPR signals arising from Cu<sub>A</sub> in D229N and E254A are similar to that of wild-type oxidase, except that the amplitude of the  $g = 2.19$  signal was slightly decreased, but there is no evidence of the presence of mononuclear or decoupled Cu<sub>A</sub> centers (see chapter V).

**Mn EPR analysis:** In CcO, the Mg atom can be replaced by a Mn atom (Hosler et al., 1995), which gives a distinct EPR hyperfine signal. The EPR spectrum of the Mn atom is sensitive to the environment of the metal center, and it can be used as a probe of the integrity of the structure of subunit I/II interface. The Mn EPR spectra of most mutants are similar to that of wild-type (Figure 4.5), indicating no structural alteration at the interface in these mutants. Unlike other carboxylate residues, both Asp-229 and Glu-254 are not surface charges, but internal carboxylate ligating the Mg center (Ostermeier et al., 1997), and thus involved in maintaining the structural integrity of the subunit II/I interface (Florens et al., 1998). The X-ray structures show that Glu-254 ligates the Mg atoms directly through its carboxyl side chain, while ligating one of the Cu atoms at the Cu<sub>A</sub> center with its carbonyl oxygen. Asp-229 ligates the Mg atom indirectly through a water molecule. EPR studies on D229N and E254A also suggest that these two mutants fail to bind Mn atoms (Figure 4.5), even when the mutant strains were grown in a medium with high levels of Mn. These results are consistent with the roles of Asp-229 and Glu-254 in Mg/Mn binding. Obviously, these two mutations cause a global change in the oxidase, as might be expected for altering internal charges in a central location.

Most of the mutants have similar visible spectra as to that of wild-type, and their Cu<sub>A</sub> and Mn EPR spectra are indistinguishable from those of the wild-type, suggesting that the metal centers in these mutants are intact; this is further supported by the results from metal analyses showing that their Cu/Fe ratios are similar to that of the wild-type



**Figure 4.5 Mn EPR spectra of wild-type cytochrome *c* oxidase and subunit II mutant enzymes.** The samples with concentrations from 30 to 50  $\mu\text{M}$  are in 10 mM Tris, pH 8.0, 40 mM KCl, 0.1% LM. The spectra were recorded at x-band using a Bruker EP-300E spectrometer, with the following settings: microwave frequency 9.44 GHz; power 20 mW; modulation amplitude 12.7G; sweep time 167.8 s; The samples were prepared as described in Hosler et al. (1995).

oxidase. The localized effect of these carboxyl mutations allow for meaningful interpretation of the binding and kinetic analyses.

### **The activities of mutant enzymes**

CcO from *R. sphaeroides* shows high activity with horse Cc; as a result, horse Cc has been used routinely in kinetics assays. However, the soluble cytochrome  $c_2$  from *R. sphaeroides* also reacts with CcO from the same strain. The maximum turnover numbers of wild-type and mutated CcO have been measured using both horse Cc and *R. sphaeroides* cytochrome  $c_2$  as the substrates in polarographic assays under the same conditions.

The maximum turnover numbers for the oxidases, measured in 50 mM  $\text{KH}_2\text{PO}_4$ , pH 6.5, in the presence of lipid, is much higher than under other conditions, with a rate of  $1700 \text{ s}^{-1}$  for wild-type oxidase with horse Cc. Under these conditions, the turnover numbers measured for all the mutants vary significantly, ranging from 1% to nearly 100% of wild-type activity. Among them, W143A, with the removal of the aromatic side chain, has the lowest activity (Table 4.1), and the more conservative change in this position, W143F, is almost equally inhibited. The significant decrease of enzyme activities associated with W143F, together with the fact that all the metal centers in this mutant are spectrally identical to wild-type, is the first indication of the importance of this residue in electron transfer from Cc to the oxidase.

Among the carboxylate-deficient mutants enzymes, D214N and D229N have the lowest turnover number, retaining about 24% of the wild-type activity, while the activity of D188N/E189Q is equivalent to that of wild-type. E157Q and E254A have about one-

third and E148Q, D195N and D151N/E152Q two-thirds of the wild-type activity. The varying levels of maximal activities observed for these mutant enzymes, which also retain wild-type spectral characteristics, appear to reflect different contributions of these carboxylate residues to the binding of Cc, due to the fact that dissociation of Cc is limiting under these assay conditions (Sinjorgo et al., 1984).

The maximum turnovers of the wild-type and carboxylate-deficient mutant enzymes have also been measured with *R. sphaeroides* cytochrome *c*<sub>2</sub> and horse Cc in 10 mM Tris, pH 8.0. Under these conditions, the turnover number for wild-type oxidase with *R. sphaeroides* cytochrome *c*<sub>2</sub> and horse Cc are about 300 s<sup>-1</sup> and 900 s<sup>-1</sup>, respectively, significantly lower than in the higher ionic strength, lower pH, phosphate buffer. The higher pH and lower ionic strength buffer renders the Cc dissociation even more limiting and the absence of lipid also lowers activity (Hosler et al., 1992). The percentages of wild-type activities retained by D188N/E189Q, D151N/E152Q, and E148Q, using either *R. sphaeroides* cytochrome *c*<sub>2</sub> or horse Cc as the substrate, follow a similar pattern of decreased to that seen with the earlier conditions (Figure 4.6). However, D214N, E157Q and D195N react with different relative rates with the two cytochromes *c*. With horse Cc, D214N, E157Q and D195N retain about 30%, 30% and 75% of wild-type activity, respectively; in contrast, they have 75% , 60% and 40% of wild-type activity, respectively, when reacting with *R. sphaeroides* cytochrome *c*<sub>2</sub>. The different behaviors of D214N, E157Q and D195N in reacting with two cytochromes *c* suggest that the interaction surface on the two cytochromes *c* differs in the vicinity of these two carboxyls.

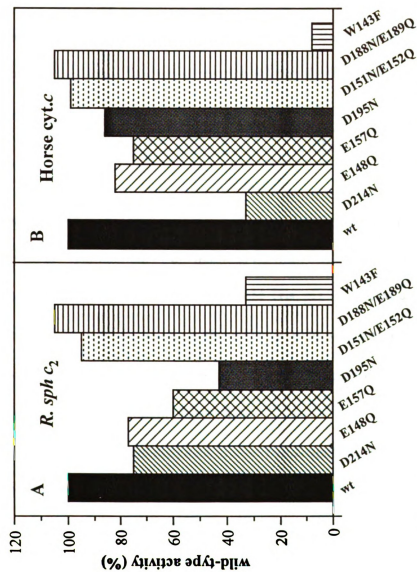
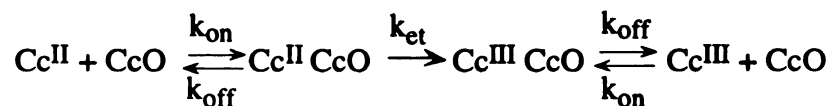


**Figure 4.6** The maximum turnover numbers of subunit II mutants with *R. sphaeroides*  $c_2$  (A) and horse heart cytochrome  $c$  (B) as substrates. The turnovers are measured polarographically in a solution of 10 mM Tris, pH 8.0, 0.05 % LM, 2.8 mM ascorbate, 0.55 mM TMPD and 30  $\mu$ M *R. sphaeroides*  $c_2$  or horse cytochrome  $c$ . The turnover numbers with horse and *R. sphaeroides* Cc for wild-type oxidase are 900 and 300  $s^{-1}$ , respectively.

### Effect of ionic strength on the interaction of cytochrome *c* with CcO

To simplify the assay system and to study ionic strength effects, the turnover numbers of wild-type and mutant CcOs have been studied by measuring the oxidation of reduced Cc in a stopped-flow spectrophotometer in the absence of additional reducing agents. In this assay, the overall reaction follows the following scheme:



Scheme 2

First, reduced Cc associates with CcO to form a complex, within which electron transfer takes place. Dissociation of the oxidized Cc from CcO is required before another reduced Cc can bind to it. In the assays with 5 mM Tris, pH 7.0 and adjusting the ionic strength with NaCl, the turnover numbers for wild-type oxidase increase from 590 s<sup>-1</sup> at 5 mM ionic strength to a maximum of 980 s<sup>-1</sup> at 75 mM ionic strength and then decrease to 290 s<sup>-1</sup> at 155 mM ionic strength (Figure 4.7).

For all the mutant enzymes, similar bell-shaped curves are observed as for wild-type oxidase, but the peak positions with the maximum activities are not all the same as that of wild-type, with the peak of activities for D214N, D195N and E148Q at 65 mM ionic strength, and E157Q at 55 mM ionic strength (Figure 4.7). In contrast, the peak activity for D188N/E189Q and D151N/E152Q is at the same ionic strength as that of wild-type. At low ionic strengths, the dissociation of Cc is likely rate limiting (Sinjorgo et al., 1984), while at very high ionic strength, the electrostatically-mediated association rates are markedly reduced. The position of the peak of activity represents the balance

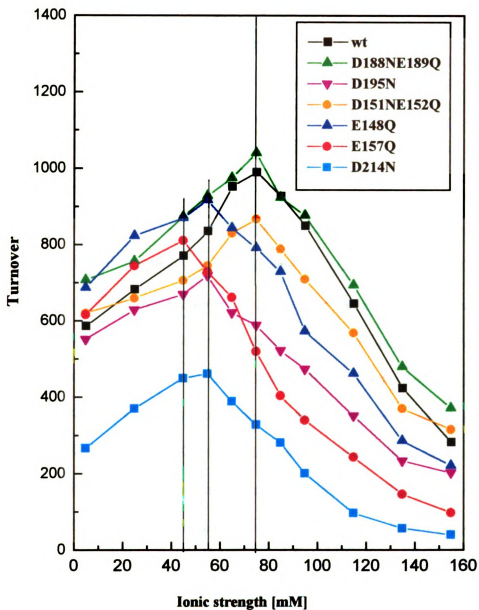


**Figure 4.7** Ionic strength dependent turnover numbers of subunit II mutants.

The turnover numbers were measured using a stopped-flow apparatus by following the oxidation of Cc at 550 nm. The reactions take place in a solution of 10 mM Tris/acetate, pH 7.0, 0.1% LM, 20  $\mu$ M reduced horse Cc.

between increasing dissociation rates and decreasing association rates, and thus is a measure of the binding strength of *Cc* to *CcO*. The shift of the peak of activity to lower ionic strengths for the mutant proteins is a measure of the relative loss of binding affinity with *Cc*, suggesting that Asp-214, Glu-148, Glu-157 and Asp-195 are in the *Cc* binding domain, while Asp-151, Glu-152, Asp-191 and Glu-189 are not.

### **Steady-state kinetics assays**

The steady-state kinetics for wild-type and mutant enzymes have been measured polarographically with *R. sphaeroides* cytochrome *c*<sub>2</sub> (Figure 4.8) and horse *Cc* (Figure 4.9) as substrates. The turnover numbers of the oxidase increase with increasing *Cc* concentrations, and the reactions display saturation kinetics (Figure 4.10). Analyses of the kinetics data revealed non-linear Eadie-Hofstee plots as observed earlier (Ferguson-Miller *et al.*, 1976), which can be most simply modeled as two different reaction sites of high and low affinity. The low  $K_M$  phase appears to represent the interaction between *Cc* and *CcO* at the high affinity site. It has been found that the low  $K_M$  value for the initial phase obtained from the polarographic assay is similar to the  $K_D$  value for the binding of *Cc* to a high-affinity site under similar conditions (Ferguson-Miller *et al.*, 1976). As a result, the  $K_M$  values obtained in these assays can be used as an indication of the binding strengths between *Cc* and *CcO*. But the complexity of the kinetics measured in the presence of the reducing agents, TMPD and ascorbate, makes a rigorous interpretation of the kinetic constants difficult.

The kinetic data have been analyzed by assuming that only the high-affinity site is involved in electron transfer, and the  $K_M$  values obtained for both phases are summarized

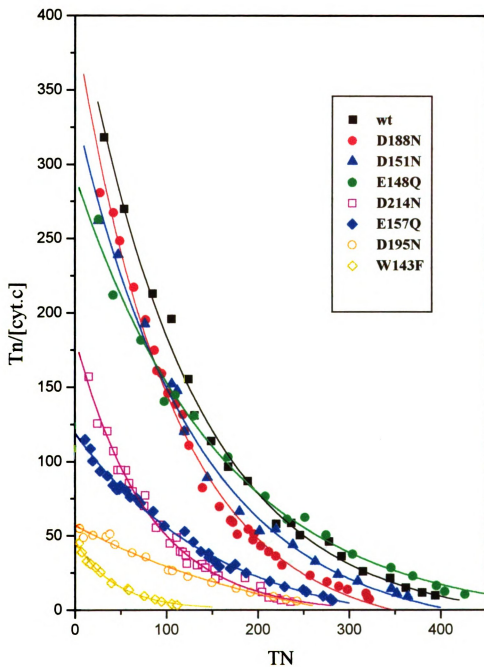


**Figure 4.8** Steady-state kinetics assay of CeO with *R. sphaeroides* cytochrome  $c_2$ .

The turnover are measured polarographically in a solution of 10 mM Tris/acetate, pH 8.0, 0.05% LM, 2.8 mM ascorbate, 0.55 mM TMPD, no lipid, with *R. sphaeroides* cytochrome  $c_2$  from 0.1 to 40  $\mu$ M. The solid lines are second-order exponential decay fitting results.



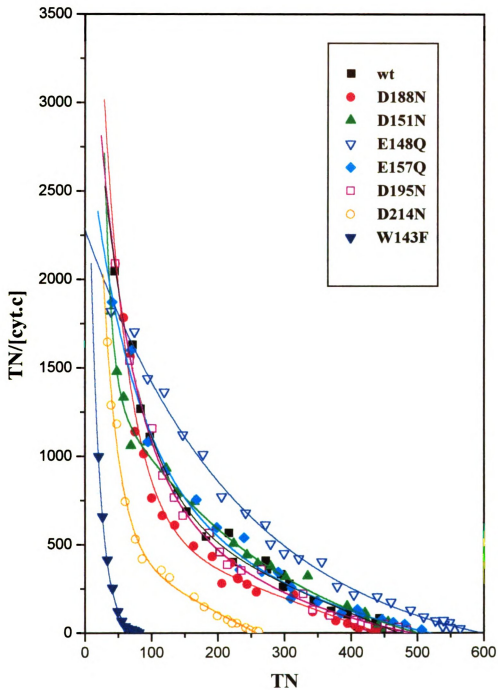


**Figure 4.9** Steady-state kinetics assay of *R. sphaeroides* cytochrome *c* oxidase with horse cytochrome *c*. The assay conditions are the same as in Figure 4.8, except with horse Cc ranging from 0.02 to 30  $\mu$ M.

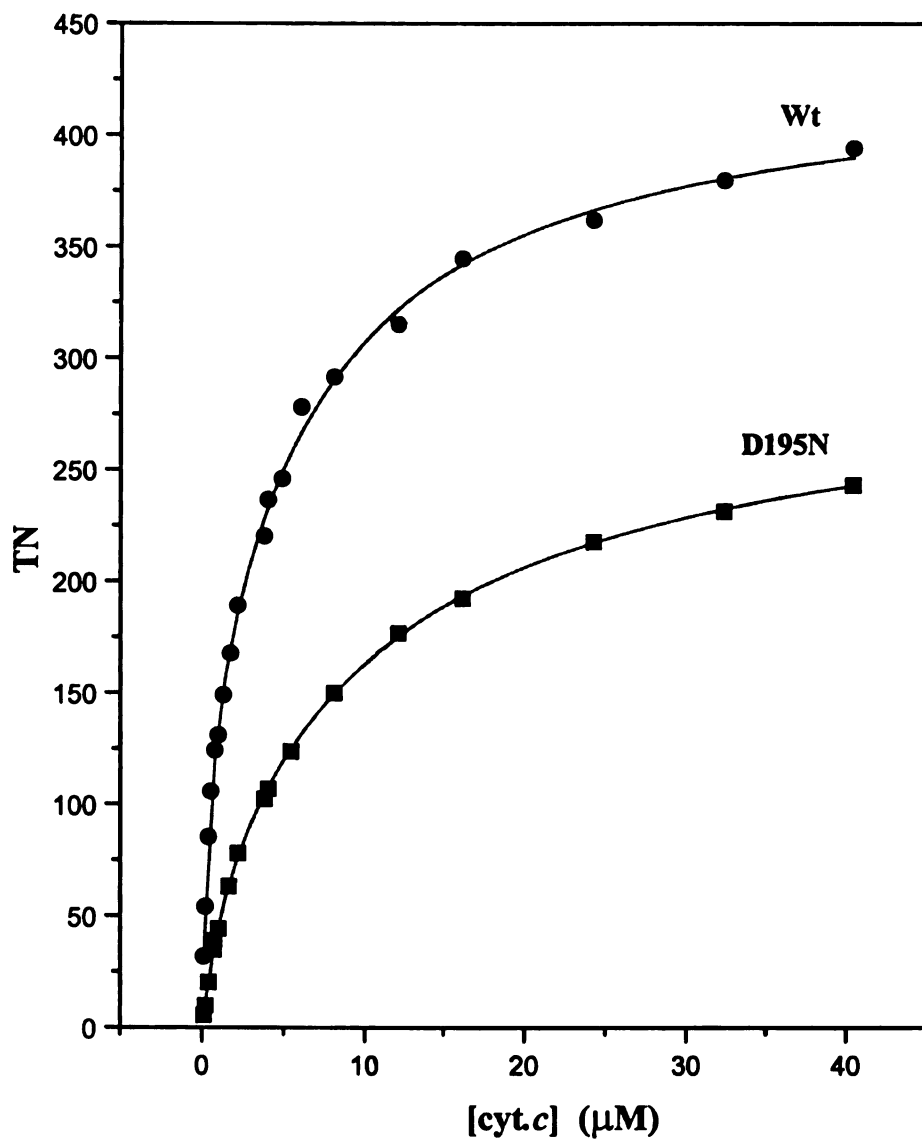


**Figure 4.10** Steady-state kinetics assay of *R. sphaeroides* CcO with *R. sphaeroides* cytochrome  $c_2$ . The experimental condition is described in the Materials and methods. The solid lines are the kinetic fitting results with Eq. 11. The  $K_M$  values for wt and D195N enzymes are listed in table 4.3.

in Table 4.3. The  $K_M$  values of the high-affinity phases for wild-type oxidase are 0.35  $\mu\text{M}$  and 0.04  $\mu\text{M}$  for *R. sphaeroides* cytochrome  $c_2$  and horse *Cc*, respectively, suggesting that horse *Cc* binds more tightly with *R. sphaeroides* CcO than does *R. sphaeroides* cytochrome  $c_2$ , but the latter *Cc* gave more readily analyzed and reproducible kinetics. The  $K_M$  values of the high-affinity phases obtained with *R. sphaeroides* cytochrome  $c_2$  for D188N/E189Q and D151N/E152Q are comparable to that of wild-type oxidase, while the values for E148Q, D195N and E157Q are two to three-fold higher than those of wild-type oxidase. These studies suggest that Asp-188, Glu-189, Asp-151 and Glu-152 are not involved in binding cytochromes *c* at all, while Glu-148, Asp-195 and Glu-157 are important contributors to the electrostatic aspect of binding to *R. sphaeroides* cytochrome  $c_2$ . It is interesting to notice that the  $K_M$  value of the high-affinity phase for D214N with *R. sphaeroides* cytochrome  $c_2$  is comparable to that of wild-type oxidase, while the value obtained with horse *Cc* is about three-fold higher than that of wild-type oxidase. So Asp-214 is likely to be involved in binding horse *Cc*, but not *R. sphaeroides* cytochrome  $c_2$ . This result is in agreement with the fact that the turnover numbers for D214N and wild-type are comparable when reacted with *R. sphaeroides* cytochrome  $c_2$ , while it is much lower for D214N when reacting with horse *Cc*.

The  $K_M$  values obtained in this study are generally very small, and the differences between those of wild-type and mutant enzymes are also very small. This is likely due to the experimental conditions used in this study, that is, at low ionic strength. Under this condition, cytochromes *c* still form tight complexes with the oxidase mutants, although the binding strengths of E148Q, D195N, E157Q and D214N are weaker. At higher ionic strength, relatively larger differences between the  $K_M$  values of wild-type and

**Table 4.3** The  $K_M$  values for the interactions of *R. sphaeroides* cytochrome *c* oxidases with *R. sphaeroides* cytochrome *c*<sub>2</sub> and horse cytochrome *c*

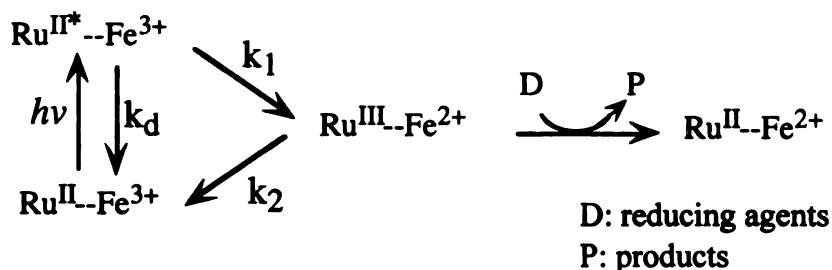
Enzymes	<i>R.</i>		<i>sph</i>		Cyt. <i>c</i> <sub>2</sub>		Horse		Cyt. <i>c</i>	
	$K_{M1}$ ( $\mu$ M)	$k_a$ ( $s^{-1}$ )	$K_{M2}$ ( $\mu$ M)	$k_b$ ( $s^{-1}$ )	$K_{M1}$ ( $\mu$ M)	$k_a$ ( $s^{-1}$ )	$K_{M2}$ ( $\mu$ M)	$k_b$ ( $s^{-1}$ )	$K_{M1}$ ( $\mu$ M)	$k_b$ ( $s^{-1}$ )
wild-type	$0.35 \pm 0.09$	$1.44 \pm 20$	$6.71 \pm 0.99$	$4.35 \pm 7$	$0.04 \pm 0.04$	$36 \pm 29$	$0.85 \pm 0.20$	$690 \pm 8$	$0.85 \pm 0.20$	$690 \pm 8$
D188N/E189Q	$0.39 \pm 0.05$	$1.45 \pm 10$	$9.56 \pm 1.32$	$392 \pm 7$	$0.02 \pm 0.01$	$80 \pm 19$	$1.00 \pm 0.11$	$445 \pm 12$	$1.00 \pm 0.11$	$445 \pm 12$
D151N/E152Q	$0.44 \pm 0.11$	$1.49 \pm 21$	$8.62 \pm 1.63$	$415 \pm 9$	$0.05 \pm 0.04$	$100 \pm 54$	$0.72 \pm 0.11$	$487 \pm 5$	$0.72 \pm 0.11$	$487 \pm 5$
E148Q	$0.66 \pm 0.20$	$192 \pm 38$	$7.13 \pm 1.46$	$475 \pm 9$	$0.09 \pm 0.03$	$219 \pm 44$	$1.17 \pm 0.22$	$582 \pm 7$	$1.17 \pm 0.22$	$582 \pm 7$
D195N	$1.64 \pm 0.38$	$105 \pm 19$	$13.11 \pm 2.07$	$300 \pm 6$	$0.12 \pm 0.04$	$220 \pm 40$	$2.32 \pm 0.75$	$499 \pm 12$	$2.32 \pm 0.75$	$499 \pm 12$
E157Q	$1.18 \pm 0.14$	$1.41 \pm 23$	$11.26 \pm 2.59$	$335 \pm 8$	$0.12 \pm 0.05$	$217 \pm 44$	$1.91 \pm 0.57$	$523 \pm 9$	$1.91 \pm 0.57$	$523 \pm 9$
D214N	$0.43 \pm 0.20$	$79 \pm 20$	$6.85 \pm 1.54$	$263 \pm 6$	$0.02 \pm 0.01$	$53 \pm 10$	$0.73 \pm 0.08$	$261 \pm 2$	$0.73 \pm 0.08$	$261 \pm 2$
E254A	$0.29 \pm 0.06$	$34 \pm 4$	$7.54 \pm 1.38$	$88 \pm 2$	-	-	-	-	-	-
W143F	$1.00 \pm 0.25$	$44 \pm 8$	$10.0 \pm 1.54$	$137 \pm 3$	$0.03 \pm 0.01$	$45 \pm 3$	$1.84 \pm 0.37$	$84 \pm 1$	$1.84 \pm 0.37$	$84 \pm 1$

mutant enzymes may be observed as in the *P. denitrificans* studies (Witt et al., 1998a), but the interpretation of the initial phases is even more complex.

**Laser flash photoreduction study of electron transfer rates into, and within, *R. sphaeroides* CcO**

**Kinetics of wild-type oxidase:**

The electron transfer reaction between Cc and the *R. sphaeroides* CcO has been studied using a flash-induced photoreduction technique. Horse Cc with ruthenium bipyridine covalently attached to Lys-55 at the bottom of Cc was used since this site is remote from the binding domain. Earlier studies have shown that the attachment of a ruthenium group at this position does not affect the interaction of Cc with CcO (Pan et al., 1993). Laser flash photolysis of Ru-55-Cc results in rapid electron transfer from excited Ru<sup>II\*</sup> to heme *c* Fe<sup>3+</sup> with a rate constant ( $k_1$ ) of  $4 \times 10^5 \text{ s}^{-1}$ , as shown in scheme 3:

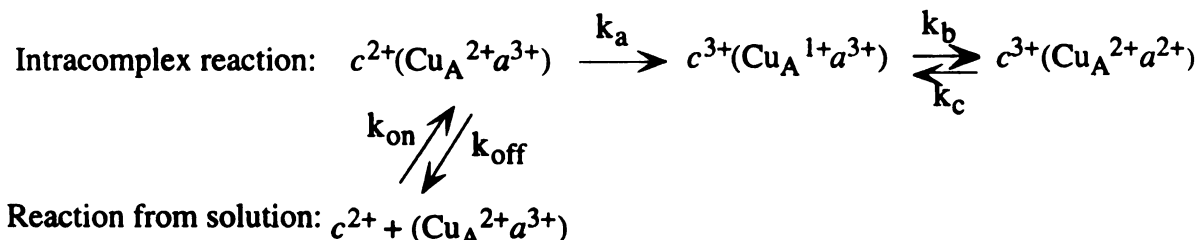


Scheme 3

Aniline and 3-carboxyl-2,2,5,5-tetramethyl-1-pyrrolidinyloxy (3-CP) are used as electron donors to reduce Ru<sup>III</sup>, preventing the back reaction  $k_2$ . The electron transfer rates from

Cc to Cu<sub>A</sub> and from Cu<sub>A</sub> to heme *a* were measured by following transients at 550 nm for Cc oxidation, 605 nm for heme *a* reduction, or 830 nm for Cu<sub>A</sub> reduction.

Electron transfer from Ru-55-Cc to CcO occurs as shown in the following scheme:



$k_{a1}$ : the intracomplex ET rate from Cc to Cu<sub>A</sub>.

$k_{a2}$ : the ET rate from free Cc to Cu<sub>A</sub>.

$k_b$ : the forward ET rate from Cu<sub>A</sub> to heme *a*.

$k_c$ : the reverse ET rate from heme *a* to Cu<sub>A</sub>.

#### Scheme 4

Under the experimental condition, where the oxidase concentration is equal to or greater than that of Ru-55-Cc, Ru-55-Cc forms a 1:1 complex with CcO at low ionic strengths. Flash photolysis of the 1:1 complex between Ru-55-Cc and CcO leads to rapid reduction of Cc, followed by reoxidation with a rate constant of  $4 \times 10^4 \text{ s}^{-1}$  (Table 4.4), as indicated by the 550 nm single exponential decay transient (Figure 4.11). The 605 nm transient indicates that heme *a* is also reduced with approximately the same rate constant. At low ionic strength, the rate constants measured by following 550 nm and 605 nm transients are independent of the concentrations of Ru-55-Cc and CcO, providing that the oxidase concentration is equal or greater than that of Ru-55-Cc, suggesting that the measured rates represent the intracomplex electron transfer rates. After each laser flash, the relative amounts of reduced heme  $a^{2+}$  and Cu<sub>A</sub><sup>1+</sup> formed upon completion of the transients were in the ratio of 6.1:1, indicating that the equilibrium constant ( $K = k_b/k_c$ ) for electron transfer between Cu<sub>A</sub> and heme *a* was 6.1 (Table 4.4).

Table 4.4 Electron transfer from Ru-55-Cc to *R. sphaeroides* cytochrome *c* oxidase

Enzymes	$k_{a1}$ ( $s^{-1}$ )	$k_{a2}$ ( $s^{-1}$ )	Fast phase (%)	$k_{2nd}$ ( $\mu M^{-1}s^{-1}$ ) @ 95 mM NaCl	$k_b$ ( $s^{-1}$ )	K ( $k_b/k_c$ )
Wild-type	40,000	-	100	310.1	$1.2 \times 10^5$	6.1
W143A	32	-	100	-	-	-
W143F	85	-	100	-	-	-
E148Q	15,000	-	100	124.8	$> 10^5$	5.7
D151N/E152Q	45,000	-	100	192.3	$> 10^5$	5.5
E157Q	12,000	260	74	58.2	$> 10^5$	4.9
D188N/E189Q	45,000	-	100	285.3	$> 10^5$	6.0
D195N	25,000	59	89	152.5	$> 10^5$	5.2
D214N	700	85	60	36.7	$> 10^5$	6.2
D229N	4,700	40	34	29.1	-	$> 20$
E254A	10,500	-	100	120	-	$> 15$

$k_{a1}$ : intracomplex ET rate from Cc to  $Cu_A$ ;  $k_{a2}$ : ET rate from free Cc to  $Cu_A$ .

$k_{2nd}$ : second-order rates.

**Figure 4.11 Photoinduced electron transfer from Ru-55-Cc to cytochrome c oxidase.** **A**, 550 nm transient for wild-type; **B**, 605 nm transient for wild-type; **C**, 605 nm transient for E157Q. The solutions contained 5 mM Tris, pH 8.0, 0.05 % LM, 10 mM aniline and 1 mM 3-CP. The enzyme and cytochrome *c* concentrations are: 15.9  $\mu\text{M}$  wild-type oxidase with 9.5  $\mu\text{M}$  of Ru-55-Cc, 14.6  $\mu\text{M}$  of E157Q with 11.4  $\mu\text{M}$  of Ru-55-Cc. The solid lines are the best fits, with one exponential for **A** and **B** with a rate of  $4 \times 10^4 \text{ s}^{-1}$ , and two exponential case for **C**, with rates of  $k_1 = 12,000 \text{ s}^{-1}$  and  $k_2 = 260 \text{ s}^{-1}$ .

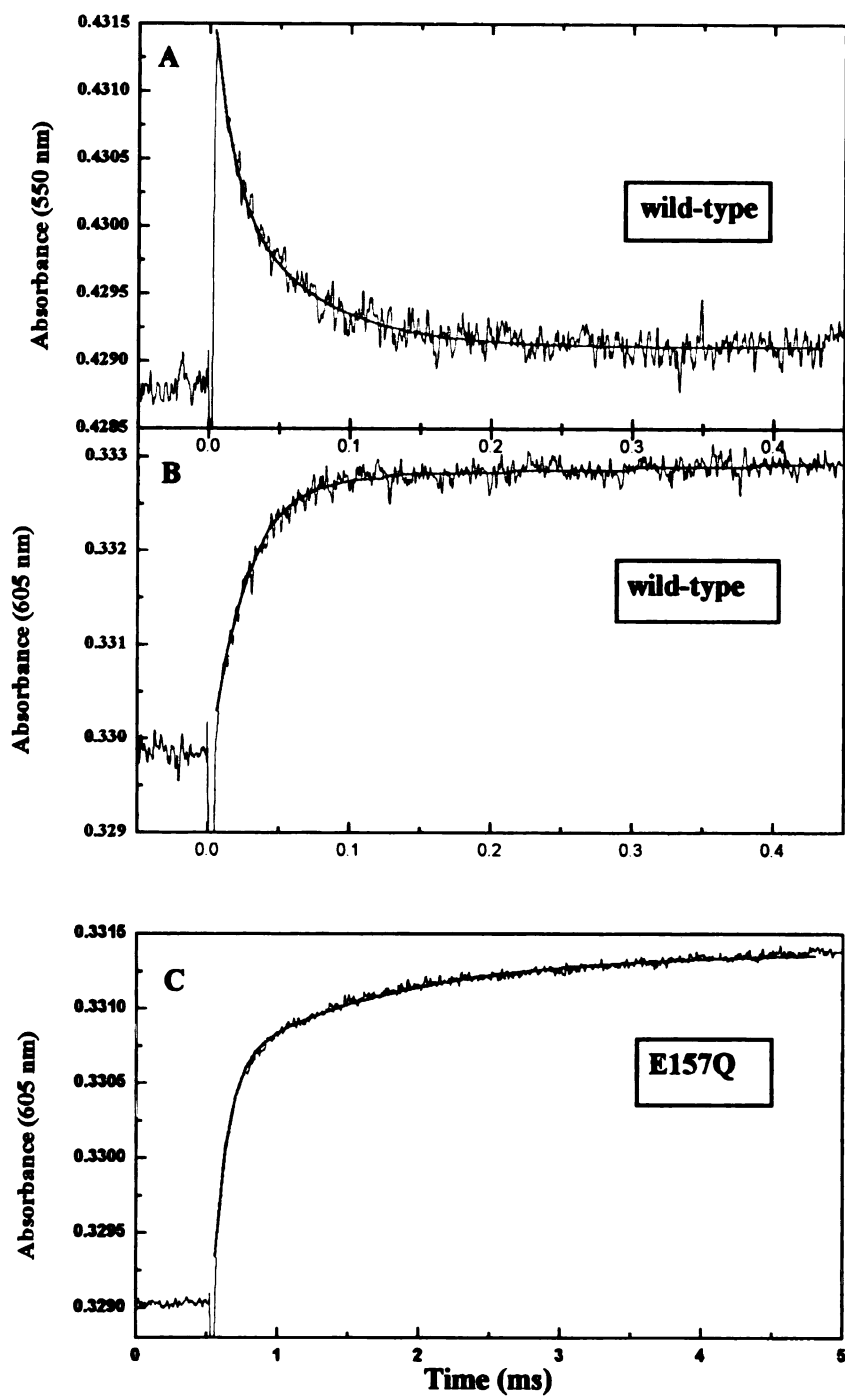


**Figure 4.11** Photoinduced electron transfer from Ru-55-Cc to cytochrome *c* oxidase

In order to measure the value of  $k_b$ , the very rapid direct photoreduction of CcO by a dimer of Ru(bpy)<sub>3</sub> has been studied. This compound, which has a charge of 4+, is likely to bind specifically to the Cc binding site on CcO and can reduce Cu<sub>A</sub> directly within 1 μs. Using this method, the rate constant  $k_b$  for electron transfer from Cu<sub>A</sub> to heme *a* was measured to be  $1.2 \times 10^5 \text{ s}^{-1}$ . The much faster rate measured for  $k_b$  than  $k_a$  can explain the similar rate constants observed for the oxidation of Cc and the reduction of heme *a* observed in this and other studies (Antalis & Palmer, 1982), since the electron transfer from Cc to Cu<sub>A</sub> will be rate-determining for both steps.

The electron transfer rate in the 1:1 complex with wild-type oxidase remains independent of ionic strength from 5 to 45 mM, and the reactions proceed according to the top line in scheme 4. Under these conditions, only fast phase reactions were observed with a constant rate ( $k_{a1}$ ) of  $4 \times 10^4 \text{ s}^{-1}$ . With further increase of ionic strength (> 45 mM), the amplitude of the fast phase gradually decreases, indicating that more Cc is dissociated from the complex. But these higher salt concentrations do not appear to alter the orientation of Cc in the complex, as evidenced by the unchanged fast phase rate observed.

At 55 mM ionic strength, a second, slow phase appears with a rate constant ( $k_{a2}$ ) of  $6900 \text{ s}^{-1}$ . The slow phase is due to the reaction of free Ru-55-Cc with CcO, following a second-order reaction according to the bottom line in scheme 4. When both fast and slow phases are present, the dissociation constant ( $K_D$ ) can be calculated using the following formula (Geren et al. (1995)):

$$K_D = (1-f) (E_0 - f C_0) / f \quad (\text{Eq. 13})$$

where  $C_0$  and  $E_0$  are the total  $Cc$  and oxidase concentrations, respectively, and  $f$  is the relative amplitude for the fast phase ( $f = Cc-CcO/(Cc_{\text{free}} + Cc-CcO)$ ). With 9.5 mM of  $Cc$  and 15.9 mM of  $CcO$ , a relative amplitude of 53% for the fast phase at 55 mM ionic strength indicates an equilibrium dissociation constant ( $K_D$ ) of 6.9 mM. At 75 mM ionic strength, the rate constant of the slow phase increases to  $7900 \text{ s}^{-1}$ , and the relative amplitude for the fast phase decreases to 32%, indicating a dissociation constant  $K_D$  of 27 mM. The fast phase rate constant ( $k_a$ ) remains constant at  $4 \times 10^4 \text{ s}^{-1}$  from 5 mM to 75 mM ionic strength, indicating that the nature of the 1:1 complex does not change with the increase in salt concentration.

At ionic strengths above 75 mM, the fast phase disappeared entirely and the rate constant of the slow phase began to decrease (Figure 4.12). The rate constants of the slow phase at each ionic strength are the same for the 550 nm and 605 nm transients. The relative amount of reduced heme  $a^{2+}$  and  $Cu_A^{+1}$  formed remain in the ratio of 6.1:1 at all ionic strengths, indicating that the equilibrium constant for electron transfer between  $Cu_A$  and heme  $a$  remains constant at  $K = 6.1$ . The rate constant of the slow phase is a linear function of the  $CcO$  concentration above 90 mM ionic strength, indicating that the slow phase is due to a bimolecular reaction between Ru-55- $Cc$  and  $CcO$ . The calculated second-order rate constant  $k_{2nd}$  decreases as the ionic strength increases, consistent with the reaction between opposite charged proteins (Figure 4.12).

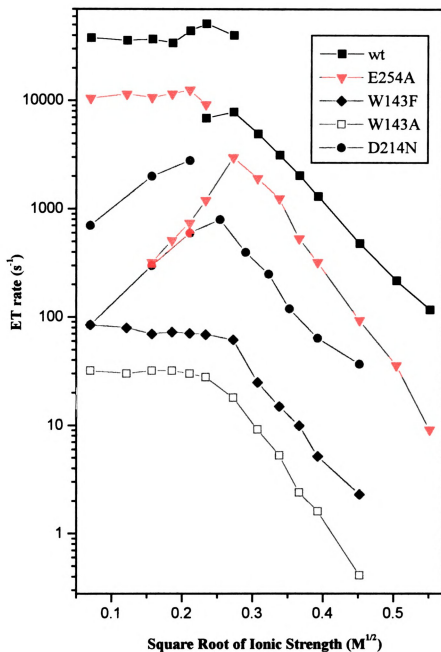


**Figure 4.12** Ionic strength dependent electron transfer from Ru-55-Cc to cytochrome c oxidase. The rates ( $k_{\text{obs}}$ ) are measured from the ruthenium-kinetics assays, with rates for both the fast and slow phases plotted together.

**Kinetics of CcO mutants:****Carboxylate-deficient mutant enzyme kinetics**

The kinetics of the ruthenium-labeled Cc interaction with the carboxylate-deficient mutant enzymes have been studied as for the wild-type oxidase. But unlike the wild-type oxidase, some mutant enzymes showed biphasic kinetics at lower ionic strength, with fast and slow phases (Figure 4.11). The slow phase represents either unbound Cc reacting from solution due to the decreased binding constant, or Cc bound in the wrong conformation. The rate constants and the amplitudes for the fast phases of mutants are listed in Table 4.4.

**Double mutants:** D151N/E152Q and D188N/E189Q double mutant enzymes have similar kinetics as to wild-type (Table 4.4). At low ionic strength, both mutant enzymes have a single fast phase, with a rate constant equivalent to that of wild-type oxidase. The peak positions for the ionic strength dependent slow phase electron transfer rate are equivalent to that of wild-type (Figure 4.13), suggesting there are similar Cc binding strengths of these two mutants and wild-type oxidase. The second-order rate constant of D151N/E152Q is lower than that of wild-type, while the rate for D188N/E189Q is closer to that of wild-type.

**E148Q:** The kinetics of the E148Q mutant is intermediate between those of wild-type and E157Q. At low ionic strength, only a single fast phase is observed with a rate constant of  $15,000 \text{ s}^{-1}$ . At 35 mM ionic strength, a slow phase appears. Like all the other oxidases, the ionic strength dependent slow phase rate follows a bell-shaped behavior (Figure 4.13), with the peak position at 55 mM ionic strength, which, obviously, is lower than the corresponding peak of wild-type oxidase.

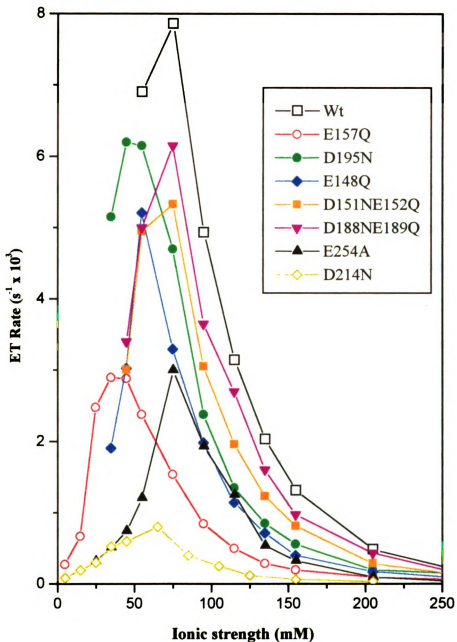


**Figure 4.13** Ionic strength dependent of the slow phase of electron transfer from Ru-55-Cc to cytochrome *c* oxidases. The rates plotted are the observed rate constants ( $k_{obs}$ ).

**E157Q and D195N:** Both E157Q and D195N mutants have two phases at low ionic strength with different rate constants (Table 4.4). The fast phase rate constant for D195N is about twice as large as that of E157Q. The rate constants of the fast phases do not change as the ionic strength is increased, but the amplitude decreases to zero by 35 mM for E157Q and 45 mM for D195N. The slow phases, the result of the interactions of free Cc with free CcO, increase to a maximum of  $2900\text{ s}^{-1}$  at 35 mM ionic strength for E157Q, and  $6200\text{ s}^{-1}$  at 45 mM ionic strength for D195N, and then decrease (Figure 4.13). Compared to wild-type oxidase, the peaks of the slow phase rates for E157Q and D195N shift to lower ionic strengths, indicating that the Cc binding strengths of these two mutants are weaker, which is in agreement with the results from ionic strength dependent turnover assays.

**D214N:** The kinetics of D214N are also altered with rate constants of  $700\text{ s}^{-1}$  and  $85\text{ s}^{-1}$  at low ionic strength (Table 4.4). Unlike wild-type and other mutants, the fast phase rate constant of D214N increases to  $2800\text{ s}^{-1}$  at 45 mM ionic strength and then disappears with further increasing of ionic strength (Figure 4.12). The rate constant of the slow phase increases to  $800\text{ s}^{-1}$  as ionic strength increasing to 65 mM, and then decreases with further increasing of ionic strength (Figure 4.12). The second-order rate constant is only  $19\text{ mM}^{-1}\text{ s}^{-1}$  at 95 mM ionic strength, compared to  $310\text{ mM}^{-1}\text{ s}^{-1}$  for wild-type oxidase (Table 4.4). The equilibrium constant for electron transfer between Cu<sub>A</sub> and heme *a* is the same as wild-type (Table 4.3), indicating that the electron transfer between Cu<sub>A</sub> and heme *a* is not altered.

**D229N and E254A:** The kinetics of D229N mutant are greatly affected as expected from their altered structural characteristics, with a biphasic transient at 5 mM

ionic strength of 4700 s<sup>-1</sup> and 40 s<sup>-1</sup>. However, under the same conditions, a single fast phase is observed for E254A with a rate constant of 10500 s<sup>-1</sup>, and the slow phase for E254A does not emerge until the ionic strength increases to 25 mM. The fast phase rate constants for D229N and E254A do not change at low ionic strengths, until the fast phases completely disappear at 55 mM ionic strength. The slow phase rate constants for D229N and E254A increased to a maximum of 400 s<sup>-1</sup> and 3000 s<sup>-1</sup>, respectively, at 75 mM ionic strength, and then decrease (Figure 4.12). Considering the heterogeneity of the sample, the slow phase observed for D229N is likely to be from the portion of C<sub>c</sub> that is in the wrong conformation in the low ionic strength buffer, resulting in a slow rate. C<sub>c</sub> in the optimal configuration with oxidase still gives much faster electron transfer rate. The rearrangement of the improperly-bound C<sub>c</sub> with increasing ionic strength, together with the fact that more C<sub>c</sub> dissociated from the complex, contributes to the observed increase in amount of the slow phase rate. The second-order rate constants for D229N and E254A decrease to 29 mM<sup>-1</sup>s<sup>-1</sup> and 120 mM<sup>-1</sup>s<sup>-1</sup> at 95 mM ionic strength, respectively. No 830 nm transient is observed for D229N, indicating that the equilibrium constant (K) between Cu<sub>A</sub> and heme *a* in this mutant is greater than 20. The K value in E254A is greater than 15. The severe kinetic changes in D229N observed from the ruthenium kinetics assay are consistent with the fact that the heme *a* center has been altered. As a consequence, the redox potentials for heme *a* are changed, altering the equilibrium constant for electron transfer between Cu<sub>A</sub> and heme *a*. In D229N, heme *a* is likely to become more positive; as a result, electrons are more likely to stay associated with heme *a*, accounting for the fact that heme *a* in the resting form of the oxidase tends to stay reduced.

It is worthy to point out that the ionic strength (75 mM) where the slow phases of reactions for D229N and E254A reach the maximum is same as that of the wild-type oxidase (Figure 4.12, 4.13), suggesting that the *Cc* binding strengths of these two mutants are identical to that of wild-type. This further implies that Asp-229 and Glu-254 are not involved in *Cc* binding, which is consistent with their locations in the protein.

The effects of mutations on both the intracomplex rate constants  $k_a$  and the second-order rate constants  $k_{2nd}$  follows the same order: D214N > D229N > E157Q > E254A > E148Q > D195N > D151N/E152Q > D188N/E189Q > wild-type; The *Cc* binding strengths for D214N, E157Q, E148Q and D195N are lower than that of wild-type, while all the other mutants are comparable to that of wild-type.

#### **W143F and W143A kinetics:**

At low ionic strength, a rate constant of  $85\text{ s}^{-1}$  is observed for W143F *CcO*. This rate is independent of the concentrations of *Cc* and *CcO*, and therefore reflects the intracomplex electron transfer from Ru-55-*Cc* to  $\text{Cu}_A$ . Because of the extremely slow electron transfer rate, the slow phase reaction, if there is one, is difficult to resolve. The intracomplex rate constant remains the same until 75 mM ionic strength, and then decreases with further increases in ionic strength, indicating dissociation of the complex (Figure 4.12).

W143A enzyme behaves in the same fashion as W143F, except that the rate constant is smaller,  $32\text{ s}^{-1}$  at low ionic strength. The complex dissociates after 75 mM ionic strength and further increase of ionic strength results in second-order reactions.

For these two mutants, the ionic strength where the intracomplex electron transfer changes to a second-order reaction is the same as for wild-type, indicating that the

dissociation constant of W143F and W143A are about the same as for wild-type. This result indicates that Trp-143 is not a major player in binding Cc, even though it strongly affects electron transfer within the Cc/CcO complex.

### **Analytical ultracentrifuge measurement of the equilibrium dissociation constant $K_D$**

A mixture of Cc and CcO at 1:1 ratio was placed in a centrifuge cell. Under the action of high centrifugal force, Cc, CcO and the Cc/CcO complex, which initially were distributed uniformly through the cell, were caused to sediment at different rates toward the bottom of the cell, based on their sizes. The complex of CcO and Cc, with a larger molecular weight, moved much faster than free Cc.

At low ionic strength solutions (below 25 mM), a single transition was observed at 410 nm in the scanned spectra (Figure 4.14), which represents the complex of CcO and Cc, suggesting that almost all Cc is bound. When the ionic strength of the solution was increased to 45 mM and above, two transitions were readily observed, one for free and one for bound Cc, indicating the presence of a significant amount of dissociated Cc. The free Cc concentration can be quantitated from its extinction at 410 nm, and the equilibrium dissociation constant was obtained at a given salt concentration (Table 4.5). Below 25 mM ionic strength, no measurable free Cc was observed for solutions with either wild-type or mutant proteins, indicating that the  $K_D$  values for all the samples were smaller than 0.2  $\mu\text{M}$ . At 65 mM ionic strength, a  $K_D$  value of 5.3  $\mu\text{M}$  was obtained for the wild-type oxidase, which was in reasonable agreement with the number (9.6  $\mu\text{M}$  at 55 mM ionic strength) obtained using the ruthenium kinetics method.

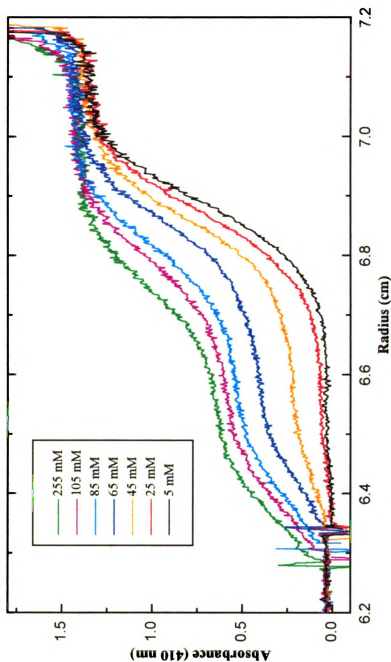


**Figure 4.14** Analytical ultracentrifugation assay of the equilibrium dissociation constant between horse cytochrome *c* and *R. sphaeroides* cytochrome *c* oxidase. The solution contained 300  $\mu$ l of 5 mM Tris-HCl, pH 8.0, 0.1% LM, with 6.0  $\mu$ M horse cytochrome *c* and 6.6  $\mu$ M wild-type oxidase. The ionic strength was adjusted with NaCl. All spectra were recorded after a 1 hr centrifugation. The ionic strength was (from bottom to top) 5, 25, 45, 65, 85, 105, and 255 mM, respectively.

**Table 4.5** Equilibrium dissociation constant  $K_D$  ( $\mu\text{M}$ ) from analytical ultracentrifuge assays for the binding of horse cytochrome *c* to *R. sphaeroides* cytochrome *c* oxidase

I (mM)	Wild-type	D188N E189Q	D151N E152Q	D195N	E148Q	E157Q	D214N	D229N	E254A	W143A	W143F
5	<0.2	<0.2	<0.2	<0.2	<0.2	<0.2	<0.2	<0.2	<0.2	<0.2	<0.2
25	<0.2	<0.2	<0.2	<0.2	<0.2	<0.2	<0.2	<0.2	<0.2	<0.2	<0.2
45	1.0	1.3	1.6	2.3	2.3	3.9	3.2	0.9	1.0	0.9	1.5
65	5.6	6.4	7.3	12	12	27	15	4.7	4.7	5.6	7.3
85	18	20	22	46	32	54	49	12	13	21	16
105	35	38	39	> 60	> 60	> 60	> 60	-	-	-	-

Both D188N/E189Q and D151N/E152Q have been shown to be very similar to wild-type oxidase in the kinetics assay, and the  $K_D$  values obtained from the centrifuge assay were also almost the same as those of the wild-type oxidase under various ionic strength conditions (Table 4.5). This further supports the conclusion that Asp-188, Glu-189, Asp-151, and Glu-152 are not involved in *Cc* binding.

The  $K_D$  values for D195N, E148Q, E157Q and D214N were two to three times larger than those of the wild-type oxidase at different ionic strengths, indicating weaker binding between these mutated oxidases and *Cc*, consistent with the kinetics assay. The changes in the binding strengths estimated from this study are consistent with the steady-state and rapid kinetics assays.

In the ultracentrifuge assay, all mutant proteins, except D229N, had essentially the same Svedberg coefficient as wild-type (9.5 S). However, D229N had a smaller Svedberg coefficient than wild-type, probably indicating loss of subunits in this unstable mutant. Thus it is more difficult to distinguish the free *Cc* band from the *Cc/CcO* complex, resulting in a much bigger error associated with the calculation for D229N. The  $K_D$  values obtained were comparable to that of wild-type oxidase, but cannot be given much confidence.

## Discussion

### **The surface region of *Cc* that interacts with various redox partners**

The interactions of *Cc* with its physiological partners, like *CcO* and *Cc* peroxidase, and nonphysiological partners, including cytochrome *b<sub>5</sub>* and plastocyanin,

have been studied thoroughly using a variety of techniques, trying to answer the question of what surface areas of these proteins are involved in *Cc* binding. Answering this question is important for understanding the mechanism and regulation of electron transfer in biological systems.

Among different redox partners, the interaction of *Cc* with *CcP* is the best characterized. The crystal structures of *CcP/Cc* complexes clearly resolve the detailed interactions between these two proteins (Pelletier & Kraut, 1992), and the electron transfer kinetics have also been well studied (Wang et al., 1996). Moreover, mutagenesis and spectroscopic studies have established that the interface resolved in the crystal structures represent the kinetically competent interaction in solution (Miller et al., 1996). Based on the evidence that *Cc* uses a similar surface region, including a cluster of conserved lysine residues, to interact with its various redox partners (Margoliash & Schejter, 1996), the *Cc/CcP* system becomes a good model for studying the interaction of *Cc* with *CcO*.

In the present study, a number of carboxyl residues in subunit II of *CcO*, as well as a centrally located tryptophan, were mutated to neutral residues, and the effects on *Cc* binding and electron transfer were studied. On the basis of these studies and with the guidance of the crystal structures of *CcO*, a *Cc* binding site is proposed (Figure 4.15).

#### **Nature of the interaction between *Cc* and *CcO*: ionic strength effects**

Previous studies have established that the interaction between *Cc* and its redox partners has a major electrostatic component, which is ionic strength dependent. The effects of ionic strength on turnover number and the second-order reaction were studied

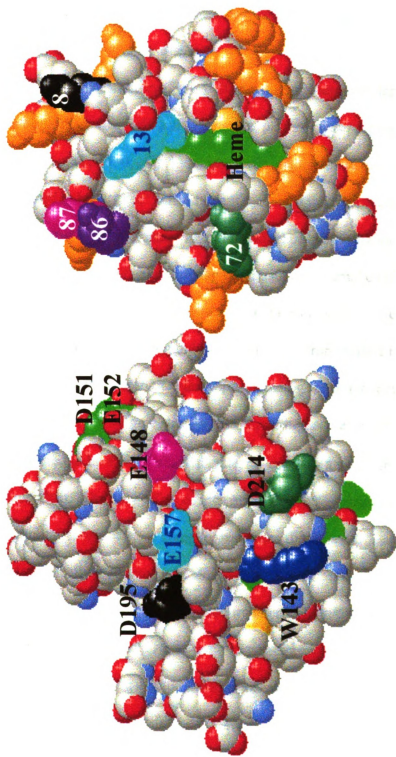


**Figure 4.15** Spacefilling models of subunit II C-terminus domain of cytochrome c oxidase (A) and horse cytochrome c (B). The oxidase structure is created from the coordinates of *P. denitrificans* oxidase, with *R. sphaeroides* oxidase numbering. The heme group in cytochrome c is shown in green, and the lysine residues are highlighted, with those proposed involved in the binding numbered.

here, and bell-shaped profiles were observed. At various intermediate ionic strengths (75 mM for wild-type), wild-type and mutant forms of CcO display the maximum electron transfer rates. Increasing or decreasing the ionic strength with respect to this peak position slows down the rates.

An interpretation of this bell-shaped ionic strength dependent profile for the reaction of Cc with CcO and other redox partners was proposed by Tollin and coworkers (Hazzard et al., 1990; 1991). At low ionic strengths, Cc and its redox partners are suggested to be "locked" into a nonoptimal configuration, accounting for the observed slow overall electron transfer rate. The effect of increasing ionic strength is proposed to cause Cc to reorient itself, allowing it to reach the optimal configuration for electron transfer, as observed at intermediate (more physiological) ionic strengths. However, in this study, we measured not only the overall electron transfer rates but also the individual rates of internal electron transfer steps, including the intracomplex rate from Cc to Cu<sub>A</sub> and heme *a*. At low ionic strength the intracomplex electron transfer rate from Cc to CcO is measured to be  $4 \times 10^4 \text{ s}^{-1}$ . This rate, observed as a single fast phase, is ionic strength independent. The only effect of increasing ionic strength on the fast phase is to decrease its amplitude, due to more complex becoming dissociated. The results indicate that the electrostatically-stabilized complex at low ionic strengths for wild-type CcO is at the optimal orientation for rapid electron transfer. The ruthenium photolysis technique allows this intracomplex, rapid electron transfer event to be resolved, while other methods using soluble reducing agents or traditional stopped-flow experiments can not detect it. Thus, the Tollin hypothesis is incorrect.

Although at low ionic strength, *Cc* is in the optimal conformation with wild-type *CcO* for rapid electron transfer, it may form a improperly-oriented complex with *CcO* when the binding domain on *CcO*, or the conformation of the oxidase, has been changed, as in the case of some mutant enzymes. At low ionic strength, D214N appears to form mostly improperly-oriented, unproductive complexes with *Cc*, as evidenced by the low intracomplex electron transfer rate observed. The addition of salt allows the complex to reorient itself to form a more optimal conformation as evidenced by the increase of the intracomplex electron transfer rate up to 45 mM ionic strengths. The severe effect observed for D214N on electron transfer suggests its critical role in orienting *Cc*.

The mutant form, D229N, is observed to adopt several conformations detected by spectral methods. In this case, slow multiphasic intracomplex rates may also be due to improperly-oriented complexes at low ionic strength. But like wild-type, its fast phase rate does not change with salt concentrations.

In the rapid kinetics assay, the slow phase normally represents the reaction of *Cc* from solution, in a second-order reaction. The formation of the bell-shaped profile for the slow phase reaction is due to the different effects of ionic strength on the  $k_{\text{on}}$  and  $k_{\text{off}}$  rates. At low ionic strength in a steady-state assay, the dissociation of oxidized *Cc* (after the rapid intracomplex electron transfer events) is rate limiting for turnover (Sinjorgo *et al.*, 1984); increasing the ionic strength increases the  $k_{\text{off}}$  rate, resulting in a much faster rate. Similarly, in the flash-induced electron transfer reactions, increasing ionic strength results in more dissociated *Cc* and *CcO* available to participate in the second order, diffusion limited reaction. However, the increasing ionic strength also decreases the  $k_{\text{on}}$  rate because of the shielding of charges by the ions in the solution. Rapid flash-induced

kinetics studies on the interaction between Cc and CcP (Mei et al., 1996) have shown that at low ionic strengths, the ionic strength effects on  $k_{\text{off}}$  were dominant, resulting in a net increase in the second order electron transfer reaction. At an intermediate ionic strength, the effects on  $k_{\text{off}}$  and  $k_{\text{on}}$  reach a balance, where the enzyme displays maximum rates. Further increase in ionic strength greatly decrease the  $k_{\text{on}}$  rate, resulting in the decrease in the overall rate.

In the multiple turnover assay measured by stopped-flow, the intracomplex electron transfer is too fast to be measured, and the overall rate measured is basically following the second-order reaction, which is equivalent to the slow phase observed in the rapid kinetics assay. However, in these two assays, different ratios of Cc/CcO have been used. In the former experiments, the Cc to CcO ratios are in the range of 400:1 to 1000:1, while in the latter, they are about 1:1. In excess, Cc will presumably bind to both the high and low-affinity sites, while at 1:1 ratio, Cc will occupy the high-affinity site first. The similar ionic strengths observed for the maximum turnover rates under steady-state conditions, and for the maximum slow phase reaction rates in the rapid kinetics assay suggest that the high-affinity site controls the overall rate, and its binding strength with Cc influences the peak position for the bell-shaped curve, as expected.

### **The effects of mutations in charged residues on Cc binding and electron transfer**

The electrostatic attraction involved in binding Cc and CcO is a long-range force that can pre-orient approaching molecules and thus enhance the proportion of productive encounters. After the molecules approach each other, solvent is partly excluded from the protein-protein interface, and the opposite charges on each molecule are partially

neutralized. Newly-formed hydrogen bonds at the interface, together with hydrophobic and van der Waals interactions, are likely to further stabilize the complex. Although some water molecules are excluded from the interface, the crystal structure of the complex between CcP/Cc (Pelletier and Kraut, 1992) shows that a number remain. These surface-bound waters are likely important for structural stability, catalysis, and molecular recognition (Kuhn et al., 1992).

The effect of mutations that neutralize negative charges in the interaction domain of CcO is expected to be at least two-fold: first, the change in electrostatic potential on the surface of CcO may affect the strength and position of docking of Cc with the oxidase; second, in a slightly (or greatly) disoriented complex, the electron transfer rate may be altered. The change of charges at the protein-protein interface will also affect water exclusion. Because water affects the shape and chemistry of the protein surface, it also contributes to the effects on docking. Thermodynamic studies on Cc reactions with carboxyl mutants of CcP show that the major difference in the thermodynamic parameters of the mutants relative to the wild-type enzyme is due to the differences in releasing of water of hydration from a neutral asparagine or glutamine residue rather than from a charged aspartate or glutamate as the two proteins interact (Erman et al., 1997), which accounts for some of the lower binding affinities among these mutant enzymes. Any changes in the retention of surface-bound water in the Cc/CcO may affect the protein-protein interface and hence the electron transfer rate, due to possible alteration of the length of the electron transfer pathway, the intervening medium, and the reorganization energies associated with the redox centers.

### **Comparison of horse and *R. sphaeroides* Cc interaction with *R. sphaeroides* CcO**

The physiological substrate for *R. sphaeroides* CcO is not clear, although studies from *P. denitrificans* suggest that the membrane-bound cytochrome  $c_{552}$  may be the direct electron donor *in vivo* (Berry and Trumpower, 1985), whereas other studies have suggested that the soluble  $c_2$  is the natural substrate (Kituchi et al., 1965). Horse Cc has been found to transfer electrons efficiently to *R. sphaeroides* oxidase, and it has been used in most of the kinetics studies. On the other hand, the soluble cytochrome  $c_2$  from *R. sphaeroides* also reacts with CcO from the same strain, albeit at a slower rate.

The interactions of wild-type and mutant CcO with cytochromes  $c$  from horse and *R. sphaeroides* were compared. The turnover number with 30  $\mu$ M horse Cc is about 3-fold higher than with *R. sphaeroides* cytochrome  $c_2$ , and the apparent binding affinity for horse Cc is about 10 times higher, as indicated by the steady-state kinetics assay. In the reactions with horse Cc and *R. sphaeroides* cytochrome  $c_2$ , D195N and D214N behave differently. With horse Cc, the turnover of D214N is significantly decreased, while with *R. sphaeroides*  $c_2$ , its turnover is significant higher. Similarly, kinetics assays have shown that the mutation in D214N has almost no effect on the binding of *R. sphaeroides* cytochrome  $c_2$ , but the binding affinity for horse Cc is decreased, suggesting that residue Asp-214 may not be important in the interaction of CcO with *R. sphaeroides* cytochrome  $c_2$ , but critical for binding horse Cc. In contrast, kinetics assays have shown that the binding affinities of D195N for both cytochromes  $c$  are decreased.

Both horse heart cytochrome  $c$  and *R. sphaeroides*  $c_2$  have been crystallized (Bushnell *et al.*, 1990; and 1cxa.pdb), and their overall structures are similar. But these

two proteins differ in many respects, including: (1) The highly conserved Lys-13 and -72 in horse *Cc* are not present in the *R. sphaeroides* cytochrome  $c_2$  (Figure 1.10). Chemical modification studies have indicated that Lys-13 and -72 are important for the interaction of horse *Cc* with its partners (Ferguson-Miller *et al.*, 1978), and the crystal structure of the *CcP/Cc(H)* complex shows the presence of a hydrogen-bond between Lys-72 and an aspartate group from *CcP* (Pelletier and Kraut, 1992). (2) *R. sphaeroides* cytochrome  $c_2$  is more acidic than horse cytochrome *c*, and the distribution of the positive potential involved in binding its partners is different (Tiede *et al.*, 1993). Horse cytochrome *c* has been found to use predominately the positive potential located at the upper left of the front face for the interactions, while the positive potential on *R. sphaeroides*  $c_2$  is distributed on the whole front face. This structural difference of these two cytochromes may cause them to react differently with *CcO*.

Asp-214 and Asp-195 of *CcO* subunit II are two of the residues that possibly interact with these two cytochromes differently. Based on the fact that Lys-13 is absent in *R. sphaeroides* cytochrome  $c_2$ , and the mutation in D214N has less effect on its binding affinity (though still a marked affect on activity), it is tempting to speculate that Asp-214 may interact with Lys-13 or Lys-72 in horse *Cc*. This model is supported by an early study which has shown that Lys-13 can cross-link with His-161 (His-217 in *R. sphaeroides*) of bovine *CcO* (Bisson *et al.*, 1982), which also places Asp-214 in the vicinity of Lys-13. However, the more inhibitory effect on binding of D195N is difficult to interpret. In the model assuming Lys-13 interacting with Asp-214, *Cc* docks “upside down” on the oxidase (See Figure 4.15), with fewer direct charge interaction possibilities for Asp-195 on *CcO* with the cluster of important lysine residues on *Cc*. It is more likely

that Lys-72 in horse Cc interacts with Asp-214 in the oxidase, and *R. sphaeroides* cytochrome  $c_2$  adopts a slightly different binding orientation as to horse Cc. As a result, due to the absence of an equivalent lysine residue to Lys-72 in horse, D214N has less inhibitory effect with *R. sphaeroides* cytochrome  $c_2$  than with horse Cc.

### **Distinction between effects on cytochrome $c$ binding and electron transfer**

Due to their different locations, carboxyl residues contribute differently to the overall Cc binding. Among the six CcO carboxyl mutants studied, D214N has the biggest effect on Cc docking and the intracomplex electron transfer, apparently forming improperly-oriented complexes at low ionic strengths. Although the intracomplex electron transfer rate between Cc and this mutant enzyme increases with increasing ionic strength, the maximum rate is still much lower than the wild-type rate. Moreover, its slow phase rate reaches a maximum at a lower ionic strength (65 mM) than that of wild-type oxidase (75 mM), indicating that the binding strength is decreased. The severe decrease of the electron transfer rate for D214N observed in this study is similar to the results of the study on the isolated Cu<sub>A</sub> domain of *P. denitrificans* oxidase with the same mutation (Lappalainen *et al.*, 1995). While the effect of the same mutation on the holoenzyme from *P. denitrificans* is less dramatic (Witt *et al.*, 1998a). Asp-214 is one of the most conserved residues in CcO, and it is also conserved in another Cu<sub>A</sub>-containing enzyme, nitrous-oxide reductase (Zumft *et al.*, 1992), which also accepts electrons from Cc. In the space-filling models of CcO, Asp-214 is located close to Trp-143, the residue identified in this and another study (Witt *et al.*, 1998b) to be the electron entry site to

$\text{Cu}_A$ . Due to its closeness to Trp-143, mutations of Asp-214 are likely to influence the precise positioning of the exposed edge of heme *c* for optimal electron transfer.

D229N and E254A are the two mutants displaying the severest structural disruption of the oxidase among all the mutant enzymes studied. This is undoubtedly due to the fact that both are internally located, not surface charge residues. In CcO, residue Glu-254 bridges the  $\text{Cu}_A$  and Mg centers, and Asp-229 stabilizes the Mg by forming a hydrogen-bond to one of its direct water ligands. Clearly, the mutations at these two residues destabilize the Mg binding site of the mutant proteins, as indicated by the Mn EPR studies (Figure 4.5). The propionic acid side chain of heme  $a_3$  is also hydrogen-bonded to one of the Mg ligands, His-411. Therefore, the loss of the Mg ion in D229N and E254A would be expected to affect the protein stability and possibly change the redox potential of heme  $a_3$ , due to the nearby charge change. The heme  $a_3$  centers in these two mutants have been found to be reduced much more slowly by dithionite than the intact heme  $a_3$  center in wild-type oxidase, indicating a change in the effective redox potentials of the heme  $a_3$  center, as also observed for other Mg-ligand mutant enzymes (Florens et al., 1998). The disruption of the Mg center also spreads to the heme *a* center through the hydrogen bond networks involving water molecules within this hydrophilic region, as indicated by the shift in the optical spectra.

The mutant enzymes E148Q, D195N and E157Q have moderate effects on Cc binding and electron transfer, but each mutant enzyme has distinct characteristics indicating different contributions to the binding of Cc and to electron transfer within the complex. The maxima of the second order rate constants determined by the photo-induced electron transfer kinetics for all these mutant enzymes is shifted to lower ionic

strengths, suggesting weaker interactions with *Cc*, in the order of E157Q > E148Q > D195N. The rapid kinetic analysis is in good agreement with the results from the binding and the steady-state kinetics assays. However, in the binding assay, all these three mutant enzymes and D214N have similar  $K_D$  values, even though their electron transfer kinetics are distinctly different, suggesting that these residues contribute differently to orienting *Cc* and to the creation of a protein-protein interface conducive to rapid electron transfer. Asp-214 appears to be more involved in correctly orienting *Cc* on the oxidase than in binding per se, compared to Glu-157.

D151N/E152Q and D188N/E189Q behave like wild-type oxidase in most aspects, and therefore residues Asp-151, Glu-152, Asp-188, and Glu-189 appear to be peripheral to the *Cc* binding domain. These two mutant enzymes also serve as excellent controls in all assays.

### **Trp-143 as the electron conduit to $Cu_A$ , and $Cu_A$ as the sole entry site for electrons from *Cc***

The interaction between *Cc* and *CcO* has been studied extensively to determine the electron transfer pathway into the oxidase. The central question has been whether  $Cu_A$  or heme *a* is the initial electron acceptor from *Cc* (Hill, 1993). Early stopped-flow experiments showed that the oxidation of reduced *Cc* at 550 nm corresponded to the rate of reduction of heme *a* as measured by absorbance changes at 605 nm and 444 nm (Wilson et al., 1975), favoring heme *a* as the initial electron acceptor (Wikström et al., 1981). But recent flow-flash (Hill, 1991) and ruthenium photolysis experiments (Pan et al., 1991a) with faster time resolution indicated that  $Cu_A$  was the initial electron acceptor. The later

assignment fits with the exposed external location of Cu<sub>A</sub> revealed in the crystal structures, which is surrounded by a cluster of surface carboxylates likely to form a Cc binding site. However, the possibility of two distinct entry sites, suggested by the complex steady-state kinetics, was not excluded by these analyses.

In this study with *R. sphaeroides* CcO and horse Cc, Cu<sub>A</sub> is also found to be the initial electron acceptor, with a rate constant of  $4 \times 10^4 \text{ s}^{-1}$ . The electron transfer rate from Cu<sub>A</sub> to heme *a* is even faster ( $1.2 \times 10^5 \text{ s}^{-1}$ ); thus heme *a* would be reduced with no measurable lag, accounting for the similar rates observed for the oxidation of Cc and the reduction of heme *a* in the early stopped-flow experiments, where the time-resolution (millisecond) was not able to distinguish either of these rates.

Trp-143 is a highly conserved residue in all the known CcO sequences and in quinol oxidases. In the crystal structure, this residue is located on the surface of subunit II about 5 Å above the Cu<sub>A</sub> center, surrounded by several conserved carboxyl groups. In this and a similar study from *P. denitrificans* (Witt *et al.*, 1998a), these carboxyl residues have been identified to be involved in Cc binding, which places Trp-143 in the middle of the Cc binding domain. In the complex of Cc and CcO, the central location of Trp-143 enables its side chain to be in close contact with the exposed heme edge of Cc, and it is likely to be the electron entry site from Cc to CcO. This residue was mutated to alanine (W143A) and phenylalanine (W143F), and EPR analyses showed that the Cu<sub>A</sub> center was essentially unaltered. In addition, Cc binding strength was the same as with wild-type oxidase, indicating that Cc binds in the normal configuration for electron transfer. However the steady-state turnover numbers and the electron transfer rates from Cc to Cu<sub>A</sub> were severely decreased up to 1000 fold. According to the theory of Onuchic

(Onuchic et al., 1992), electron transfer in proteins depends not only on the driving force, the reorganization energies, and the distance between the redox centers, but also the intervening medium. In the complexes of *Cc* with W143A and W143F, the presence of an intact  $\text{Cu}_A$  center and the normal *Cc* binding conformation suggest that the driving force and the reorganization energies are not likely altered. So the remaining factors that might account for the observed decreased in rate are change in distance or intervening medium. In W143A, the removal of the indole group might be expected to produce a gap between heme *c* and  $\text{Cu}_A$ . While due to the flexibility of the protein, this gap may be filled through the rearrangement of the protein. In the case of the phenylalanine substitution for tryptophan, the replacement of the indole group with a phenyl group, is even less likely to change the distance between heme *c* and  $\text{Cu}_A$ . Nevertheless, in both mutants, the electron transfer rate is almost equally inhibited, suggesting that the nature of the intervening medium and perhaps the unique character of the indole ring, is critical for electron transfer. The involvement of a tryptophan residue in electron injection is not without precedent. In ribonucleotide reductase protein R2 (Parkin et al., 1998), a surface tryptophan residue is also found to mediate electron injection into protein. While the question of whether the residual activities retained by W143A and W143F represent the electron transfer through the replaced side chains or neighboring residues cannot be answered in this study.

In the polarographic steady-state turnover assay, the maximum rate measured for the oxidase reflects the rate-limiting step in the overall reaction, either the reduction of *Cc* by TMPD, the association or dissociation of *Cc* from *CcO* depending on ionic strength conditions, or any internal electron or proton transfer steps within *CcO*. Normally the

intrinsic rates of electron transfer within the protein far exceed overall activity, indicating other limiting factors, but the turnovers measured for W143A and W143F (Table 4.1) are comparable to the rates measured from *Cc* to  $Cu_A$  in the ruthenium kinetic experiments (Table 4.4). Thus, in these mutants, the electron transfer from *Cc* to  $Cu_A$  has become the overall rate limiting step, even at high concentrations of *Cc* where steady-state kinetics imply the possibility of a second interaction of *Cc*. These results strongly suggest that  $Cu_A$  is the sole electron acceptor from *Cc*, and that any additional interaction of *Cc* feed through  $Cu_A$  as well.

#### **A model of *Cc*/*CcO* interaction**

In the space-filling model of the C-terminus of subunit II (Figure 4.15), Asp-214, Asp-195, Glu-157 and Glu-148, are shown to be located in a pocket surrounding the highly conserved aromatic region, with Asp-214 located close to Trp-143 on the surface. The strong inhibitory effect of even conservative mutations of Trp-143 indicate the likelihood that it is the point of closest approach to heme *c* and the electron entry site to  $Cu_A$ .

The high degree of conservation and physical closeness of Asp-214 to Trp-143 are consistent with its location in the middle of the *Cc* binding domain, as suggested by the major changes in the kinetics associated with alteration of this residue. Glu-157, Glu-148 and Asp-195, with moderate effects on kinetics, are concluded to be located in the binding domain, but not so central as to strongly affect the chemistry of the interaction and the electron transfer process itself. This binding site for *Cc* would enable the exposed heme edge on *Cc* to be in close contact with the aromatic residues, possibly excluding

water and enhancing the electron transfer rate between Cc and Cu<sub>A</sub>. In this model, Asp-151 and Glu-152 are located at the edge of the binding domain, and Asp-188, Glu-189 well outside it, unlikely to be involved in Cc binding, as the data suggest.

In our proposed model, the porphyrin of Cc is close to Trp-143, and Asp-214 interacts with Lys-72 from horse Cc, and Asp-195, Glu-157 and Glu-148 are close to Lys-8, -13, and -87, respectively.

Early studies found that Glu-254 was modified by EDC, a water-soluble derivatizing agent for carboxyls, but that Cc protected it from labeling (Millett *et al.*, 1983), which led to the conclusion that it was part of the Cc binding domain. However the crystal structures of oxidase show that the residue is buried inside the protein. Interesting, the crystal structure of bovine CcO indicates that Glu-254 is at a hydrophilic region, and a possible water channel, located at the interface of subunits I and II, and connecting to the surface of the protein (Tsukihara *et al.*, 1996). This channel is likely to be the pathway that EDC takes to reach Glu-254. The protection of Glu-254 from labeling by EDC in the presence of Cc also suggests that Cc is bound close to, or on top of, this channel, in such a way that blocks the accessibility of EDC to Glu-254. In this scenario, residues in subunit I, besides the ones identified in subunit II, may also contribute to the binding of Cc. A recent study of *P. denitrificans* CcO has identified the involvement of an aspartate residue (Asp-257 in *P. denitrificans*) in Cc binding, but unfortunately, this residue is not conserved in *R. sphaeroides* oxidase.

## Summary

Mutagenesis studies and kinetics analyses suggest that Asp-214, Glu-157, Glu-148 and Asp-195 in the subunit II of *R. sphaeroides* CcO form the high-affinity binding site for Cc. This arrangement places Trp-143 in the middle of the binding site, suggesting its key role in electron entry to Cu<sub>A</sub>. Asp-214, next to Trp-143 in the 3-D structure, is possibly located at the center of the high affinity site, while Glu-157, Glu-148 and Asp-195 are more peripheral. Residues from subunit I may also contribute to the binding. Asp-151, Glu-152, Asp-188, and Glu-189 are not involved in Cc binding. Internally located Asp-229 and Glu-254 are found to be critical to the integrity of the overall structure.

This study identifies several important residues in binding Cc, but the orientation of Cc, when it approaches this site and ultimately binds, were not. Without crystal structures of Cc/CcO complexes, this model may be tested by computational analysis of docking possibilities, and complementary structural analysis of Cc, which is currently underway.

## CHAPTER V

### **Importance of electronic coupling of the two coppers in the Cu<sub>A</sub> center for electron transfer, not proton pumping**

This work was done in collaboration with Dr. Frank Millett at the University of Arkansas and Dr. Gerald Babcock, and will be published in two papers (In preparation):

Importance of electronic coupling of the two coppers in the Cu<sub>A</sub> center for electron transfer, not proton pumping

Zhen, Y., Mills, D., Hoganson, C. W., Babcock, G., and Ferguson-Miller, S

The Role of Cu<sub>A</sub> in mediating electron transfer from cytochrome *c* to heme *a* in cytochrome *c* oxidase: Effects of mutation of Cu<sub>A</sub> ligands on rapid electron transfer kinetics

Wang, K., Zhen, Y., Durham, B., Ferguson-Miller, S., and Millett, F.

Part of this work will also be published as a book chapter in Frontiers in Cellular Bioenergetics: Molecular Biology, Biochemistry and Physiopathology Papa, S., Guerrieri, F. & Tager, J. M., Eds. (Plenum Press, New York), coauthored with Mills, D., Hoganson, C. W., Lucas, R. L., Shi, W., Babcock, G., and Ferguson-Miller, S., (1998), in press.

## Introduction

CcO contains an unusual Cu<sub>A</sub> center at the C-terminal extramembrane domain of subunit II. Unlike the type 1 (or blue) and type 2 copper centers (Solomon & Lowery, 1993), which show distinct hyperfine structures at the g<sub>II</sub> region in the X-band EPR spectra, the hyperfine splitting of Cu<sub>A</sub> cannot be resolved using the same microwave frequency. In addition, the optical spectrum of CcO have an unique broad peak in the near-IR region centered at 830 nm, which has been assigned to be from Cu<sub>A</sub> center (Greenwood et al., 1988), providing an optical marker for kinetics studies.

The difference between Cu<sub>A</sub> and other copper centers lies in its unique binuclear character which gives it distinct EPR and optical spectra. Previous spectroscopic studies have suggested that the Cu<sub>A</sub> center in CcO is in a mixed-valence [Cu(1.5)-Cu(1.5)] configuration (Beinert et al., 1962), with one electron delocalized at two copper nuclei. This model has been confirmed from the crystallographic studies of CcO from *Paracoccus denitrificans* and bovine heart (Iwata et al., 1995; Tsukihara et al., 1995). Furthermore, the crystal structure of the soluble domain of quinol oxidase with an engineered Cu<sub>A</sub> center also shows a similar Cu<sub>A</sub> center as in CcO (Wilmanns et al., 1995). All the structures reveal that the binuclear Cu<sub>A</sub> center is bridged by two cysteines (Cys-252 and Cys-256 in *Rhodobacter sphaeroides*), with two histidines (His-217 and His-260) as the terminal ligands for each copper atom. A methionine (Met-263) ligates one of the copper atoms through a relatively weak bond, while the other copper atom is ligated by the carbonyl oxygen of a glutamate residue (Glu-254). The four ligands of each copper atom form a distorted tetrahedral coordination, with the two copper atoms in a symmetric environment. The structures also reveal that Glu-254 not only ligates Cu<sub>A</sub> using its

carbonyl group but also uses its carboxyl side chain to ligate Mg, placing the Mg center in proximity to Cu<sub>A</sub>.

The redox active Cu<sub>A</sub> center is located at the C-terminus of subunit II, close to the outside surface of the protein where C<sub>c</sub> must interact. This arrangement enables electrons to be transferred rapidly from C<sub>c</sub> to Cu<sub>A</sub>, with a rate constant of  $6 \times 10^4 \text{ s}^{-1}$  measured using the ruthenium photoexcitation technique (Geren et al., 1995). The electron is transferred from Cu<sub>A</sub> to the low spin heme *a* with a rate constant of  $1.8 \times 10^4 \text{ s}^{-1}$ , and then to the binuclear center. The electron transfer rates from heme *a* to the heme *a*<sub>3</sub>-Cu<sub>B</sub> binuclear center, a pH dependent step (Hållen & Nilsson, 1992), have been measured to be in the range of  $3 \text{ s}^{-1}$  to  $1 \times 10^5 \text{ s}^{-1}$  (Greenwood & Gibson, 1967; Antalis & Palmer, 1982; Hill, 1991; Oliveberg & Malmström, 1991), dependent on the redox states of the enzyme and the methods used. Direct electron transfer between Cu<sub>A</sub> and heme *a*<sub>3</sub> has not been observed. Besides its involvement in electron transfer, Cu<sub>A</sub> has also been suggested to be the proton pumping site (Chan & Li, 1990).

Electron transfer in proteins is dependent on the driving force, the reorganization energy of the redox centers and the distance between them (Marcus & Sutin, 1985). The role of the structure of the intervening protein is still not clear, and opposite theories about it currently exist (Onuchic et al., 1992; Moser et al., 1995). In CcO, Cu<sub>A</sub> is 19 Å from heme *a* and 22 Å from heme *a*<sub>3</sub> (Tsukihara et al., 1995). The relatively equal distance for Cu<sub>A</sub> to the two heme groups, together with the fact that the electron transfer rate from Cu<sub>A</sub> to heme *a* is much faster than to heme *a*<sub>3</sub>, leads to the question of whether there are features of the Cu<sub>A</sub> center itself, or the intervening protein structure, that contribute to the apparent selectivity for transferring the electron to heme *a*. The ability

of the binuclear  $\text{Cu}_A$  center to delocalize an electron over a large area, and the smaller reorganization energy associated with electron transfer from  $\text{Cu}_A$  to heme *a* have been suggested to account for the difference (Ramirez et al., 1995; Brzezinski, 1996). A more efficient electron transfer pathway from  $\text{Cu}_A$  to heme *a* has also been suggested to be important; this pathway involves one of the  $\text{Cu}_A$  ligand, His-260, the peptide bond between a pair of conserved arginines at the interface of subunit I and II, and several hydrogen bonds linking them and the propionate substituent of the heme *a* porphyrin ring (Iwata et al., 1995; Ramirez et al., 1995).

*CcO* from *R. sphaeroides* has proven to be a good model system for studying the structure and function of this important enzyme by using genetic techniques (Hosler et al., 1992;1993). Several mutants have been made by substituting the  $\text{Cu}_A$  ligands. These mutants have been designed to alter its binuclear character, or the predicted pathway to heme *a*, in order to address the following questions:

- 1) Is the binuclear character of the  $\text{Cu}_A$  center essential for rapid, direct electron transfer and coupled proton translocation?
- 2) Is there a through-bond pathway between  $\text{Cu}_A$  and heme *a* that accounts for the speed and direction of electron flow?

## Methods and Materials

**Site-directed mutagenesis:** Three methods were used to construct mutants: the Kunkel method (Kunkel, 1985), the Batt method (Vandeyar et al., 1988), and the overlap extension PCR method (Ho et al., 1989).

In both Kunkel and Batt methods, single-stranded DNA from the derivative of M13mp19, containing the 683 bp *EcoRI/HindIII* fragment from plasmid pYJ302 (Figure 2.6 in Chapter II), was used as the template for oligonucleotide-mediated mutagenesis. However, the major differences between these two methods is the way of removing the wild-type parent strand after synthesizing the mutant strand. In the Kunkel method, a uracil-containing single stranded template DNA was isolated when the bacteriophages were used to infect *E. coli* strain CJ236 (*duf ung<sup>-</sup> F'*), and this wild-type parent strand was degraded after transforming the heteroduplex molecule containing the second complementary strand to another wild-type *E. coli* strain. In the Batt method, the newly synthesized complementary strand with the mutation was methylated due to the fact that 5-methyl-dCTP was used in the synthesis reaction. The methylation protected the synthesized strand from digestion by *MspI*, *HhaI* and exonuclease III, while the wild-type strand was digested. By degrading the parent strands, the chance of finding plaques with the desired mutations was greatly increased. To confirm the presence of the desired mutation, single-stranded DNA from different plaques was sequenced. Double-stranded DNA isolated from the cells infected by the phages with the desired mutation was digested with *NcoI* and *EcoRV*, and the whole *coxII/III* operon with the desired mutation was recovered following the procedure shown in Figure 2.6 (in Chapter II). C256S and

H260N were constructed using the Kunkel method; while M263L, H217C, H217G, H260G and H260C used the latter approach.

Compared with the above methods, the PCR method was the most efficient. In this method, double-stranded DNA from plasmid pYJ302 was the template for the PCR reaction, and high fidelity *pfu* polymerase was used to extend the primers in the presence of nucleotides and templates. For each mutant, four primers were involved; two of them were complementary to the flanking pUC19 sequences located at each end of the *NcoI/EcoRV* sequence in pYJ302, equivalent to the “universal” primers; and the other two primers, carrying the mutation, were partially complementary to each other and to the template. Two PCR reactions were run as shown in Figure 5.1, to generate the mutated *NcoI/EcoRV* fragment. The PCR product was cloned into pUC19, and was sequenced before cloning back to the *coxII/III* operon as shown in Figure 2.6. A mutant (LpM) that altered the loop region below the Cu<sub>A</sub> site to make it resemble a blue-copper protein was created using this method.

The following primers were used to generate the corresponding mutants, with the mutated codons underlined:

H217C: GACGTGATCTGCTCCTGGAC  
 H217G: CGACGTGATCGGATCCTGGACCG  
 C256S: CGGAGCTGTCCGGCATCTC  
 H260N: GGCATCTCGAACGCCTACA  
 H260C: CGGCATCTCGTGCGCCTACAT  
 H260G: CGGCATCTCGGGCGCCTACATG  
 M263L: CACGCCTACTTGCCGATCA

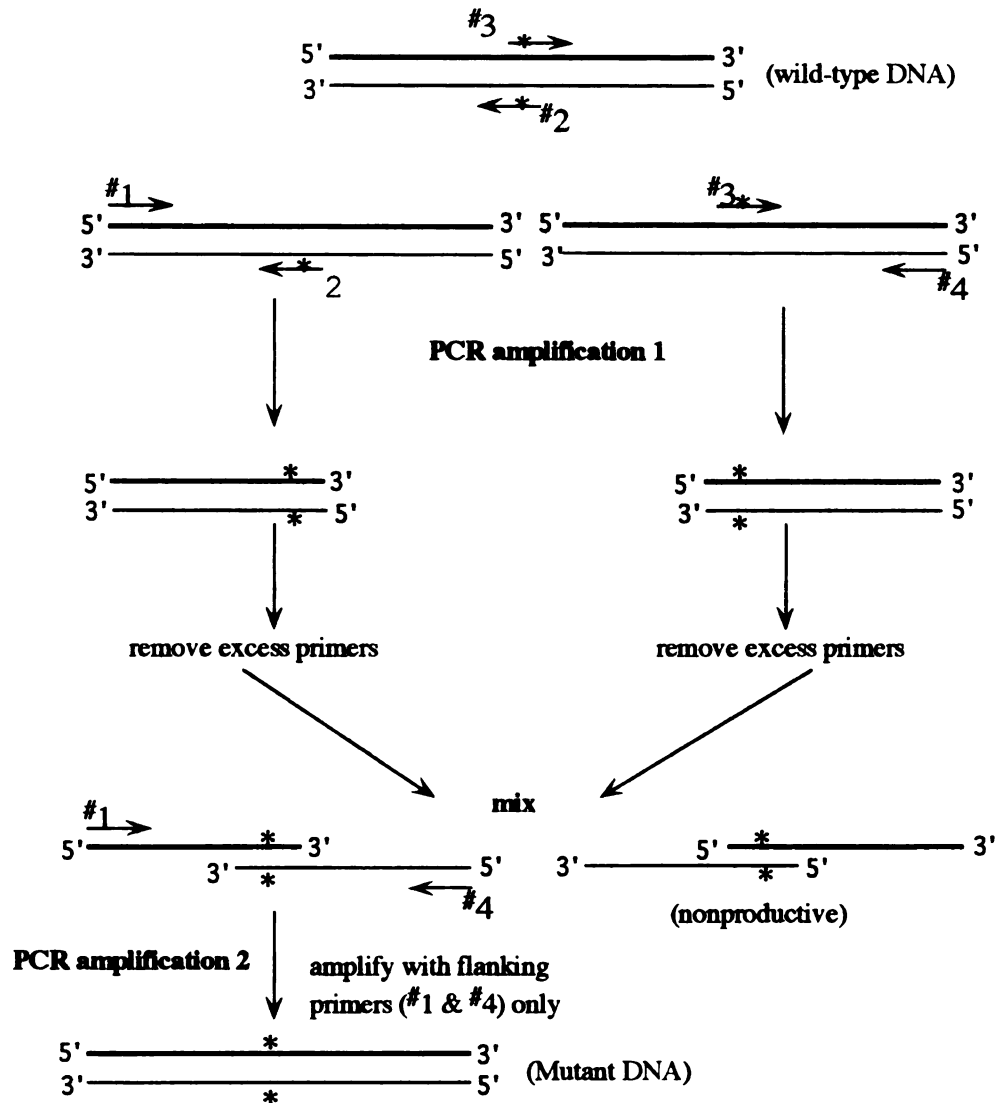


**Figure 5.1 Schematic representation of site-specific mutagenesis using the overlap extension method.** Four primers are involved, with two mutant primers (#2, #3) and two flanking primers (#1, #4). The \* indicates the locations of the mutation.

In the PCR reaction for creating LpM, the following four primers were used, which resulted in the replacement of the Cu<sub>A</sub>-binding loop, Cys<sup>252</sup>-Ser-Glu<sup>254</sup>-Ile-Cys<sup>256</sup>-Gly-Ile-Ser-His<sup>260</sup>-Ala-Tyr-Met<sup>263</sup>-Pro-Ile, with a sequence of Cys-Ser-Glu-Pro-Gly-His-Ser-Ala-Leu-Met-Lys-Gly.

- LpM: (1) AGTCACGACGTTGTAAAAC  
 (2) CAGGAAACAGCTATGAC  
 (3) TCATCAGTGCCGAGTGCCTGGCTCCGAACACTGGCCG  
 (4) GCACTCGGCACTGATGAAGGGGACGGTCAAGGTCGTGT

**Gene expression and protein purification:** All mutants, except LpM, were expressed from the derivatives of pRK415-1, containing the mutated *coxII/III* operons, after conjugating with the subunit II deletion strain YZ200. H260N and M263L, along with LpM, were also overexpressed using the system described in chapter III, and purified using metal-affinity chromatography.

**Visible spectra:** Spectra were recorded using a Perkin Elmer Lambda 40P UV-Vis spectrometer. The dithionite-reduced minus ferricyanide-oxidized difference spectra were recorded for the solubilized whole membranes, and dithionite-reduced spectra for the purified oxidase.

**Activity assay:** The maximum turnover numbers of the purified oxidases were measured polarographically as described in Hosler et al. (1992).

**Metal assay:** Metal analyses were done using inductively coupled plasma (ICP) emission spectroscopy at the chemical analysis laboratory at the University of Georgia and total-reflection X-ray fluorescence spectrometry (TXRF) at the physics department

of the University of Göteborg, Sweden. The sample concentrations were in the range of 30-70 mM.

**EPR spectra:** Measurements were performed as described in Hosler et al., (1992), with the exception that the samples were in 10 mM Tris-HCl, 40 mM KCl, pH 8.0, 0.1 % lauryl maltoside. The sample preparations for high Mg/low Mn content, or low Mg/high Mn content oxidases were the same as described in Hosler et al. (1995). The EPR spectra were recorded using a Bruker EP-300E spectrometer.

**Flash photolysis:** Transient absorbance measurements were carried out in a 1 cm glass microcuvette by flash photolysis of 300 ml solutions containing about 10 mM of CcO and an equal or lesser amount of ruthenium labeled horse Cc, in order to measure a 1:1 reaction between Cc and CcO. Also included were 10 mM aniline and 1 mM 3-carboxyl-2,2,5,5-tetramethyl-1-pyrrolidinyloxy free radical (3-CP) to prevent the oxidation of reduced Cc by Ru(III). Ru-55-Cc, a horse Cc derivative with the inorganic complex, ruthenium trisbipyridine (Ru(bpy)<sub>3</sub>), covalently attached at the Lys-55 position, was used in the experiments. Upon a laser flash, electron transfer from Cc to the Cu<sub>A</sub> center of CcO was measured by monitoring the decrease of absorbance at 550 nm for Ru-55-Cc oxidation and at 830 nm for Cu<sub>A</sub> reduction, and the increase of absorbance at 605 nm for heme *a* reduction. The ionic strength dependencies for electron transfer from Ru-55-Cc to wild-type and mutated CcO were determined. The ionic strength of the sample solution was varied using a 5.0 M NaCl stock solution.

## Results

Kinetics studies have shown that the Cu<sub>A</sub> center is the initial electron acceptor from Cc (Hill, 1993). To study the significance of the binuclear character of Cu<sub>A</sub>, several mutants have been made by mutating Cu<sub>A</sub> ligands, creating H217C, H217G, C256S, H260C, H260G, H260N, M263L and LpM, aiming to alter the Cu<sub>A</sub> center to different degrees.

The subunit II C-terminal domain of CcO shares a similar structure with blue copper proteins, such as azurin and amicyanin (van der Oost et al., 1992), in which the mononuclear copper atom is ligated by two histidines, one cysteine, and one methionine residue. Sequence analysis has indicated that one of the differences between Cu<sub>A</sub> domain and blue copper proteins is the length of the loop involved in binding the copper atoms. In the Cu<sub>A</sub> domain, the loop is longer than the corresponding ones in the blue copper proteins and possesses an extra cysteine residue, enabling Cu<sub>A</sub> site to bind two copper atoms. By replacing the shorter loop in azurin (Hay et al., 1996) and amicyanin (Dennison et al., 1995), copper sites similar to the Cu<sub>A</sub> in CcO can be created in these proteins. Aiming to create a copper site at the Cu<sub>A</sub> center similar to the type I copper centers, the longer Cu<sub>A</sub> binding loop (Cys-Ser-Glu-Ile-Cys-Gly-Ile-Ser-His-Ala-Tyr-Met-Pro-Ile) has been replaced by the corresponding one (Cys-Ser-Glu-Pro-Gly-His-Ser-Ala-Leu-Met-Lys-Gly) from azurin in *Pseudomonas aeruginosa*. The Mg ligand Glu-254 has been retained by replacing a phenylalanine residue in the original azurin sequence.

### **Expression levels of the mutants in cell membranes**

All the mutated oxidase genes have been expressed and the protein located in the membranes, but their expression levels are severely decreased (Figure 5.2). Furthermore, the  $\alpha$ -peaks for H217C, C256S and H260G are blue-shifted, suggesting structural alterations of the heme groups in these mutants. The low amount of oxidase may be due to instability of the mutated protein, or to the potential loss of the plasmid in these mutated strains as observed frequently in this study.

In H217G and H260G, the replacements of the histidine residues with glycine create cavities inside the protein, which were occupied originally by the imidazole side chain of the histidine residues. Previous studies in myoglobin and azurin (den Blaauwen et al., 1991; Depillis et al., 1994) have shown that these His-to-Gly mutants can be rescued by exogenously added imidazole groups, when growing the cells with the mutated protein or incubating the purified protein in the presence of imidazole. Under these conditions, exogenous imidazole groups can occupy the cavities created by the specific mutations, and be involved in metal binding. A wide range of small organic ligands, like pyridine, phenol and methyl-substituted imidazole, can replace imidazole in these chemical “rescue” experiments. This method is an alternative for site-directed mutagenesis to alter the metal ligands. A similar approach was tried for H260G and H217G by growing the corresponding *R. sphaeroides* cell strains in the presence of imidazole in the Sistrom’s medium. Unfortunately, the cells did not grow in the presence of 10 mM imidazole, the concentration used in the experiments with myoglobin and azurin. With 2 mM imidazole, the cells grew, but photosynthetically, indicated by the greenish color of the medium. Low concentrations (0.5 mM to 1 mM) of imidazole did

**Figure 5.2 Optical spectra of Cu<sub>A</sub> ligands mutants.** **A.** The reduced-minus-oxidized membranes spectra for the nonoverexpressed wild-type and mutants strains. **B.** The reduced-minus-oxidized membranes spectra for the overexpressed wild-type, M263L, H260N and LpM strains. **C.** The reduced spectra of the purified oxidases from wild-type, M263L and H260N.

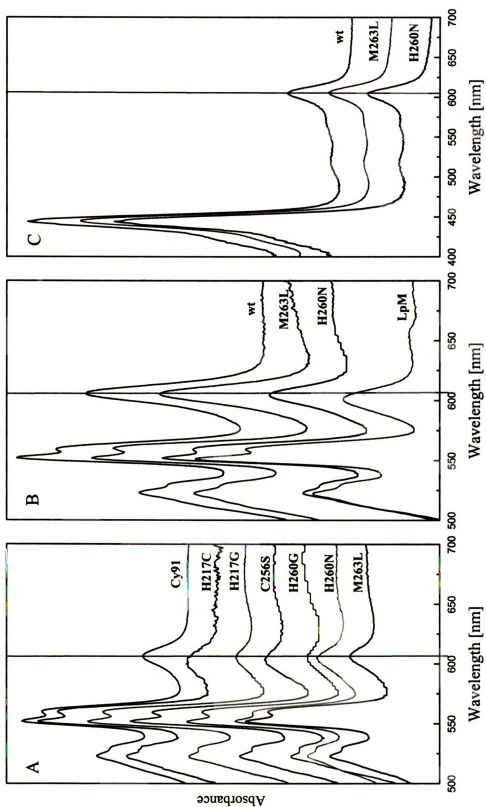


Figure 5.2 Optical spectra of  $\text{Cu}_A$  ligand mutants.

not enhance the oxidase expression level in the membrane. It was not yet attempted to overexpress these two mutant enzymes and study chemical rescue with the purified enzymes.

The oxidase expression levels in H260N and M263L strains are slightly higher than other mutant strains, and the oxidase genes in these two strains, together with the LpM mutant, have been overexpressed using the overexpression system described in chapter III. As a result, the oxidase expression levels are increased four to five-fold (Figure 5.2).

The purified LpM has a shifted reduced spectrum ( Panel B in Figure 5.2), with the  $\alpha$  and Soret peaks centered at 601 nm and 440 nm, respectively. EPR analysis of this mutant has shown that the  $\text{Cu}_A$  signal is completely gone, and the characteristics of a type I copper signal are not present either, suggesting that the attempt to convert the  $\text{Cu}_A$  center to a type I copper center have failed. Without the  $\text{Cu}_A$  center, the 830 nm absorption peak from  $\text{Cu}_A$  is not present either, and the purified oxidase has no activity measured polarographically.

H260N and M263L have been well characterized, and the following sections focus on these two mutants.

### **Spectral characterizations of H260N and M263L**

**Optical spectra** In the reduced CcO, the two heme groups have strong absorbance in the 444 to 605 nm region, with the low spin heme  $\alpha$  contributing about 80% to the  $\alpha$ -peak, and 50% to the Soret peak. Structural disturbance of the two heme groups is likely to cause spectral shifts of the  $\alpha$  and Soret peaks.

The reduced spectrum of M263L is almost identical to that of wild-type (Panel C in Figure 5.2), with respect to the peak positions and the Soret to  $a$ -peak ratio, suggesting that the mutation has no apparent effect on the structures of the two heme groups on subunit I. The  $a$  peak of the reduced spectrum for H260N blue-shifts about 1 nm, indicating a structural disturbance of the heme  $a$  center; however, its Soret/ $a$  ratio is the same as that of wild-type, suggesting no differential loss of either heme. Since CO can quantitatively bind at the binuclear center at subunit I giving a distinctive spectrum, its binding capability is used to check the integrity of this center. For H260N and M263L, their CO-binding abilities are similar to that of wild-type (Table 5.1), indicating that the high spin heme  $a_3$  and  $Cu_B$  centers are not disturbed structurally.

Although the reduced heme spectra of H260N and M263L are similar to that of the wild-type, both hemes are reduced much slower than those in wild-type oxidase when using dithionite as the reducing agent. The reduction of heme  $a_3$  lags behind when heme  $a$  is completely reduced, suggesting an altered (decreased) redox potential of heme  $a_3$ . It is curious to notice that the heme  $a_3$  in H260N and M263L can be reduced much faster when TMPD is used as the reducing agent, even though its redox potential is higher than dithionite.

In wild-type CcO from *R. sphaeroides*, the near-IR absorption band for  $Cu_A$  is at 850 nm, with an extinction coefficient of  $2.0 \text{ cm}^{-1}\text{mM}^{-1}$  for the oxidized minus reduced spectra (Figure 4.3 in chapter IV). The corresponding absorbance in H260N and M263L are severely decreased (Figure 5.3), with extinction coefficients of 0.77 and  $1.34 \text{ cm}^{-1}\text{mM}^{-1}$ , respectively. The 830 nm bands also shift to 920 nm, suggesting that the  $Cu_A$  centers in these two mutants are altered.

**Table 5.1** Characteristics of *R. sphaeroides* cytochrome *c* oxidase subunit II H260N and M263L enzymes

Enzyme	Optical spectra		$\epsilon_{(630)}$ cm <sup>2</sup> mM <sup>-1</sup>	Turnover (s <sup>-1</sup> )	EPR spectra		Cu/Fe ratio		CO- binding	Proton pumping
	$\alpha$ -peak	Soret/ $\alpha$			Cu <sub>A</sub>	Mn	ICP	TXRF		
wild-type	606	5.6	2.06	1700	normal	normal	1.51	1.26	100%	Yes
H260N	605	5.6	0.77	15	distorted	normal	1.49	1.22	100%	Yes
M263L	606	5.6	1.34	150	distorted	altered	1.49	1.17	100%	Yes

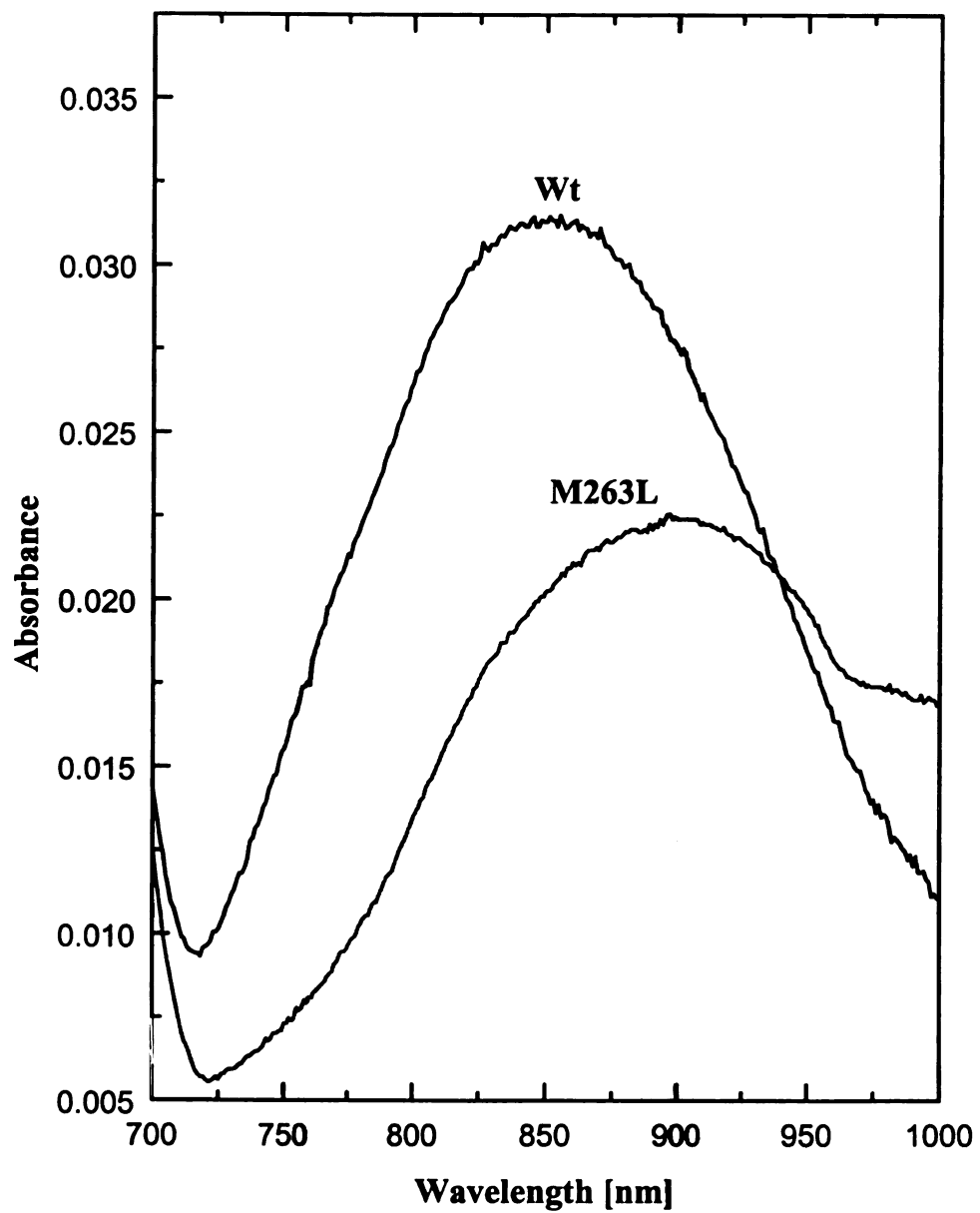


**Figure 5.3** Near-infrared spectra of the wild-type and M263L enzymes.  
The spectra were recorded as described in Figure 4.3.

**Metal analyses** Although the  $\text{Cu}_A$  centers are disrupted in H260N and M263L as resolved in the optical spectral assay, metal analysis done by using ICP gives almost identical Cu/Fe ratios for these two mutants as for wild-type. The overall Cu/Fe ratios measured by TXRF are lower than the numbers obtained from ICP method, but the ratios measured for the two mutants are generally comparable to that of wild-type. The inconsistency of the Cu/Fe ratios measured using different methods reflects the difficulty of measuring the Cu/Fe ratio accurately due to contaminating Fe and Cu and possible presence of partially denatured species.

**EPR spectra** Electron paramagnetic resonance spectroscopy has been used extensively to study the molecular environment of the metal centers in CcO, and it reveals the presence of signals for heme  $a$  and  $\text{Cu}_A$  in the “resting” oxidized form of the enzyme (Figure 5.4). Due to antiferromagnetic coupling between high spin heme  $a_3$  and  $\text{Cu}_B$ , these two metal centers are EPR invisible. The signals at  $g = 2.83, 2.31$  and  $1.62$  arise from the low spin heme  $a$ ; those at  $g = 2.19$  and  $2.00$ , from  $\text{Cu}_A$  (Hosler et al., 1992). In the wild-type oxidase, the theoretical seven-line hyperfine characteristic for a mixed-valence  $\text{Cu}_A$  center in the  $g_{\parallel}$  region, as observed in nitrous-oxide reductase (Kroneck et al., 1988), is not resolved in CcO at the X-band frequency. Instead, a signal with a value of  $g = 2.19$  is present in this region in bovine and in *R. Sphaeroides* oxidases. In studies with the  $\text{Cu}_A$  domain from *P. denitrificans*, partial hyperfine structures from  $\text{Cu}_A$  have been resolved around the  $g = 2.19$  region (Farrar et al., 1995). Previous studies in *R. sphaeroides* showed that the amplitude of this  $g = 2.19$  signal is greater than bovine at low temperatures but decreases when the temperature rises to 100K (Hosler et al., 1992), suggesting that it is not solely from  $\text{Cu}_A$ . The signal at  $g = 4.3$  is from contaminating

**Figure 5.4** **Cu<sub>A</sub> and heme EPR spectra of wild-type, M263L and H260N.**  
A. Cu<sub>A</sub> EPR spectra of wild-type, M263L and H260N enzymes.  
B. The CcO oxidases Mn EPR spectra of wild-type, M263L and H260N enzymes. EPR spectra of 30 to 50 μM oxidases in 10 mM Tris, pH 8.0, 40 mM KCl, 0.1% LM were recorded at X-band using a Bruker EP-300E spectrometer. The related g values are indicated in the plots. The Cu<sub>A</sub> EPR spectra were recorded at 10 K with the following settings: microwave frequency 9.482 GHz; microwave power 2 mW; modulation amplitude 12.7 G; sweep time 335.5 s; The *inset* in panel A is the enlarged g<sub>||</sub> region of M263L. This spectrum was recorded using a more concentrated (70 μM) M263L sample. The Mn EPR spectra were recorded in 100 K, with the following settings: microwave frequency 9.44 GHz; microwave power 20 mW; modulation amplitude 12.7 G; sweep time 167.8 s; The samples were prepared as described in Hosler *et al.* (1995).

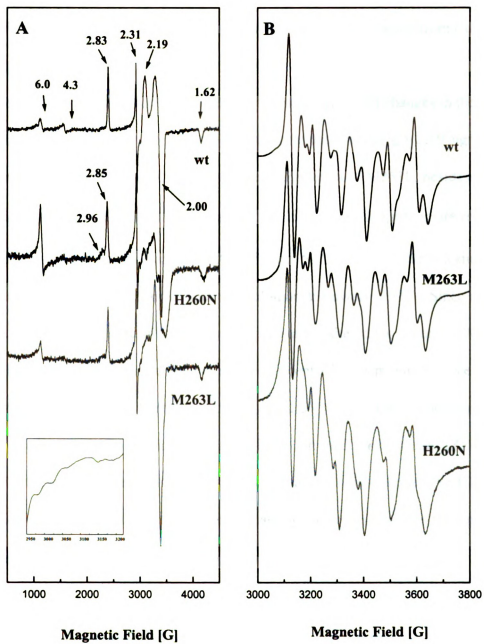


Figure 5.4 EPR spectra of wild-type, M263L and H260N enzymes.

iron. Although high spin heme  $a_3$  is EPR silent, the spectrum of the “resting” form of wild-type CcO from *R. sphaeroides* always has a weak signal at  $g = 6.0$  region, which arises from a small portion of ferric heme  $a_3$  which has been decoupled from  $\text{Cu}_B$ , possibly due to loss of  $\text{Cu}_B$ .

The EPR spectra of H260N and M263L reveal significant changes in the  $\text{Cu}_A$  centers in these two mutants (Figure 5.4). With the mutations, the  $g = 2.19$  signal is broadened in both H260N and M263L. In the EPR spectra of M263L, besides the hyperfine structures resolved at the  $g_{\perp}$  region, the four hyperfine splitting are resolved in the  $g_{\parallel}$  region, with a splitting constant ( $A_{\parallel}$ ) of about 50 G characteristic of a single copper nucleus coupled with an unpaired electron (Solomon & Lowery, 1993). Since metal analysis indicates there are still two copper atoms at the altered  $\text{Cu}_A$  center in M263L, the EPR spectrum suggests that the binuclear  $\text{Cu}_A$  center in this mutant has been converted from a mixed-valence state  $[\text{Cu}(1.5)\text{-Cu}(1.5)]$  to a decoupled configuration  $[\text{Cu}(1)\text{-Cu}(2)]$ . A similar result was obtained in CcO from *P. denitrificans* (Zickermann et al., 1995), in which the equivalent residue was mutated to isoleucine. For H260N, the alteration of the  $\text{Cu}_A$  center is even more dramatic, with the amplitude of the signal at the  $g_{\perp}$  region significantly decreased, but again two copper appear to be retained.

In the EPR spectrum of M263L (Figure 5.4), the three heme  $a$  signals are at the same positions as those of wild-type oxidase, suggesting that heme  $a$  is intact in this mutant. However, a small signal at  $g = 2.96$  position appears. In *R. sphaeroides*, the heme  $a$  EPR at  $g = 2.83$  has been interpreted to indicate that one of the two histidine ligands has a strong hydrogen bond leading to the equivalent of a deprotonated histidine in the oxidized state (Hosler et al., 1992). Two neutral histidine ligands would shift the

signal to  $g = 2.96$  as in bovine. The presence of both  $g = 2.83$  and  $2.96$  signals in M263L suggests that CcO in M263L is present in two conformations, with the majority in the wild-type conformation.

Like M263L, H260N is not a homogeneous sample, as indicated by the presence of both  $g = 2.83$  and  $2.96$  signals. Moreover, the  $g = 2.83$  signal present in wild-type is shifted to  $g = 2.85$  position in H260N, suggesting that the environment of heme  $a$  is slightly altered, consistent with the optical spectrum. In H260N, the  $g = 6.0$  signal is much larger than that in wild-type CcO, indicating some high spin heme  $a_3$  decoupled from  $\text{Cu}_B$ . However, the fraction of decoupled heme  $a_3$  is very small and does not represent significant loss of  $\text{Cu}_B$ , since it does not change the Cu/Fe ratio significantly, as indicated by the metal assay results

In *R. sphaeroides* CcO, it has been shown that the Mg atom located at the interface of subunit I and II can be replaced by Mn when the cells are grown in a high concentration of Mn (Hosler et al., 1995), and the distinct EPR spectra of Mn can be used as a probe to check the structural integrity of the interface. The Mn EPR spectra have been recorded for wild-type and two mutant enzymes as shown in Figure 5.4. Clearly, the Mn EPR spectrum of H260N is altered as compared to that of the wild-type CcO, suggesting that the effect of alteration of the  $\text{Cu}_A$  center is spread to the Mg/Mn site. The crystal structures of CcO show that His-260 ligates one of the two copper atoms along with Glu-254, which also ligates the Mg atom directly (Tsukihara et al., 1995). The mutation of residue His-260 will inevitably alter the positions of Glu-254 and other nearby residues, thereby causing structural change at the Mg/Mn center. In

contrast, the Mn EPR spectrum of M263L did not show any change, suggesting that the mutational effect of M263L is more localized.

**Activity assay** Due to the severe disruption of the  $\text{Cu}_A$  center, the activities of these two mutant enzymes were significantly decreased, with about 1% and 10% of wild-type activity retained for H260N and M263L, respectively (Table 5.1). The residual activity measured for H260N is not due to any exogenous activity, and can be inhibited by cyanide. The slow dithionite reduction of heme  $a$  and  $a_3$  observed may be partially due to the overall slow turnover numbers of these enzymes. More likely, dithionite reduces heme  $a$  by donating electrons to  $\text{Cu}_A$  first. But the even slower reduction of heme  $a_3$  in both mutants is likely due to the change of the redox potential of this center (see below).

#### **Time-resolved kinetics of electron transfer in H260N and M263L**

Ruthenium photoexcitation is a unique technique to measure the electron transfer rates from  $\text{Cc}$  to  $\text{Cu}_A$ , and then from  $\text{Cu}_A$  to heme  $a$  (Pan *et al.*, 1993; (Geren *et al.*, 1995). In this experiment, Ru-55-Cc was chosen as the substrate. Laser excitation of a 1:1 complex between Ru-55-Cc and CcO results in rapid electron transfer from Ru-55-Cc to CcO as described in Chapter IV.

At low ionic strength, when the wild-type oxidase concentration is equal to or greater than that of Ru-55-Cc, Ru-55-Cc forms a 1:1 complex with CcO. Laser flash photolysis of the complex results in rapid electron transfer with a rate constant of  $40,000 \text{ s}^{-1}$  as measured by following the rapid decrease of absorbance at 550 nm and the increase at 605 nm (Figure 4.11 in chapter IV). The measured rate constants are independent of the concentrations of Ru-55-Cc and CcO, suggesting that the measured rates represent the

intracomplex electron transfer rates. By using a dimer of Ru(bpy)<sub>3</sub> as the direct substrate of CcO, the electron transfer rate ( $k_b$ ) from Cu<sub>A</sub> to heme *a* is  $1.2 \times 10^5 \text{ s}^{-1}$ . After each laser flash, the relative amounts of the reduced heme  $a^{2+}$  and Cu<sub>A</sub><sup>1+</sup> forms can be measured, and are found to be in the ratio of 6.1:1, indicating that the equilibrium constant ( $K = k_b/k_c$ ) for electron transfer between Cu<sub>A</sub> and heme *a* is 6.1 (Table 5.2).

The redox potential difference ( $\Delta E^0$ ) between heme *a* and Cu<sub>A</sub> can be calculated using the following equation:

$$\Delta E^0 = E_a^0 - E_{\text{CuA}}^0 = 59 \times \log K \quad (\text{Eq. 14})$$

where  $K$  is the equilibrium constant between Cu<sub>A</sub> and heme *a*. The calculated  $\Delta E^0$  value for wild-type oxidase is about 46 mV, suggesting that heme *a* is more positive than Cu<sub>A</sub>.

The electron transfer rate between Ru-55-Cc and CcO is ionic strength dependent. With the increasing of ionic strength, some of the Ru-55-Cc dissociates from the complex. Free Ru-55-Cc can only react with CcO by first re-binding to it, thus, there is a second, slow rate of electron transfer. The amplitude of the fast phase decreases with the increasing of ionic strength, meantime, the amplitude and the rate of the slow phase rate increases. A plot of the slow phase rates versus ionic strengths for the wild-type is given in Figure 5.5. At 75 mM ionic strength, the slow phase of wild-type CcO displays a maximum electron transfer rate at  $7900 \text{ s}^{-1}$ .

Unlike wild-type CcO, which has a single fast phase at low ionic strength, M263L mutant displayed triphasic kinetics at 5 mM ionic strength, with rate constants of  $16,000 \text{ s}^{-1}$ ,  $250 \text{ s}^{-1}$ , and  $20 \text{ s}^{-1}$  as judged by following the 550 nm transients (Table 5.2). The fast phase is due to electron transfer within a preformed complex between Ru-55-Cc and M263L, while the slow phase is due to the reaction of uncomplexed Ru-55-Cc with the

**Table 5.2 Electron transfer from Ru-55-Cc to cytochrome c oxidase H260N and M263L enzymes**

Enzymes	$k_r$ ( $s^{-1}$ )	$k_m$ ( $s^{-1}$ )	$k_s$ ( $s^{-1}$ )	% (fast phase)	$k_b$ ( $s^{-1}$ )	$k_c$ ( $s^{-1}$ )	K ( $k_b/k_c$ )	$\Delta E$ (mV) ( $E_a - E_{CuA}$ )	$k_{cat}$ ( $s^{-1}mM^{-1}$ ) (@ 95 mM NaCl)
wild-type	40,000	-	-	100	120,000	20,000	6.1	49	310
H260N	13,000	78	16	30	60	300	0.2	-41	35
M263L	16,000	250	20	25	50	500	0.1	-59	53

$k_p$ ,  $k_m$ , and  $k_s$  are the triphasic rates for ET from Cyt. c to  $Cu_A$  by following 550 nm transients.

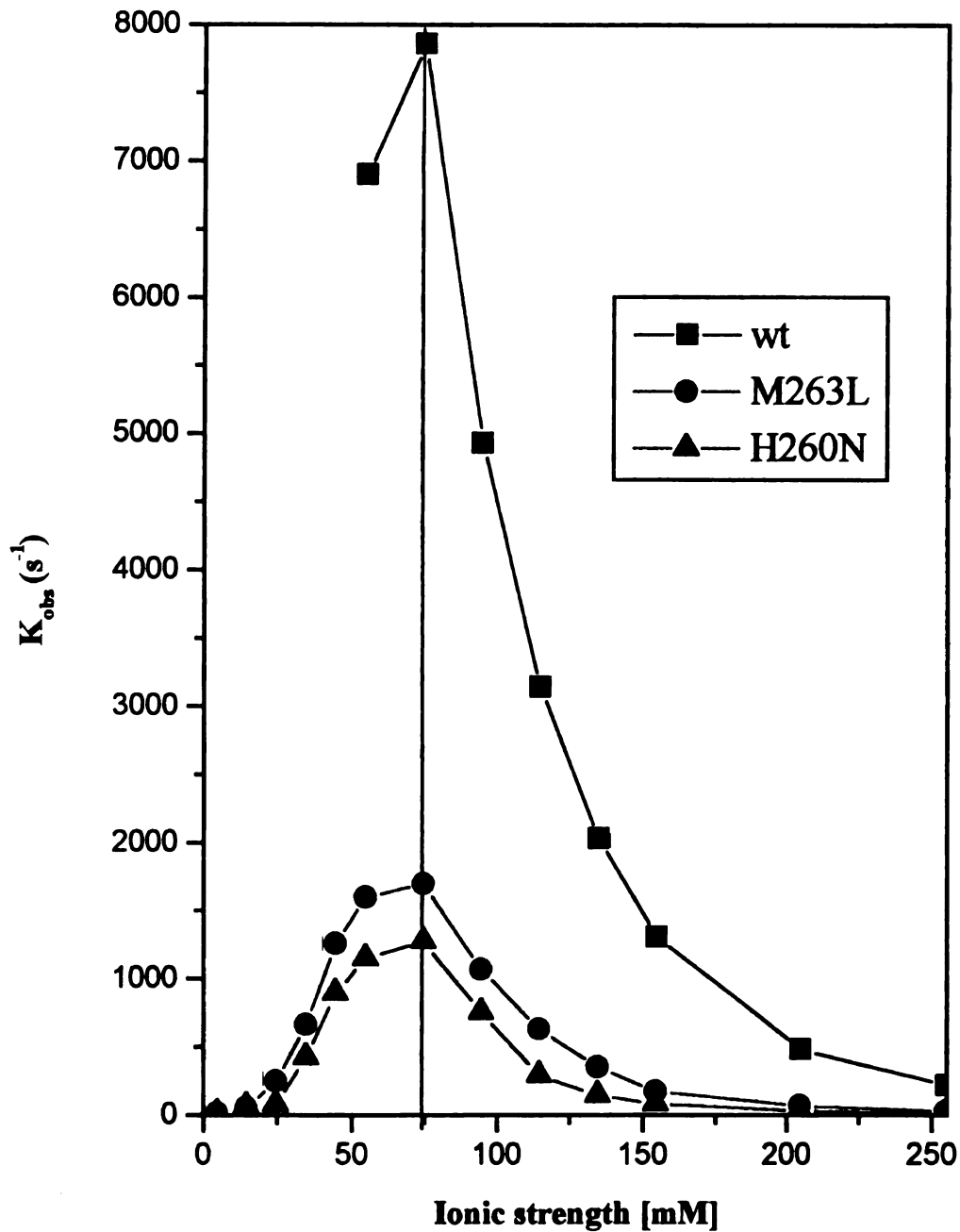


**Figure 5.5** Ionic strength dependent electron transfer from Ru-55-Cc to wild-type, M263L and H260N enzymes. The slow phase electron transfer rates in the ruthenium kinetics assay were plotted against the ionic strength of the solution.

free oxidase. The amplitude of the fast phase is smaller (25%) compared to the slowest phase (45%). The intermediates phase (35%) disappeared with increasing ionic strength, while the rate constant for the fast phase does not change throughout the ionic strengths of 5 to 55 mM, and then disappears at high salt content. Meantime, the slow phase of the 550 nm transient increased to a maximum of  $1700\text{ s}^{-1}$  at 75 mM ionic strengths, and then decreased as the ionic strength was further increased, following a similar pattern to that of the wild-type oxidase. The peak position for the ionic strength dependent slow phase reaction of M263L is the same as that of the wild-type (Figure 5.5), suggesting that although the electron transfer rate has decreased, the Cc binding affinity of this mutant is similar to that of wild-type.

The amplitude of the 605 nm transient is very small (Figure 5.6), and its rate constant is similar to the slow phase rate constants of the 550 nm transients, increasing with the ionic strength to a plateau value of  $550\text{ s}^{-1}$  from 40 to 70 mM, and then decreasing with the further increasing of ionic strength (Figure 5.7).

For M263L, the amplitude of the 830 nm transient is much larger than for wild-type, suggesting that the reoxidation of  $\text{Cu}_A$  by transfer to heme  $a$  is much slower. The rate constants for the 830 nm transients have nearly the same rate constants as the 550 nm transients at all ionic strengths, indicating that the rates measured by following 550 nm and 830 nm transients are represent the initial electron transfer from Cc to  $\text{Cu}_A$ .

The relative yields of reduced  $\text{Cu}_A^{+1}$  and heme  $a^{2+}$  were measured in the M263L reaction, and the calculated equilibrium constant (K) is 0.1 (Table 5.2), independent of ionic strength. The calculated  $\Delta E^0$  value for M263L is about -59 mV, indicating that the redox potential of  $\text{Cu}_A$  in M263L is more positive than that of heme  $a$  rather than 50 mV

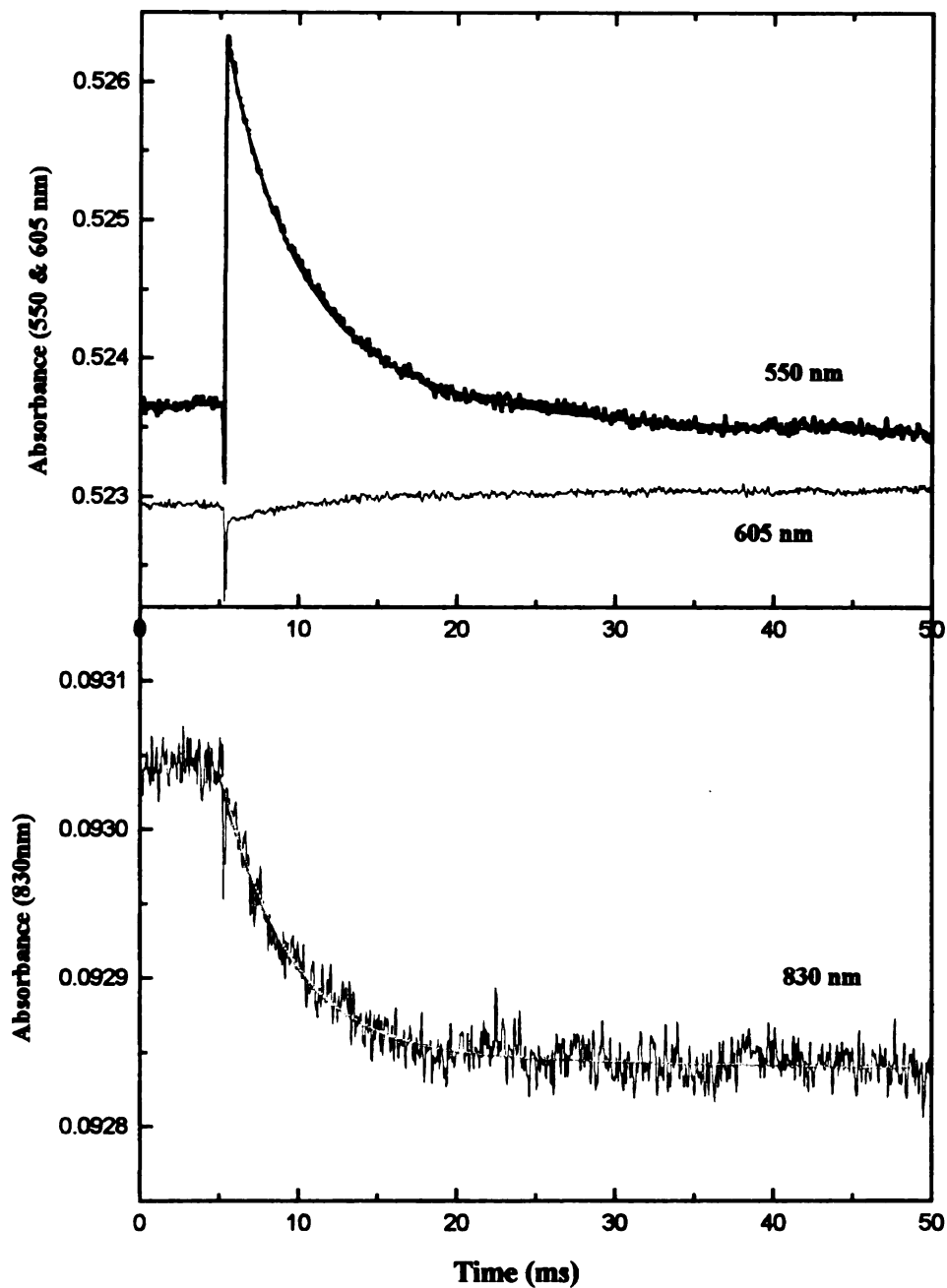


**Figure 5.6** Electron transfer between Ru-55-Cc and M263L at 150 mM NaCl. The solution contained 5 mM Tris, pH 8.0, 0.05% LM, 10 mM aniline and 1 mM 3-CP, 20  $\mu$ M M263L oxidase, 10  $\mu$ M Ru-55-Cc, and 150 mM NaCl. The solid lines are single exponential fits.

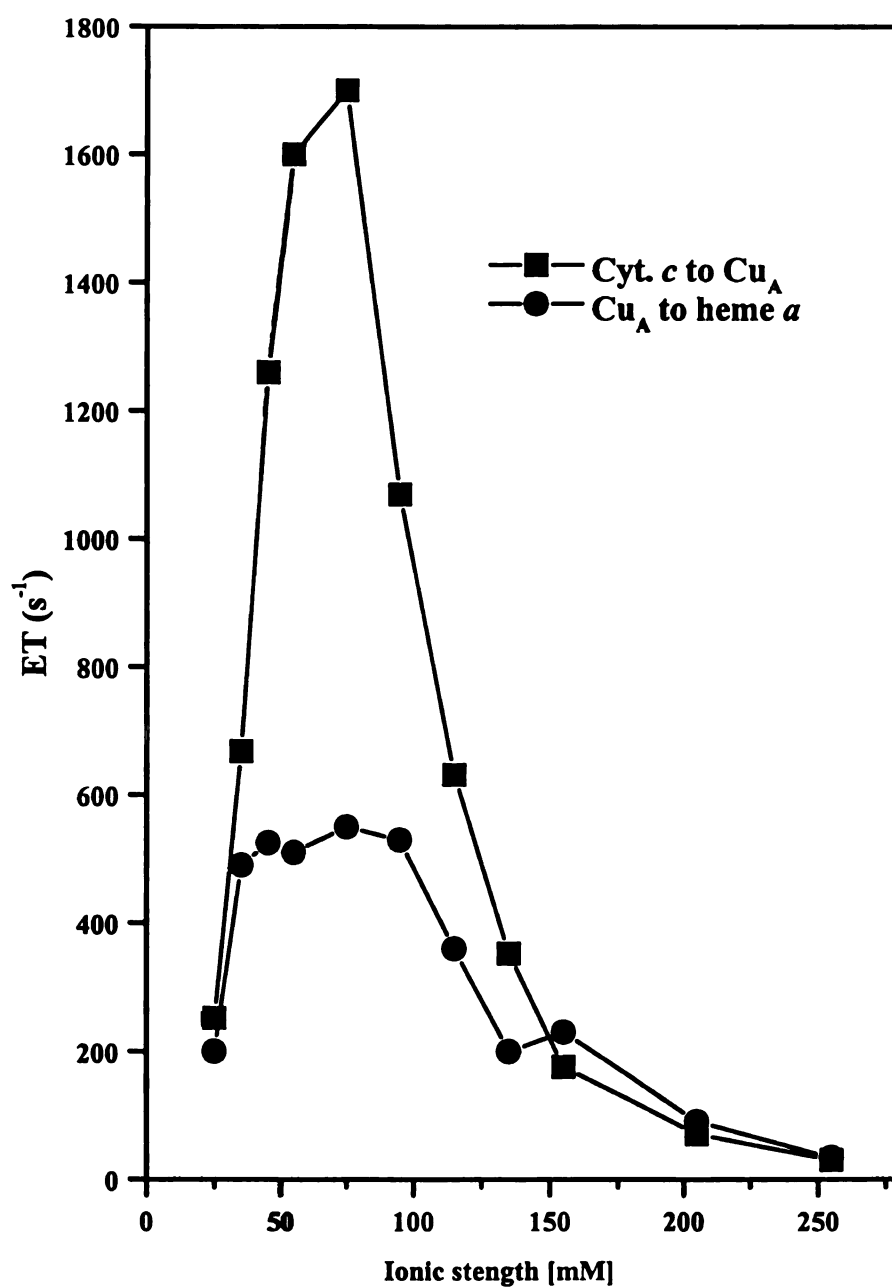


**Figure 5.7** Ionic strength dependence of the slow phase of electron transfer from Ru-55-Cc to Cu<sub>A</sub> and from Cu<sub>A</sub> to heme *a* in M263L enzyme. The solution contained 10 μM Ru-55-Cc and 15 μM M263L in 5 mM Tris, pH 8.0.

more negative, representing a change of about 110 mV and making it unfavorable for electron transfer from Cu<sub>A</sub> to heme *a*. As a result, the rate constant of the 605 nm transient never exceeds the 550 nm transient, even when that of the 550 nm transient is 1700 s<sup>-1</sup> (Figure 5.7). The observed rate constant for heme *a* reduction is given by  $k_{605} = k_b + k_c$ . With an equilibrium constant of 0.1, and a maximum electron transfer rate of 550 s<sup>-1</sup> at 150 mM ionic strength the calculated values for  $k_b$  and  $k_c$  are 50 and 500 s<sup>-1</sup>, respectively ( for wild-type,  $k_b = 12,000$  s<sup>-1</sup> and  $k_c = 2000$  s<sup>-1</sup>).

The kinetic properties of H260N are similar to that of M263L. At 5 mM Tris-HCl, three phases were observed with rate constants of 11,000 s<sup>-1</sup>, 78 s<sup>-1</sup>, and 16 s<sup>-1</sup>, with amplitudes of 30%, 20% and 50%, respectively. As the ionic strength was increased, the rate constant of the fast phase remained approximately constant, the rate constant of the slow phase increased, and the intermediate phase disappeared. The rate constant of the slow phase reached a maximum of 1300 s<sup>-1</sup> at 75 mM ionic strength, and then decreased with further increases in ionic strength (Figure 5.5). The maximum rate constant for the 605 nm transients is 360 s<sup>-1</sup>, even though the rate constant of the slow phase of 550 nm transient reaches a maximum of 1300 s<sup>-1</sup> at 75 mM ionic strength. ). The calculated equilibrium constant (K) between Cu<sub>A</sub> and heme *a* for H260N is 0.2 (Table 5.2), indicating  $\Delta E^0$  value between CuA and heme *a* of -41 mV, yielding a value for  $k_b$  and  $k_c$  of 60 and 300 s<sup>-1</sup>, respectively.

### **Proton translocation**

Purified *R. sphaeroides* CcO displays proton pumping activity when reconstituted into phospholipid vesicles, with a stoichiometry of 0.7 H<sup>+</sup>/e<sup>-</sup> (Figure 5.8).



**Figure 5.8 Proton pumping activities of the purified M263L and H260N enzymes.** Proton translocation following reconstitution of the purified enzymes into phospholipid vesicles was measured at 22°C by a spectroscopic method in 2.4 ml of 50  $\mu$ M NaHCO<sub>3</sub>-KOH, pH 7.4, 45 mM KCl, 44 mM sucrose, 50  $\mu$ M phenol red, pH 7.4 using an Aminco DW-2 spectrophotometer and a 556.8-504.7 nm wavelength pair. **A.** Immediate acidification of the medium occurred upon injection of reduced horse heart cytochrome *c*. **B.** A second addition of cytochrome *c* after the complete uncoupling of the vesicles with 5  $\mu$ M CCCP, initiated rapid alkalization of the medium

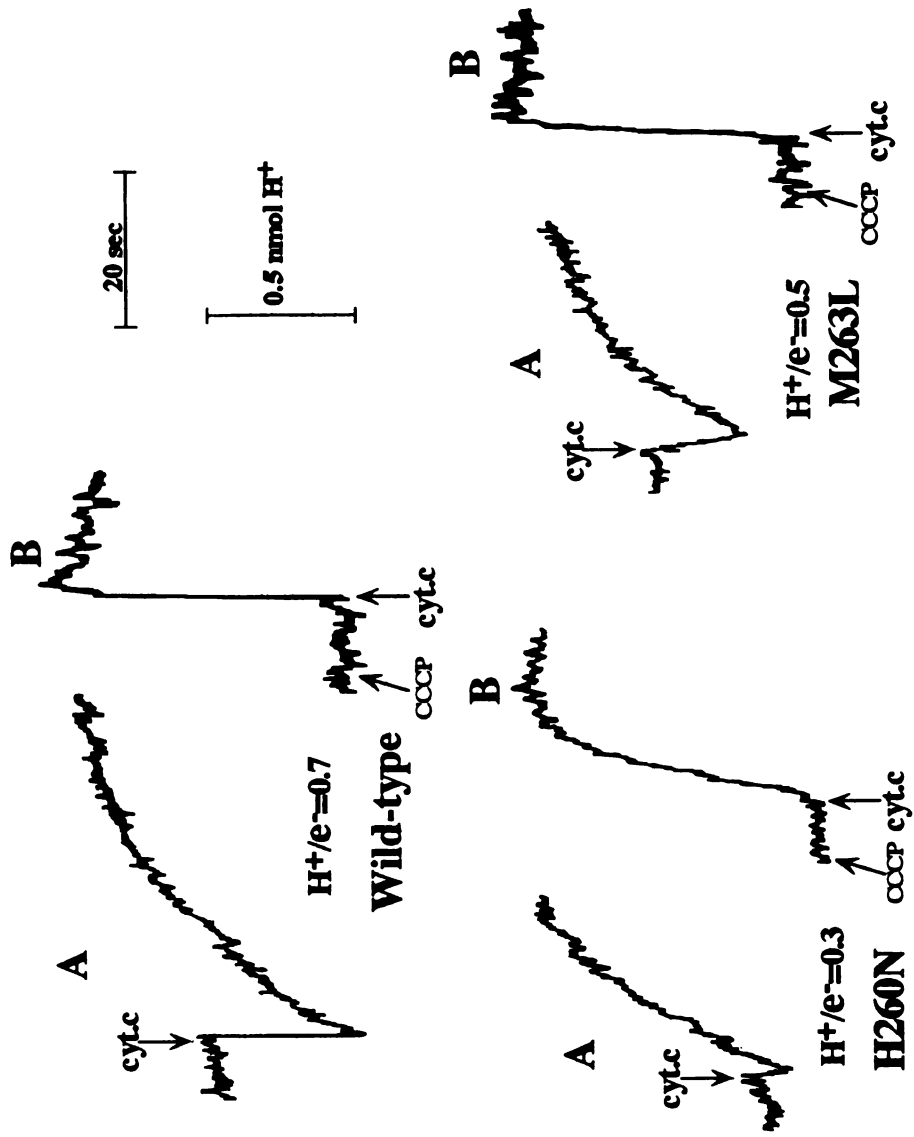


Figure 5.8 Proton pumping activities of the purified M263L and H260N.

The proton-pumping activities for H260N and M263L have also been measured after reconstituting into phospholipid vesicles. The addition of reduced horse Cc leads to immediate acidification due to proton pumping activity, followed by a slow alkalization due to the overall net proton consumption for water formation (Figure 5.8). The presence of 5 mM CCCP allows rapid equilibrium of protons across the lipid bilayer, resulting in the observed net alkalization. Both M263L and H260N show proton pumping activity with stoichiometries of  $0.5 \text{ H}^+/\text{e}^-$  and  $0.3 \text{ H}^+/\text{e}^-$ , respectively. The smaller  $\text{H}^+/\text{e}^-$  measured for H260N is likely due to the slower turnover of this mutant, resulting in a competing back leak of protons into the vesicle.

## Discussion

### The CcO expression levels in subunit II mutants

$\text{Cu}_A$  has been on the center stage of CcO studies for the past decade, and it has always been associated with controversies (Beinert, 1997), until its nature was revealed recently through crystallographic studies. The crystal structures have shown that the  $\text{Cu}_A$  center in CcO is a binuclear copper center, with two copper atoms in close proximity in a configuration that allows them to share the unpaired electron.

In order to study the unique binuclear character of  $\text{Cu}_A$  center, several CcO mutants have been created in *R. sphaeroides* by altering the  $\text{Cu}_A$  ligands. When the genes were expressed in cell membranes, these altered oxidases display severely decreased expression levels, making the purification of some of them difficult. It has been observed that the expression levels of the CcO subunit II mutant genes from *R. sphaeroides*

generally correlate with their activities; the higher its activity, the higher its expression level. So the low expression levels observed for most of the subunit II mutants suggest their activities are very low, too. Most of the mutants alter the heme *a* centers to different degrees, as evidenced by the shift in the optical spectra. In contrast, although some subunit I CcO mutants from *R. sphaeroides* have similar low activities, their expression levels are comparable to that of the wild-type. The distinction between subunit I and II mutants may be due to the fact that subunit I is generally more stable as it is protected in the membrane. Most of the subunit II mutants tend to disrupt the association between subunit I and II; as a result, the oxidases become more labile and destabilized.

Another important difference may relate to the pressure to partially or completely eliminate the oxidase-carrying plasmid in low activity mutants; it may be easier to lose the *coxII/III* operon region than the region encoding subunit I. The loss of plasmid would result in variable but increasing poor synthesis of oxidase, which has observed with the subunit II mutants.

The attempt to convert the Cu<sub>A</sub> center to a type I copper site in LpM by changing the Cu<sub>A</sub>-binding loop failed, which may be due to the fact that the mutagenized loop in subunit II is restricted to certain conformations unsuitable for binding a blue copper center, as a result of the interaction with subunit I. In small blue copper proteins, the loop may have more flexibility.

#### **The effects of mutations in H260N and M263L**

Metal determination using ICP and TXRF suggests that the two copper atoms are still present in the altered Cu<sub>A</sub> centers in M263L and H260N. EPR studies show that

characteristics of a type I copper center appear in the altered Cu<sub>A</sub> center in M263L. This is very likely since, in the native Cu<sub>A</sub> center, the two copper are in a symmetrical configuration and share the unpaired electron. Mutating ligands of the copper atoms will likely change the coordination geometry of these copper atoms, resulting in a change of the coordination symmetry between them and the localization of the electron to one of the copper atoms. This is likely to be the case in H260N, although no clear hyperfine structure has been resolved in the g<sub>||</sub> region.

In the Cu<sub>A</sub> center, Met-263 and His-260 are involved in binding different copper atoms, and the bond between His-260 and the copper atom it binds is much shorter (1.9 Å) than the one with methionine (2.5 Å). Therefore, the mutation of His-260 is likely to have more severe effects, as evidenced by the changes of EPR spectra, the low activity of H260N, and the alteration of the Mn site in this mutant.

Electron transfer rates depend on the redox potentials of the metal centers, their relative reorganizational energies, and the distance or electronic coupling between them. The redox potential of bovine Cc is 260 mV in solution, and may be even lower (220-230 mV) when bound to CcO (Schroedl & Hartzell, 1977). The redox potentials for Cu<sub>A</sub> and heme *a* have been reported to be about 250 and 360 mV (Wilson et al., 1972 ; 1976), respectively, which enables electrons to be transferred from Cc , through Cu<sub>A</sub> to heme *a*. Although the redox potentials for Cu<sub>A</sub> and heme *a* in *R. sphaeroides* CcO have not been reported yet, the value for Cu<sub>A</sub> will be similar to the one in bovine oxidase based on their similar characteristics, while the redox potential of heme *a* may be different from the one in bovine oxidase, as indicated by its different optical and EPR spectra. Actually, in *R. sphaeroides* CcO the redox potential difference between heme *a* and Cu<sub>A</sub> calculated from

the rapid kinetics assay is about 46 mV, suggesting that the redox potential of heme *a* is about 300 mV, assuming the redox potential of Cu<sub>A</sub> is same as the one in bovine oxidase. This redox potential of heme *a* still enables electrons to be transferred from lower potential Cu<sub>A</sub> to heme *a*.

In M263L, the calculated  $\Delta E^0$  value is about -59 mV, suggesting that the redox potential of Cu<sub>A</sub> is now higher, rather lower, than that of heme *a*. Spectral characterization of M263L has shown that heme *a* in this mutant is not altered, suggesting that its redox potential has a wild-type value of 300 mV. In that case the redox potential of Cu<sub>A</sub> must have increased to 360 mV in the mutant, accounting for the unfavorable electron transfer to heme *a*. The situation in H260N is more complex than in M263L, with the redox potentials for both Cu<sub>A</sub> and heme *a* likely to be changed due to the structural alterations as indicated in the EPR spectrum. The redox potential of Cu<sub>A</sub> is about 41 mV higher than that of heme *a*, which also results in inhibition of electron transfer from Cu<sub>A</sub> to heme *a*.

In most of the blue copper centers, methionine is a long axial ligand for the copper atoms, and it can be replaced by all other amino acids without losing the blue color of the protein (Karksson et al., 1991). In stellacyanin, this residue is even naturally replaced by leucine (Bergman et al., 1977). Mutagenesis studies on azurin have shown that substitution of the methionine with leucine, or other amino acid with hydrophobic side chains, results in a large increase in redox potential of the copper center. This is likely due to that fact that the hydrophobic side chains exclude water from the metal site, resulting in the increase of the redox potential (Malmström, 1994). In CcO, the methionine residue is also solvent-exposed, and the leucine substitution in M263L will likely increase

the redox potential of the Cu<sub>A</sub> center in a similar way as in azurin. Decoupling the two coppers should also increase the reorganization energy, resulting in inhibition of electron transfer.

The Cu<sub>A</sub> center has been investigated in other systems. In CcO from *P. denitrificans* (Zickermann et al., 1995), mutation of the methionine to isoleucine also decouples the interaction between the two copper atoms. In the studies with the soluble Cu<sub>A</sub> domain from *P. denitrificans* (Farrar et al., 1995) and the engineered *CyoA* domain from quinol oxidase (Kelly et al., 1993), mutations of the methionine residue tend to destabilize the proteins, and this residue has been suggested to have an important structural role. The residues equivalent to His-260 in *R. sphaeroides* have been mutated in these studies too. In the Cu<sub>A</sub> domain from *P. denitrificans* (Farrar et al., 1995), the H260N mutation retains two copper atoms, but decouples the interaction between them, while the same mutation in the *CyoA* domain retains only one copper atom (Kelly et al., 1993). The different results observed for the same mutation in the holoenzyme and in the Cu<sub>A</sub> domains suggest that the stabilities of soluble Cu<sub>A</sub> domains are lower than the holoenzymes.

The crystal structures of CcO reveal that there is an extensive hydrogen-bond network at the interface of subunits I and II (Ostermeier et al., 1997). Within this network, His-260 is hydrogen-bonded to a highly conserved arginine pair in subunit I, which, in turn, also interacts with heme *a* through covalent and hydrogen bonds. This arginine pair is also hydrogen-bonded to the propionate substituent of heme *a*<sub>3</sub> and to the Mg site. In H260N, the alteration of the hydrogen bond interactions and the Mg site will undoubtedly disturb the whole hydrogen-bond network in this region, and could account

for the structural and redox potential changes observed for heme *a*<sub>1</sub> and heme *a*<sub>3</sub>.

### **The disruption of the proposed electron transfer pathway in H260N**

Whether the rate of long-range electron transfer in proteins depends on only the distance and mass between the redox centers (Moser et al., 1995) or on specific pathways between them (Onuchic et al., 1992) is still not clear. The hydrogen-bond between His-260 and the arginine pair in subunit I has been proposed to form a part of a through-bond electron transfer pathway from Cu<sub>A</sub> to heme *a* (Iwata *et. al.*, 1995; Ramirez *et. al.*, 1995; Tsukihara *et. al.*, 1996). The H260N mutation will undoubtedly disrupt this hydrogen-bond interaction, and this could account for an even lower intrinsic electron transfer than that expected from disruption of the Cu<sub>A</sub> center and alteration in its redox potential, as compared to M263L. However, given the severe changes in structure and redox potentials of Cu<sub>A</sub> and heme *a* in this mutant, it is not possible to draw any conclusions regarding the pathway model based on this mutant alone.

Besides being an initial electron acceptor, Cu<sub>A</sub> was originally proposed to be involved in proton pumping (Chan & Li, 1990). Arguments against this model are based on the fact that quinol oxidases, which are homologous to CcO but do not have Cu<sub>A</sub> centers, can pump protons. In this study, the characteristic of coupling between the two copper atoms was found not to be important for proton pumping.

## Summary

Results discussed in this paper show that the rate of electron entry and transfer in CcO is determined by the unique structure of the binuclear Cu<sub>A</sub> center. Mutations of the copper ligands in M263L and H260N lead to decoupling the interaction between the two copper atoms and change the redox potential of this center, resulting in strong inhibition (240-fold in M263L) of electron transfer between Cu<sub>A</sub> and heme *a*. These results also support the model that Cu<sub>A</sub> is the sole input site for electrons from Cc. The coupling between the two copper atoms is not important for the proton pumping activity of this enzyme.

**CHAPTER VI**  
**SUMMARY AND PERSPECTIVES**

### **Deletion of subunit II**

In order to use site-directed mutagenesis technique to study the structure and function of subunit II of CcO from *R. sphaeroides*, it was necessary to delete the subunit II gene from the chromosome. Previously, a *R. sphaeroides* strain had been created in which the *coxII/III* operon was disrupted through insertional inactivation (Cao et al., 1992). Although the inactivation of the *coxII/III* operon resulted in the loss of the characteristic CcO spectrum from the membrane of the mutant strain, and CcO could be recovered in this mutant strain through complementation with the whole *coxII/III* operon, this strain was not a good system for site-directed mutagenesis, because of the potential for gene recombination between the inactivated copy in the chromosome and the copy in the plasmid used for the complementation.

Through homologous recombination, the *coxII/III* operon (*coxII*, *orf1*, *orf3* and partial *coxIII*) was deleted from the genomic DNA in YZ200 and replaced by a Sm/Sp antibiotic resistance gene. The deletion was confirmed through genetic and spectroscopic analyses. Moreover, YZ200 could be complemented with a plasmid-borne copy of the *coxII/III* operon, which makes it a good system for site-directed mutagenesis studies. In combination with strain YZ200, two systems have been set up, which enable all the residues in subunit II of CcO from *R. sphaeroides* to be mutated. YZ200 and the two systems have been thoroughly tested in the subsequently studies, and proved to be successful.

### **Overexpression and purification of CcO**

In wild-type *R. sphaeroides* strains, the content of CcO in the membrane is very low, characterized by the lower *a/b* ratios (0.2 for Ga and 2.4.1, and 0.35 for Cy91). For some of subunit II mutants (like H217C and C256S), which severely disrupt the enzymatic function, the enzyme expression level in the membranes is even lower, and the enzyme cannot be purified using the conventional anion-exchange chromatography.

The *aa*<sub>3</sub>-type CcO genes in *R. sphaeroides* have been successfully overexpressed up to seven-fold by ligating the two operons of CcO genes together and introducing them back into *R. sphaeroides* strains. Growth at high pH achieves even higher expression. The overexpression system allows all the mutants, regardless of their activities, to be purified in large amounts for further biochemical and biophysical analyses. A high-yield protocol for purifying homogenous oxidase by coupling Ni-affinity chromatography and anion-exchange chromatography has also been devised. In the overexpression system, the six histidine tag is located at the C-terminal of subunit I; as a result, the Ni-NTA purified enzymes, including the wild-type, have a fraction with a variable amount of subunit I alone, while the subunits II and III are lost in the purification. For mutants, like D229N and E254A, which have a disrupted subunit I/II interface, the fraction of subunit I is more significant than in wild-type. The presence of subunit I alone, along with the holoenzyme, tends to complicate the characterization of the enzyme. In combination with the anion-exchange chromatography, the fraction of subunit I, and the two fractions with intact and partially cleaved subunit II can be separated, resulting in a more homogenous sample.

Although CcO in most of the mutants can be overexpressed, the strains that have lower oxidase activities tend to partially delete the overexpression plasmid (pRK-pYJ123H) in the process of storage at low temperature and re-growth, while retaining the Tc-resistant phenotype. These cells tend to stick to the agar plates, and are difficult to remove using an inoculation loop, and they also grow much faster in the liquid medium. In order to acquire a large amount of enzyme from these strains, it is necessary to grow cells from newly-conjugated colonies.

### **Structural significance of the binuclear Cu<sub>A</sub> center and its control on electron transfer**

To study the structural significance of the binuclear center, the Cu<sub>A</sub> ligands have been mutated and, among the mutants, H260N and M263L have been thoroughly characterized. In M263L, the Cu<sub>A</sub> center was severely altered, and the coupling between the two copper atoms was disrupted, resulting in a copper center with properties of blue copper centers. The two copper atoms at the Cu<sub>A</sub> center are still present and all the other metal centers are intact in this mutant. In M263L, the decoupling of the two copper atoms results in the increase of the redox potential of the altered Cu<sub>A</sub> center by about 110 mV, as measured from the ruthenium kinetics assay, which severely inhibits the electron transfer from Cu<sub>A</sub> to heme *a* ( $50 \text{ s}^{-1}$  vs.  $120,000 \text{ s}^{-1}$  in wild-type). The decoupling of the Cu<sub>A</sub> center in M263L is also likely to increase the reorganization energy associated with the electron transfer, which also contributes to the slow electron transfer rates in this mutant. The mutational effect in H260N on the overall structure is more dramatic than in M263L. Besides the Cu<sub>A</sub> center, both the heme *a* and Mg sites are also affected. In this

mutant, the redox potential difference between Cu<sub>A</sub> and heme *a* is also altered, resulting in the inhibition of the electron transfer rate from Cu<sub>A</sub> to heme *a*. For these two mutants, it is necessary to measure the redox potentials of the Cu<sub>A</sub> center independently to confirm the results measured from the rapid kinetics assay. The binuclear character of the Cu<sub>A</sub> center is obviously critical for maintaining the right redox potential to facilitate the rapid electron transfer from Cc to heme *a*, while it is not important for the proton pumping function of the enzyme, since M263L and H260N still retain the proton pumping activity although the binuclear center is altered.

In M263L and H260N, the heme *a*<sub>3</sub> centers are difficult to reduce with dithionite. So it is necessary to use FTIR techniques to check the structural intactness of the binuclear centers of these two mutants (Hosler et al., 1994). However, in a recent theoretical analysis done by Michel and coworkers (Kannt et al., 1998), they found that residue Lys-227 in subunit II becomes protonated when the heme *a*<sub>3</sub>-Cu<sub>B</sub> center is reduced. So it is likely that the mutations in M263L and H260N change (most likely lower) the pK of Lys-227, resulting in difficulty in protonating this residue and in the reduction of the binuclear center. Clearly, more experiments are required to confirm this theory.

### **Residues involved in Cc binding**

Early studies have suggested that negatively charged carboxyl groups in subunit II of CcO are important in binding Cc. In this study, the conserved carboxyl residues (E148, D152, E157, D195, D214, D229, E254) in subunit II of *R. sphaeroides*, along with the nonconserved D188/E189, were mutated to neutral charge.

Physical characterization, including optical spectra, EPR and metal analysis, have shown that the metal centers in E148Q, D151N/E152Q, E157Q, D188N/E189Q, D195N and D214N are not altered, suggesting that the change of activities of these mutants are due to the localized effect of removing these carboxyl groups. In contrast, the heme *a* and Mg centers in D229N and E254A are disturbed, which is consistent with their locations at the interface of subunits I and II, either as direct ligands to the Mg center or hydrogen-bonded to the heme *a* centers through a hydrogen-bond network. The mutations in D188N/E189Q and D151N/E152Q have almost no effect on their overall activities when reacting with either horse or *R. sphaeroides* Cc, while the activities of E148Q, E157Q, D195N and D214N are decreased to different degrees; moreover, D195N and D214N behave differently in the reaction with horse or *R. sphaeroides* Cc, suggesting that horse and *R. sphaeroides* cytochromes *c* react differently with CcO from *R. sphaeroides*.

These mutants have been analyzed using the laser flash photolysis technique. At low ionic strength for the wild-type oxidase, a fast phase, representing the intracomplex electron transfer from Ru-55-Cc and Cu<sub>A</sub>, is observed, followed by electron transfer from Cu<sub>A</sub> to heme *a*. The intracomplex electron transfer rate from Cc to Cu<sub>A</sub> does not change as the ionic strength is increased from 5 to 75 mM, suggesting that increasing ionic strength does not change the configuration of Cc in the complex. At ionic strengths above 75 mM, Cc is completely dissociated from the complex, and the electron transfer reaction follows a second-order reaction. D151N/E152Q and D188N/E189Q have similar kinetics as wild-type, with rate constants equivalent to that of the wild-type oxidase.

E148Q, E157Q, D195N and D214N all have severely altered rapid kinetics, and most of them have fast and slow phases at low ionic strength. The fast phase is due to

the intracomplex electron transfer, and the slow phase reaction is due to either *Cc* in the wrong conformation or reaction from the solution due to the decreased binding affinity. The ionic strength dependent second-order reaction assay indicated that the binding strengths of these mutants for *Cc* are decreased, suggesting their involvement in *Cc* binding. This conclusion is also supported by the ultracentrifugation assay and the steady-state kinetics assay, which show that the equilibrium dissociation constant ( $K_D$ ) for binding horse *Cc* and the  $K_M$  values are increased, which also suggests that the binding strength for *Cc* is decreased. As controls, D151N/E152Q and D188N/E189Q do not display decreased *Cc* binding strengths.

Although the lysine residues in *Cc* that are involved in binding to *CcO* have been identified early, and several carboxyl residues in *CcO* that are involved in the binding have been identified in this study, it is still not clear how these lysine and carboxyl residues interact with each other, which can only be answered through computational and crystallographic studies.

### **Trp-143, the electron entry site, and $Cu_A$ , the solo initial electron acceptor in *CcO***

The  $Cu_A$  center has been shown to be the initial electron acceptor in *CcO*, but the possibility of a direct electron transfer pathway from *Cc* to heme *a* has not been ruled out. The mutations in W143F and W143A decrease the intracomplex electron transfer rate to 500-fold and 1200-fold, respectively, while the  $Cu_A$  centers in these two mutants are intact, and the *Cc* binding strength of these two mutants are similar to that of wild-type. So Trp-143 in subunit II is likely to be the electron entry site to *CcO*. In these

two mutants, the electron transfer rates from  $Cc$  to  $Cu_A$  are comparable to the overall turnover of the enzyme, suggesting that  $Cu_A$  is the solo initial electron acceptor in  $CcO$ .

In the C-terminus of subunit II, Trp-143 is surrounded by residues E148, E157, D195 and D214, which have been identified to be important in binding  $Cc$ . This arrangement may enable the heme edge of  $Cc$  to be in close contact with Trp-143, facilitating rapid electron transfer between them. In the recent collaboration with Victoria Roberts at the Scripps Institute, we have also found that one of the most energetically favorable orientations for  $Cc$ , predicted from the computational docking experiment, also places the heme edge of  $Cc$  within 5.0 Å of Trp-143, which is in agreement with the mutational study results. But the preliminary docking study cannot address the charge-charge interaction issue. A theoretical calculation done by P. Dutton at the University of Pennsylvania also places Trp-143 in the middle of the electron transfer pathway. All these results confirm the importance of Trp-143 in transfer electron from  $Cc$  to  $CcO$ . In Dutton's calculation, beside Trp-143, the other residues around Trp-143, like Tyr-144 and Tyr-159, have also been identified to be located at the electron entry "patch" to  $CcO$ . Further studies are required to test his theory.

## **APPENDIX**

## ABSTRACTS

1. Hosler, J.P., Espe, M., Fetter, J., Shapleigh, J.P., Thomas, J., Tecklenburg, M.M.J., Kim, Y., **Zhen, Y.**, Gennis, R.B., Babcock, G.T. and Ferguson-Miller, S. (1993) Metal center ligation and proton pumping in cytochrome *c* oxidase. Workshop on Structure-Function of Ion-Translocating Complexes, Freiburg, Germany
2. **Zhen, Y.**, Fetter, J., and Ferguson-Miller, S. (1995) Site-directed mutagenesis study of subunit II of *R. sphaeroides* cytochrome *c* oxidase. Inorganic Biochemistry Summer Workshop. University of Georgia, Athens
3. **Zhen, Y.**, Fetter, J., and Ferguson-Miller, S. (1996) Site-directed mutagenesis study of subunit II of cytochrome *c* oxidase. *Biophysical J.* 70 A353.
4. **Zhen, Y.**, Qian, J., Hosler, J. P., Follmann, K., Nilsson, T., Hayward, T., and Ferguson-Miller, S. (1996) Overexpression of cytochrome *c* oxidase in *Rhodobacter sphaeroides*. Canadian Federation of Biological Societies 39th Meeting . London, Ontario.
5. **Zhen, Y.**, Wang, K., Mills, D., Ferguson-Miller, S. and Millett, F. (1997) The binuclear character of Cu<sub>A</sub> in cytochrome *c* oxidase is important for electron transfer, not for proton pumping. Gordon Research Conference on Inorganic Biochemistry. Ventura, CA
6. **Zhen, Y.**, Wang, K., Mills, D., Ferguson-Miller, S., and Millett, F. (1997) The binuclear character of Cu<sub>A</sub> in cytochrome *c* oxidase is important for electron transfer, not for Proton Pumping. *Biophysical J.* 72 A93.
7. **Zhen, Y.**, Wang, K., Millett, F., and Ferguson-Miller, S. (1997) Rapid kinetic analysis of cytochrome *c* react with cytochrome *c* oxidase mutants: Definition of the interaction domain. Gordon Research Conference on Bioenergetics. Andover, New Hampshire.
8. **Zhen, Y.**, Wang, K., Sadoski, R., Grinnell, S., Geren, L., Ferguson-Miller, S., Durham, B. and Millett, F. (1998) Definition of interaction domain for the reaction of cytochrome *c* with *R.sphaeroides* cytochrome *c* oxidase. *Biophysical J.* 74 A77
9. Karpefors, M., Ädelroth, P., **Zhen, Y.**, Ferguson-Miller, S., and Brzezinski, P. (1998) Electron transfer from Cu<sub>A</sub> to heme *a* in in cytochrome *c* oxidase is controlled by proton transfer to the binuclear center. *Biochim. Biophys. Acta* vol. 10 p91

## **BIBLIOGRAPHY**

Aasa, R., Albracht, S. P. J., Falk, K.-E., Lanne, B. & Vanngard, T. (1976) EPR signals from cytochrome *c* oxidase. *Biochim. Biophys. Acta* 422: 260-272.

Adman, E. T. (1991) *Copper Protein Structures* (Adv. Prot. Chem.), vol. 42.

Allen, J. P., Feher, G., Yeates, T. O., Rees, D. C., Deisenhofer, J., Michel, H. & Huber, R. (1986) Structural homology of reaction centers from *Rhodospseudomonas sphaeroides* and *Rhodospseudomonas viridis* as determined by x-ray diffraction. *Proc. Natl. Acad. Sci. U S A* 83: 8589-93.

Amber, B. P., Bartsch, R. G., Daniel, M., Kamen, M. D., McLellan, L., Meyer, T. E. & Beeumen, J. V. (1981) Amino acid sequences of bacterial cytochrome *c'* and *c<sub>556</sub>*. *Proc. Natl. Acad. Sci. USA* 78: 6854-6857.

Antalis, T. M. & Palmer, G. (1982) Kinetic characterization of the interaction between cytochrome oxidase and cytochrome *c*. *J. Biol. Chem.* 257: 6194-6206.

Antholine, W. E., Kastrau, D. H. W., Steffens, G. C. M., Buse, G., Zumft, W. G. & Kroneck, P. M. H. (1992) A comparative EPR investigation of the multicopper proteins nitrous-oxide reductase and cytochrome *c* oxidase. *Eur. J. Biochem.* 209: 875-881.

Anthony, G., Reimann, A. & Kadenbach, B. (1993) Tissue-specific regulation of bovine heart cytochrome *c* oxidase activity by ADP via interaction with subunit VIa. *Proc. Natl. Acad. Sci. (USA)* 90: 1652-1656.

Antonini, G., Malatesta, F., Sarti, P. & Brunori, M. (1991) Control of Cytochrome Oxidase Activity. A transient spectroscopy study. *J. Biol. Chem.* 266: 13193-13202.

Avigliano, L., Vecchini, P., Sirianni, P., Marcozzi, G., Marchesini, A. & Mondovi, B. (1983) A reinvestigation on the quaternary structure of ascorbate oxidase from *Cucurbita pepo medullosa*. *Mol. Cell. Biochem.* 56: 107-12.

Babcock, G. T. & Callahan, P. M. (1983) Redox-linked hydrogen bond strength changes in cytochrome *a*: Implications for a cytochrome oxidase proton pump. *Biochemistry* 22: 2314-2319.

Babcock, G. T., Espe, M., Hoganson, C., Lydakis-Simantiris, N., McCracken, J., Shi, W., Styring, S., Tommos, C. & Warncke, K. (1997) Tyrosyl radicals in enzyme catalysis: some properties and a focus on photosynthetic water oxidation. *Acta. Chem. Scand.* 51: 533-40.

Babcock, G. T., Vickery, L. E. & Palmer, G. (1976) Electronic state of heme in cytochrome oxidase. I. Magnetic circular dichroism of the isolated enzyme and its derivatives. *J. Biol. Chem.* 251: 7907-19.

Babcock, G. T. & Wikström, M. (1992) Oxygen activation and the conservation of energy in cell respiration. *Nature* 356: 301-309.

Bartsch, R. G. in *The Photosynthetic Bacteria* Clayton, R. K. & Sistrom, W. R., Eds. (Plenum Press, New York, 1978) pp. 249-280.

Bartsch, R. G., Ambler, R. P., Meyer, T. E. & Cusanovich, M. A. (1989) Effect of aerobic growth conditions on the soluble cytochrome content of the purple phototrophic bacterium *Rhodobacter sphaeroides*: induction of cytochrome  $c_{554}$ . *Arch. Biochem. Biophys.* 271: 433-440.

Behr, J., Hellwig, P., Mantele, W. & Michel, H. (1998) Redox dependent changes at the heme propionates in cytochrome *c* oxidase from *Paracoccus denitrificans*: direct evidence from FTIR difference spectroscopy in combination with heme propionate  $^{13}\text{C}$  labeling. *Biochemistry* 37: 7400-6.

Beinert, H. (1997) Copper A of cytochrome *c* oxidase, a novel, long-embattled, biological electron-transfer site. *Eur. J. Biochem.* 245: 521-32.

Beinert, H., Griffiths, D., E, Wharton, D. C. & Sands, R. H. (1962) Properties of the copper associated with cytochrome *c* oxidase as studied by paramagnetic resonance spectroscopy. *J. Biol. Chem* 237: 2337-2345.

Bergman, C., Gandvik, E. K., Nyman, P. O. & Strid, L. (1977) The amino acid sequence of stellacyanin from the lacquer tree. *Biochem. Biophys. Res. Commun.* 77: 1052-1059.

Berry, E., Huang, L., Zhang, Z., Chi, Y. & Kim, K. (1998) Structure of the mitochondrial cytochrome  $bc_1$  complex: pathways for electron transfer involving a mobile iron-sulfur protein and two exposed edges of the cytochrome *c*, heme. *J. Biophys.* 74: A329.

Berry, E. A. & Trumpower, B. L. (1985) Isolation of ubiquinol oxidase from *Paracoccus denitrificans* and resolution into cytochrome  $bc_1$  and cytochrome *c-aa3* complexes. *J. Biol. Chem.* 260: 2458-2467.

Berry, E. A. & Trumpower, B. L. (1987) Simultaneous determination of hemes *a*, *b*, and *c* from pyridine hemochrome spectra. *Anal. Biochem.* 161: 1-15.

Bisson, R., Jacobs, B. & Capaldi, R. A. (1980) Binding of arylazidocytocrome *c* derivatives to beef heart cytochrome *c* oxidase: cross-linking in the high- and low-affinity binding sites. *Biochemistry* 19: 4173-8.

Bisson, R., Steffens, G. C. M., Capaldi, R. A. & Buse, G. (1982) Mapping of the cytochrome *c* binding site on cytochrome *c* oxidase. *FEBS Lett.* 144: 359-363.

Bjerrum, M. J., Casimiro, D. R., Chang, I. J., Di Bilio, A. J., Gray, H. B., Hill, M. G., Langen, R., Mines, G. A., Skov, L. K., Winkler, J. R. & et al. (1995) Electron transfer in ruthenium-modified proteins. *J. Bioenerg. Biomembr.* 27: 295-302.

Blackburn, N. J., Barr, M. E., Woodruff, W. H., Van der Oost, J. & Vries, S. (1994) Metal-metal bonding in biology: EXAFS evidence for a 2.5 Å copper-copper bond in the Cu<sub>A</sub> center of cytochrome oxidase. *Biochemistry* 33: 10401-10407.

Blair, D. F., Ellis, J., Walther R., Wang, H., Gray, H. B. & Chan, S. I. (1986) Spectroelectrochemical study of cytochrome *c* oxidase: pH and temperature dependences of the cytochrome potentials. *J. Biol. Chem.* 261: 11524-11537.

Blair, D. F., Martin, C. T., Gelles, J., Wang, H., Brudvig, G. W., Stevens, T. H. & Chan, S. I. (1983) The metal centers of cytochrome *c* oxidase: Structures and Interactions. *Chemica. Scripta.* 21: 43-53.

Bombelka, E., Richter, F.-W., Stroh, A. & Kadenbach, B. (1986) Analysis of the Cu, Fe, and Zn contents in cytochrome *c* oxidases from different species and tissues by proton-induced x-ray emission (PIXE). *Biochem. Biophys. Res. Commun.* 140: 1007-1014.

Bose, S., Hendler, R. W., Shrager, R. I., Chan, S. I. & Smith, P. D. (1997) Multichannel analysis of single-turnover kinetics of cytochrome *aa*<sub>3</sub> reduction of O<sub>2</sub>. *Biochemistry* 36: 2439-49.

Bott, M., Ritz, D. & Hennecke, H. (1991) The *Bradyrhizobium japonicum* *cycM* gene encodes a membrane-anchored homolog of mitochondrial cytochrome *c*. *J. Bacteriol.* 173: 6766-6772.

Bradford, M. M. (1976) A rapid and sensitive method for the quantitation of microgram quantities of protein utilizing the principle of protein-dry binding. *Anal. Biochem.* 72: 248-254.

Brandner, J. P., McEwan, A. G., Kaplan, S. & Donohue, T. J. (1989) Expression of the *Rhodobacter sphaeroides* cytochrome *c*<sub>2</sub> structure gene. *J. Bact.* 171: 360-368.

Brautigan, D. L., Ferguson-Miller, S. & Margoliash, E. (1978) Mitochondrial cytochrome *c*: Preparation and activity of native and chemically modified cytochromes *c*. *Methods Enzymol.* 53: 128-164.

Brzezinski, P. (1996) Internal electron-transfer reactions in cytochrome *c* oxidase. *Biochemistry* 35: 5612-5.

Brzezinski, P. & Malmstrom, B. G. (1987) The mechanism of electron gating in proton pumping cytochrome *c* oxidase: the effect of pH and temperature on internal electron transfer. *Biochim. Biophys. Acta* 894: 29-38.

Brzezinski, P. & Malmström, B. G. (1986) Electron-transport-driven proton pumps display nonhyperbolic kinetics in the oxidation of ferricytochrome *c* catalyzed by cytochrome *c* oxidase. *Proc. Natl. Acad. Sci.* 83: 4282-4286.

Brzezinski, P., Sundahl, M., Adelroth, P., Wilson, M. T., el-Agez, B., Wittung, P. & Malmstrom, B. G. (1995) Triplet-state quenching in complexes between Zn-cytochrome *c* and cytochrome oxidase or its Cu<sub>A</sub> domain. *Biophys. Chem.* 54: 191-7.

Brzezinski, P. & Wilson, M. T. (1997) Photochemical electron injection into redox-active proteins. *Proc. Natl. Acad. Sci. U S A* 94: 6176-9.

Cann, J. R. Interacting macromolecules: The theory and practice of their electrophoresis, ultracentrifugation, and chromatography. Horecker, B., Eds., Molecular Biology (Academic Press, New York and London, 1970).

Cao, J., Hosler, J., Shapleigh, J., Gennis, R., Revzin, A. & Ferguson-Miller, S. (1992) Cytochrome *aa3* of *Rhodobacter sphaeroides* as a model for mitochondrial cytochrome *c* oxidase. *J. Biol. Chem.* 267: 24273-24278.

Cao, J., Shapleigh, J., Gennis, R., Revzin, A. & Ferguson-Miller, S. (1991) The gene encoding cytochrome *c* oxidase subunit II from *Rhodobacter sphaeroides*; Comparison of the deduced amino acid sequence with sequences of corresponding peptides from other species. *Gene* 101: 133-137.

Chan, S. I. & Li, P. M. (1990) Cytochrome *c* Oxidase: Understanding nature's design of a proton pump. *Biochemistry* 29: 1-12.

Chance, B., Saronio, C. & Leigh, J. S., Jr. (1975(a)) Functional intermediates in the reaction of membrane-bound cytochrome oxidase with oxygen. *J. Biol. Chem.* 250: 9226-37.

Chance, B., Saronio, C. & Leigh, J. S., Jr. (1975(b)) Functional intermediates in reaction of cytochrome oxidase with oxygen. *Proc. Natl. Acad. Sci. U S A* 72: 1635-40.

Chang, C. H., Tiede, D., Tang, J., Smith, U., Norris, J. & Schiffer, M. (1986) Structure of *Rhodospseudomonas sphaeroides* R-26 reaction center. *FEBS Lett.* 205: 82-6.

Chory, J., Donohue, T. J., Varga, A. R., Staehelin, L. A. & Kaplan, S. (1984) Induction of the photosynthetic membranes of *Rhodospseudomonas sphaeroides*: biological and morphological studies. *J. Bacteriol.* 159: 540-554.

Cohen-Bazire, G., Sistrom, W. R. & Stanier, R. Y. (1957) Kinetic studies of pigment synthesis by non-sulfur purple bacteria. *J. Cell Comp. Physiol.* 49: 25-68.

Cooper, C. E. (1989) The steady-state kinetics of cytochrome *c* oxidation by cytochrome oxidase. *Biochim. Biophys. Acta* 1017: 187-203.

Cramer, W. A., Martinez, S. E., Huang, D., Tae, G. S., Everly, R. M., Heymann, J. B., Cheng, R. H., Baker, T. S. a. & Smith, J. L. (1994) Structural aspects of the cytochrome *b<sub>f</sub>* complex; structure of the lumen-side domain of cytochrome *f*. *J. Bioenerg. Biomembr.* 26: 31-47.

- Curry, W. B., Grabe, M. D., Kurnikov, I. V., Skourtis, S. S., Beratan, D. N., Regan, J. J., Aquino, A. J., Beroza, P. & Onuchic, J. N. (1995) Pathways, pathway tubes, pathway docking, and propagators in electron transfer proteins. *J. Bioenerg. Biomembr.* 27: 285-93.
- Cusanovich, M. A. (1971) Molecular weight of some cytochrome *cc'*. *Biochim. Biophys. Acta* 236: 238-241.
- Daldal, F., Cheng, S., Applebaum, J., Davidson, E. & Prince, R. C. (1986) Cytochrome *c*<sub>2</sub> is not essential for photosynthetic growth of *Rhodospseudomonas Capsulata*. *Proc. Nat. Acad. Sci. USA* 83: 2012-2016.
- Davies, J. & Smith, D. I. (1978) Plasmid-determined resistance to antimicrobial agents. *Ann. Rev. Microbiol.* 32: 469-518.
- Davis, R. W., Botstein, D. & Roth, J. R. *Advanced Bacterial Genetics* (Cold Spring Harbor Laboratory, Cold Spring Harbor, NY, 1980).
- de Gier, J. L., Schepper, M., Reijnders, W. N. M., van Dyck, S. J., Slotboom, D. J., Warner, A., Saraste, M., Krab, K., Finel, M., Stouthamer, A. H., van Spanning, R. J. M. & van der Oost, J. (1996) Structural and functional analysis of *aa*<sub>3</sub>-type and *cbb*<sub>3</sub>-type cytochrome *c* oxidases of *Paracoccus denitrificans* reveals significant differences in proton-pumping design. *Mol. Microbiol.* 20: 1247-1260.
- Deisenhofer, J., Epp, O., Miki, K., Huber, R. & Michel, H. (1984) X-ray structure analysis of a membrane protein complex. Electron density map at 3 Å resolution and a model of the chromophores of the photosynthetic reaction center from *Rhodospseudomonas viridis*. *J. Mol. Biol.* 180: 385-98.
- den Blaauwen, T., van de Kamp, M. & Canters, G. W. (1991) Type I and II copper sites obtained by external addition of ligands to a HIS117Gly azurin mutant. *J. Am. Chem. Soc.* 113: 5050-5052.
- Dennison, C., Vijgenboom, E., De Vries, S., Van der Oost, J. & Canters, G. W. (1995) Introduction of a Cu<sub>A</sub> site into the blue copper protein amicyanin from *Thiobacillus versutus*. *FEBS lett.* 365: 92-94.
- Depillis, G. D., Decatur, S. M., Barrick, D. & Boxer, S. G. (1994) Functional cavities in proteins: a general method for proximal ligands substitution in myoglobin. *J. Am. Chem. Soc.* 116: 6981-6982.
- Dietz, R., Nastainczyk, W. & Ruf, H. H. (1988) Higher oxidation states of prostaglandin H synthase. Rapid electronic spectroscopy detected two spectral intermediates during the peroxidase reaction with prostaglandin G<sub>2</sub>. *Eur. J. Biochem.* 171: 321-8.
- Donohue, T. & Kaplan, S. (1991) Genetic techniques in *Rhodospirillaceae*. *Methods Enzymol.* 204: 459-485.

Donohue, T. J., McEwan, A. G., Van Doren, S., Crofts, A. R. & Kaplan, S. (1988) Phenotypic and genetic characterization of cytochrome *c*<sub>2</sub> Deficient mutants of *Rhodobacter sphaeroides*. *Biochemistry* 27: 1918-1925.

Duport, C., Meyer, C., Naud, I. & Jouanneau, Y. (1994) A new gene expression system based on a fructose-dependent promoter from *Rhodobacter capsulatus*. *Gene* 145: 103-108.

Durham, B., Pan, L. P., Long, J. E. & Millett, F. (1989) Photoinduced electron-transfer kinetics of singly labeled ruthenium bis(bipyridine) dicarboxybipyridine cytochrome *c* derivatives. *Biochemistry* 28: 8659-65.

Einarsdottir, O. & Caughey, W. S. (1984) Zinc is a constituent of bovine heart cytochrome *c* oxidase preparations. *Biochem. Biophys. Res. Commun.* 124: 836-42.

Einarsdottir, O. & Caughey, W. S. (1985) Bovine heart cytochrome *c* oxidase preparations contain high affinity binding sites for magnesium as well as for zinc, copper, and heme iron. *Biochem. Biophys. Res. Commun.* 129: 840-7.

Erman, J. E., Kresheck, G. C., Vitello, L. B. & Miller, M. A. (1997) Cytochrome *c*/cytochrome *c* peroxidase complex: Effect of binding-site mutations on the thermodynamics of complex formation. *Biochemistry* 36: 4054-4060.

Errede, B., Haight, G. J. & Kamen, M. (1976) Oxidation of ferrocyanide by mitochondrial cytochrome *c* oxidase. *Proc. Natl. Acad. Sci.* 73: 113-117.

Errede, B. & Kamen, M. D. (1978) Comparative kinetic studies of cytochromes *c* reactions with mitochondrial cytochrome *c* oxidase and reductase. *Biochemistry* 17: 1015-1027.

Espe, M. P., Hosler, J. P., Ferguson-Miller, S., Babcock, G. T. & McCracken, J. (1995) A continuous wave and pulsed EPR characterization of the Mn<sup>2+</sup> binding site in *Rhodobacter sphaeroides* cytochrome *c* oxidase. *Biochemistry* 34: 7593-7602.

Farrar, J. A., Lappalainen, P., Zumft, W. G., Saraste, M. & Thomson, A. J. (1995) Spectroscopic and mutagenesis studies on the Cu<sub>A</sub> centre from the cytochrome-*c* oxidase complex of *Paracoccus denitrificans*. *Eur. J. Biochem.* 232: 294-303.

Ferguson-Miller, S. & Babcock, G. (1996) Heme/copper terminal oxidases. *Chem. Rev.* 96: 2889-2907.

Ferguson-Miller, S., Brautigan, D. & Margoliash, E. (1976) Correlation of the kinetics of electron transfer activity of various eukaryotic cytochrome *c* with binding to mitochondrial cytochrome *c* oxidase. *J. Biol. Chem.* 251: 1104-1115.

Ferguson-Miller, S., Brautigan, D. L. & Margoliash, E. (1978) Definition of cytochrome *c* binding domains by chemical modification. *J. Biol. Chem.* 253: 149-159.

Fetter, J. R., Qian, J., Shapleigh, J., Thomas, J. W., García-Horsman, J. A., Schmidt, E., Hosler, J., Babcock, G. T., Gennis, R. B. & Ferguson-Miller, S. (1995) Possible proton relay pathways in cytochrome *c* oxidase. *Proc. Natl. Acad. Sci. U.S.A.* 92: 1604-1608.

Fishel, L. A., Villafranca, J. E., Mauro, J. M. & Kraut, J. (1987) Yeast cytochrome *c* peroxidase: Mutagenesis and expression in *Escherichia coli* show tryptophan-51 is not the radical site in compound I. *Biochemistry* 26: 351-60.

Fitch, J., Cannac, V., Meyer, T. e., Cusanovich, M. A., Tollin, G., Van Beeumen, J., Rott, M. A. & Donohue, T. J. (1989) Expression of a cytochrome *c*<sub>2</sub> isozyme restores photosynthetic growth of *Rhodobacter sphaeroides* mutants lacking the wild-type cytochrome *c*<sub>2</sub> gene. *Arch. Biochem. Biophys.* 271: 502-507.

Florens, L., Hoganson, C., McCracken, J., Fetter, J., Mills, D. A., Babcock, G. T. & Ferguson-Miller, S. in *The phototropic prokaryotes* Preschek, G., Eds. (Plenum Press, 1998), vol. *in press*.

Flory, J. E. & Donohue, T. J. (1995) Organization and expression of the *Rhodobacter sphaeroides* *cycFG* operon. *J. Bacteriol.* 177: 4311-4320.

Flory, J. E. & Donohue, T. J. (1997) Transcriptional control of several aerobically induced cytochrome structural genes in *Rhodobacter sphaeroides*. *Microbiology* 143: 3101-3110.

Frank, V. & Kadenbach, B. (1996) Regulation of the H<sup>+</sup>/e<sup>-</sup> Stoichiometry of cytochrome *c* oxidase from bovine heart by intramitochondrial ATP/ADP ratios. *FEBS Lett.* 382: 121 -124.

Friedrich, T., Abelmann, A., Brors, B., Guenebaut, V., Kintscher, L., Leonard, K., Rasmussen, T., Scheide, D., Schlitt, A., Schulte, U. & Weiss, H. (1998) Redox components and structure of the respiratory NADH:ubiquinone oxidoreductase (complex I). *Biochem. Biophys. Acta* 1365: 215-219.

Francisz, W., Scholes, C. P., Hyde, J. S., Wei, Y. H., King, T. E., Shaw, R. W. & Beiner, H. (1979) Hyperfine structure resolved by 2 to 4 GHz EPR of cytochrome *c* oxidase. *J. Biol. Chem.* 254: 7482-4.

Fujita, N., Mori, H., Yura, T. & Ishihana, a. (1994) Systematic sequencing of the *Escherichia coli* genome: Analysis of the 2.4-4.1 min (110,917-193,643) region. *Nucleic Acids res.* 22: 1637-1639.

Gabellini, N. & Sebald, w. (1986) Nucleotide Sequence and Transcription of the *fbc* Operon from *Rhodopseudomonas sphaeroides*: Evaluation of the deduced amino acid sequences of the FeS protein, cytochrome *b* and cytochrome *c*<sub>1</sub>. *Eur. J. Biochem.* 154: 569-579.

Garber, E. & Margoliash, E. (1990) Interaction of cytochrome *c* with cytochrome *c* oxidase: An understanding of the high- to low-affinity transition. *Biochim. Biophys. Acta* 1015: 279-287.

- García-Horsman, J., Barquera, B., Rumbley, J., Ma, J. & Gennis, R. B. (1994a) The superfamily of heme-copper respiratory oxidases. *J. Bacteriol.* 176: 5587-5600.
- García-Horsman, J. A., Berry, E., Shapleigh, J. P., Alben, J. O. & Gennis, R. B. (1994b) A novel cytochrome *c* oxidase from *Rhodobacter Sphaeroides* that lacks Cu<sub>A</sub>. *Biochemistry* 33: 3113-3119.
- García-Horsman, J. A., Puustinen, A., Gennis, R. B. & Wikström, M. (1995) Proton transfer in cytochrome *bo*<sub>3</sub> ubiquinol oxidase of *Escherichia coli*: Second-site mutations in subunit I that restore proton pumping in the mutant Asp135→Asn. *Biochemistry* 34: 4428-4433.
- Gennis, R. B., Casey, R. P., Azzi, A. & Ludwig, B. (1982) Purification and characterization of the cytochrome *c* oxidase from *Rhodopseudomonas sphaeroides*. *Eur. J. Biochem.* 125: 189-195.
- Georgiadis, K. E., Jhon, N.-I. & Eiansdottir, O. (1994) Time-resolved optical absorption studies of intramolecular electron transfer in cytochrome *c* oxidase. *Biochemistry* 33: 9245-9256.
- Geren, L. M., Beasley, J. R., Fine, B. R., Saunders, A. J., Hibdon, S., Pielak, G. J., Durham, B. & Millett, F. (1995) Design of a ruthenium-cytochrome *c* derivative to measure electron transfer to the initial acceptor in cytochrome *c* oxidase. *J. Biol. Chem.* 270: 2466 - 2662.
- Gibson, Q. & Greenwood, C. (1963) Reactions of cytochrome oxidase with oxygen and carbon monoxide. *Biochem. J.* 86: 541-554.
- Gray, H. B. & Winkler, J. R. (1996) Electron transfer in proteins. *Annu. Rev. Biochem.* 65: 537-61.
- Gray, K., Grooms, M., Myllykallio, H., Moomaw, C., Slaughter, C. & Daldal, F. (1994) *Rhodobacter capsulatus* contains a novel *cb*-type cytochrome *c* oxidase without a Cu<sub>A</sub> center. *Biochemistry* 33: 3120-3127.
- Greenwood, C. & Gibson, Q. H. (1967) The reaction of reduced cytochrome *c* oxidase with oxygen. *J. Biol. Chem.* 242: 1782-1787.
- Greenwood, C., Hill, B. C., Barber, D., Eglinton, D. G. & Thomson, A. J. (1983) The optical properties of Cu<sub>A</sub> in bovine cytochrome *c* oxidase determined by low-temperature magnetic-circular-dichroism spectroscopy. *Biochem. J.* 215: 303-16.
- Greenwood, C., Thomson, A. J., Barrett, C. P., Peterson, J., George, G. N., Fee, J. A. & Reichardt, J. (1988) Some spectroscopic views of the Cu<sub>A</sub> Site in cytochrome *c* oxidase preparations. *Ann. NY Acad. Sci.* 550: 47-52.
- Griffiths, D. E. & Wharton, D. C. (1961) Studies of the electron transport system: XXXVI. properties of copper in cytochrome oxidase. *J. Biol. Chem.* 236: 1857-1862.

- Hagerhall, c. (1997) Succinate:quinone oxidoreductases variations on a conserved theme. *Biochim. Biophys. Acta* 1320: 107-141.
- Hällén, S. & Nilsson, T. (1992) Proton transfer during the reaction between fully reduced cytochrome oxidase and dioxygen: pH and deuterium isotope effects. *Biochemistry* 31: 11853-11859.
- Haltia, T., Finel, M., Harms, N., Nakari, T., Raitio, M., Wikström, M. & Saraste, M. (1989) Deletion of the gene for subunit III leads to defective assembly of bacterial cytochrome oxidase. *EMBO J.* 8: 3571-3579.
- Haltia, T., Saraste, M. & Wikström, M. (1991) Subunit III of cytochrome *c* oxidase is not involved in proton translocation: A site-directed mutagenesis study. *EMBO J.* 10: 2015-2021.
- Haltia, T., Semo, N., Arrondo, J. L., Goni, F. M. & Freire, E. (1994) Thermodynamic and structural of cytochrome *c* oxidase from *Paracoccus denitrificans*. *Biochemistry* 33: 9731-9740.
- Han, S., Ching, Y.-C. & Rousseau, D. L. (1990) Ferryl and hydroxy intermediates in the reaction of oxygen with reduced cytochrome *c* oxidase. *Nature* 348: 89-90.
- Hansson, O., Karlsson, B., Aasa, R., Vanngard, T. & Malmstrom, B. G. (1982) The structure of the paramagnetic oxygen intermediate in the cytochrome *c* oxidase reaction. *EMBO J.* 1: 1295-7.
- Hatefi, Y. (1985) The mitochondrial electron transport and oxidative phosphorylation system. *Annu. Rev. Biochem.* 54: 1015-1069.
- Hay, M., Richards, J. H. & Lu, Y. (1996) Construction and characterization of an azurin analog for the purple copper site in cytochrome *c* oxidase. *Proc. Natl. Acad. Sci. USA* 93: 461-4.
- Hazzard, J., McLendon, G., Cusanovich, M. & Tollin, G. (1990) Formation of electrostatically-stabilized complex at low ionic strength inhibits interprotein electron transfer between yeast cytochrome *c* and cytochrome *c* peroxidase. *Biochem. Biophys. Res. Commun.* 172: 1157-62.
- Hazzard, J., Rong, S. & Tollin, G. (1991) Ionic strength dependence of the kinetics of electron transfer from bovine mitochondrial cytochrome *c* to bovine cytochrome *c* oxidase. *Biochemistry* 30: 213-222.
- Hellwig, P., Behr, J., Ostermeier, C., Richter, O. M., Pfitzner, U., Odenwald, A., Ludwig, B., Michel, H. & Mantele, W. (1998) Involvement of glutamic acid 278 in the redox reaction of the cytochrome *c* oxidase from *Paracoccus denitrificans* investigated by FTIR spectroscopy. *Biochemistry* 37: 7390-9.

- Hill, B. C. (1991) The reaction of the electrostatic cytochrome *c*-cytochrome oxidase complex with oxygen. *J. Biol. Chem.* 266: 2219-2226.
- Hill, B. C. (1993) The sequence of electron carriers in the reaction of cytochrome *c* oxidase with oxygen. *J. Bioenerg. Biomembr.* 25: 115-120.
- Hill, B. C. (1994) Modeling the sequence of electron transfer reactions in the single turnover of reduced, mammalian cytochrome *c* oxidase. *J. Biol. Chem.* 269: 2219-2226.
- Ho, S. N., Hunt, H. D., Horton, R. M., Pullen, J. K. & Pease, L. R. (1989) Site-directed mutagenesis by overlap extension using the polymerase chain reaction. *Gene* 77: 51-59.
- Hoeren, F. U., Berks, B. C., Ferguson, S. J. & McCarthy, J. E. (1993) Sequence and expression of the gene encoding the respiratory nitrous-oxide reductase from *Paracoccus denitrificans*. New and conserved structural and regulatory motifs. *Eur. J. Biochem.* 218: 49-57.
- Hofacker, I. & Schulten, K. (1997) Oxygen and proton pathways in cytochrome *c* oxidase. *Proteins: Structure, Function & Genetics* 30: 100-107.
- Holm, L., Saraste, M. & Wikström, M. (1987) Structural models of the redox centres in cytochrome oxidase. *EMBO J.* 6: 2819-2823.
- Hosler, J. P., Espe, M. P., Zhen, Y., Babcock, G. T. & Ferguson-Miller, S. (1995) Analysis of site-directed mutants locates a non-redox-active metal near the active site of cytochrome *c* oxidase of *Rhodobacter sphaeroides*. *Biochemistry* 34: 7586-7592.
- Hosler, J. P., Ferguson-Miller, S., Calhoun, M. W., Thomas, J. W., Hill, J., Lemieux, L., Ma, J., Georgiou, C., Fetter, J., Shapleigh, J. P., Tecklenburg, M. M. J., Babcock, G. T. & Gennis, R. B. (1993) Insight into the active-site structure and function of cytochrome oxidase by analysis of site-directed mutants of bacterial cytochrome *aa<sub>3</sub>* and cytochrome *bo*. *J. Bioenerg. Biomembr.* 25: 121-136.
- Hosler, J. P., Fetter, J., Tecklenburg, M. M. J., Espe, M., Lerma, C. & Ferguson-Miller, S. (1992) Cytochrome *aa<sub>3</sub>* of *Rhodobacter sphaeroides* as a model for mitochondrial cytochrome *c* oxidase. *J. Biol. Chem.* 267: 24264-24272.
- Hosler, J. P., Kim, Y., Shapleigh, J., Gennis, R., Alben, J., Ferguson-Miller, S. & Babcock, G. (1994) Vibrational characteristics of mutant and wild-type carbon-monooxygenase cytochrome *c* oxidase: evidence for a linear arrangement of heme *a*, *a<sub>3</sub>*, and Cu<sub>A</sub>. *J. Am. Chem. Soc.* 116: 5515-5516.
- Iwata, S., Lee, J. W., Okada, K., Lee, J. K., Iwata, M., Rasmussen, B., Link, T. A., Ramaswamy, S. & Jap, B. K. (1998) Complete structure of the 11-subunit bovine mitochondrial cytochrome *bc<sub>1</sub>* complex. *Science* 281: 64-71.

Iwata, S., Ostermeier, C., Ludwig, B. & Michel, H. (1995) Structure at 2.8 Å resolution of cytochrome *c* oxidase from *Paracoccus denitrificans*. *Nature* 376: 660-669.

Iwata, S., Saynovits, M., Link, T. A. & Michel, H. (1996) Structure of a water soluble fragment of the 'Rieske' iron-sulfur protein of the bovine heart mitochondrial cytochrome *bc<sub>1</sub>* complex determined by MAD phasing at 1.5 Å resolution. *Structure* 4: 567-579.

Jenney Jr., F. E. & Daldal, F. (1993) a novel membrane-associated *c*-type cytochrome *cyt c<sub>y</sub>*, can mediate the photosynthetic growth of *Rhodobacter capsuatus* and *Rhodobacter sphaeroides*. *EMBO J.* 12: 1283-1292.

Junemann, S. (1997) Cytochrome *bd* terminal oxidase. *Biochim. Biophys. Acta* 1321: 107-127.

Kadenbach, B., Jarausch, J., Hartmann, R. & Merle, P. (1983) Separation of mammalian cytochrome *c* oxidase into 13 polypeptides by a sodium dodecyl sulfate-gel electrophoretic procedure. *Anal. Biochem.* 129: 517-521.

Kaminski, P. A., Kitts, C. L., Zimmerman, Z. & Ludwig, R. A. (1996) *Azorhizobium caulinodans* uses both cytochrome *bd* (quinol) and cytochrome *cbb<sub>3</sub>* (cytochrome *c*) terminal oxidases for symbiotic N<sub>2</sub> fixation. *J. Bacteriol.* 178: 5989-5994.

Kang, C. H., Brautigam, D. L., Osheroff, N. & Margoliash, E. (1978) Definition of cytochrome *c* binding domains by chemical modification. Reaction of carboxydinitrophenyl- and trinitrophenyl-cytochromes *c* with baker's yeast cytochrome *c* peroxidase. *J. Biol. Chem.* 253: 6502-10.

Kannt, A., Roy, C., Lancaster, D. & Michel, H. (1998) The coupling of electron transfer and proton translocation: electrostatic calculations on *Paracoccus denitrificans* cytochrome *c* oxidase. *Biophys. J.* 74: 708-21.

Karksson, B. G., Nordling, M., Pascher, T., Tsai, L. C., Sjolín, L. & Lundberg, L. G. (1991) Casette mutagenesis of Met121 in azurin from *Pseudomonas aeruginosa*. *Protein Eng.* 4: 343-349.

Keilin, D. & Hartree, E. F. (1939) Cytochrome and cytochrome oxidase. *Proc. R. Soc. (Lond.)* B127: 167-191.

Kelly, M., Lappalainen, P., Talbo, G., Haltia, T., van der Oost, J. & Saraste, M. (1993) Two cysteines, two histidines, and one methionine are ligands of a binuclear purple copper center. *J. Biol. Chem.* 268: 16781-16787.

Kiley, P. J. & Kaplan, S. (1988) molecular genetics of photosynthetic membrane biosynthesis in *Rhodobacter sphaeroides*. *Microbiol. Rev.* 52: 50-69.

Kituchi, G., Saito, Y. & Motokawa, Y. (1965) On cytochrome oxidase as the terminal oxidase of dark respiration of non-sulfur purple bacteria. *Biochem. Biophys. Acta* 94: 1-14.

- Konstantinov, A. A., Siletsky, S., Mitchell, D., Kaulen, A. & Gennis, R. (1997) The roles of the two proton input channels in cytochrome *c* oxidase from *Rhodobacter sphaeroides* probed by the effects of site-directed mutations on time-resolved electrogenic intraprotein proton transfer. *Proc. Natl. Acad. Sci. (USA)* 94: 9085-9090.
- Kovach, M. E., Phillips, R. W., Elzer, P. H., Roop II, R. M. & Peterson, K. M. (1994) pBBR1MCS: A broad-host-range cloning vector. *BioTechniques* 16: 800-802.
- Krebs, M. P. & Khorana, H. G. (1993) Mechanism of light-dependent proton translocation by bacteriorhodopsin. *J. Bacteriol.* 175: 1555-1560.
- Kroneck, P. M. H., Anotholine, W. E., Riester, J. & Zumft, W. G. (1988) The cupric site in nitrous oxide reductase contains a mixed-valence [Cu(II),Cu(I)] binuclear center: a multifrequency electron paramagnetic resonance investigation. *FEBS lett.* 242: 70-74.
- Kroneck, P. M. H., Antholine, W. A., Riester, J. & Zumft, W. G. (1989) The nature of the cupric site in nitrous oxide reductase and of Cu<sub>A</sub> in cytochrome *c* oxidase. *FEBS Lett.* 248: 212-213.
- Kuhn, L. A., Siani, M. A., Pique, M. E., Fisher, C. L., Getzoff, E. D. & Tainer, J. A. (1992) The interdependence of protein surface topography and bound water molecules revealed by surface accessibility and fractal density measures. *J. Mol. Biol.* 228: 13-22.
- Kunkel, T. A. (1985) Rapid and efficient site-specific mutagenesis without phenotypic selection. *Proc. Natl. Acad. Sci. USA* 82: 488-492.
- Langen, R., Chang, I. J., Germanas, J. P., Richards, J. H., Winkler, J. R. & Gray, H. B. (1995) Electron tunneling in proteins: coupling through a beta strand. *Science* 268: 1733-5.
- Lappalainen, P., Aasa, R., Malmström, B. G. & Saraste, M. (1993) Soluble Cu<sub>A</sub>-binding domain from the *Paracoccus* cytochrome *c* oxidase. *J. Biol. Chem.* 268: 26416-26421.
- Lappalainen, P. & Saraste, M. (1994) The binuclear Cu<sub>A</sub> center of cytochrome *c* oxidase. *Biochim. Biophys. Acta.* 1187: 222-225.
- Lappalainen, P., Watmough, N. J., Greenwood, C. & Saraste, M. (1995) Electron transfer between cytochrome *c* and the isolated Cu<sub>A</sub> domain: identification of substrate-binding residues in cytochrome *c* oxidase. *Biochemistry* 34: 5824-5830.
- Larsson, S., Kallebring, B., Wittung, P. & Malmstrom, B. G. (1995) The Cu<sub>A</sub> center of cytochrome *c* oxidase: electronic structure and spectra of models compared to the properties of Cu<sub>A</sub> domains. *Proc. Natl. Acad. Sci. U S A* 92: 7167-71.

- Li, P. M., Gelles, J., Chan, S. I., Sullivan, R. J. & Scott, R. A. (1987a) Extended x-ray absorption fine structure of copper in Cu<sub>A</sub>-depleted, *p*-(hydroxymercuri)benzoate-modified, and native cytochrome *c* oxidase. *Biochemistry* 26: 2091-2095.
- Li, P. M., Malmström, B. G. & Chan, S. I. (1989) The nature of Cu<sub>A</sub> in cytochrome *c* oxidase. *FEBS Lett.* 248: 210-211.
- Li, Y., Naqui, A., Frey, T. G. & Chance, B. (1987b) A new procedure for the purification of monodisperse highly active cytochrome *c* oxidase from bovine heart. *Biochem. J.* 242: 417-23.
- Liao, G.-L. & Palmer, G. (1996) The reduced minus oxidized difference spectra of cytochrome *a* and *a*<sub>3</sub>. *Biochim. Biophys. Acta* 1274: 109-111.
- Long, J. E., Durham, B., Okamura, M. & Millett, F. (1989) Role of specific lysine residues in binding cytochrome *c*<sub>2</sub> to the *Rhodobacter sphaeroides* reaction center in optimal orientation for rapid electron transfer. *Biochemistry* 28: 6970-6974.
- Magnus, K. A., Hazes, B., Ton-That, H., Bonaventura, C., Bonaventura, J. & Hol, W. G. (1994) Crystallographic analysis of oxygenated and deoxygenated states of arthropod hemocyanin shows unusual differences. *Proteins* 19: 302-9.
- Malmstrom, B. (1994) Rack-induced bonding in blue-copper proteins. *European Journal of Biochemistry* 223: 711-718.
- Malmstrom, B. G. & Aasa, R. (1993) The nature of the Cu<sub>A</sub> center in cytochrome *c* oxidase. *FEBS Lett.* 325: 49-52.
- Malmstrom, B. G. & Vangard, T. (1960) Electron spin resonance of copper proteins and some model complexes. *J. Mol. Biol.* 2: 118-124.
- Marcus, R. A. & Sutin, N. (1985) Electron transfers in chemistry and biology. *Biochim. Biophys. Acta* 811: 265-322.
- Margoliash, E. & Schejter, A. in *Cytochrome c: A multidisciplinary approach* Scott, R. A. & Mauk, A. G., Eds. (University science books, Sausalito, California, 1996).
- Martin, C. T., Scholes, C. P. & Chan, S. I. (1988) On the nature of cysteine coordination to Cu<sub>A</sub> in cytochrome *c* oxidase. *J. Biol. Chem.* 263: 8420-8429.
- Martinze, S. E., Huang, D., Ponomarev, M., Cramer, W. A. & Smith, J. L. (1996) The heme redox center of chloroplast cytochrome *f* is linked to a buried five-water chain. *Protein. sci.* 5: 1081.
- Mather, M., Springer, P., Hensel, S., Buse, G. & Fee, J. A. (1993) Cytochrome oxidase genes from *Thermus thermophilus*: nucleotide sequence of the fused gene and analysis of the deduced primary structures for subunits I and III of cytochrome *caa*<sub>3</sub>. *J. Biol. Chem.* 268: 5395-5408.

Mei, H., Wang, K., McKee, S., Wang, X., Waldner, J. L., Pielak, G. J., Durham, B. & Millett, F. (1996) Control of formation and dissociation of the high-affinity complex between cytochrome *c* and cytochrome *c* peroxidase by ionic strength and the low-affinity binding site. *Biochemistry* 35: 15800-6.

Meyer, T. E. & Cusanovich, M. A. (1985) Soluble cytochrome composition of the purple phototrophic bacterium *Rhodospseudomonas sphaeroides* ATCC 17023. *Biochim. Biophys. Acta* 807: 308-391.

Meyer, T. E. & Kamen, M. D. in *Advances in protein chemistry* (Academic Press, Inc., 1982), vol. 25, pp. 105-212.

Miller, M. A., Geren, L., Han, G. W., Saunders, A., Beasley, J., Pielak, G. J., Durham, B., Millett, F. & Kraut, J. (1996) Identifying the physiological electron transfer site of cytochrome *c* peroxidase by structure-based engineering. *Biochemistry* 35: 667-73.

Miller, M. A., Liu, R. Q., Hahm, S., Geren, L., Hibdon, S., Kraut, J., Durham, B. & Millett, F. (1994) Interaction domain for the reaction of cytochrome *c* with the radical and the oxyferryl heme in cytochrome *c* peroxidase compound I. *Biochemistry* 33: 8686-93.

Millett, F. in *Cytochrome c: A multidisciplinary approach* A, S. R. & Maurk, A. G., Eds. (University science books, Sausalito, CA, 1996).

Millett, F., Darley-Usmar, V. & Capaldi, R. A. (1982) Cytochrome *c* is cross-linked to subunit ii of cytochrome *c* oxidase by a water-soluble carbodiimide. *Biochemistry* 21: 3857-3862.

Millett, F., de Jong, C., Paulson, L. & Capaldi, R. A. (1983) Identification of specific carboxylate groups on cytochrome *c* oxidase that are involved in binding cytochrome *c*. *Biochemistry* 22: 546-552.

Millett, F. & Durham, B. in *Metal Ions in Biological Systems* Sigel, H. & Siegel, A., Eds. (Marcel Dekker, Inc., Basel, Switzerland, 1991), vol. 27, pp. 223-264.

Millett, F., Miller, M. A., Geren, L. & Durham, B. (1995) Electron transfer between cytochrome *c* and cytochrome *c* peroxidase. *J. Bioenerg. Biomembr.* 27: 341-51.

Mitchell, D. M., Ädelroth, P., Hosler, J. P., Fetter, J. R., Brzezinski, P., Pressler, M. A., Aasa, R., Malmström, B. G., Alben, J. O., Babcock, G. T., Gennis, R. B. & Ferguson-Miller, S. (1996) A ligand-exchange mechanism of proton pumping involving tyrosine-422 of subunit I of cytochrome oxidase is ruled out. *Biochemistry* 35: 824-828.

Mitchell, D. M. & Gennis, R. B. (1995) Rapid purification of wildtype and mutant cytochrome *c* oxidase from *Rhodobacter sphaeroides* by  $\text{Ni}^{2+}$ -nta affinity chromatography. *FEBS Lett.* 368: 148-150.

Mitchell, P. (1976) Possible Molecular Mechanisms of the Protonmotive Function of Cytochrome Systems. *J. Theor. Biol.* 62: 327-367.

- Mitchell, P. & Moyle, J. (1965) Stoichiometry of proton translocation through the respiratory chain and adenosine triphosphatase systems of rat liver mitochondria. *Nature* 208: 147-51.
- Moore, G. R. & Pettigrew, G. W., Eds., Cytochrome *c*: evolutionary, structural and physiochemical aspects (Springer Verlag, Berlin, 1990).
- Morgan, J. E., Verkhovsky, M. I. & Wikström, M. (1994) The histidine cycle: a new model for proton translocation in the respiratory heme-copper oxidases. *J. Bioenerg. Biomembr.* 26: 599-608.
- Moser, C. C., Keske, J. M., Warncke, K., Farid, R. S. & Dutton, P. L. (1992) Nature of biological electron transfer. *Nature* 355: 796 - 802.
- Moser, C. C., Page, C. C., Farid, R. & Dutton, P. L. (1995) Biological electron transfer. *J. Bioenerg. Biomembr.* 27: 263-274.
- Moubarak, A., Pan, L. P. & Millett, F. (1987) Fluorescein mercuric acetate specifically displaces zinc from cytochrome oxidase. *Biochem. Biophys. Res. Commun.* 143: 1030-6.
- Nano, F. & Kaplan, S. (1982) Expression of the transposable lac operon Tn951 in *Rhodospseudomonas sphaeroides*. *J. Bacteriol.* 152: 924-927.
- Naqui, A., Powers, L., Lundeen, M., Constantinescu, A. & Chance, B. (1988) On the environment of zinc in beef heart cytochrome *c* oxidase: An x-ray absorption study. *J. Biol. Chem.* 263: 12342-12345.
- Nicholls, P. & Sone, N. (1984) Kinetics of cytochrome *c* and TMPD oxidation by cytochrome *c* oxidase from the *Thermophilic bacterium*, PS3. *Biochim. Biophys. Acta* 767: 240-7.
- Nilsson, T. (1992) Photoinduced electron transfer from tris(2,2'-bipyridyl)ruthenium to cytochrome *c* oxidase. *Proc. Natl. Acad. Sci. U S A* 89: 6497-501.
- Nobrega, M. P., Nobrega, F. G. & Tzagoloff, A. (1990) COX10 codes for a protein homologous to the ORF1 product of *Paracoccus denitrificans* and is required for the synthesis of yeast cytochrome oxidase. *J. Biol. Chem.* 265: 14220-14226.
- Oblad, M., Selin, E., Malmstrom, B., Strid, L., Aasa, R. & Malmstrom, B. G. (1989) Analytical characterization of cytochrome oxidase preparations with regard to metal and phospholipid contents, peptide composition and catalytic activity. *Biochim. Biophys. Acta* 975: 267-70.
- Ogura, T., Takahashi, S., Shinzawa-Itoh, K., Yoshikawa, S. & Kitagawa, T. (1991) Time-Resolved Resonance Raman Investigation of Cytochrome Oxidase Catalysis: Observation of a New Oxygen-Isotope Sensitive Raman Band. *Bull. Chem. Soc. Jpn.* 64: 2901-2907.

- Oliveberg, M., Hallén, S. & Nilsson, T. (1991) Uptake and release of protons during the reaction between cytochrome *c* oxidase and molecular oxygen: A flow-flash investigation. *Biochemistry* 30: 436-440.
- Oliveberg, M. & Malmström, B. G. (1991) Internal electron transfer in cytochrome *c* oxidase: evidence for a rapid equilibrium between cytochrome *a* and the bimetallic site. *Biochemistry* 30: 7053-7057.
- Onuchic, J. N., Beratan, D. N., Winkler, J. R. & Gray, H. B. (1992) Pathway analysis of protein electron-transfer reactions. *Annu Rev Biophys Biomol Struct* 21: 349-77.
- Osheroff, N., Brautigan, D. L. & Margoliash, E. (1980) Definition of enzymic interaction domains on cytochrome *c*. Purification and activity of singly substituted carboxydinitrophenyl-lysine 7, 25, 73, 86, and 99 cytochromes *c*. *J. Biol. Chem.* 255: 8245-51.
- Ostermeier, C., Harrenga, A., Ermler, U. & Michel, H. (1997) Structure at 2.7 Å resolution of the *Paracoccus denitrificans* two-subunit cytochrome *c* oxidase complexed with an antibody Fv fragment. *Proc. Natl. Acad. Sci. USA* 94: 10547-10553.
- Overfield, R. E., Wraight, C. A. & Devault, D. (1979) Microsecond photooxidation kinetics of cytochrome *c*<sub>2</sub> from *Rhodopseudomonas sphaeroides*: In vivo and solution studies. *FEBS Lett.* 105: 137-142.
- Pan, L.-P., Hazzard, J. T., Lin, J., Tollin, G. & Chan, S. I. (1991a) The electron input to cytochrome *c* oxidase from cytochrome *c*. *J. Am. Chem. Soc.* 113: 5908-5910.
- Pan, L. P., Durham, B., Wolinska, J. & Millett, F. (1988) Preparation and characterization of singly labeled ruthenium polypyridine cytochrome *c* derivatives. *Biochemistry* 27: 7180-4.
- Pan, L. P., Hibdon, S., Liu, R.-Q., Durham, B. & Millett, F. (1993) Intracomplex electron transfer between ruthenium-cytochrome *c* derivatives and cytochrome *c* oxidase. *Biochemistry* 32: 8492-8498.
- Pan, L. P., Li, Z., Larsen, R. & Chan, S. I. (1991b) The nature of Cu<sub>x</sub> in cytochrome *c* oxidase. *J. Biol. Chem.* 266: 1367-1379.
- Parkin, S. E., Chen, S., Ley, B. A., Mangravite, L., Edmondson, D. E., Huynh, B. H. & Bollinger, J. M., Jr. (1998) Electron injection through a specific pathway determines the outcome of oxygen activation at the diiron cluster in the F208Y mutant of *Escherichia coli* ribonucleotide reductase protein R2. *Biochemistry* 37: 1124-30.
- Pelletier, H. & Kraut, J. (1992) Crystal structure of a complex between electron transfer partners, cytochrome *c* peroxidase and cytochrome *c*. *Science* 258: 1748-1755.
- Pettigrew, G. W. & Moore, G. R., Eds., Cytochrome *c*: biological aspects (Springer Verlag, Berlin, 1987).

- Pfenning, N. & Truper, H. G. *Bergey's manual of determinative bacteriology*.  
Buchanan, R. E. & Gibson, N. E., Eds., (Williams and Wilkins Co., Baltimore, 1974).
- Poulos, T., Freer, S., Alden, R., Edwards, S., Skogland, U., Takio, K., Eriksson, B.,  
Xuong, N., Yonetani, T. & Kraut, J. (1980) The crystal structure of cytochrome *c*  
peroxidase. *J. Biol. Chem.* 255(2): 575-580.
- Proshlyakov, D. A., Ogura, T., Shinzawa-Itoh, K., Yoshikawa, S., Appelman, E. H. &  
Kitagawa, T. (1994) Selective resonance raman observation of the "607 nm" form  
generated in the reaction of oxidized cytochrome *c* oxidase with hydrogen peroxide. *J.*  
*Biol. Chem.* 269: 29385-29388.
- Proshlyakov, D. A., Ogura, T., Shinzawa-Itoh, K., Yoshikawa, S. & Kitagawa, T.  
(1996) Microcirculating system for simultaneous determination of Raman and  
absorption spectra of enzymatic reaction intermediates and its application to the  
reaction of cytochrome *c* oxidase with hydrogen peroxide. *Biochemistry* 35: 76-82.
- Proshlyakov, D. A., Pressler, M. A. & Babcock, G. T. (1998) Dioxygen activation and  
bond cleavage by mixed-valence cytochrome *c* oxidase. *Proc. Natl. Acad. Sci. U S A* 95:  
8020-5.
- Puustinen, A., Bailey, J. A., Dyer, R. B., Mecklenburg, S. L., Wikström, M. &  
Woodruff, W. H. (1997) Fourier transform infrared evidence for connectivity between  
Cu<sub>B</sub> and glutamic acid 286 in cytochrome *bo*<sub>3</sub> from *Escherichia coli*. *Biochemistry* 36:  
13195-200.
- Puustinen, A., Morgan, J. E., Verkhovsky, M., Thomas, J. W., Gennis, R. B. &  
Wikström, M. (1992) The low spin heme site of cytochrome *o* from *E. coli* is  
promiscuous with respect to heme type. *Biochemistry* 31: 10363-10369.
- Qian, J., Shi, W., Pressler, M., Hoganson, C., Mills, D., Babcock, G. T. & Ferguson-  
Miller, S. (1997) Aspartate-407 in *Rhodobacter sphaeroides* cytochrome *c* oxidase is  
not required for proton pumping or Mn binding. *Biochemistry* 36: 2539-2543.
- Ramirez, B. E., Malmstrom, B. G., Winkler, J. R. & Gray, H. B. (1995) The currents of  
life: The terminal electron-transfer complex of respiration. *Proc. Natl. Acad. Sci. USA*  
92: 11949 - 11951.
- Regan, J. J., Di Bilio, A. J., Langen, R., Skov, L. K., Winkler, J. R., Gray, H. B. &  
Onuchic, J. N. (1995) Electron tunneling in azurin: the coupling across a beta-sheet.  
*Chem. Biol.* 2: 489-96.
- Rich, P. R. (1995) Toward understanding the chemistry of oxygen reduction and  
proton translocation in iron - copper respiratory oxidases. *Aust. J. Plant Physiol.* 22:  
479 - 484.

- Rieder, R. & Bosshard, H. R. (1980) Comparison of the binding sites on cytochrome *c* for cytochrome *c* oxidase, cytochrome *bc*<sub>1</sub>, and cytochrome *c*<sub>1</sub>. *J. Biol. Chem.* 255: 4732-4739.
- Riistama, S., Puustinen, A., Garcia-Horsman, A., Iwata, S., Michel, H. & Wikström, M. (1996) Channelling of dioxygen into the respiratory enzyme. *Biochim. Biophys. Acta* 1275: 1-4.
- Rott, M. A. & Donohue, T. J. (1990) *Rhodobacter sphaeroides* *spd* mutations allow cytochrome *c*<sub>2</sub>-independent photosynthetic growth. *J. Bacteriol.* 172: 1954-1961.
- Rott, M. A., Fitch, J., Mery, T. E. & Donohue, T. J. (1992) Regulation of cytochrome *c*<sub>2</sub> isoform in wild-type and cytochrome *c*<sub>2</sub> mutants strains of *Rhodobacter sphaeroides*. *Arch. Biochem. Biophys.* 292: 576-582.
- Rott, M. A., Witthuhn, V. C., Schike, B. A., Soranno, M., Ali, A. & Donohue, T. J. (1993) Genetic evidence for the role of isocytchrome *c*<sub>2</sub> in photosynthetic growth of *Rhodobacter sphaeroides* *Spd* Mutants. *J. Bacterol.* 175: 358-366.
- Rumbley, J., Nickels, E. F. & Gennis, R. B. (1997) One-step purification of histidine-tagged cytochrome *bo*<sub>3</sub> from *Escherichia coli* and demonstration that associated quinone is not required for the structural integrity of the oxidase. *Biochim. Biophys. Acta* 1340: 131-142.
- Saiki, K., Mogi, T. & Anraku, Y. (1992) Heme O biosynthesis in *Escherichia coli*: The *CyoE* gene in the cytochrome *bo* operon encodes a protoheme IX farnesyltransferase. *Biochem. Biophys. Res. Commun.* 189: 1491-1497.
- Saiki, K., Mogi, T., Hori, H., Tsubaki, M. & Anraku, Y. (1993) Identification of the functional domains in heme O synthase. *J. Biol. Chem.* 268: .
- Saraste, M. (1990) Structural features of cytochrome oxidase. *Q. Rev. Biophys.* 23: 331-366.
- Saraste, M., Raito, M., Jalli, T., Chepuri, V., Lemieux, L. & Gennis, R. B. (1989) Cytochrome *o* from *Escherichia coli* is structurally related to cytochrome *aa*<sub>3</sub>. *Ann. NY Acad. Sci.* 550: 314-324.
- Schägger, H., Link, T. A., Engel, W. D. & von Jagow, G. (1986) Isolation of the eleven protein subunits of the *bc*<sub>1</sub> complex from beef heart. *Methods Enzymol.* 126: 224-37.
- Schroedl, N. A. & Hartzell, C. R. (1977) Oxidative titrations of reduced cytochrome *aa*<sub>3</sub>: correlation of midpoint potentials and extinction coefficients observed at three major absorption bands. *Biochemistry* 16: 4961-5.
- Scott, R., Zumft, W. G., Coyle, C. L. & Dooley, D. M. (1989) *Pseudomonas stutzeri* N<sub>2</sub>O reductase contains Cu<sub>A</sub>-type sites. *Proc. Natl. Acad. Sci. USA* 86: 4082-4086.

- Scott, R. A. & Mauk, A. g., Eds., *Cytochrome c: A multidisciplinary approach* (University Science Books, Sausalito, California, 1996).
- Shapleigh, J. P. & Gennis, R. B. (1992) Cloning, sequencing, and deletion from the chromosome of the gene encoding subunit I of the *aa<sub>3</sub>*-type cytochrome *c* oxidase of *Rhodobacter sphaeroides*. *Mol. Microbiol.* 6: 635-642.
- Sinjorgo, K. M., Meijling, J. H. & Muijsers, A. O. (1984) The concept of high- and low-affinity reactions in bovine cytochrome *c* oxidase steady-state kinetics. *Biochim. Biophys. Acta* 767: 48-56.
- Sinjorgo, K. M., Steinebach, O. M., Dekker, H. L. & Muijsers, A. O. (1986) The effects of pH and ionic strength on cytochrome *c* oxidase steady-state kinetics reveal a catalytic and a non-catalytic interaction domain for cytochrome *c*. *Biochim. Biophys. Acta* 850: 108-15.
- Slutter, C. E., Sanders, D., Wittung, P., Malmstrom, B. G., Aasa, R., Richards, J. H., Gray, H. B. & Fee, J. A. (1996) Water-soluble, recombinant Cu<sub>A</sub>-domain of the cytochrome *ba<sub>3</sub>* subunit II from *Thermus thermophilus*. *Biochemistry* 35: 3387-95.
- Smith, H. T., Ahmed, A. J. & Millett, F. (1981) Electrostatic interaction of cytochrome *c* with cytochrome *c<sub>1</sub>* and cytochrome oxidase. *J. Biol. Chem.* 256: 4984-90.
- Smith, H. T., Staudenmayer, N. & Millett, F. (1977) Use of specific lysine modifications to locate the reaction site of cytochrome *c* with cytochrome oxidase. *Biochemistry* 16: 4971-4974.
- Smith, L. & Davies, H. C. (1991) The reactions of the oxidase and reductases of *Paracoccus denitrificans* with cytochromes *c*. *J. Bioenerget. Biomemb.* 23: 303-319.
- Smith, M. B. & Millett, F. (1980) A 19F nuclear magnetic resonance study of the interaction between cytochrome *c* and cytochrome *c* peroxidase. *Biochim. Biophys. Acta* 626: 64-72.
- Solomon, E. I. & Lowery, M. D. (1993) Electronic structure contributions to function in bioinorganic chemistry. *Science* 259: 1575-81.
- Solomon, E. I., Sundaram, U. M. & Machonkin, T. E. (1996) Multicopper oxidases and oxygenases. *Chem. Rev.* 96: 2563-2606.
- sone, n., kutoh, e. & sato, k. (1990) A cytochrome *o*-type oxidase of the *Thermophilic bacterium* ps3 grown under air-limited conditions. *J. Biochem.* 107: 597-602.
- Speck, S. H. & Margoliash, E. (1984) Characterization of the interaction of cytochrome *c* and mitochondrial ubiquinol-cytochrome *c* reductase. *J. Biol. Chem.* 259: 1064-1072.

- Staudenmayer, N., Smith, M. B., Smith, H. T., Spies, F. K., Jr. & Millett, F. (1976) An enzyme kinetics and <sup>19</sup>F nuclear magnetic resonance study of selectively trifluoroacetylated cytochrome *c* derivatives. *Biochemistry* 15: 3198-205.
- Steffens, G. C., Soulimane, T., Wolff, G. & Buse, G. (1993) Stoichiometry and redox behaviour of metals in cytochrome *c* oxidase. *Eur. J. Biochem.* 213: 1149-57.
- Steffens, G. C. M., Biewald, R. & Buse, G. (1987) Cytochrome *c* oxidase is a three-copper, two-heme-A protein. *Eur. J. Biochem.* 164: 295-300.
- Steffens, G. J. & Buse, G. in *Cytochrome Oxidase* King, T. E., Orii, Y., Chance, B. & Okunuki, K., Eds. (Elsevier, 1979a) pp. 79-90.
- Steffens, G. J. & Buse, G. (1979b) Studies on Cytochrome *c* Oxidase, IV. Primary Structure and Function of Subunit II. *Hoppe-Seyler's Z. Physiol. Chem.* 360: 613-619.
- Steinrücke, P., Gerhus, E., Jetzek, M., Turba, A. & Ludwig, B. (1991) The cytochrome *c* reductase/oxidase respiratory pathway of *Paracoccus denitrificans*: Genetic and functional studies. *J. Bioenerget. Biomemb.* 23: 227-239.
- Steinrücke, P., Steffens, G. C. M., Pankus, G., Buse, G. & Ludwig, B. (1987) Subunit II of cytochrome *c* oxidase from *Paracoccus denitrificans* DNA sequence, gene expression and the protein. *Eur. J. Biochem.* 167: 431-439.
- Stevens, T. H., Martin, C. T., Wang, H., Brudvig, G. W., Scholes, C. P. & Chan, S. I. (1982) The nature of Cu<sub>A</sub> in cytochrome *c* oxidase. *J. Biol. Chem.* 257: 12106-12113.
- Taha, T. S. M. & Ferguson-Miller, S. (1992) Interaction of cytochrome *c* with cytochrome *c* oxidase studied by monoclonal antibodies and a protein modifying reagent. *Biochemistry* 31: 9090-9097.
- Tahirov, T. H., Misaki, S., Meyer, T. E., Cusanovich, M. A., Higuchi, Y. & Yasuoka, N. (1996) High-resolution crystal structures of two polymorphs of cytochrome *c*' from the purple phototropic bacterium *Rhodobacter capsulatus*. *J. Mol. Biol.* 259: .
- Tait, R. C. & Boyer, H. W. (1978) On the nature of tetracycline resistance controlled by the plasmid psc101. *Cell* 13: 73-81.
- Thomas, J. W., Calhoun, M. W., Lemieux, L. J., Puustinen, A., Wikström, M., Alben, J. O. & Gennis, R. B. (1994) Site-directed mutagenesis of residues within helix VI in subunit I of the cytochrome *bo*<sub>3</sub> ubiquinol oxidase from *Escherichia coli* suggests that tyrosine 288 may be a Cu<sub>B</sub> ligand. *Biochemistry* 33: 13013-21.
- Thomas, J. W., Puustinen, A., Alben, J. O., Gennis, R. B. & Wikström, M. (1993) Substitution of asparagine for aspartate-135 in subunit I of the cytochrome *bo* ubiquinol oxidase of *Escherichia coli* eliminates proton-pumping activity. *Biochemistry* 32: 10923-10928.

- Thompson, D. A., Gregory, L. & Ferguson-Miller, S. (1985) Cytochrome *c* oxidase depleted of subunit III: Proton-pumping, respiratory control, and pH dependence of the midpoint potential of cytochrome *a*. *J. Inorg. Biochem.* 23: 357-364.
- Thony-Meyer, L., Beck, C., Preisig, O. & Hennecke, H. (1994) The *ccoNOQP* gene cluster codes for a *cb*-type cytochrome oxidase that functions in aerobic respiration of *Rhodobacter capsulatus*. *Mol. Microbiol.* 14: 705-716.
- Tiede, D. M., Vashishta, A.-C. & Gunner, M. R. (1993) Electron-transfer kinetics and electrostatic properties of the *Rhodobacter sphaeroides* reaction center and soluble *c*-cytochrome. *Biochemistry* 32: 4515-4531.
- Trumpower, B. L. (1990(a)) Cytochrome *bc*<sub>1</sub> complexes of microorganisms. *Microbiol. Rev.* 54: 101-129.
- Trumpower, B. L. (1990(b)) The protonmotive Q cycle. *J. Biol. Chem.* 265: 11409-11412.
- Trumpower, B. L. & Gennis, R. B. (1994) Energy transduction by cytochrome complexes in mitochondrial and bacterial respiration: the enzymology of coupling electron transfer reactions to transmembrane proton translocation. *Annu. Rev. Biochem.* 63: 675-716.
- Tsukihara, T., Aoyama, H., Yamashita, E., Tomizaki, T., Yamaguchi, H., Shinzawa-ito, K., Nakashima, R., Yaono, R. & Yoshikawa, S. (1995) Structure of metal sites of oxidized bovine heart cytochrome *c* oxidase at 2.8 Å. *Science* 269: 1069-1074.
- Tsukihara, T., Aoyama, H., Yamashita, E., Tomizaki, T., Yamaguchi, H., Shinzawa-Itō, K., Nakashima, R., Yaono, R. & Yoshikawa, S. (1996) The whole structure of the 13-subunit oxidized cytochrome *c* oxidase at 2.8 Å. *Science* 272: 1136-1144.
- Turba, A., Jetzek, M. & Ludwig, B. (1995) Purification of *Paracoccus denitrificans* cytochrome *c*<sub>552</sub> and sequences analysis of the gene. *Eur. J. Biochem.* 231: 259-265.
- Tzagoloff, A., Capitanio, N., Nobrega, M. P. & Gatti, D. (1990) Cytochrome oxidase assembly in yeast requires the product of *COX11*, a homology of the *P. denitrificans* protein encoded by ORF3. *EMBO J.* 9: 2759-2764.
- Tzagoloff, A., Nobrega, M., Gorman, N. & Sinclair, P. (1993) On the function of yeast *COX10* and *COX11* gene products. *Biochem. Mol. Biol. Int.* 31: 593-598.
- van der Oost, J., Lappalainen, P., Musacchio, A., Warne, A., Lemieux, L. J., Rumbley, J., Gennis, R. B., Aasa, R., Pascher, T., Malmström, B. G. & Saraste, M. (1992) Restoration of a lost metal-binding site: construction of two different copper sites into a subunit of the *E. coli* quinol oxidase complex. *EMBO J.* 11: 3209-3217.
- Vandeyar, M. A., Weiner, M. P., Hutton, C. J. & Batt, C. A. (1988) A simple and rapid method for the selection of oligodeoxynucleotide-directed mutants. *Gene* 65: 129-133.

Vanneste, W. H. (1966) The stoichiometry and absorption spectra of components *a* and *a*<sub>3</sub> in cytochrome *c* oxidase. *Biochemistry* 5: 838-848.

Varotsis, C. & Babcock, G. T. (1990) Appearance of the  $\nu(\text{Fe}^{\text{IV}}=\text{O})$  vibration from a ferryl-oxo intermediate in the cytochrome oxidase/dioxygen reaction. *Biochemistry* 29: 7357-7362.

Varotsis, C., Zhang, Y., Appelman, E. H. & Babcock, G. T. (1993) Resolution of the reaction sequence during the reduction of O<sub>2</sub> by cytochrome oxidase. *Proc. Natl. Acad. Sci. USA* 90: 237-241.

von Wachenfeldt, C., De vries, S. & Van der Oost, J. (1994) The Cu<sub>A</sub> site of the *caa*<sub>3</sub>-type oxidase of *Bacillus subtilis* is a mixed-valence binuclear copper center. *FEBS lett.* 340: 109-113.

Wang, K., Mei, H., Geren, L., Miller, M. A., Saunders, A., Wang, X., Waldner, J. L., Pielak, G. J., Durham, B. & Millett, F. (1996) Design of a ruthenium-cytochrome *c* derivative to measure electron transfer to the radical cation and oxyferryl heme in cytochrome *c* peroxidase. *Biochemistry* 35: 15107-19.

Waxman, D. J. & Strominger, J. L. (1983) penicillin-binding proteins and the mechanism of action of  $\beta$ -lactam antibiotics. *Ann. Rev. Biochem.* 52: 825-869.

Weber, P. C., Bartsch, R. G., Cussanovich, M. A., Hamlin, R. C., Howard, A., Jordan, S. R., Kamen, M. D., Meyer, T. E., Weatherford, D. W., Xuong, D. W. & Salemme, F. R. (1980) Structure of cytochrome *c*: A dimeric, high-spin haem protein. *Nature* 286: 302-304.

Wikström, M. (1977) Proton pump coupled to cytochrome *c* oxidase in mitochondria. *Nature* 266: 271-273.

Wikström, M. (1984) Pumping of protons from the mitochondrial matrix by cytochrome oxidase. *Nature* 308: 558-560.

Wikström, M. (1989) Identification of the electron transfers in cytochrome oxidase that are coupled to proton-pumping. *Nature* 338: 776-778.

Wikström, M., Bogachev, A., Finel, M., Morgan, J. E., Puustinen, A., Raitio, M., Verkhovskaya, M. L. & Verkhovsky, M. I. (1994) Mechanism of proton translocation by the respiratory oxidases: The histidine cycle. *Biochim. Biophys. Acta* 1187: 106-111.

Wikström, M., Krab, K. & Saraste, M. *Cytochrome Oxidase - A Synthesis* (Academic Press, New York, 1981).

Wikström, M. & Morgan, J. E. (1992) The dioxygen cycle: spectral, kinetic and thermodynamic characteristics of ferryl and peroxy intermediates observed by reversal of the cytochrome oxidase reaction. *J. Biol. Chem.* 267: 10266-10273.

- Wilmanns, M., Lappalainen, P., Kelly, M., Sauer-Eriksson, E. & Saraste, M. (1995) Crystal structure of the membrane-exposed domain from a respiratory quinol oxidase complex with an engineered dinuclear copper center. *Proc. Natl. Acad. Sci.(USA)* 92: 11955-11959.
- Wilson, D. F., Erecinska, M. & Owen, C. S. (1976) Some properties of the redox components of cytochrome *c* oxidase and their interactions. *Arch. Biochem. Biophys.* 175: 160-72.
- Wilson, D. F., Linsay, G. & Brocklehurst, E. S. (1972) Heme-heme interactions in cytochrome oxidase. *Biochim. Biophys. Acta* 256: 277-286.
- Wilson, M. T., Greenwood, C., Brunori, M. & Antonini, E. (1975) Kinetic studies on the reaction between cytochrome *c* oxidase and ferrocycytochrome *c*. *Biochem. J.* 147: 145-53.
- Witt, H. & Ludwig, B. (1997) Isolation, analysis, and deletion of the gene coding for subunit IV of cytochrome *c* oxidase in *Paracoccus denitrificans*. *J. Biol. Chem.* 272: 5514-7.
- Witt, H., Malatesta, F., Nicoletti, F., Brunori, M. & Ludwig, B. (1998a) Cytochrome-*c*-binding site on cytochrome oxidase in *Paracoccus denitrificans*. *Eur. J. Biochem.* 251: 367-73.
- Witt, H., Malatesta, F., Nicoletti, F., Brunori, M. & Ludwig, B. (1998b) Tryptophan 121 of subunit II is the electron entry site to cytochrome-*c* oxidase in *Paracoccus denitrificans*. Involvement of a hydrophobic patch in the docking reaction involvement of a hydrophobic patch in the docking reaction. *J. Biol. Chem.* 273: 5132-6.
- Witt, H., Wittershagen, A., Bill, E., Kolbesen, B. O. & Ludwig, B. (1997) Asp-193 and Glu-218 of subunit II are involved in the Mn<sup>2+</sup>-binding of *Paracoccus denitrificans* cytochrome *c* oxidase. *FEBS Lett.* 409: 128-30.
- Witt, H., Zickermann, V. & Ludwig, B. (1995) Site-directed mutagenesis of cytochrome *c* oxidase reveals two acidic residues involved in the binding of cytochrome *c*. *Biochim. Biophys. Acta* 1230: 74-6.
- Wittung, P., Kallebring, B. & Malmstrom, B. G. (1994) The cupredoxin fold is found in the soluble Cu<sub>A</sub> and CyoA domains of two terminal oxidase. *FEBS Lett.* 349: 286-288.
- Woodruff, W. H. (1993) Coordination dynamics of heme-copper oxidases. The ligand shuttle and the control and coupling of electron transfer and proton translocation. *J. Bioenerg. Biomem.* 25: 177-88.
- Xia, D., Yu, C.-A., Kim, H., Xia, J.-Z., Kachurin, A. M., Zhang, L., Yu, L. & Deisenhofer, J. (1997) crystal structure of the cytochrome *bc*<sub>1</sub> complex from bovine heart mitochondria. *Science* 277: 60-66.

Yasui, M., Harada, S., Kai, Y., Kasai, N., Kusunoki, M. & Matsuura, Y. (1992) Three-dimensional structure of ferricytochrome *c*' from *Rhodospirillum rubrum* at 2.8 Å resolution. *J. Biochem.* 111: 317-324.

Yoshikawa, S., Shinzawa-Itoh, K., Nakashima, R., Yaono, R., Yamashita, E., Inoue, N., Yao, M., Fei, M. J., Libeu, C. P., Mizushima, T., Yamaguchi, H., Tomizaki, T. & Tsukihara, T. (1998) Redox-coupled crystal structural changes in bovine heart cytochrome *c* oxidase. *Science* 280: 1723-9.

Yoshikawa, S., Tera, T., Takahashi, Y., Tsukihara, T. & Caughey, W. S. (1988) Crystalline cytochrome *c* oxidase of bovine heart mitochondrial membrane: Composition and x-ray diffraction studies. *Proc. Natl. Acad. Sci. USA* 85: 1354-1358.

Yu, L., Dong, J.-H. & Yu, C.-A. (1986) Characterization of purified cytochrome *c*<sub>1</sub> from *Rhodobacter sphaeroides* R-26. *Biochim. Biophys. Acta* 852: 203-211.

Yu, L., Mei, Q.-C. & Yu, C.-A. (1984) Characterization of purified cCytochrome *bc*<sub>1</sub> complex from *Rhodopseudomonas sphaeroides* R-26. *J. Biol. Chem.* 259: 5752-5760.

Yun, C.-H., Barquera, B., Iba, K., Takamiya, K.-i., Shapleigh, J., Crofts, A. R. & Gennis, R. B. (1994) Deletion of the gene encoding cytochrome *b*<sub>562</sub> from *Rhodobacter sphaeroides*. *FEMS Microbio. Letts.* 120: 105-110.

Zhang, Z., Huang, L., Shulmeister, V. M., Chi, Y. I., Kim, K. K., Hung, L. W., Crofts, A. R., Berry, E. A. & Kim, S. H. (1998) Electron transfer by domain movement in cytochrome *bc*<sub>1</sub>. *Nature* 392: 677-84.

Zhen, Y., Qian, J., Follmann, K., Hosler, J., Hayward, T., Nilsson, T. & Ferguson-Miller, S. (1998) Overexpression and purification of cytochrome *c* oxidase from *Rhodobacter sphaeroides*. *Protein Expr. Purif.* 13: 326-336.

Zickermann, V., Verkhovsky, M., Morgan, J., Wikström, M., Anemuller, S., Bill, E., Steffens, G. C. & Ludwig, B. (1995) Perturbation of the Cu<sub>A</sub> site in cytochrome-*c* oxidase of *Paracoccus denitrificans* by replacement of Met227 with isoleucine. *Eur. J. Biochem.* 234: 686-93.

Zickermann, V., Wittershagen, A., Kolbesen, B. O. & Ludwig, B. (1997) Transformation of the Cu<sub>A</sub> redox site in cytochrome *c* oxidase into a mononuclear copper center. *Biochemistry* 36: 3232-6.

Zumft, W. G. (1997) Cell biology and molecular basis of denitrification. *Microbiol. Mol. Biol. Rev.* 61: 533-616.

Zumft, W. G., Dreusch, A., Lochelt, S., Cuypers, H., Friedrich, B. & Schneider, B. (1992) Derived amino acid sequences of the *nosZ* gene (respiratory N<sub>2</sub>O reductase) from *Alcaligenes eutrophus*, *Pseudomonas aeruginosa* and *Pseudomonas stutzeri* reveal potential copper-binding residues. Implications for the Cu<sub>A</sub> site of N<sub>2</sub>O reductase and cytochrome *c* oxidase. *Eur. J. Biochem.* 208: 31-40.

MICHIGAN STATE UNIV. LIBRARIES



31293016885224